

31+8923

UNLIMITED

AGARD-AR-350

AGARD-AR-350

# AGARD

ADVISORY GROUP FOR AEROSPACE RESEARCH & DEVELOPMENT

7 RUE ANCELLE, 92200 NEUILLY-SUR-SEINE, FRANCE

Processed / Not Processed by DIMS

Joy SEPT 02  
.....signed.....date

NOT FOR DESTRUCTION

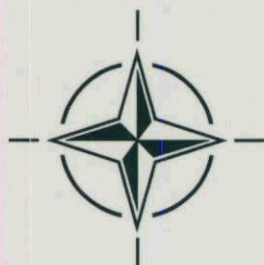
AGARD ADVISORY REPORT 350

## Structural Assessment of Solid Propellant Grains

(l'Évaluation structurale des blocs de poudre à propergol solide)

*Report of the Propulsion and Energetics Panel Working Group 25.*

*This Advisory Report was prepared at the request of the Propulsion and Energetics Panel of AGARD.*



**NORTH ATLANTIC TREATY ORGANIZATION**

Published December 1997

Distribu... Cover

UNLIMITED



# AGARD

ADVISORY GROUP FOR AEROSPACE RESEARCH & DEVELOPMENT

7 RUE ANCELLE, 92200 NEUILLY-SUR-SEINE, FRANCE

**AGARD ADVISORY REPORT 350**

## **Structural Assessment of Solid Propellant Grains**

(l'Évaluation structurale des blocs de poudre à propergol solide)

Report of the Propulsion and Energetics Panel Working Group 25.

This Advisory Report was prepared at the request of the Propulsion and Energetics Panel of AGARD.



North Atlantic Treaty Organization  
*Organisation du Traité de l'Atlantique Nord*

# The Mission of AGARD

According to its Charter, the mission of AGARD is to bring together the leading personalities of the NATO nations in the fields of science and technology relating to aerospace for the following purposes:

- Recommending effective ways for the member nations to use their research and development capabilities for the common benefit of the NATO community;
- Providing scientific and technical advice and assistance to the Military Committee in the field of aerospace research and development (with particular regard to its military application);
- Continuously stimulating advances in the aerospace sciences relevant to strengthening the common defence posture;
- Improving the co-operation among member nations in aerospace research and development;
- Exchange of scientific and technical information;
- Providing assistance to member nations for the purpose of increasing their scientific and technical potential;
- Rendering scientific and technical assistance, as requested, to other NATO bodies and to member nations in connection with research and development problems in the aerospace field.

The highest authority within AGARD is the National Delegates Board consisting of officially appointed senior representatives from each member nation. The mission of AGARD is carried out through the Panels which are composed of experts appointed by the National Delegates, the Consultant and Exchange Programme and the Aerospace Applications Studies Programme. The results of AGARD work are reported to the member nations and the NATO Authorities through the AGARD series of publications of which this is one.

Participation in AGARD activities is by invitation only and is normally limited to citizens of the NATO nations.

The content of this publication has been reproduced directly from material supplied by AGARD or the authors.



*Printed on recycled paper*

Published December 1997

Copyright © AGARD 1997  
All Rights Reserved

ISBN 92-836-1063-6



*Printed by Canada Communication Group Inc.  
(A St. Joseph Corporation Company)  
45 Sacré-Cœur Blvd., Hull (Québec), Canada K1A 0S7*

# **Propulsion and Energetics Panel Working Group 25 On Structural Assessment of Solid Propellant Grains**

**(AGARD AR-350)**

## **Executive Summary**

The recorded use of solid propellant rockets in battle spans many centuries. Today the solid propellant rocket maintains a prominent position supplying propulsion for a wide range of missiles. Numerous systems are in service or development and the future of solid propellant rockets seems assured well into the next century. The capability to design, develop and manufacture solid propellant rockets is spread widely across the NATO countries and the trend is for these technologies to become yet more widespread.

Solid propellant rocket motors are the primary propulsion choice for short and medium range missiles. Even the growing interest in ramjet and ramrocket propulsion technology required for the longer range applications carries with it the need for a solid propellant boost motor to accelerate the missile to a velocity sufficient to sustain the airbreathing mode.

Within the overall matrix of solid propellant rocket motor technologies, grain structural integrity remains a challenging area for design engineers. It is a key discipline that governs performance, reliability and service life. The environments in which rocket motors are asked to operate are becoming more and more severe, particularly for air-carried missiles where low and high temperature extremes are experienced. The ability to predict and verify adequate structural margins for such systems is vital.

The technical problems are common for all workers in the field. However, the analysis methods employed, and the design standards required, differ from one country to another and even from company to company within the same country. This lack of standardisation presents problems when assessing foreign design proposals, when participating in multinational projects, and in the ownership of foreign missile systems where safety and serviceability need to be monitored. The growing pressure for longer service life compounds the problem. There is a clear need for knowledge and understanding of the methods, standards and criteria used in each NATO country.

AGARD Propulsion and Energetics Panel established Working Group 25 to address these problems within the sphere of tactical weapon systems. The Working Group comprised AGARD Propulsion Panel Members and specialists from amongst the NATO countries. This report presents the findings of Working Group 25. It is intended to be used as a reference document for rocket motor design engineers, stress engineers, and rheologists as well as government procurement and monitoring agencies. The task of the Working group was to compare methods of structural analysis and failure prediction of solid propellant motor grains in use in the NATO countries, highlight differences and suggest standardisations or recommended approaches wherever possible. Although the scope of this work was restricted to tactical systems in particular, much of the material presented within this report will also have relevance to solid propellant rocket motors and gas generators for use in civil space systems and strategic missiles.

# L'évaluation structurale des blocs de poudre à propergol solide

(AGARD AR-350)

## Synthèse

La première utilisation des fusées à propergol solide sur le champ de bataille date de plusieurs siècles. Aujourd'hui, la fusée à propergol solide maintient sa position préminente, assurant la propulsion d'une large gamme de missiles. De nombreux systèmes sont soit en service, soit en développement, ce qui semble garantir l'avenir des fusées à propergol solide pendant une bonne partie du siècle prochain. Les compétences en matière de conception, de développement et de fabrication des fusées à propergol solide sont dispersées dans l'ensemble des pays membres de l'OTAN et la tendance actuelle en ce qui concerne ces technologies va dans le sens d'une dissémination encore plus grande.

Les moteurs-fusée à propergol solide représentent la meilleure solution de propulsion pour les missiles à courte et à moyenne portées. Même l'intérêt grandissant montré pour les technologies de propulsion des statoréacteurs et statofusées nécessaires pour une plus longue portée fait appel à un booster à propergol solide pour accélérer le missile à une vitesse suffisante pour lui permettre le mode aérobic soutenu.

Dans le contexte de la matrice globale des technologies des moteurs-fusée à propergol solide, l'intégrité structurale du bloc de poudre est un domaine qui doit continuer à motiver les ingénieurs-concepteurs. Il s'agit d'une discipline clé qui régit les performances, la fiabilité et la durée de vie. Les environnements opérationnels des moteurs-fusée sont de plus en plus extrêmes, en particulier pour les missiles aéroportés, qui sont exposés à de très grands écarts de température. La capacité de prévoir et de vérifier des marges structurales adéquates est vitale pour de tels systèmes.

Les problèmes techniques sont communs à tous ceux qui travaillent dans ce domaine. Cependant, les méthodes d'analyse utilisées et les normes de conception varient d'un pays à l'autre, voire même d'un établissement à l'autre au sein d'un même pays. Ce manque de standardisation pose des problèmes au niveau de l'évaluation d'avant projets d'étude reçus de soumissionnaires étrangers, de la participation aux projets multinationaux, et aux possesseurs de systèmes d'armes étrangers, dont la sûreté et la disponibilité doivent être contrôlées en permanence. Ce problème se trouve amplifié par la demande de plus en plus pressante de durées de vie plus longues. De toute évidence, la nécessité se fait sentir d'une coordination des méthodes, des normes et des critères utilisés dans chacun des pays membres de l'OTAN.

Le Panel AGARD de propulsion et d'énergétique a créé le Groupe de travail No. 25 pour examiner ces problèmes dans le cadre des systèmes d'armes tactiques. Il était composé de membres du Panel PEP, ainsi que d'autres spécialistes des différents pays membres de l'OTAN. Ce rapport présente les conclusions du WG25. Document de référence, il est destiné aux ingénieurs-concepteurs des moteurs-fusée, aux ingénieurs spécialistes des phénomènes de contrainte et aux spécialistes de la rhéologie, ainsi qu'aux agences gouvernementales d'approvisionnement et de contrôle. Le groupe a eu pour mandat de faire la comparaison des méthodes d'analyse structurale et de prédiction de défaillance des blocs de poudre des moteurs à propergol solide utilisés par les pays membres de l'OTAN, de mettre en lumière toutes les différences constatées et, dans la mesure du possible, de faire des propositions de normalisation ou de tentatives de solution. Bien que la portée de ces travaux ait été limitée en particulier aux systèmes tactiques, bon nombre des sujets traités dans ce rapport s'appliquent aux moteurs-fusée à propergol solide et aux générateurs de gaz destinés aux systèmes spatiaux civils et aux missiles stratégiques.

# Contents

	<b>Page</b>
<b>Executive Summary</b>	iii
<b>Synthèse</b>	iv
<b>Recent Publications of the Propulsion and Energetics Panel</b>	vi
<b>Propulsion and Energetics Panel Working Group 25 Membership</b>	viii
<b>Acknowledgements</b>	ix
	<b>Reference</b>
<b>Chapter 1 Overview of Solid Propellant Rocket Motor Design</b>	1
<b>Chapter 2 Application of Structural Integrity Assessment</b>	2
<b>Chapter 3 Structural Analysis</b>	3
<b>Chapter 4 Material Characterisation</b>	4
<b>Chapter 5 Failure Criteria</b>	5
<b>Chapter 6 Margin of Safety Determination</b>	6
<b>Chapter 7 Verification</b>	7
<b>Chapter 8 Recommendations and Conclusions</b>	8

# Recent Publications of the Propulsion and Energetics Panel

## CONFERENCE PROCEEDINGS (CP)

### **Interior Ballistics of Guns**

AGARD CP 392, January 1986

### **Advanced Instrumentation for Aero Engine Components**

AGARD CP 399, November 1986

### **Engine Response to Distorted Inflow Conditions**

AGARD CP 400, March 1987

### **Transonic and Supersonic Phenomena in Turbomachines**

AGARD CP 401, March 1987

### **Advanced Technology for Aero Engine Components**

AGARD CP 421, September 1987

### **Combustion and Fuels in Gas Turbine Engines**

AGARD CP 422, June 1988

### **Engine Condition Monitoring — Technology and Experience**

AGARD CP 448, October 1988

### **Application of Advanced Material for Turbomachinery and Rocket Propulsion**

AGARD CP 449, March 1989

### **Combustion Instabilities in Liquid-Fuelled Propulsion Systems**

AGARD CP 450, April 1989

### **Aircraft Fire Safety**

AGARD CP 467, October 1989

### **Unsteady Aerodynamic Phenomena in Turbomachines**

AGARD CP 468, February 1990

### **Secondary Flows in Turbomachines**

AGARD CP 469, February 1990

### **Hypersonic Combined Cycle Propulsion**

AGARD CP 479, December 1990

### **Low Temperature Environment Operations of Turboengines (Design and User's Problems)**

AGARD CP 480, May 1991

### **CFD Techniques for Propulsion Applications**

AGARD CP 510, February 1992

### **Insensitive Munitions**

AGARD CP 511, July 1992

### **Combat Aircraft Noise**

AGARD CP 512, April 1992

### **Airbreathing Propulsion for Missiles and Projectiles**

AGARD CP 526, September 1992

### **Heat Transfer and Cooling in Gas Turbines**

AGARD CP 527, February 1993

### **Fuels and Combustion Technology for Advanced Aircraft Engines**

AGARD CP 536, September 1993

### **Technology Requirements for Small Gas Turbines**

AGARD CP 537, March 1994

### **Erosion, Corrosion and Foreign Object Damage Effects in Gas Turbines**

AGARD CP 558, February 1995

### **Environmental Aspects of Rocket and Gun Propulsion**

AGARD CP 559, February 1995

### **Loss Mechanisms and Unsteady Flows in Turbomachines**

AGARD CP 571, January 1996

### **Advanced Aero-Engine Concepts and Controls**

AGARD CP 572, June 1996

### **Service Life of Solid Propellants Systems**

AGARD CP 586, May 1997

### **Aircraft Fire Safety**

AGARD CP 587, September 1997

## **ADVISORY REPORTS (AR)**

**Producibility and Cost Studies of Aviation Kerosines** (*Results of Working Group 16*)

AGARD AR 227, June 1985

**Performance of Rocket Motors with Metallized Propellants** (*Results of Working Group 17*)

AGARD AR 230, September 1986

**Recommended Practices for Measurement of Gas Path Pressures and Temperatures for Performance Assessment of Aircraft Turbine Engines and Components** (*Results of Working Group 19*)

AGARD AR 245, June 1990

**The Uniform Engine Test Programme** (*Results of Working Group 15*)

AGARD AR 248, February 1990

**Test Cases for Computation of Internal Flows in Aero Engine Components** (*Results of Working Group 18*)

AGARD AR 275, July 1990

**Test Cases for Engine Life Assessment Technology** (*Results of Working Group 20*)

AGARD AR 308, September 1992

**Terminology and Assessment Methods of Solid Propellant Rocket Exhaust Signatures** (*Results of Working Group 21*)

AGARD AR 287, February 1993

**Guide to the Measurement of the Transient Performance of Aircraft Turbine Engines and Components** (*Results of Working Group 23*)

AGARD AR 320, March 1994

**Experimental and Analytical Methods for the Determination of Connected — Pipe Ramjet and Ducted Rocket Internal Performance** (*Results of Working Group 22*)

AGARD AR 323, July 1994

**Recommended Practices for the Assessment of the Effects of Atmospheric Water Ingestion on the Performance and Operability of Gas Turbine Engines** (*Results of Working Group 24*)

AGARD AR 332, September 1995

## **LECTURE SERIES (LS)**

**Design Methods Used in Solid Rocket Motors**

AGARD LS 150, April 1987

AGARD LS 150 (Revised), April 1988

**Blading Design for Axial Turbomachines**

AGARD LS 167, June 1989

**Comparative Engine Performance Measurements**

AGARD LS 169, May 1990

**Combustion of Solid Propellants**

AGARD LS 180, July 1991

**Steady and Transient Performance Prediction of Gas Turbine Engines**

AGARD LS 183, May 1992

**Rocket Motor Plume Technology**

AGARD LS 188, June 1993

**Research and Development of Ram/Scramjets and Turboramjets in Russia**

AGARD LS 194, December 1993

**Turbomachinery Design Using CFD**

AGARD LS 195, May 1994

**Mathematical Models of Gas Turbine Engines and their Components**

AGARD LS 198, December 1994

## **AGARDOGRAPHS (AG)**

**Measurement Uncertainty within the Uniform Engine Test Programme**

AGARD AG 307, May 1989

**Hazard Studies for Solid Propellant Rocket Motors**

AGARD AG 316, September 1990

**Advanced Methods for Cascade Testing**

AGARD AG 328, August 1993

## **REPORTS (R)**

**Rotorcraft Drivetrain Life Safety and Reliability**

AGARD R 775, June 1990

**Impact Study on the use of JET A Fuel in Military Aircraft during Operations in Europe**

AGARD R 801, January 1997

**The Single Fuel Concept and Operation Desert Shield/Storm**

AGARD R 810, January 1997 (*NATO Unclassified*)

**Propulsion and Energy Issues for the 21st Century**

AGARD R 824, March 1997

# Propulsion and Energetics Panel Working Group 25 Members

## Chairman

A. Whitehouse (Panel Member)  
Royal Ordnance plc  
Rocket Motors  
Kidderminster  
Worcestershire  
DY11 7RZ, United Kingdom

## Canada

Mr. B. Jones  
British Aerospace Limited  
P.O. Box 874  
660 Berry Street  
Winnipeg, Manitoba, R3C 2S4

## France

Mr. J. Thepenier  
SNPE Defense Espace  
33160 Saint-Médard-en-Jalles

Mr. R. Couturier (Panel Member)  
Defense Espace du SNPE  
Centre de Recherches du Bouchet  
BP 2  
91710 Vert le Petit

Mr. P. Donguy (Panel Technical Assessor)  
S.E.P.  
24, rue Salomon de Rothschild  
BP 303  
92156 Suresnes Cedex

## Germany

Dipl. Ing. H. Besser (Panel Member)  
Bayern-Chemie GmbH  
Postfach 1131  
84544 Aschau a. Inn

Mr. L. Eineder  
Bayer-Chemie GmbH  
Postfach 1131  
84544 Aschau a. Inn

## The Netherlands

Dr. F. Zee  
Aerospace Propulsion Products B.V.  
P.O. Box 697  
4600 Ar Bergen Op Zoom

## Turkey

Prof. E. Tekkaya  
Middle East Technical University  
06531 Ankara

Mr. M. Cakiroglu  
ESTAN Missile Industries Inc.  
P.O. Box 30  
Elmadag, Ankara

## United Kingdom

Dr. J. Buswell  
DRA, Fort Halstead  
Sevenoaks, Kent, TN14 7BP

Mr. G.S. Faulkner  
Royal Ordnance plc  
Rocket Motors  
Kidderminster  
Worcestershire  
DY11 7RZ

Dr. J. Margetson (Technical Editor)  
Defence Research Consultancy  
c/o Royal Ordnance plc  
Westcott, Aylesbury  
Bucks, HP18 ONZ

Sqn Ldr. Ian Maxey  
Project Manager, Rocketry and Lifeing  
Propulsion Research (PR) WX4  
DRA Fort Halstead  
Sevenoaks, Kent TN17 7BP

## United States

Mr. L. Meyer (Panel Member)  
OL-AC PL/RK  
5 Pollux Drive  
Edwards AFB, CA 93524 7084

Mr. R. Leighton  
OLAC, PL/RKAM  
4, Draco Drive  
Edwards AFB, California 93514-7190

Mr. R. Pritchard  
Naval Air Warfare Center  
Weapons Division  
China Lake, CA 94555-6001

## Panel Executive Office

### From Europe

PEP, RTO-OTAN  
92200 Neuilly-sur-Seine  
France

### From US & Canada

PEP, RTO-NATO  
PSC 116  
APO AE 09777

Tel. 33 (1) 55 61 22 85  
Fax: 33 (1) 55 61 22 98/99

# Acknowledgements

I would like to thank the following guest members and consultants who contributed significantly to this report.

G. Francis	Micon Ltd, USA
H. Chelner	Micon Ltd, USA
G. Spinks	DERA, Fort Halstead, UK
G. Collingwood	Thiokol, USA
S. Ozupek	University of California
B. Gondouin	SNPE, France
E. Koc	Tubitak-Sage, Turkey
S.Y. Ho	AMRL, Australia
C. Cook	Ordnance Board, UK

**A. Whitehouse**  
**WG-25 Chairman**

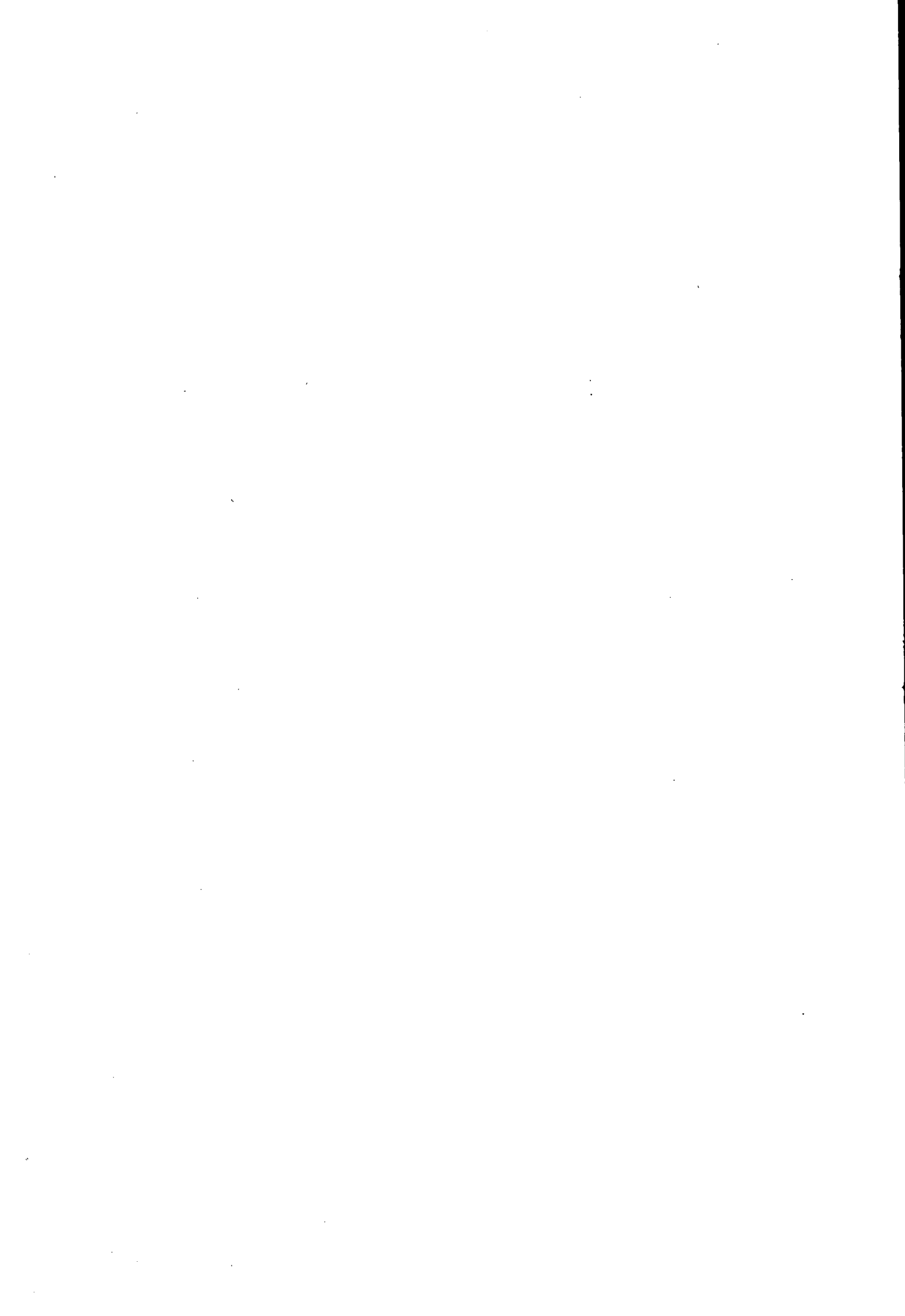


# **CHAPTER 1**

## **OVERVIEW OF SOLID PROPELLANT ROCKET MOTOR DESIGN**

### **TABLE OF CONTENTS**

<b>1.1</b>	<b>GENERAL CHARACTERISTICS</b>	<b>1-1</b>
<b>1.2</b>	<b>ROCKET MOTOR DESIGN FEATURES</b>	<b>1-5</b>
1.2.1	Rocket Motor Case Construction	1-5
1.2.2	Grain Design	1-6
1.2.3	Grain Configurations	1-7
1.2.4	Nozzleless Motors	1-8
1.2.5	Propellant	1-9
<b>1.3</b>	<b>SERVICE ENVIRONMENTS</b>	<b>1-11</b>
<b>1.4</b>	<b>OPERATIONAL LOADS</b>	<b>1-11</b>
<b>1.5</b>	<b>REFERENCES</b>	<b>1-12</b>



## Chapter 1

# OVERVIEW OF SOLID PROPELLANT ROCKET MOTOR DESIGN

### 1.1 GENERAL CHARACTERISTICS

This chapter gives a brief overview of solid propellant rocket motor design features and the service environments in which solid rockets are required to operate. The concerns of the rocket motor designer arising from grain structural integrity are placed into this context.

The majority of present day tactical missile systems use solid propellant motors as the source of propulsive power. The rocket motor is normally a structurally important component in the missile airframe and typically represents 50 - 60 % of the total system mass. Solid rocket motors can produce very high power outputs enabling short to medium range flight profiles that would be impossible with other forms of propulsion. For longer range missions solid rocket motors become unacceptably heavy due to the mass of propellant that needs to be carried in these situations and air-breathing engines gain favour.

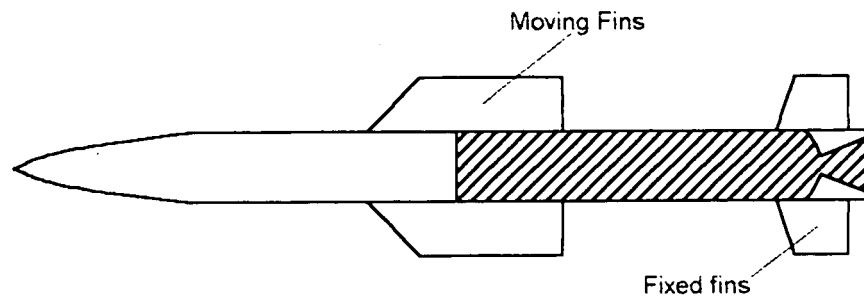
The thrust-time profile of a solid rocket motor is normally predetermined and is dictated by the propellant grain geometry. Boost-sustain profiles can be obtained from a single propellant grain or separate boost and sustain motors may be incorporated into the missile design. The use of separate motors to achieve boost-sustain thrust profiles simplifies the motor design but increases overall system mass. Some missiles incorporate discarding boost motors to overcome this mass penalty. An emerging concept which provides a degree of thrust profile management is the 'Pulse Motor'. Here two discrete propellant grains within the same combustion chamber are separated by a frangible bulkhead or intermediary nozzle. The second grain is ignited on demand at some time after the first grain has burnt out. Whatever the propellant grain layout a blastpipe may be needed in order to create space at the rear of the missile airframe to house control surface actuation equipment and/or achieve missile centre of gravity requirements. Some generic missile configurations are shown in fig 1.1. Examples of in-service tactical missile systems spanning air-to-air, ground-to-air and anti-tank applications are shown in figs 1.2 and 1.5.

Relative to its liquid propellant and air breathing counterparts the solid rocket motor is simple in design, has few parts, is robust and requires little if any maintenance. It is however required to operate in more severe and varied environments than any other form of propulsion system. Functional pretest of the main active element of a solid rocket motor, the propellant grain, is not possible. Furthermore, malfunction of the propellant grain generally leads to excessive combustion pressure and violent rupture of the motor case. There is therefore a clear need to specify, design for and verify high levels of reliability for solid propellant grains. Strategies for achieving this are the principal concerns of this Working Group report.

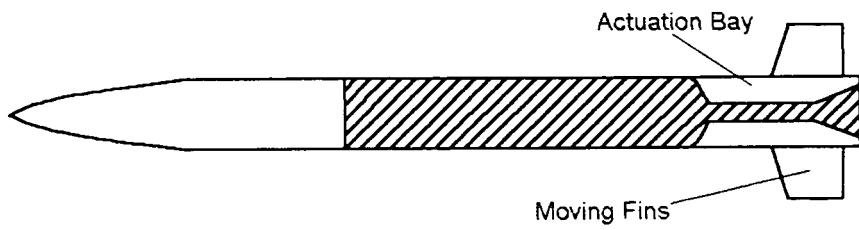
Whilst solid propellant rocket motors form the main subject of this report, there is another class of solid propellant operated device that often shares similar characteristics and grain structural integrity problems i.e. the gas generator. Gas generators are required to produce a supply of hot gas rather than propulsive thrust. For missile applications they are used to:

- i) provide power for actuation systems, separation or ejection devices.
- ii) provide a source of hot, fuel-rich gas for air-breathing ramrockets.
- iii) provide a source of hot gas for ignition of the main propellant grain.

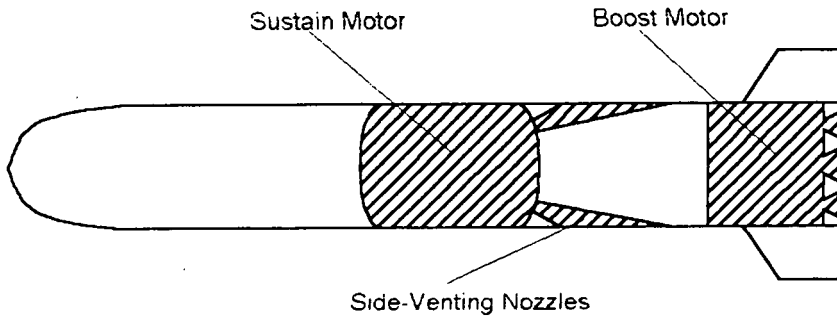
The aforementioned comments concerning propellant grain reliability apply equally well to gas generators.



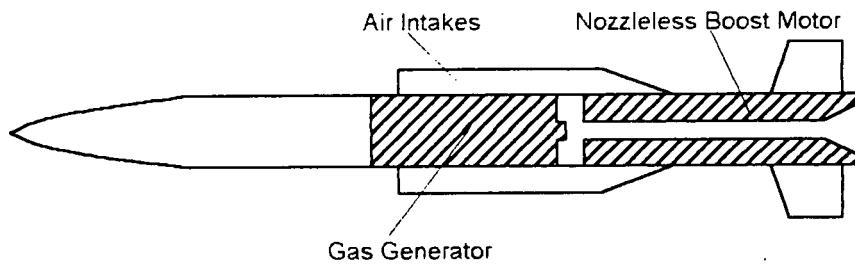
**Air-to-Air Missile**



**Air-to-Air Missile**



**Ant-Tank Missile**



**Integrated Ramrocket**

**Figure 1.1** Some Generic Missile Configurations



**Figure 1.2** BAe ASRAAM (Advanced Short Range Air to Air Missile)  
(photo Matra-Bae Dynamics)

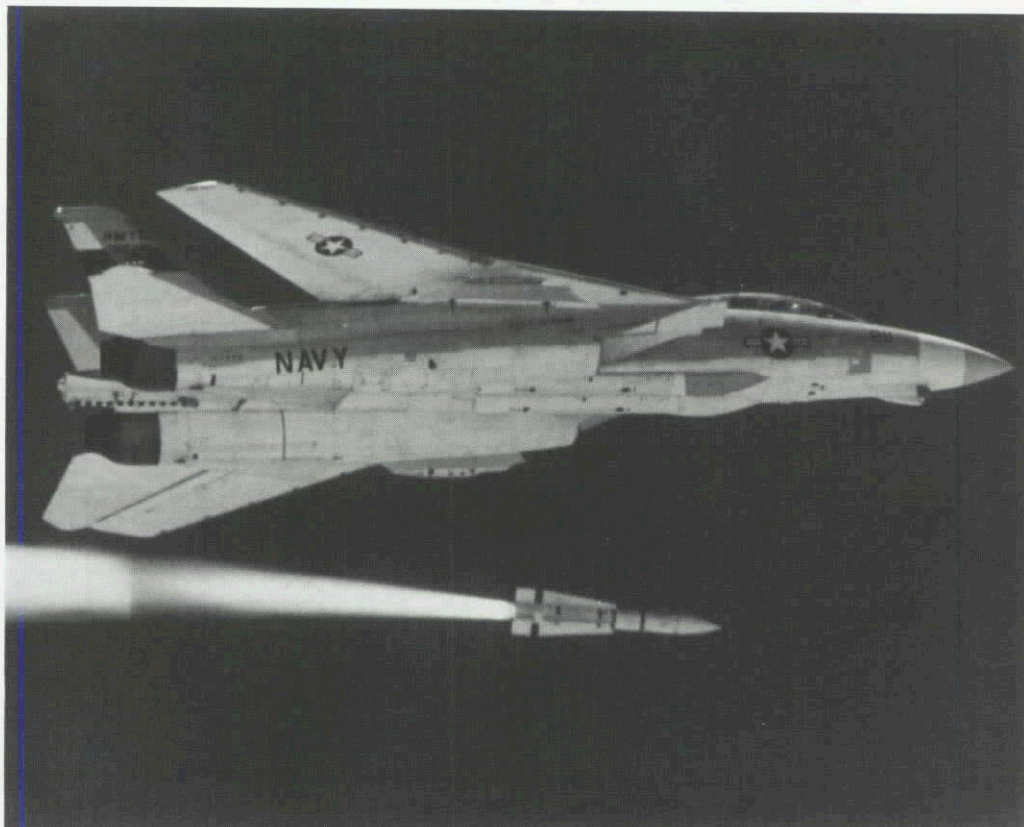


**Figure 1.3** Phoenix Missile Launch (photo NAWC)



**Figure 1.4** BAe Rapier Air Defence Missile (photo Matra-BAe Dynamics)



**Figure 1.5** Surface to Air System with TVC (photo SNPE)

## 1.2 ROCKET MOTOR DESIGN FEATURES

The design features of a typical solid rocket motor are shown in fig 1.6. The solid propellant grain burns at high pressure producing high temperature gas which vents through a converging-diverging nozzle to provide thrust. The structure of the rocket motor case, blastpipe and nozzle must be protected from the high temperature efflux by carefully chosen insulating materials. There are many complex interactions between the various components of a solid rocket and the design process involves iterative optimisation. A detailed analysis of the design process is given in AGARD LS-150 'Design Methods in Solid Rocket motors', [1]. The basic constructional elements are discussed briefly below.

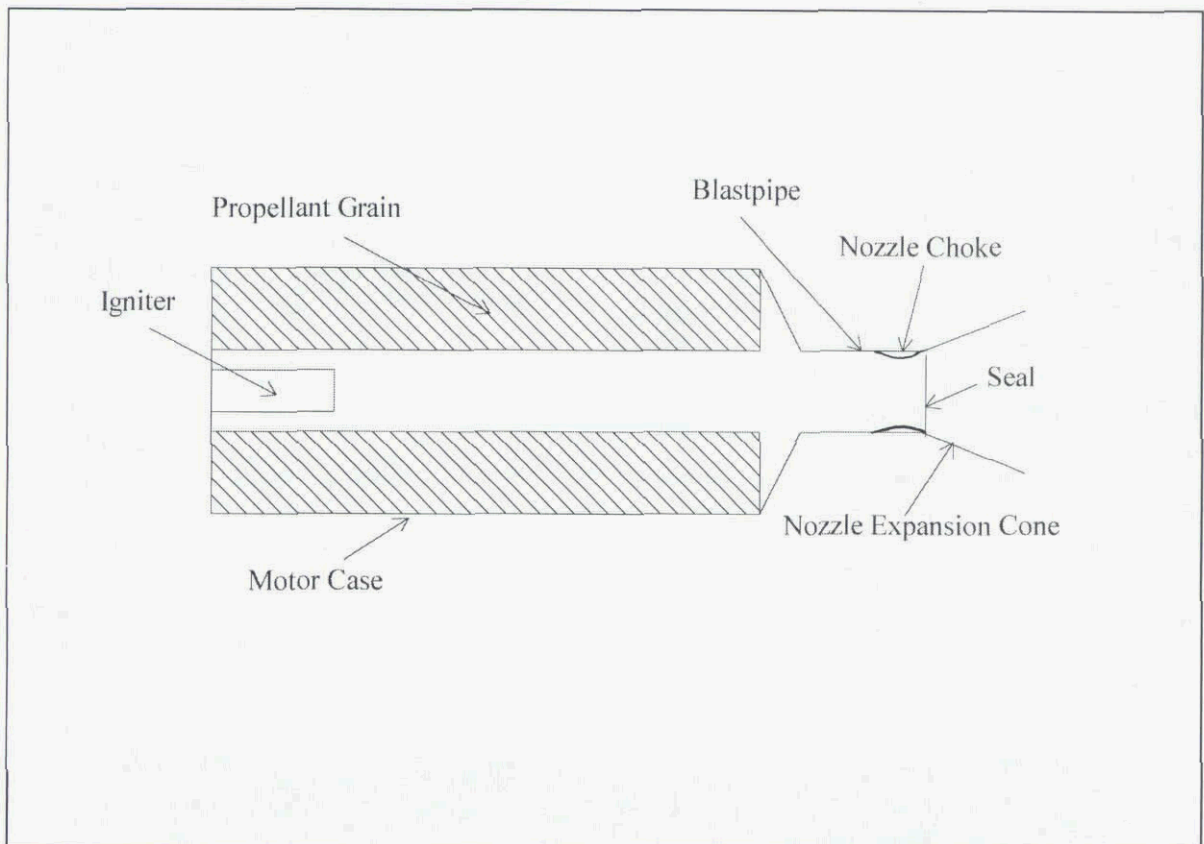


**Figure 1.6** Typical Rocket Motor Features

### 1.2.1 Rocket Motor Case Construction

The rocket motor case provides containment for the propellant grain, a pressure vessel during motor burn and a structural member to carry missile loads. Traditionally, the most common type of rocket motor case has been monolithic metallic employing high strength steel, aluminium or titanium and various forms of fabrication and forming. In recent years over winding techniques have been developed using high strength fibres such as Kevlar or carbon. A monolithic metal shell is overwound with fibres that may in some instances be braided together. For certain applications this form of construction results in a very efficient low mass case having good Insensitive Munition properties.

Steel Strip Laminate motor bodies are fabricated by coating high strength steel strip with adhesive and winding over a mandrel. End fittings are also secured by adhesive joints. This form of construction results in an efficient structure due to the use of very high strength steel which would be difficult to work by conventional means and also has good Insensitive Munition properties.

Composite rocket motor cases are manufactured by winding resin impregnated high strength fibres, usually carbon, over a suitably shaped mandrel. After cure of the resin the mandrel is removed to leave a very strong and lightweight structure. A novel technique for constructing rocket motors with composite cases has been pioneered in France. First the propellant grain is cast and cured inside an elastomeric bag which will constitute the internal insulation. The case is then wound over the propellant grain and cured

at a temperature compatible with the propellant. This manufacturing technique removes the need for a sufficiently large aperture at one end of the case to withdraw the propellant casting mandrel allowing a more efficient pressure vessel design. The stresses induced by propellant cooldown after cure are also virtually eliminated. The design of filament wound cases is discussed in some detail in ref. [1]. Composite cases are very light and also offer good Insensitive Munition properties.

### 1.2.2 Grain Design

The initial geometry of a solid propellant grain entirely dictates the subsequent burning surface area evolution and hence the mass flow rate and thrust profile. In this sense the thrust-time profile of a conventional solid rocket motor is pre-determined. The absolute magnitude of the thrust profile is determined by the surface area in conjunction with propellant burn rate pressure dependency, propellant density and thermochemical properties and the nozzle geometry.

A thrust-time requirement is usually prescribed by the missile designer. The grain designer must then try to meet this requirement as closely as possible and this gives rise to a wide range of geometrical configurations some of which are illustrated in fig 1.7. There are however further design constraints. Grain geometry affects stress levels within the propellant and hence structural integrity. Manufacturing difficulties involved in grain casting or extrusion must be considered. The internal gas flow must be such as to minimise combustion instabilities or erosive burning.

Boost-sustain thrust characteristics are frequently required in order to optimise the missile flight profile and range. As the boost to sustain thrust ratio increases so it becomes more difficult to achieve the required thrust tailoring by surface area evolution alone. For high boost-sustain ratios a cast-on-cast grain configuration is sometimes used. In this configuration the surface area evolution is typically neutral and the thrust control is achieved by the use of two propellants, a fast burning 'boost' propellant is cast on top of a slower burning 'sustain' propellant to form a single grain. Such grains may be cast in the motor and case-bonded or cast externally and cartridge loaded into the motor. The concerns for structural analyst here are the mismatch in mechanical properties between boost and sustain propellants and the propellant to propellant bond strength.

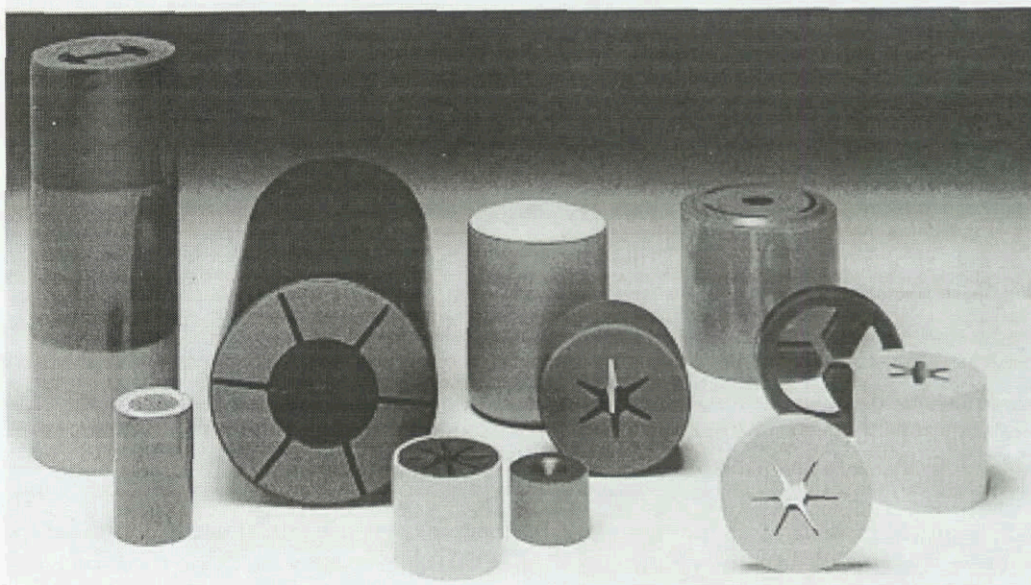


**Figure 1.7** Examples of Grain Shapes

The modelling of three-dimensional surface evolution is a complex numerical task and is performed by high speed computers using CAD software. Modern software now enables an integrated surface modelling/structural analysis/ballistic analysis approach. Solid geometry parameters obtained during

surface modelling can be passed directly to finite element mesh generators and ballistics modules greatly reducing the time taken for design optimisation.

### 1.2.3 Grain Configurations

Grain configurations fall into two classes; cartridge loaded and case-bonded.

#### i) Cartridge Loaded

Cartridge loaded grains are manufactured prior to assembly into the rocket motor and are restrained in the motor by mechanical means such as support plates and rubber pads or by adhesive bonds, usually to the case forward closure. 'Inhibition' coatings may be applied to some grain surfaces to prevent burning and so modify the surface evolution as desired or to facilitate charge support during burning. The outer surfaces of cartridge loaded grains are frequently inhibited for this reason. The cartridge loaded configuration, given adequate clearances between the case and grain, allows unconstrained thermal expansion and contraction of the propellant grain minimising thermally induced stresses. Volumetric efficiency is lower than the case-bonded configuration and case design must encompass a full diameter opening to allow motor assembly. An example configuration is shown in fig 1.8.

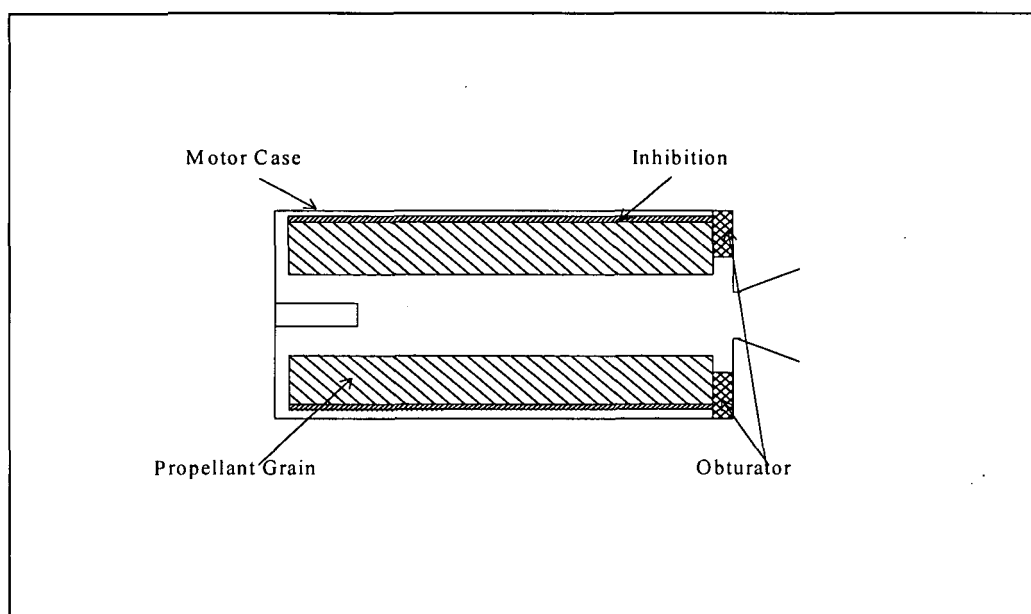


**Figure 1.8** Cartridge Loaded Grain

#### ii) Case-Bonded

Case-bonded grains are formed by casting or injecting propellant directly into the internally insulated motor case. The propellant internal conduit geometry is created by a mandrel located in the motor case prior to propellant casting. A bond between the propellant and the case wall insulation is formed as the propellant cures. An intermediary layer of adhesive or rubber between the propellant and insulation is sometimes present to aid bonding. Once the propellant is fully cured the mandrel is removed to leave the finished grain. Case-bonded grains are volumetrically efficient and ease thermal protection of the case during burn since propellant is a good insulator. The constraint of the propellant grain by the case and the mismatch in coefficient of thermal expansion between propellant and case strongly influences the stress/strain state of the grain under thermal and pressure loads. The grain design and propellant selection must make allowance for this. Stress relieving features are commonly incorporated into case-bonded grains. These can take the form of stress relieving boots or flaps at the ends of the grain or geometrical features such as radial slots, as illustrated in fig 1.9, or other cast in features.

Nearly all case-bonded grains have a central conduit and are radially burning in order to reduce stress concentrations. However, end burning grains may in some cases be case-bonded when used in conjunction with a particular form of insulation incorporating regularly spaced enclosed voids. This gives the insulation the ability to move with the propellant under thermally induced strains and avoids high stresses along the insulation to propellant bondline.

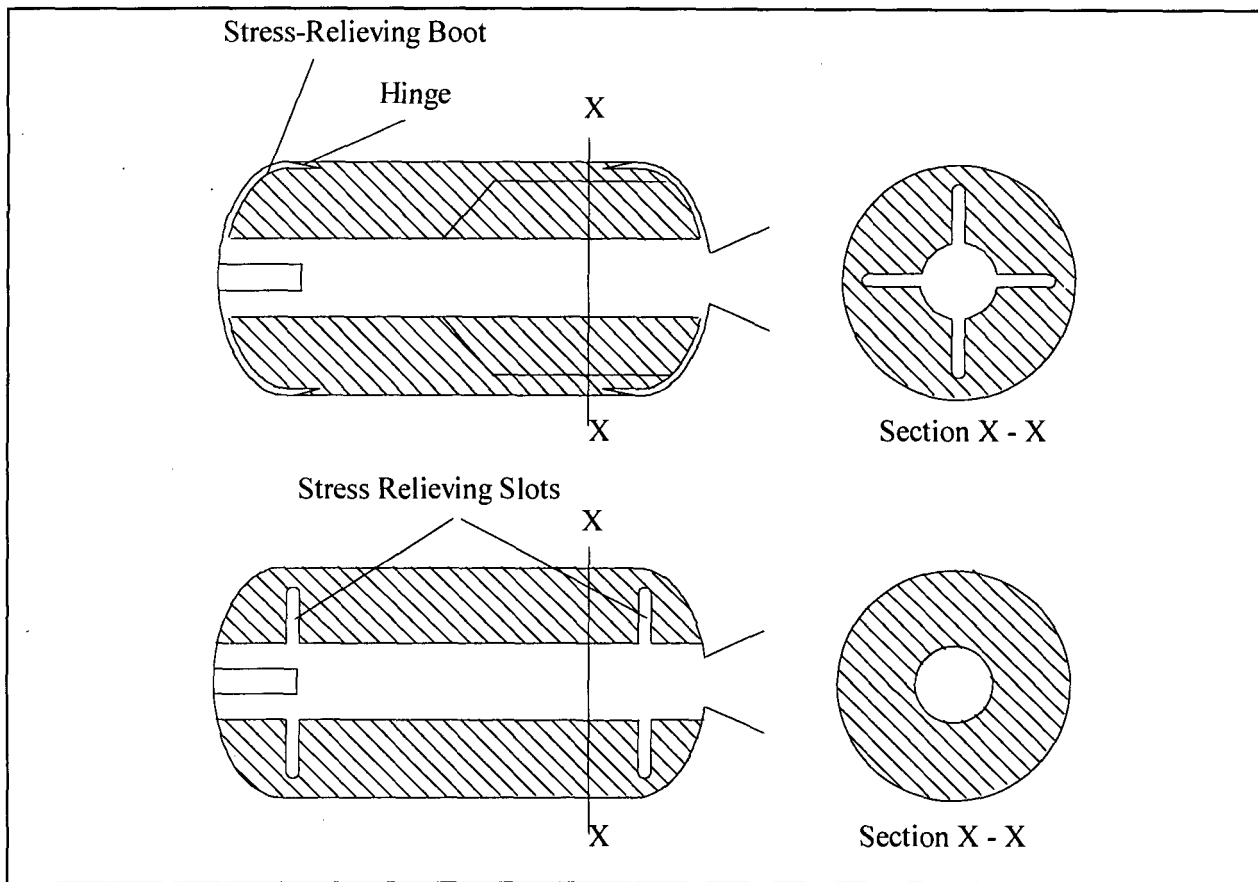


**Figure 1.9** Case-Bonded Grain Configurations

#### 1.2.4 Nozzleless Motors

The nozzleless motor concept is illustrated schematically in fig 1.10. The propellant grain is case-bonded and has a cylindrical central conduit. There is no converging-diverging nozzle as in conventional rocket motors, instead the exhaust forms an aerodynamic choke point at the rear of the central conduit. An expansion cone is cast into the propellant grain to aid expansion of the exhaust and increase thrust. The principal application of nozzleless motors is as integrated boost propulsion for ramjets or ramrockets. In this configuration the boost motor grain is cast into the ramjet combustor. Conventional rocket motors require a much smaller nozzle throat than the ramjet itself. A separate rocket nozzle which ejects prior to ramjet operation must therefore be provided within the combustor. This adds cost and complexity to the system and introduces an aircraft safety hazard for air-launched applications due to the ejected debris. Nozzleless motors in contrast avoid the need for such complication and offer an attractive solution despite their intrinsically lower thrust efficiency.

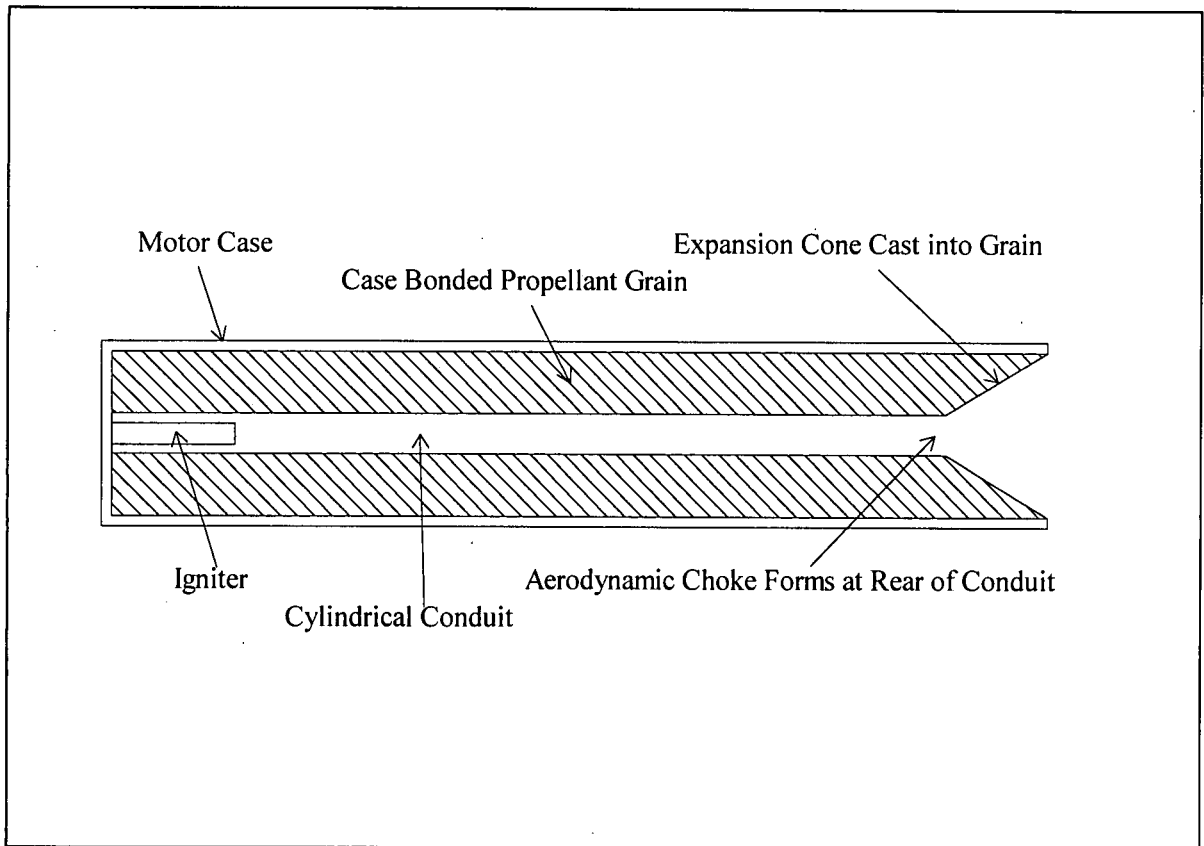


**Figure 1.10** Nozzleless Rocket Motor

### 1.2.5 Propellant

Some idealised requirements when developing or selecting a propellant for a given application may be stated. The propellant should have the required burning rate at the motor design pressure with a low pressure and temperature dependency. It should have a high specific impulse and density for rocket applications. For gas generator use other considerations such as clean, low temperature combustion products may apply. It should be easily ignited yet meet safe handling and sensitiveness criteria. The propellant must be easily processed during manufacture and be suitable for forming into a wide range of grain configurations. The ingredients should be cheap and easily obtainable. The finished propellant should have good mechanical properties (strength and extensibility) over a wide temperature range. Its properties should not deteriorate with age or exposure to environmental influences. To meet all of these requirements is very difficult and in practice many compromises have to be made. Two principal classes of propellant have emerged which offer usable characteristics and have found widespread military use. These are double-base and composite and are described in summary below. Further information can be found in ref. [2].

#### i) Double-Base or Homogeneous Propellant

This is the oldest class of propellants in use today and is derived from gun propellant technology. In their simplest form double-base propellants consist of a colloidal solution of nitro-cellulose in nitro-glycerine. After suitable processing a dough can be formed which is then extruded to the required grain cross section. Control of burning rate is achieved by the addition of small quantities of ballistic modifiers such as metal salts. However double-base propellants have a tendency to unstable burning often requiring the addition of particulate matter to the propellant to provide acoustic damping in the combustion chamber or the use of mechanical baffles and damping devices in the chamber. The extrusion process is well suited to high volume manufacture but limits the grain geometry design and precludes case-bonded grains. Large numbers of cartridge loaded rocket grains were made during the Second World War using this technique.

In order to overcome these limitations a cast double-base (CDB) family of propellants has been developed. A casting powder consisting of approximately 1mm by 1mm right circular cylinders is

manufactured by extrusion of nitro-cellulose or nitro-cellulose/nitro-glycerine. A casting mould or motor body with former is then filled with casting powder and a nitro-glycerine based casting liquid is added. The finished propellant results after curing for a few days at elevated temperature. A wide variety of complex three-dimensional grain designs can be made using this technique.

The mechanical properties of cast double-base propellants may be enhanced by the addition of an elastomer to the casting liquid. The formulation may then be manipulated to optimise propellant extensibility and modulus over a wide temperature range. This family of propellants is known as Elastomer Modified Cast Double Base (EMCDB). For all classes of CDB propellants specific impulse may be increased by adding nitramines such as RDX or HMX to the casting powder. Ammonium perchlorate and aluminium may also be added to the basic CDB propellant system to form composite modified cast double base (CMCDB) propellants.

Cross linked Double Base propellants (XLDB) are another variant of the double-base propellant family and are formed by a casting process using a slurry of polymers ( nitro-cellulose and synthetic polymers), energetic plasticisers (nitro-glycerine and others), fillers plus a curing agent. The resulting propellant has reasonable elastomeric properties and may be case-bonded.

#### ii) Composite or Heterogeneous Propellants

Composite propellants are based upon an organic polymer which serves as both binder and fuel with a solid oxidiser. Metallic additives such as aluminium powder may be used to increase density-impulse product. Nearly all present day composite propellants for tactical rocket motors use hydroxy-terminated polybutadiene (HTPB) as a binder as this offers the optimum combination of thermodynamic and mechanical properties. Some earlier composite propellants employed carboxy-terminated polybutadiene (CTPB) or a polyurethane as a binder. The inferior mechanical properties of these propellants compared to HTPB limited their use. In large space booster and strategic systems a polybutadiene - acrylic acid acrylonitrile (PBAN) binder is commonly used. For rocket applications ammonium perchlorate (AP) is used as an oxidiser almost without exception. It is easy to obtain, can be milled to a range of particle sizes to facilitate burning rate control and is chemically stable. The principal drawback of ammonium perchlorate is the presence of large amounts of hydrogen chloride in the combustion products which forms dense smoke in certain atmospheric conditions and is corrosive in nature. Ammonium nitrate (AN) is some times used to replace ammonium perchlorate particularly in gas generator propellants. Crystalline phase changes have limited the temperature range of AN propellants although much current research is directed towards this problem. The cyclic nitramine HMX is sometimes used to replace a portion of the ammonium perchlorate to reduce the chlorine content in the exhaust. AP based composite propellants will absorb atmospheric moisture if not properly protected. This can result initially in a degradation of strain capability leading to break down of the AP-binder matrix on prolonged exposure. The rocket motor design must therefore provide adequate environmental sealing and/or desiccation when an AP composite propellant is used.

#### (iii) Future Propellants

A review of some recent work on new formulations is given in ref. [4]. New oxidisers such as ammonium dinitrate (ADN), CL20 and hydrazinium nitroformate (HNF), [5] are currently receiving much research attention in an effort to find a replacement for ammonium perchlorate. Similarly, energetic binders such as glycidyl azide polymer (GAP) and polyimmo are being developed. The prospects are for higher energy propellants having low smoke signatures. However it is highly likely that these new propellants based upon energetic binders will have inferior low temperature mechanical properties relative to the current HTPB formulations. This will reinforce yet further the importance of grain structural integrity analysis.

### 1.3 SERVICE ENVIRONMENTS

There are three broad classes of service environment for tactical weapon systems; land, air and sea. Each has specific aspects which impinge upon rocket motor design and grain structural integrity.

For land-based systems and to some extent for air-carried and naval systems the thermal environment prior to missile flight is generally governed by the climate at the deployment location although some long term storage may take place in temperature controlled magazines. Some but not all ship-borne systems have the benefit of temperature controlled magazines during operational deployment. Climatic models comprising diurnal temperature and humidity cycles and graphs of the yearly probability of occurrence of a given diurnal cycle may be found in STANAG 2895, [3]. Solar heating in unshaded conditions must be taken into account as must temperature rises induced by storage in containers or buildings. An analysis of the climatic and storage conditions provides information on temperature maxima and minima and cyclic variations. This may be incorporated into structural analyses and cumulative damage models. Climatic data may also be used to assess the extent of propellant ageing and to determine appropriate accelerated ageing trials using the Arrhenius equation and known activation energies. Air carried systems are subjected to additional thermal conditions generated by the aircraft flight profile. These may take the form of forced cooling as in high altitude low speed flight or forced heating as in low altitude high speed flight. In the case of forced heating or 'aeroheating' high temperatures may be experienced in the case-propellant bondline region (for case-bonded grains) and a high temperature gradient may be created radially through the grain. Here, thermally induced stress must be carefully considered.

Many shoulder-launched land-based systems suffer a self induced high acceleration environment. A common arrangement in such systems is an 'eject' motor which propels the missile to a safe distance before ignition of the main motor. The eject motor must burn entirely within its travel up the launch tube in order to avoid blast overpressures on exit. It therefore generates a high thrust for a short time sometimes combined with a spin force. The main motor must withstand this acceleration and still function correctly.

Transportation (air, sea and road) imposes both shock and vibration environments on service rocket motors. Tests and analyses must be performed during development and qualification to verify that the motor can withstand these conditions. Vibration environments for air carried weapons may be severe, particularly in the case of helicopter carried systems. Ship borne systems are subjected to specific vibration and shock environments arising from the maritime warfare environment. More detailed analyses of service environments and rocket motor environmental testing may be found in refs. [6], [7], [8] and [9].

### 1.4 OPERATIONAL LOADS

The propellant grain experiences significant loads during motor operation. These may be considered in two classes.

i) Loads arising from pressure distributions within the combustion chamber. The gaseous products of combustion are accelerated within the combustion chamber to sonic velocity at the nozzle throat. This process together with the distributed evolution of gas from the propellant burning surface produces spatial variations in the pressure acting upon the grain surface. Present day computational fluid dynamic computer codes are able to model these flow processes to a reasonable accuracy and can provide input data for structural analyses.

ii) Loads arising from the motion of the rocket motor. These loads arise from inertial forces imparted by the motor thrust or missile manoeuvres.

Both of these load types can occur simultaneously and can interact through a complex coupling between grain distortion and internal pressure distribution.

**1.5 REFERENCES**

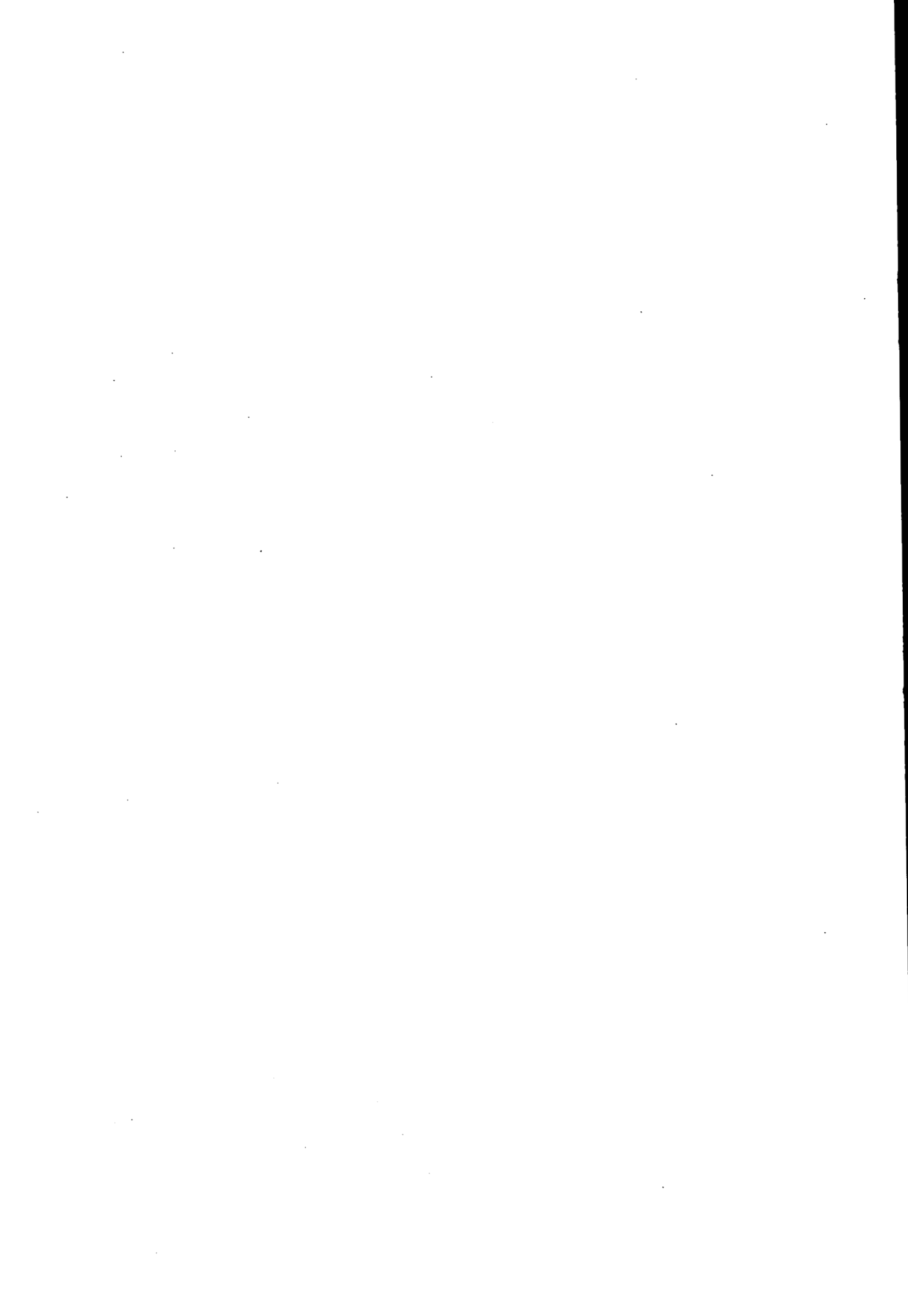
- [1] AGARD LS-150 *Design Methods in Solid Rocket Motors*, 1987
- [2] Davenas, A.; **Solid Rocket Propulsion Technology**, Pergamon Press, 1993
- [3] STANAG 2895 *Extreme Climatic Conditions and Derived Conditions for Use in Defining Design/Test Criteria for NATO Forces' Materiel*, NATO, 1990
- [4] Doriath, G.; d'Andrea, B.; *New Solid Propellants and Production Processes*, **5th AAAF International Symposium**, 22-24 May 1996, Paris.
- [5] Schoyer, H.F.R.; Schnorhk, A.J.; Korting, P.A.O.G.; van Lit, P.J.; Mul, J.M.; Gadiot, G.M.H.J.L.; Meulenbrugge, J.J.; *High Performance Propellants Based on Hydrazinium Nitroformate*, **Journal of Propulsion and Power**, Vol 11, No 4, July-August 1995
- [6] Maxey, I.; *Environmental Data for Rocket Motor Service Life Assessment*, **87th AGARD Propulsion and Energetics Panel Symposium, Service Life of Solid Propellant Systems**, 6-10 May 1996, Athens.
- [7] Laurencon, N.; *Operational conditions and Life Cycle of Solid Rocket Motors for Tactical Missiles*, **87th AGARD Propulsion and Energetics Panel Symposium, Service Life of Solid Propellant Systems**, 6-10 May 1996, Athens.
- [8] Chevalier, M.; Laurent, J.M.; *Programme General d'Essais Vieillessement : Application a un Missile Air Sol*, **87th AGARD Propulsion and Energetics Panel Symposium, Service Life of Solid Propellant Systems**, 6-10 May 1996, Athens.
- [9] Nugeyre, J.C.; Herran, B.; *Evaluation de la Duree de Vie des Moteurs Tactiques*, **87th AGARD Propulsion and Energetics Panel Symposium, Service Life of Solid Propellant Systems**, 6-10 May 1996, Athens

# **CHAPTER 2**

## **APPLICATION OF STRUCTURAL INTEGRITY ASSESSMENT**

### **TABLE OF CONTENTS**

<b>2.1</b>	<b>NEED FOR STRUCTURAL INTEGRITY ASSESSMENT</b>	<b>2-1</b>
<b>2.2</b>	<b>EMPLOYMENT OF STRUCTURAL INTEGRITY ASSESSMENT</b>	<b>2-2</b>
2.2.1	Role	2-2
2.2.2	Use During Design and Development	2-2
<b>2.3</b>	<b>STRUCTURAL INTEGRITY ASSESSMENT PROCESS</b>	<b>2-3</b>
2.3.1	Main Aspects	2-3
2.3.2	Topic Coverage	2-3
<b>2.4</b>	<b>REQUIREMENTS AND SPECIFICATIONS</b>	<b>2-4</b>
<b>2.5</b>	<b>REFERENCES</b>	<b>2-5</b>



## Chapter 2

### APPLICATION OF STRUCTURAL INTEGRITY ASSESSMENT

#### 2.1 NEED FOR STRUCTURAL INTEGRITY ASSESSMENT

The structural integrity assessment process, which is used to evaluate the ability of a solid propellant grain (including its bondline system) to perform satisfactorily under the operating conditions specified throughout its life cycle, is a major consideration in the design and evaluation of solid propellant rocket motors and gas generators. It provides a systematic examination of the structural response of the grain to its applied loading requirements and permits analysis of potential failure modes in the grain.

There is a clear need to determine a set of reasonable and practical procedural requirements that should be followed in structural integrity assessment. This is necessary so that specifications can be set to bound the process and to document the required stages. If this was carried out, the information on the conduct of structural integrity assessment - either in general or for a specific application - in one NATO country could be exchanged with and be understood by others. This would in turn allow the purchasing nation to make a more reliable and confident prediction of safety for their use of the motor or gas generator throughout its life cycle. It would also enable NATO nations to direct their activities on structural integrity assessment in a most effective and useful manner. Clearly, if this interchange of information is to be accomplished then it is essential that participating parties appreciate and understand what procedures are adopted with regard to the application of the structural integrity assessment. This document seeks to address this communication problem in detail. It consists of contributions from participating organisations in NATO countries describing the current methodologies adopted and, in some instances, the differences in approach and interpretation used to perform the structural integrity assessment of solid propellant grains.

Rocket motors and gas generators which use a solid propellant grain present the engineer with a unique set of structural integrity and service life assessment problems. The difficulties associated with performing an assessment of a grain are varied and complex. Complexities arise, for example, from the non-linear rate dependent and temperature dependent properties of the propellant, the interaction of the propellant grain with the bondline system and case, and the varied loadings - temperature, mechanical, pressure, acoustic - which the assembly must withstand for a long lifetime and yet still function without failure. If the grain suffers a structural failure, either before or during the operational phase, the resultant changes to the burning characteristics which will inevitably occur may lead to catastrophic failure upon ignition. It should be appreciated that the structural integrity assessment process has an important input, and indeed complements, the service life assessment of a solid propellant grain. However, within the scope of this Working Group's activity, the attention has been focused on the structural integrity assessment alone. Moreover, it has concentrated on the assessment of tactical systems, as strategic and space booster motor assessments include a number of specialised aspects which require separate consideration. The purpose of this Chapter is to describe the main uses and features of structural integrity assessment, whilst later sections of the document will describe the key elements and means of carrying out the process in detail.

After long experience of the inherent problems in assessing solid rocket motors and gas generators, it is generally agreed that a formalised approach to structural integrity assessment is a major contributor to obtaining the required high level of assurance that a propellant grain can withstand the in-service loads. In the past the structural integrity analysis of the grain was limited in its theoretical scope, due predominantly to lack of computational power, and relied heavily on a safety analysis of the grain being carried out prior to the motor entering service. The safety analysis was based on the use of proof firings and over-tests during the development and final production stages to assess whether a safety margin existed. With the availability of increased computational power, the structural integrity analysis became more analytical and more related to risk assessment. The initial thrust of this work was centred in the USA, where many strategic and tactical solid rocket motors were developed, and different aspects of the structural integrity method were researched and proved under the auspices of the Chemical Propulsion Information Agency (CPIA) and the Joint Army Navy NASA Air Force (JANNAF) propulsion

committees. This work was also developed in other nations and enhanced through national and co-operative programmes and international exchange agreements. The development of these methods have been particularly needed to cope with the increasingly more stringent requirements - performance, reliability and cost - applied to a solid propellant rocket motor, whilst there is also nowadays a greater need to assess the probability and consequence of failures for safety accountability reasons.

## **2.2 EMPLOYMENT OF STRUCTURAL INTEGRITY ASSESSMENT**

### **2.2.1 Role**

The role and extent to which structural integrity assessment is employed varies dependant on the relevant stage in the design, development, validation or use of a grain in a particular application for a solid rocket motor or gas generator. It can be applied whether the propellant is either a double-base or composite type and whether the grain is of a cartridge-loaded or a case-bonded form. The assessment provides a systematic examination of possible failure modes against the loading requirements and thus qualification, verification and surveillance programmes can be tailored to areas of perceived or greatest risk. It has primarily been developed as an aid to the design process of a grain and to determine risks in motor development and service use. The analysis process also enables both design and through-life trade-off studies to be conducted, by allowing either changes in the design factors or differences in operating limits and loading to be considered, and, if needed, further grain optimisation to be carried out. Structural integrity assessment is a useful aid to determining the appropriate extent of testing required to show a structurally sound grain design for, and subsequent to, entry to service of the motor. This in turn allows service life to be determined more accurately, thus enabling whole life management to be planned and to determine where In-Service surveillance activities, such as non-destructive testing, are best employed. It is also a useful basis for failure investigations and to investigate problems.

### **2.2.2 Use During Design and Development**

#### **2.2.2.1**

In the first stage of designing a rocket motor and bidding for the contract, an outline design is prepared in sufficient detail to assess the overall performance against the requirements, identify risk areas, and estimate costs to enable a costed programme to be put together. Some grain design is performed, together with basic structural integrity assessment - although this may not be fully detailed - perhaps by using simplified models and data from a similar or equivalent propellant and grain. The service environmental requirement may not be completely defined at this stage.

#### **2.2.2.2**

Following contract award, the detailed design stage takes place. Manufacturing drawings for an initial prototype are created and detailed grain to core interfaces are specified. Some limited propellant testing is carried out to support the structural analysis. The full grain geometry is confirmed by ballistic modelling and structural integrity analysis. Grain structural margins are identified from the analysis. Optimisation and refinement of the grain is carried out. Some sub-scale motors may be tested to provide basic verification that the requirements are being met.

#### **2.2.2.3**

During the Development stage, limited environmental testing is performed, usually involving full-scale motors to confirm performance characteristics and to examine potential risk areas. Motors may be subjected to selected environmental extremes followed by test firing to establish confidence in the design. Analogue or sub-scale motors may also be used to confirm structural integrity for specific critical conditions. In addition, it is usual to carry out further propellant testing to support the strength analysis; this may, for instance, require accelerated ageing of samples, followed by mechanical properties testing.

During the Development stage, some pre-qualification testing may be conducted to reduce the risks. For example, air-carried missile projects may require that a pre-flight test programme on the full motor may be undertaken in order to obtain clearance for motor use in air-carried and free-flight tests.

#### **2.2.2.4**

The Qualification testing stage provides formal verification evidence that the conditions of the technical and environmental requirement are met. The full ageing characteristics of the solid propellant grain are

determined via a programme of testing of the motor and all materials which simulates the service environment. From this the reduction in grain structural design margin with age may be determined. This stage is completed with Final (Type) Qualification testing of the motor for its intended application; this process is detailed in such NATO requirement documents as STANAGs 4297, 4325 and 4337 [1,2,3].

## 2.3 STRUCTURAL INTEGRITY ASSESSMENT PROCESS

### 2.3.1 Main Aspects

There are, generally, two main aspects in structural integrity assessment: structural analysis of the grain and strength analysis. Typically, the structural analysis consists of a determination of the stresses, strains and deformations the grain may be subjected to under prescribed loading conditions during its life cycle. The strength analysis, when coupled with appropriate failure data and criteria for the propellant and bondline materials leads to an evaluation of the grains' Margin of Safety (MS). The MS provides a measure of the ability of the grain to meet the loads that arise in the storage, use and operation of the motor; a positive MS is needed to ensure safe and satisfactory operation throughout the service life. Patently, this is not the same as the safety factor or margin that a user specifies for the overall system, which considers many other aspects such as the tolerable risks to the launch crew and platform or the intended use of the system. During the outline design stage, the structural analysis is based on many simplifying assumptions and may be somewhat limited, whilst for the final design a comprehensive and detailed analysis is conducted, combining the structural analysis and strength analysis phases. The Working Group has agreed that the elements defining the structural integrity assessment cycle are those depicted in Fig 2.1, where the figures in parentheses refer to the relevant Chapter numbers in this report.

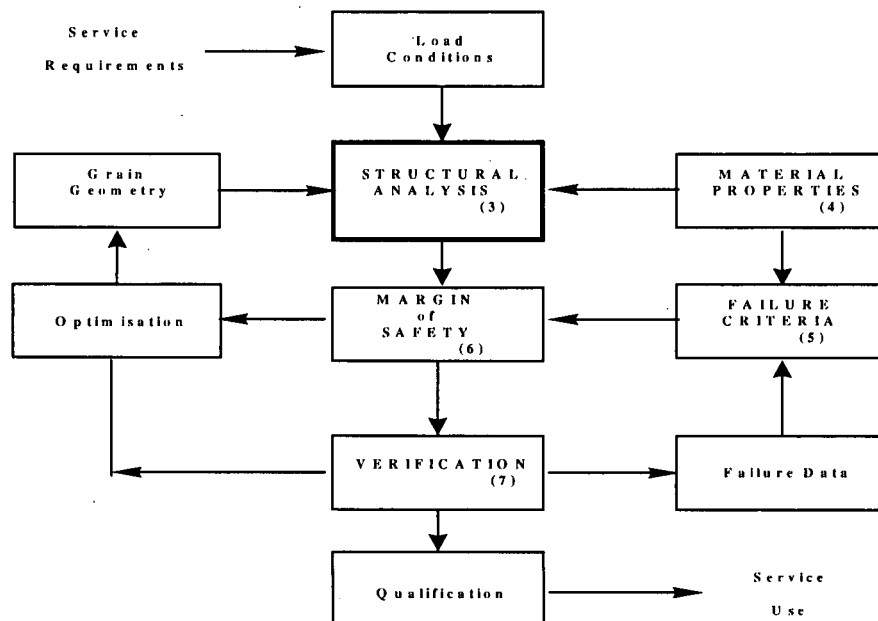


Fig 2.1 - Outline Structural Integrity Assessment Cycle

### 2.3.2 Topic Coverage

The key modules depicted in Fig 2.1 are described in detail in the following Chapters of this document:

#### 2.3.2.1

In Chapter 3 the structural analysis procedures that are generally utilised in the solid rocket motor industry for analysing the stress and strain response of the grain geometry, and associated bondline system, are described. The information presented considers the different constitutive models (i.e. elastic, hyperelastic, linear and non-linear viscoelastic) which are used as the basis for the analysis, the finite

element solution procedure and interpretation of results, and the basic material characterisation inputs and the definition of the loading requirements necessary to perform the analysis.

#### 2.3.2.2

The inputs to the structural analysis need a detailed description of the response of the materials for a representative spectrum of strain rates and temperatures. Failure properties of the materials - such as strain capacity and ultimate strength, etc. - are also needed for the strength analysis. These materials characterisation issues are dealt with in Chapter 4. An overview is also given of the tests that are currently used in NATO to characterise the material behaviour.

#### 2.3.2.3

Any structural abnormality that deters the solid propellant grain from performing its mission can be regarded as a failure. In Chapter 5 the basic failure types and theories, together with their applications, which are currently used by the NATO countries are discussed. In addition, Chapter 5 reviews such aspects as multi-axiality effects, cumulative damage concepts and fracture mechanics considerations.

#### 2.3.2.4

After the structural analysis and the selection of an appropriate failure criteria, a strength analysis is the next step in determining the structural integrity of the grain and bondline system. The results can be expressed in terms of Margin of Safety, Safety Ratio or Safety Factor. There are important distinctions between these different measures of safety and the manner in which they are used by the different NATO participants in the Working Group are discussed in detail in Chapter 6.

#### 2.3.2.5

In Chapter 7, details are given of the main methods of verification which can be used during the design and development stages of a solid rocket motor or gas generator project to verify the predictions of the structural response of the grain to the loads imposed during its life cycle. Verification may also be used to determine the limits of the motor's reliable working conditions with a high level of confidence.

#### 2.3.2.6

Finally, Chapter 8 provides a summary of the Working Group's agreements and their recommendations for the future objectives concerning structural integrity assessment.

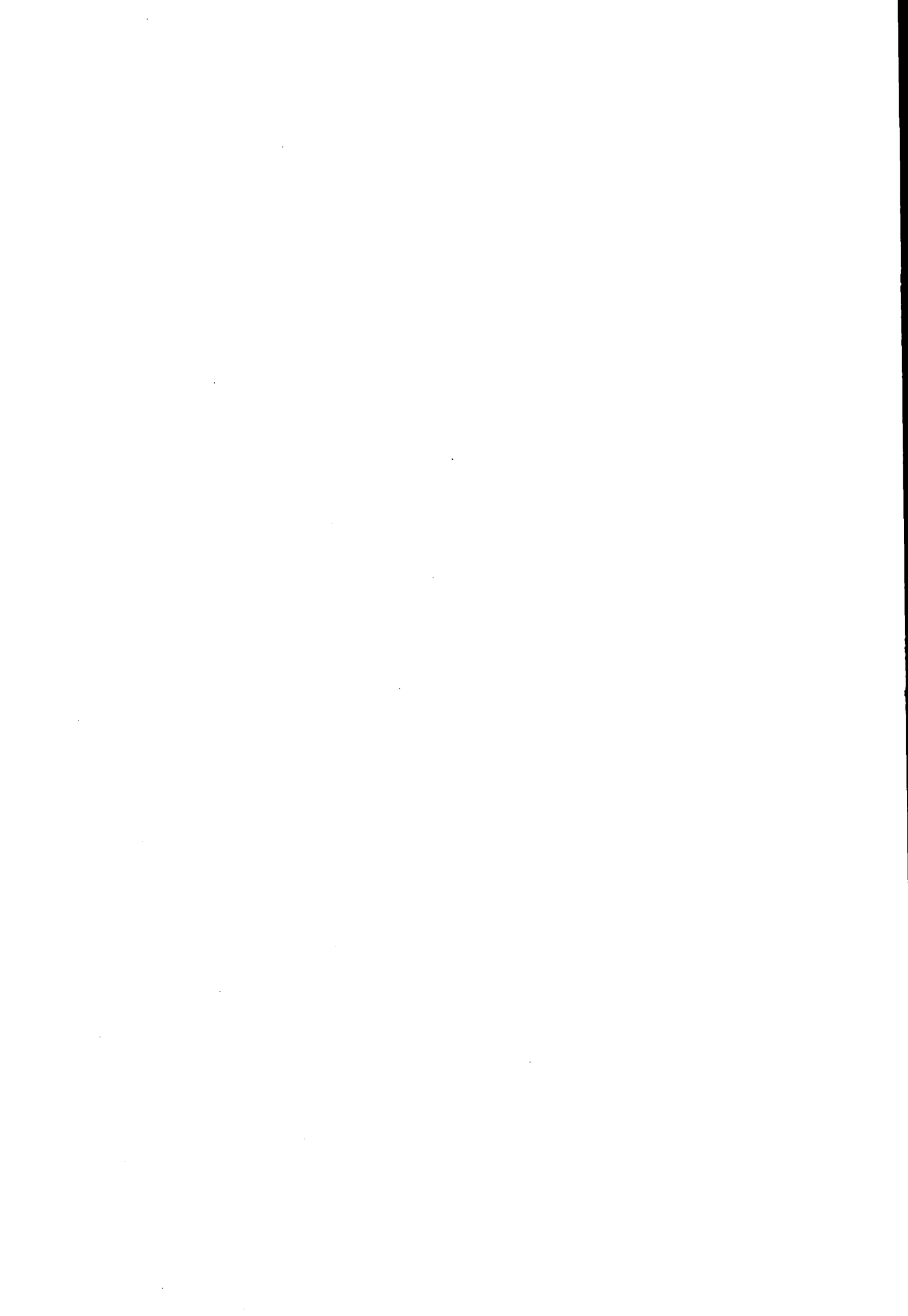
## 2.4 REQUIREMENTS AND SPECIFICATIONS

At present most NATO nations do not define requirements for the process of structural integrity assessment or for establishing the required margin of safety. It is however known that there are a number of design specifications used in differing countries that specify aspects of the design process and means of validating the safety. Additionally, some nations require the design and verification processes to be registered and validated, including specific requirements on recording and documenting the analysis process. These include the use of a Structural Design Record (SDR) for aerospace and missile structural components to record strength and fatigue calculations and factors. Although not traditionally used for motor grains, the format of them are amenable to be used for many aspects of reporting the structural integrity assessment process. Meanwhile, the requirements for margin of safety may in some projects be set by the Prime Contractor, who is charged to provide the necessary design assurance, whereas in others the margin of safety may be set by the procurement authority or Government agency. Moreover, the requirements for tactical systems may differ from those set for strategic or man-rated rockets, or be dependent upon the intended use. Thus, unlike many other design activities, standards to be followed in carrying out the process of deriving a margin of safety or documenting the calculations and the data are not regularly set out in NATO documents such as STANAGs, nor are they contained in National specifications such as Military or Defence Standards or Specifications. The results of grain structural assessments are, therefore, difficult to interpret by anyone outside the analysis team and are often unsuitably or inadequately documented to be able to exchange with other Nations.

The Working Group have considered these different aspects and in Chapter 8 recommend that future solid rocket motor projects adopt the use of a Grain Structural Assessment Report (GSAR) and suggest the format and suitable aspects to be considered in the GSAR.

## 2.5 REFERENCES

- [1] *Appraisal of the Safety and Suitability for Service of NATO Munitions, incorporating Allied Ordnance Publication AOP-15, "Guidance on the Assessment of the Safety & Suitability for Service of Munitions for NATO Armed Forces", (1985), STANAG 4297, NATO AC/310.*
- [2] *Standard Environmental and Safety Tests for Air-launched Munitions, STANAG 4325, NATO AC/310, (1991).*
- [3] *Surface Launched Munitions, Appraisal, Safety and Environmental Tests, STANAG 4337, NATO AC/310, (1994).*



# CHAPTER 3

## STRUCTURAL ANALYSIS

### TABLE OF CONTENTS

<b>3.1</b>	<b>INTRODUCTION</b>	<b>3-1</b>
	3.1.1 The Finite Element Method	3-1
<b>3.2</b>	<b>MODEL DEFINITION</b>	<b>3-2</b>
	3.2.1 Problem Definition	3-2
	3.2.1.1 Two Dimensional Analysis	3-4
	3.2.1.2 Three Dimensional Analysis	3-4
	3.2.2 Finite Element Model Definition	3-5
	3.2.2.1 Element Selection	3-5
	3.2.2.2 Boundary Condition Application	3-11
<b>3.3</b>	<b>MATERIAL DEFINITION</b>	<b>3-12</b>
	3.3.1 Constitutive Laws	3-12
	3.3.1.1 Linear Elastic (Hookean Material Law)	3-12
	3.3.1.2 Non-linear Elastic	3-13
	3.3.1.3 Linear Viscoelastic	3-13
	3.3.1.4 Non-linear Viscoelastic	3-14
	3.3.1.5 Material Model Stability	3-15
	3.3.2 Case Materials	3-15
	3.3.2.1 Metal Properties	3-15
	3.3.2.2 Composite Case Properties	3-16
	3.3.3 Insulation/Inhibitor (Rubber/Polymeric) Materials	3-16
	3.3.4 Propellant Grain	3-16
<b>3.4</b>	<b>LOAD DEFINITION</b>	<b>3-17</b>
	3.4.1 Ignition Pressurisation	3-17
	3.4.2 Thermally Induced Loads	3-18
	3.4.3 Acceleration	3-18
	3.4.4 Vibration	3-18
	3.4.5 Slump (Storage)	3-18
	3.4.6 Air Carry Reaction Loads	3-18
	3.4.7 Aerodynamic Heating	3-18
	3.4.8 Combined Loads	3-18
<b>3.5</b>	<b>SOLUTION PROCEDURE</b>	<b>3-19</b>
	3.5.1 Linear (small displacement)	3-19
	3.5.2 Non-linear (large displacement)	3-19
	3.5.3 Path Dependent	3-19

<b>3.6</b>	<b>RESULTS INTERPRETATION</b>	<b>3-19</b>
3.6.1	Accuracy	3-20
3.6.2	Solution Interpretation	3-21
3.6.3	Result Computations	3-21
3.6.3.1	Principal Stress and Strain	3-21
3.6.3.2	Hydrostatic Stress	3-21
3.6.3.3	Deviatoric Stress	3-21
3.6.3.4	von Mises Stress	3-21
3.6.4	Example Result Plots	3-22
<b>3.7</b>	<b>PRELIMINARY ANALYSES</b>	<b>3-23</b>
3.7.1	Stress Response and Effective Modulus Calculation	3-23
3.7.1.1	Basic Assumptions	3-23
3.7.1.2	Primary Relationships	3-25
<b>3.8</b>	<b>SELECTED MATERIAL MODEL EQUATIONS</b>	<b>3-26</b>
3.8.1	Linear Elastic Material Models	3-26
3.8.1.1	Equations for Plane Stress/Strain	3-26
3.8.1.2	Equations for Axisymmetry	3-28
3.8.2	Non-linear Elastic Material Models	3-29
3.8.2.1	The Deformation Gradient	3-29
3.8.2.2	Strain Energy Density	3-30
3.8.2.3	Mooney-Rivlin Material Models	3-31
3.8.2.4	Ogden Material Model	3-32
3.8.2.5	Classical Problems in Hyperelasticity	3-33
3.8.2.6	Classical Geometrically Non-Linear Problems	3-39
<b>3.9</b>	<b>FINITE ELEMENT CODES</b>	<b>3-43</b>
<b>3.10</b>	<b>CONCLUSIONS</b>	<b>3-44</b>
<b>3.11</b>	<b>REFERENCES</b>	<b>3-45</b>

## Chapter 3

# STRUCTURAL ANALYSIS

### 3.1 INTRODUCTION

The structural analysis of solid propellant grains presents several difficulties due primarily to the complex structure itself as well as the unique material behaviour associated with the solid propellant and constituent components. Some of the problems encountered in even the simplest problems include; whether to assume elastic, hyperelastic, viscoelastic, or combinations of these material behaviours; when infinitesimal strain (small deformation) theory is applicable; whether the problem can be reduced dimensionally or through symmetry; inclusion of complex boundary conditions (e.g. contact problems, etc) or loading (e.g. load histories, etc). A consequence of the complexity involved in the analysis of solid propellant grains is that approaches taken by different analysts can vary significantly. This is especially true when international cooperation is required. The objective of this chapter is to provide the analysts with a common basis of reference which describes the structural analysis procedures that are generally utilised in the solid rocket motor industry. The structural analysis of the solid rocket propellant grain is a central activity in the structural integrity evaluation process and interfaces with all the other activities described in this technical document. For example, before a structural analysis can be performed it is necessary to obtain the required input data. This data typically must come from the results of the material testing which is described in detail in chapter 4. Likewise the results obtained from a structural analysis ultimately will be used to demonstrate the structural integrity of the solid propellant grain through the procedures used to predict failure (chapter 5) and calculation of margin of safety (chapter 6) of the solid rocket motor grain.

In the past, choosing a structural analysis method was significantly influenced by the resources available (time, cost, manpower, computer resources) and accuracy required. With the dramatic improvements seen in computational capabilities the adoption of more complex methods is much less dependent on resources. Hence, sophisticated analytical tools, based on the finite element approach, are now extensively used for performing the structural analysis.

A disadvantage associated with computational methods is that the underlying method is hidden from the analyst. It is hoped that by explaining some of the underlying mathematics the analyst will be better equipped to interpret the solutions provided by the finite element method. Also, recommended (or agreed upon) approaches to the structural analysis of solid propellant grains will be discussed as an aid to better communication between analysts.

The focus of this chapter will be on the finite element method, however, other analysis techniques (typically simpler, preliminary methods) are in common use. Some highly recommended reading for an overview of design and structural assessment of solid propellant grains can be found in references 1 and 2. Additionally, excellent resources [3,4,5] exist that explain the Finite Element Method in much greater detail than will be covered in this chapter.

#### 3.1.1 The Finite Element Method

The finite element method, used to solve a wide variety of scientific, engineering and general mathematical boundary value problems, has a history thoroughly rooted in engineering practice. In fact the method grew out of techniques originally developed to solve engineering problems. In the late 1800's and early 1900's methods were developed, based on variational techniques (Rayleigh, Ritz, et al.) and "weighted residuals" (Galerkin, et al.), that led directly to the development of the finite element method.

The basic underlying approach of the method is to take a complex problem and break it down into parts represented by simple mathematical functions from which a system of linear equations can be assembled and hopefully solved. Mathematically, the approach used in the finite element method is to choose a function basis (a linearly independent set of functions) and find a linear combination of these functions that

that minimizes the error between the resulting solution and the "exact" solution (i.e. the solution to the posed boundary value problem). The resulting linear equations, formed from each element, are assembled into a large system of equations. The solution is found (at discrete points or nodes) by solving the assembled matrix problem. It can be shown, for well posed boundary value problems, that the finite element technique does result in a solution that is as close to the true solution as possible for the defined model.

Due to the resulting large (typically sparse) system of equations, significant computational resources are usually required. Therefore, this has led to the development of finite element computer programs (to assemble, manage, and solve the system of equations) and supporting programs to aid in modelling (creation of the finite elements, material definitions, and boundary conditions) and solution interpretation. Many computer codes exist both commercially and in the public domain that can handle problems ranging from the very simple analysis to large complex analyses.

Finite element techniques were first applied to the structural analysis of solid propellant rocket motors (SRMs) in the early 1960s. Performing the structural analysis of SRMs poses some specific challenges to the analyst. Of particular significance are the materials typically used in SRMs. For example, the propellant grain material can exhibit highly complex non-linear thermo-viscoelastic behaviour under certain combined time and temperature loading histories. This non-linear, viscoelastic behaviour has yet to be adequately modeled for all loading conditions possible in SRMs. However, given relatively simple load histories current state-of-the-art analysis tools can be readily applied. Additional difficulties arise when case/grain interaction must be taken into account. If the case itself exhibits complex behaviour, such as with filament wound composite cases, then inclusion of the case model is important. Complex geometries, such as nonaxisymmetric features, frequently require analysis. However, with some insight as to where the critical regions are for a particular design and loading condition the analyst can make possible simplifications (i.e. making assumptions that may only affect non-critical regions).

The following sections describe modelling procedures, problem assumptions, solution procedures, and result interpretation representative of the kind of methodology typically used in performing structural analyses of solid propellant rocket motor grains utilising the finite element technique as well as an approach to preliminary analysis.

## **3.2 MODEL DEFINITION**

To successfully compute a solution to any boundary value problem the problem must be well posed. In other words, it is necessary that the model include properly defined geometry, material properties, and boundary conditions such that the resulting system is numerically tractable (i.e. the resulting system of equations is non-singular). And in the same light, it is necessary that the element shape function and integration rule combination be selected such that no "spurious" energy modes occur (see section 3.2.2.1). It is also recommended that the problem complexity be reduced to a minimum by making use of simplifying assumptions. These topics are discussed in more detail in the following paragraphs.

### **3.2.1 Problem Definition**

First consideration for performing the structural analysis is to determine how to most easily model the problem while still retaining the desired degree of accuracy. For example, if the problem involves modelling geometry, material properties and boundary conditions that do not vary in the circumferential direction then it makes sense to assume that the solution will also not vary circumferentially. This assumption allows a two dimensional idealisation of the grain geometry to be considered with results computed only in the plane of symmetry. Results may be computed for the out-of-plane direction as a post-processing operation. Other examples where simplifications can be introduced are "plane" problems where the out-of-plane stress or strain is a known constant. Additionally, if the geometry has natural planes of symmetry then the model can be reduced accordingly. For example, take a typical cross-section of a SRM with a slotted grain. The slots, in this example, occur at regular angular intervals. A typical finite element model for the full geometry is shown in Fig 3.1 (assuming either plane stress or plane strain).

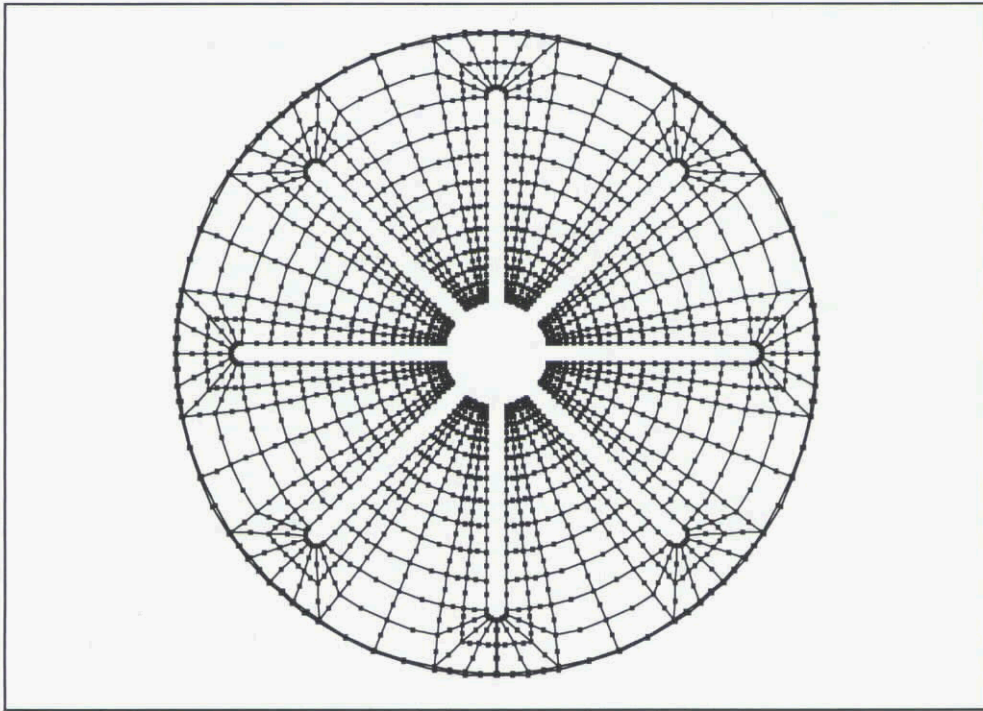


**Figure 3.1** - Full motor model

However, it is apparent that this model is highly symmetric and that through the use of displacement type boundary conditions advantage can be taken of this symmetry to reduce the model to only a single repeated segment. Fig 3.2 shows a possible model that, given purely symmetric loading, will result in a solution exactly equivalent to the full motor model. Note that boundary conditions are shown for an internal pressure load (indicated by arrows with tails) with the necessary displacements (indicated by arrows without tails) defining the lines of symmetry only.

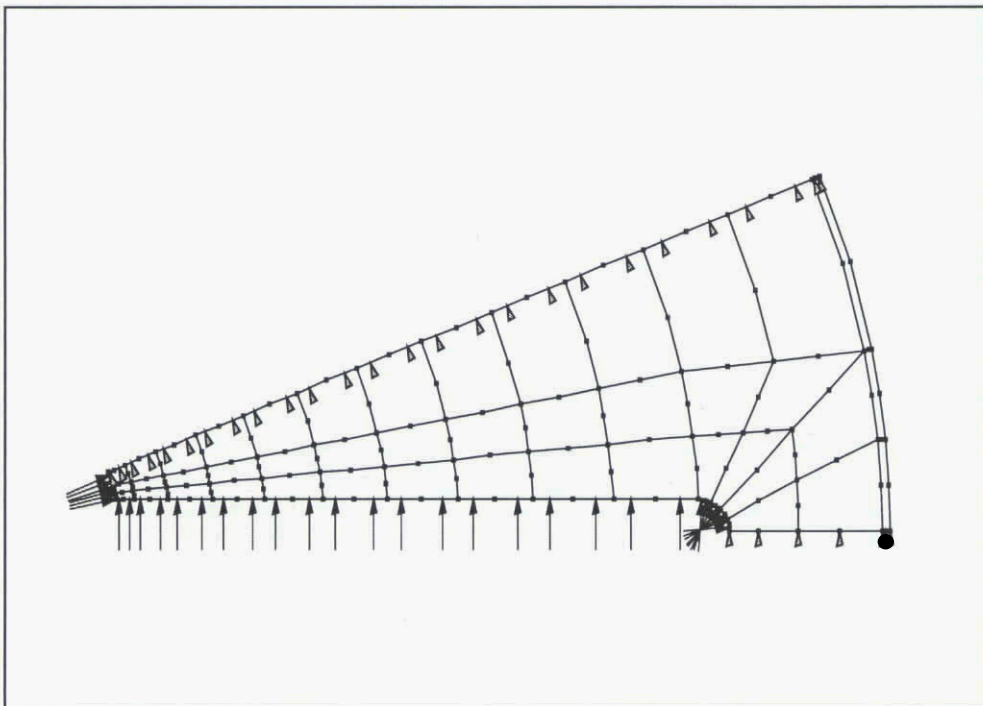


**Figure 3.2** - Partial motor model

In general, the dimension of the model is dependent on the physical dimension of the problem (considering geometry only) and the load dimension (which depends on actual load application). For example, a simple rocket motor with a circular bore, that is internally pressurised, can be reduced to a two dimensional problem (it can be geometrically modeled exactly assuming axisymmetry). The loading is also two dimensional (again modeled exactly assuming axisymmetry), therefore, the resulting model need not be modeled with greater than two dimensions. However, for the same physical model but with a transversely applied load (such as a transverse acceleration due to horizontal storage) the loading is two dimensional only in the cross-sectional plane. For this situation the overall model dimension must be three dimensional.

### 3.2.1.1 Two Dimensional Analysis

The types of assumptions that can be used to restrict the problem to two dimensions include the following.

**Plane strain/stress:** In this case, the out-of-plane stress or strain is assumed to be zero. For example, in very thin structures, that are not loaded out of the plane spanned by the structure, the plane stress assumption can be utilised. Likewise for very long structures or structures that are constrained in the "out-of-plane" direction the plane strain assumption may be valid. In either case, the corresponding out-of-plane stress or strain may be computed after the solution is found by making use of this assumption. The field equations, relating stress to strain (linear Hooke's constitutive law) and strain to displacements (assuming infinitesimally small strains), that result from the plane stress/strain assumptions are given in section 3.8.1.1. Additionally, a modified plane strain assumption is commonly used when the out-of-plane strain is known and can be assumed constant.

**Axisymmetric geometry/loading:** As discussed in section 3.2.1, for problems where the geometry, material properties, and boundary conditions do not vary with circumferential direction, axisymmetry can be assumed. The field equations (again, those relating stress to strain and strain to displacements, as above) that result from the axisymmetric assumption are given in section 3.8.1.2.

**Approximate 3D:** Other possible simplifying assumptions can be used to approximate three dimensional behaviour. Non-axisymmetric loading, for example, can be approximated by modelling the loading as a Fourier series approximation and superposing the results. Also some non-axisymmetric features (e.g. fins) can be modeled approximately through use of special elements that simulate structural response of fin regions or even by modelling the fin region with orthotropic material properties (giving the approximate behaviour of the propellant grain in the hoop direction). Fig 3.3 shows an example motor modelled as axisymmetric, but containing non-axisymmetric features (the fins are modelled with approximate 3D elements which are shown shaded in the figure). It should be noted that use of approximate 3D assumptions to model nonaxisymmetric features effectively models the behaviour of the feature in an "average" sense and does not account for complex three dimensional interactions (e.g. stress/strain concentrations along the bottom of fin slots).

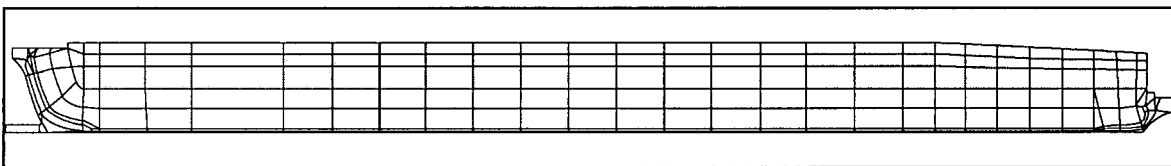


Figure 3.3 - Axisymmetric model with non-axisymmetric features

### 3.2.1.2 Three dimensional analysis

In some cases, it may be necessary to model the problem as a fully three dimensional problem. However, even for a three dimensional model it may still be possible to take advantage of symmetry. This particular point can be illustrated with reference to the storage of a rocket motor under slump loading conditions. For a horizontally stored motor a full three dimensional model most likely will be required. However, as a result of the loading symmetry it is only necessary to model half of the motor (i.e. a 180 degree segment). Likewise, if the motor is geometrically symmetric about the mid-plane the motor model

may again be reduced by half (making the final model one quarter the size of the original model).

### 3.2.2 Finite Element Model Definition

After a complete definition of the problem (geometry, loading conditions, and problem simplifications) has been determined, development of the finite element model can proceed. Several considerations must be made before undertaking the finite element model development. A general element class must typically be selected depending on several factors including computational accuracy, efficiency, and modelling ease. Also, critical regions in the physical model should be identified (typically based on common sense and/or experience) where the finite element mesh should be refined for higher accuracy. These topics will be discussed in the following sections.

#### 3.2.2.1 Element Selection

Typically the structural analysis of a SRM requires the use of solid continuum elements, therefore, discussion of element selection will be restricted to these classes of elements.

Element selection requires consideration of the problem order, shape function, and integration rule. Normally the user of most finite element programs is shielded from having to consider these factors, but it can be useful to have some understanding of how these effect element behaviour since some combinations may produce numerical instabilities while others are computationally inefficient.

Fig 3.4 shows a set of two-dimensional elements typically used for modelling solid structures. These elements are shown with the recommended integration rules for problems with two degrees of freedom at each node (such as a two dimensional structural problem where the solution is two displacements for each node). Fig 3.5 illustrates some possible element choices for three-dimensional modelling.

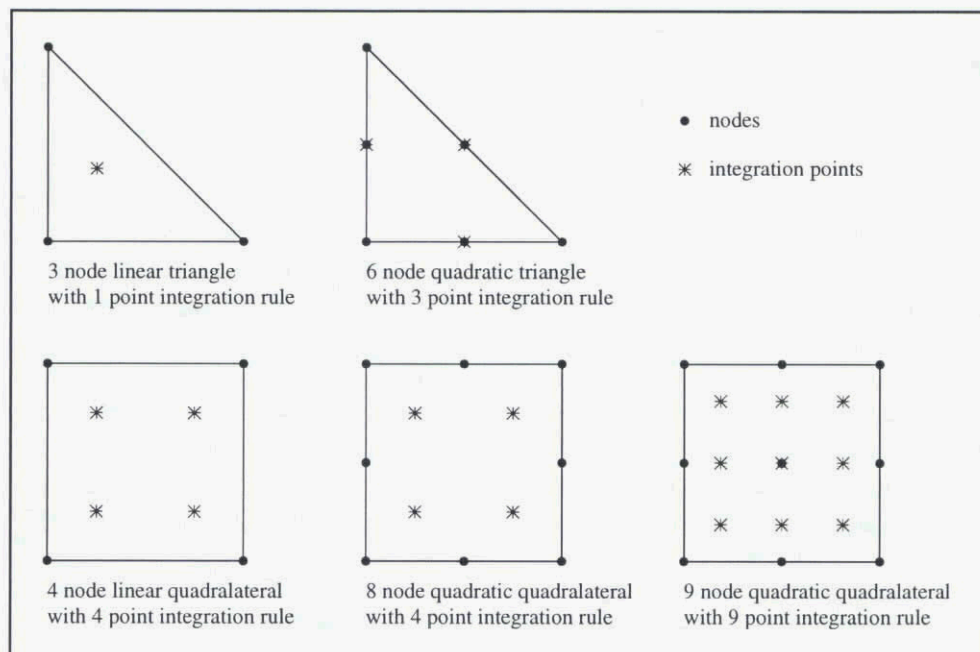


Figure 3.4 - 2D elements

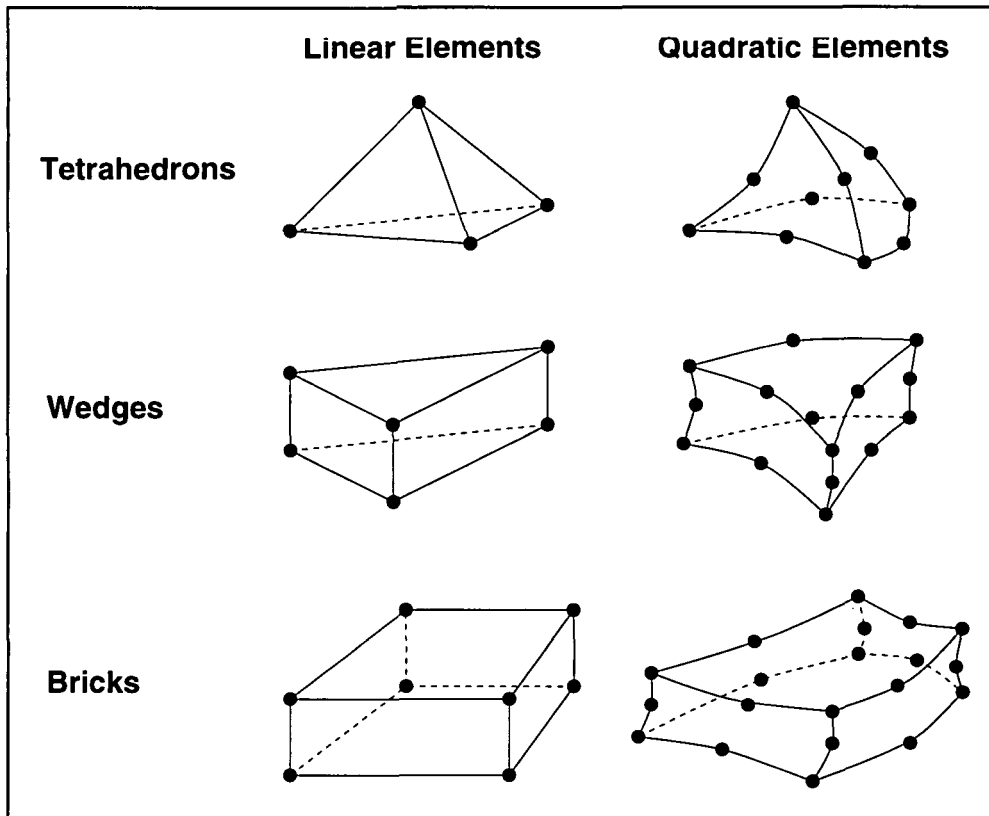
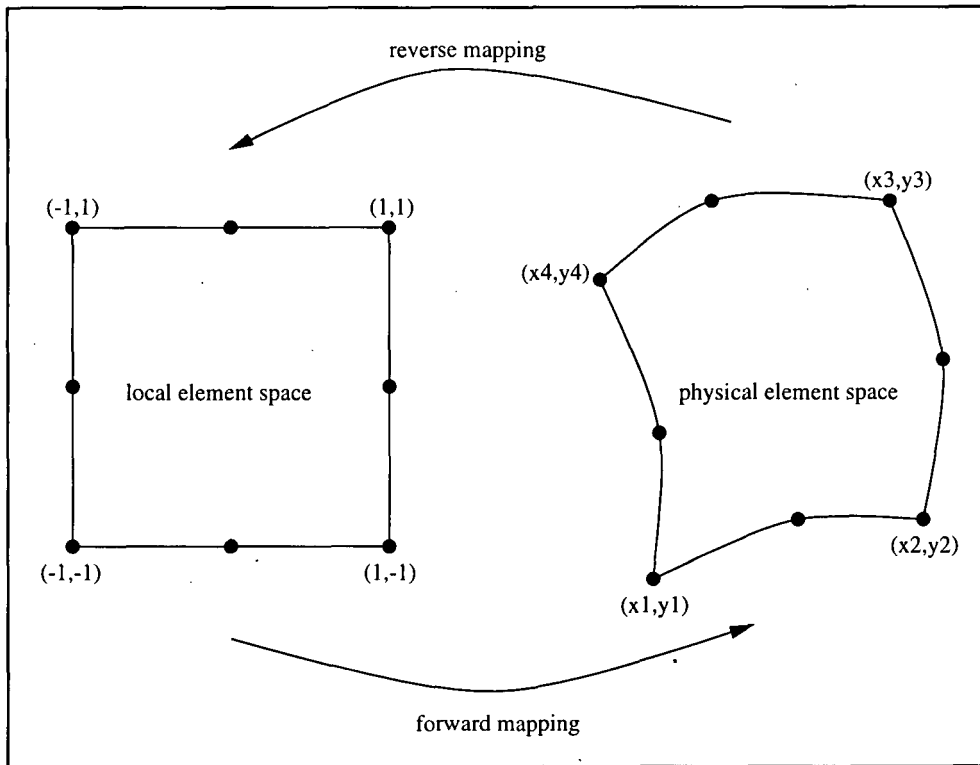


Figure 3.5 - 3D elements

### Element Types

To categorise elements it is best to consider the shape function, element order, and integration rule. These terms will be discussed in detail in the following paragraphs.

For isoparametric elements, the shape function defines the mapping between the physical element and the local element coordinate space (as illustrated in Fig. 3.6). This local element space is chosen to simplify element integration and is only used internally during the assembly phase of the solution. It is through the use of these shape functions that the user is able to model virtually any shape desired by "distorting" the elements to conform to the physical model shape. However, there is a limit to the amount of distortion that can be achieved by these elements (or more accurately, the shape functions). A good measure of the element "distortion" is the so called "Jacobian" which is defined as the point-by-point area ratio between the physical element and the local element (actually the Jacobian is defined as the mapping itself and the area ratio is in fact the determinant of the Jacobian operator). If the element "distortion" is not excessive then the Jacobian will be non-zero everywhere in the element space.



**Figure 3.6 - Element spaces**

Additionally, for consistency, it is typically required that the Jacobian be the same sign for every element which insures consistent element orientation. Fig. 3.7 shows an example of a highly distorted element. The placement of the upper right corner node is such that the resulting mapping is "folded". The plotted contours shows the distribution of the Jacobian over the element which in fact changes sign along the "fold". This region along the "fold" is an area where the mapping is not invertible (i.e. the Jacobian is zero or ill-conditioned). The general "rule of thumb" is to not allow the interior angle of any corner nodes to exceed 135 degrees. It is also a requirement that the node number ordering be the same for all elements and the usual convention is to define the element node numbers counterclockwise around all elements. If an element is excessively distorted then it must be divided into smaller elements such that the resulting elements have less distortion.

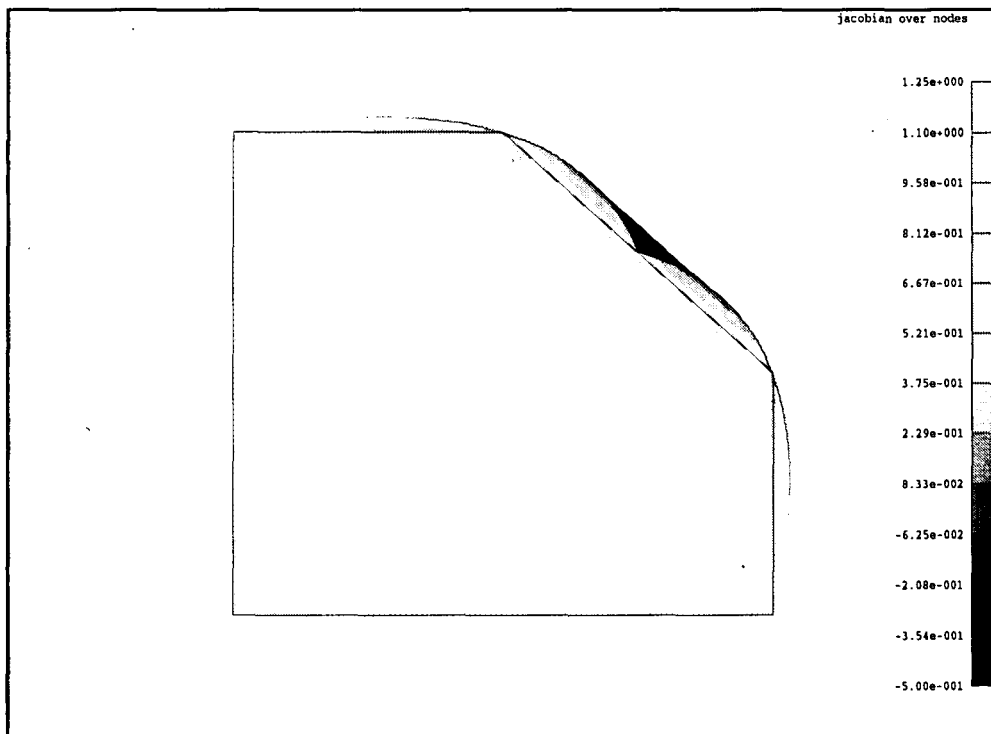


Figure 3.7 - Jacobian distribution of a malformed element

Any collection of functions can potentially be used as shape functions. However, to satisfy the solution requirements these chosen functions must be smooth (to satisfy continuity), accurate (the functions must form a complete basis), and convenient (numerically tractable). Polynomials have been found to effectively satisfy these conditions. The user is typically given only the choice of order for the polynomials. Linear shape functions refer to first order polynomials, quadratic shape functions refer to second order, cubic to third order, etc. Within any particular model the same order shape functions must be utilised throughout unless special transition elements are used (which are not necessarily available in all finite element programs).

Different element shapes are typically available which include triangles and rectangles (quadrilaterals) for two dimensional problems (see Fig. 3.4) and tetrahedrals, wedges, and bricks for three dimensional problems (see Fig. 3.5). Different element shapes may be combined in a model freely (as long as shape function order is consistent). However, standard practice is to use rectangular (for two dimensional problems) and bricks (for three dimensional problems) whenever possible. Additionally, second order (quadratic) shape functions are used with a particular preference for the "Serendipity" based family of shape functions (the eight node quadrilateral for two dimensional problems and the twenty node brick for three dimensional problems). Preference is given to these elements because of computational efficiency and modelling convenience (no interior nodes). However, there is a possible stability problem with these elements when used with particular integration rules (as discussed in the next section).

### Integration Rule

During the assembly phase of the finite element solution, element contributions are computed by integrating over the element. For two dimensional problems, for example, the integration over the element,  $\Omega_e$ , is of the form,

$$\int_{\Omega_e} g(x,y) dx dy \quad (3.1)$$

where the form of the function,  $g(x,y)$ , is determined by the shape function.

For relatively simple functions it would be possible to determine a closed form solution to the integral, however, in general practice numerical integration methods are employed. In fact, it can be shown that, for the class of shape functions discussed, numerical integration utilising the Gaussian quadrature formula can result in an exact integration for very little computational effort. The quadrature formula for the above integral is stated as,

$$\int_{\Omega} g(x,y) dx dy = \sum_{i=1}^{N_i} g(x_i, y_i) \cdot w_i \quad (3.2)$$

where the number of integration points,  $N_i$ , the location of the integration points,  $x_i, y_i$ , and the quadrature weights,  $w_i$ , define the integration rule. Integration rules have been tabulated for use with various element types. In general, it is necessary to choose an integration rule such that the element is fully integrated (i.e. the resulting integration is exact), however, there may be some advantages to under integrating (e.g. reducing computational requirements). A good example of an under integrated element is the eight node quadrilateral used in two dimensional structural problems. This element is typically used with a two-by-two Gaussian quadrature rule (four integration points). This results in a slightly under integrated element, but is very efficient computationally with very little effect in accuracy compared to the higher order nine noded element. A consequence of this under integration is that this element contains an extra "zero energy mode". Zero energy modes are non-trivial solutions that result in no work. An example of a zero energy mode is rigid body translation. Rigid body translations (and rotations) are preventable through proper application of displacement boundary conditions. However, extra or "spurious" zero energy modes may not be so easily considered. Fig. 3.8 shows the zero energy modes for the eight node quadrilateral with four integration points. As it happens the extra mode contained in this element is non-communicable. This means that connected elements do not "communicate" or pass on this spurious mode to adjoining elements.

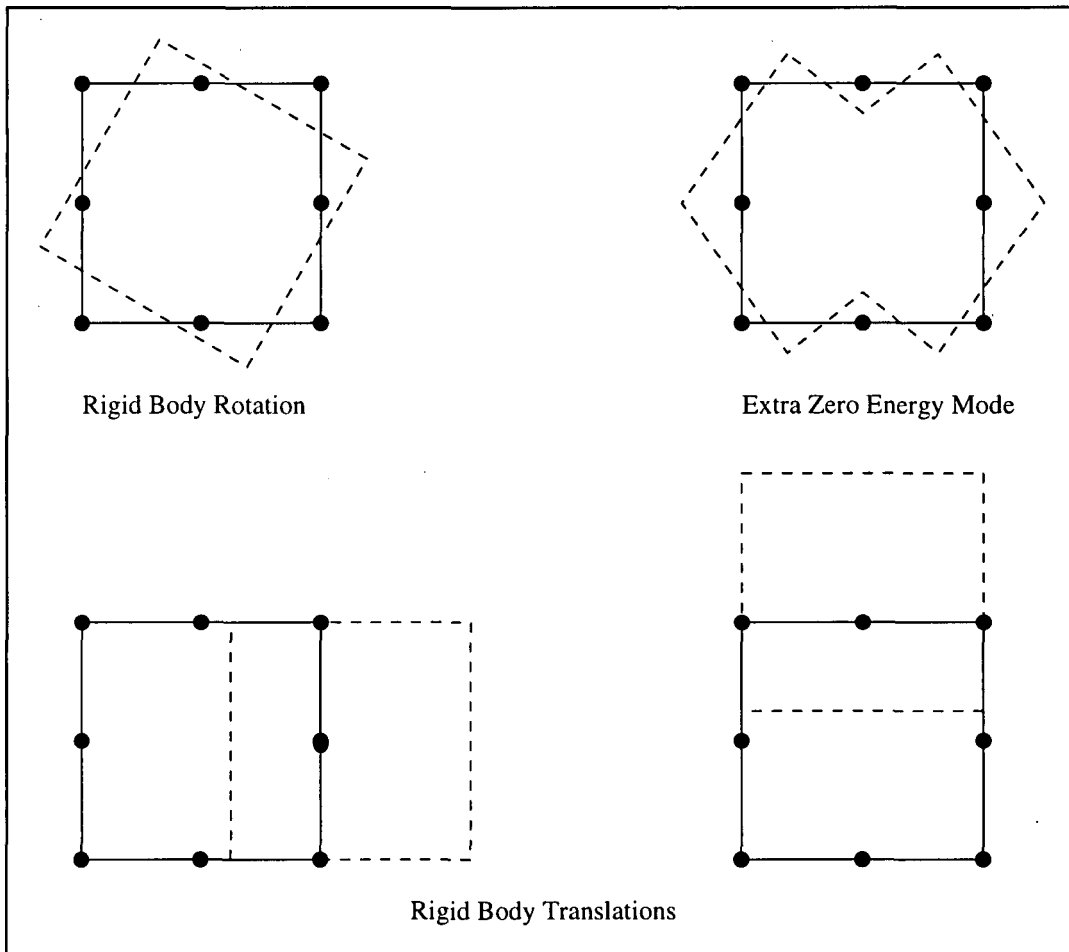


Figure 3.8 - Zero energy modes for the 8-node quadrilateral

### Reformulated Elements

Incompressibility or near-incompressibility requires special treatment. Most finite element codes, used in the structural analysis of solid propellants, have "reformulated" element types that allow the extra constraint implied by incompressibility to be modelled. Even near-incompressibility is modelled more accurately by the reformulated elements. It can be shown that as the Poisson's ratio (referring to a Hookean material) approaches 0.5 the bulk response becomes dominant. In fact, for a Poisson's ratio equal to 0.5 the bulk modulus becomes infinite and in this limiting case the solution is numerically intractable. For this situation reformulated elements - elements that use a material formulation with an additional degree of freedom - may be used. This degree of freedom is essentially the volume change for the element which controls bulk behaviour (compressibility). For these reformulated elements the bulk behaviour is treated separately from the shear behaviour and the volume change becomes an additional unknown which is either solved for (for nearly incompressible materials) or constrained (for incompressible materials). It is recommended that for elements using linear elastic (Hookean) material behaviour with a Poisson's ratio greater than 0.45 that the above mentioned reformulated elements are used.

### Refinement

Most structural analyses require an iterative approach to provide accurate results. In the first instance a coarse model might be considered with subsequent refinements to the model being made as a better understanding of the critical regions emerges. Many approaches have been utilised by analysts to model refined regions. Typically, only the critical regions are remeshed, leaving the rest of the model coarse (preferably without altering nodal locations). Critical regions are identified by noting where the solution (displacement) or any combination of solution derivatives (such as stress or strain) varies significantly in

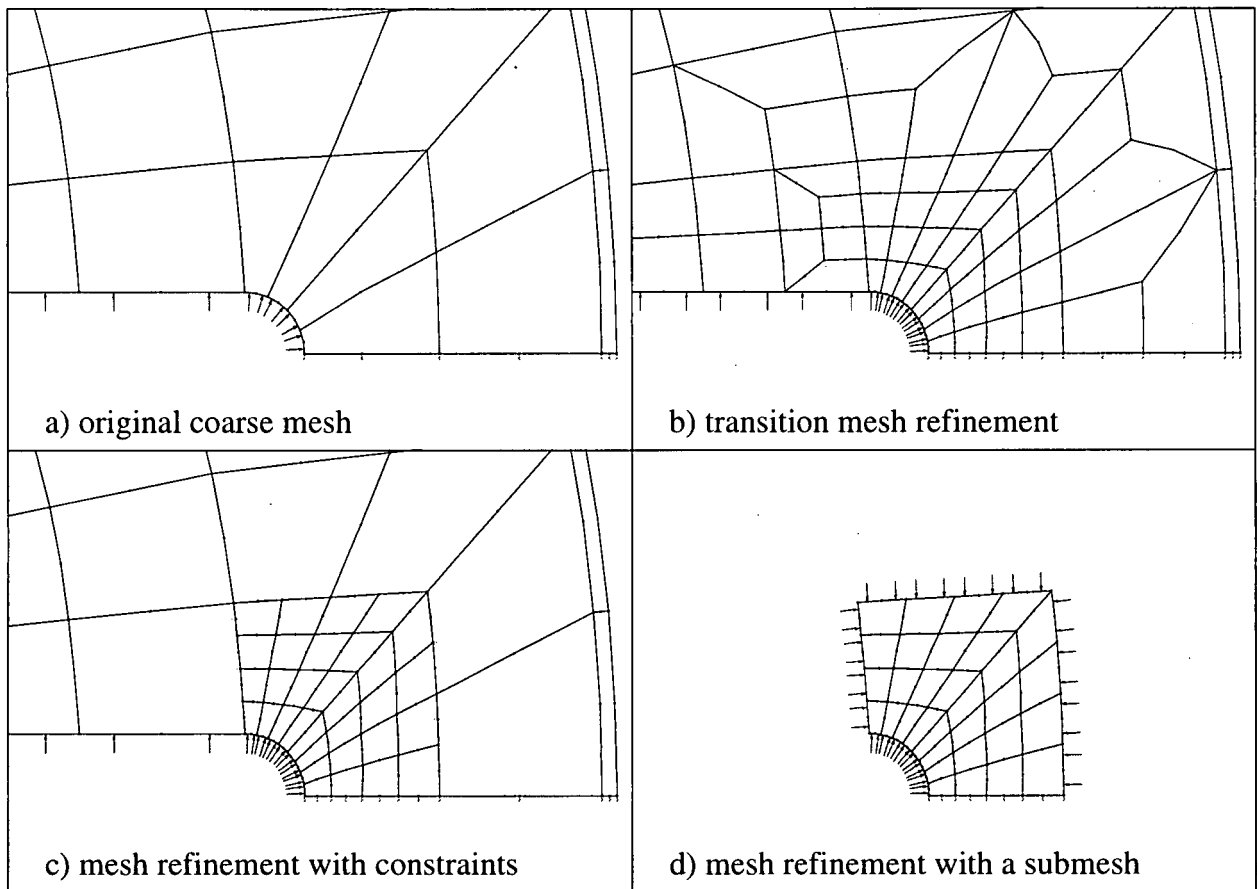


Figure 3.9 - Mesh refinement approaches

a localised area. These are typically areas of high stress or strain concentration. Common approaches to mesh refinement include use of transition elements (to join a coarse mesh to a fine mesh), "multipoint" constraints (linking degrees of freedom), and separate modelling of the refined region with boundary conditions applied to simulate the rest of the model. Each approach has its advantages and disadvantages. An example of the use of transition elements is shown in Fig. 3.9b. This approach has the advantage of ease of modelling without significant remeshing or alteration of the surrounding mesh. It has the disadvantages of requiring a transition region and not making use of previously computed results. The "multipoint" constraint approach (shown in Fig. 3.9c) has the same advantages without requiring a transition region. However, again previously computed results are not utilised. Finally, a separate model can be created for the critical region only. Boundary conditions would be applied to this model that would simulate the stress field computed in the previous analysis. This method has the advantage of making use of previously computed results, but has the disadvantage of being more difficult to model (unless the finite element code has this capability).

### 3.2.2.2 Boundary condition application

For a model to represent a well posed boundary value problem sufficient boundary conditions must be applied to prevent the introduction of any zero energy modes. Additional boundary conditions must also be applied to reflect the actual loading conditions (which clearly must exist for there to be a nontrivial problem).

#### Boundary Condition Types

There are basically two distinct categories of boundary conditions, constraints (displacements, temperatures, etc) and loads (forces, fluxes, etc). Constraint type boundary conditions can be thought of as boundary conditions that reduce the total number of degrees of freedom in the problem. Effectively, they modify the left hand side of the system of equations, the solution vector, by replacing unknowns with known quantities and are used to prevent zero energy modes. An example of this type of boundary condition is the displacement boundary condition which is used to prevent rigid body motion (i.e. a zero energy mode). Loads can be thought of as modifications to the right hand side of the system of

equations, in other words, a forcing function. Additionally, both constraints and loads may be applied at nodes or distributed along element faces or sides. Nodal boundary conditions directly modify the specified global degree of freedom whereas distributed boundary conditions are integrated over the element face or side and typically are applied with reference to the elements local coordinate system. An example of a nodal boundary condition would be a point force where a force value is assigned to a specific node in a specific global direction. An example of a distributed boundary condition would be a pressure applied normal to a specific element face (or side).

### 3.3 MATERIAL DEFINITION

List of symbols used in this section:

- $E$  - Young's modulus of elasticity
- $\sigma$  - stress
- $\epsilon$  - strain
- $t$  - real time
- $\xi$  - reduced time
- $a_T$  - time-temperature shift factor
- $T$  - temperature
- $T_o$  - reference temperature
- $E(t)$  - Relaxation Modulus
- $\sigma(t)$  - stress history
- $\epsilon(t)$  - strain history

A major challenge posed to the structural analyst of solid propellant grains is how to model the material behaviour. The materials typically found in solid rocket motors exhibit complex behaviour under even simple loading conditions. This complex material behaviour, under various loading conditions, has yet to be completely mathematically described by any one material constitutive law (the mathematical description of the material behaviour). Therefore, choice of a material constitutive law is highly dependent on loading conditions (and possible loading history).

#### 3.3.1 Constitutive Laws

Material constitutive laws, for problems in structural mechanics, define the relationship between stress and strain. In other words, for a given strain level the material constitutive law will return the corresponding stress. Also, it is important to adopt the correct strain-displacement relationship since any assumptions made in this respect will effect the stress-strain relationship.

##### 3.3.1.1 Linear Elastic (Hookean Material Law)

The simplest material law is a linear relationship, where the material law is simply a set of constants. This material law is known as Hooke's law and can be expressed mathematically as,

$$\sigma = E \epsilon \quad (3.3)$$

where  $E$  is a tensor quantity defining the material constitutive law and consists of a set of material stiffnesses typically determined empirically through material testing. A complete specification for an anisotropic material (no planes of material symmetry) would require 21 constants (actually the stiffness tensor  $E$  contains 36 entries but is always symmetric about the diagonal and therefore only 21 are independent). Section 3.8.1 defines the relationships between the material stiffness and the engineering material constants for plane and axisymmetric problems.

Some consequences of linearity are that the following principles apply,

1) Superposition:

$$\sigma(\boldsymbol{\varepsilon}_1 + \boldsymbol{\varepsilon}_2) = \sigma(\boldsymbol{\varepsilon}_1) + \sigma(\boldsymbol{\varepsilon}_2) \quad (3.4)$$

2) Homogeneity:

$$\sigma(\beta \boldsymbol{\varepsilon}) = \beta \sigma(\boldsymbol{\varepsilon}) \quad (\beta = \text{constant}) \quad (3.5)$$

where  $\boldsymbol{\varepsilon}_1$  and  $\boldsymbol{\varepsilon}_2$  are two different strains.

Metallic rocket motor cases and other metallic components are typically modeled assuming linear elastic material behaviour.

### 3.3.1.2 Non-linear Elastic

If the stress-strain relationship does not vary linearly and does not exhibit any hysteresis (energy loss) then the material is said to be nonlinearly elastic. An example of a material law falling into this category is a simple hyperelastic constitutive law typically used to model rubber materials. Some commonly used material constitutive laws are those due to Mooney-Rivlin and Ogden as discussed in section 3.8.2. Nonlinear elastic laws can be used to model unfilled rubber such as the insulation or inhibitor materials.

### 3.3.1.3 Linear Viscoelastic

Some materials, like solid propellants, that exhibit time dependent behaviour are treated as simple viscoelastic materials. Furthermore, if the principles of superposition and homogeneity apply then the material behaviour is linear.

For a simple, nonaging, linear viscoelastic material the stress is related to an arbitrary strain history through a convolution integral of the form,

$$\sigma = \int_0^t E(t - \tau) \frac{d\boldsymbol{\varepsilon}}{d\tau} d\tau \quad (3.6)$$

where  $E(t)$  is the relaxation modulus which is typically obtained from constant strain level tests (see chapter 4.)

For nonisothermal behaviour (temperature dependent) it is common to assume that the material is described by a thermorheologically simple model. That is, the temperature dependence may be separated from the time dependence through the use of a time-temperature shift and the substitution of a so called "reduced time" for real time in the convolution integral. The above integral then becomes what is generally known as the Boltzmann superposition integral,

$$\sigma = \int_0^{\xi} E(\xi - \bar{\xi}) \frac{d\boldsymbol{\varepsilon}}{d\bar{\xi}} d\bar{\xi} \quad (3.7)$$

where, for an isothermal loading,  $\xi = t/a_T$  is the reduced time and  $a_T$  is a time-temperature shift factor (obtained from experimental data) which is a function of temperature. For a nonisothermal loading history (temperature varies with time) the reduced time is typically calculated using the relationship postulated by Moreland-Lee,

$$\xi = \int_0^t (1/a_T) dt \quad (3.8)$$

To obtain a complete set of relaxation modulus data a series of constant strain level tests are carried out for temperatures within the required operating temperature range for the motor. Relaxation modulus curves are obtained from each test and translated into a single master relaxation modulus curve. The individual shifted values, recorded as a function of temperature, define the shift factor curve. This time-temperature shift data is frequently modelled using the Williams-Landel-Ferry (WLF) function as follows,

$$\log a_T = \frac{-C_1(T - T_o)}{(C_2 + T - T_o)} \quad (3.9)$$

where  $T_o$  is the reference temperature (i.e. the temperature where  $a_T = 1$ ). For detailed information on the characterisation and material data reduction for viscoelastic materials see chapter 4.

If viscoelasticity is not an available material option in the selected finite element code then an effective modulus, which represents the time dependent viscoelastic behaviour in some approximate sense, may be used with an elastic material law. This effective modulus is calculated using the Boltzmann superposition integral (shown above) for a simple uniaxial strain history. This approach assumes that the strains throughout the region modeled with the effective modulus value are proportional to the simple strain history used. The procedure is to calculate a stress history from the strain history thereby giving an effective modulus as,

$$E_{eff}(t) = \sigma(t)/\epsilon(t) \quad (3.10)$$

which is the instantaneous secant modulus at time  $t$ . A detailed discussion of a recommended procedure for calculating stress response and effective moduli from an arbitrary strain history is given in section 3.7.1.

#### 3.3.1.4 Non-linear Viscoelastic

It is beyond the scope of this chapter to cover all the various nonlinear theories which have been developed to describe solid propellant material behaviour. However, some documents [6,7,8] are readily available that cover, in depth, many of the emerging theories and indicate where they may be applicable. Some discussion on common issues and a brief introduction to some nonlinear models follows.

The most obvious source of nonlinearity in solid propellants or polymers arises from the material's dependence on external factors such as strain, strain rate and temperature. Other nonlinearities due to geometric effects like large rotations or load-deformation interaction also contribute to nonlinear behaviour. Geometric effects are accounted for through strain-displacement relationships which keep higher order rotational terms. Nonlinearity due to the dependence of a load's direction and magnitude on the structure's response to the load can be dealt with using finite element solution algorithms. This section will focus on some of the nonlinear constitutive theories implemented in finite element codes for the analysis of propellant materials. Most of these theories handle material nonlinearities by including terms in the linear viscoelastic constitutive equation to give observed behaviour.

It has been shown that a coupling effect exists when a propellant is simultaneously strained and cooled [9,10]. As a result, linear viscoelastic stress-strain results underpredict observed data. This type of nonlinearity was treated by Lee [9] using a modified modulus approach. Another method of treating straining-cooling coupling was proposed by Cost [11]. Other than a modified definition of reduced time,

Cost's constitutive model has the same form as that for linear viscoelasticity.

Nonlinearities caused by variations in strain rate whether caused by changes in temperature or imposed boundary conditions were studied by Swanson in 1980. In 1983, Swanson developed another constitutive model [12] using the Green-Lagrange definition of strain. Green strains differ from the small strain relationships in so far as the Green strains retain second order derivatives of displacement. This permits rotational geometric nonlinearities to be taken into account. In addition, a strain dependant softening function and a strain rate function was used which took into account the evolution of damage and changes in dilatation (see, for example, Schapery models referenced below).

Solid propellant constitutive theories either currently in use or of interest include the following.

Lee model for coupled thermomechanical effects [9]

Cost model for combined straining and cooling [11]

Farris model with time-independent bulk response and time-dependant deviatoric response [6]

Swanson and Christensen model [12]

Simo model with uncoupled volumetric and deviatoric response [13]

Özüpek model for cyclic loading [14]

Schapery models for deformation and fracture behaviour of particulate composites [15,16,17,18]

Park adaptation of Schapery model for solid propellants [19]

### 3.3.1.5 Material Model Stability

Realistic analyses of solid rocket motors require material models which are not only accurate but also stable. When performing a finite element analysis, stability is determined by the material tangent stiffness matrix. This matrix characterises the incremental relation between stress and strain, and is typically positive definite, i.e. it has only positive eigenvalues. As long as the matrix stays positive definite the material model is stable. Loss of stability of the model occurs when an eigenvalue of the matrix changes sign. As a result of this computations may fail to converge.

Material model generation, i.e. determination of material constants and functions by fitting the model to test data, should be followed by the determination of the range of deformations for which the model is stable and hence useful for finite element calculations. For hyperelastic materials, a criterion has been established to check the stability of the selected models. For nonlinear viscoelastic materials, however, there is no corresponding criterion available.

### 3.3.2 Case Materials

List of symbols used in this section:

$E_1, E_2$  - principal moduli in fibre and transverse directions

$\nu_{12}, \nu_{23}$  - in-plane and out-plane Poisson's ratios

$G_{12}$  - in-plane shear modulus

The case of a solid rocket motor can, depending on the geometry and loading conditions, greatly influence the propellant grain structural integrity. It may be possible to model the case through appropriate boundary conditions, however, greater accuracy (correspondence to actual motor conditions) can be expected if the case is modeled. This is especially true for composite (e.g. filament wound) cases.

#### 3.3.2.1 Metal Properties

For most applications, isotropic material properties are obtained from standard engineering references. If unusual environments require specialised properties then specific testing may be required.

### 3.3.2.2 Composite Case Properties

There are certain complexities associated with material property definition of composite filament wound cases. A typical composite case "layup" consists of several layers of a fibre and matrix (the binder material) either wound or applied as a prefabricated part (probably separately wound). Each layer will have a natural principal direction aligned with the fibre (the primary load carrying direction) with material isotropy only in the transverse plane (the plane perpendicular to the fibre direction). Therefore, it is necessary to treat each layer as a transversely isotropic material (which, in reality, is a simplification). The material properties typically used to define a transverse isotropic lamina (single layer or ply) are the two principal moduli ( $E_1, E_2$ ), the in-plane and out-plane Poisson's ratios ( $\nu_{12}, \nu_{23}$ ) and the in-plane shear modulus ( $G_{12}$ ). These material properties are found either from uniaxial tests of the lamina loaded in the fibre direction and transverse to the fibre direction or from a micromechanics approach [20,21]. The micromechanics approach derives lamina (or composite) properties from the constituent properties (the material properties of the fibre and matrix separately). This approach is typically used when lamina properties are not available (as fibre and matrix properties can be readily obtained from the manufacturer).

Once lamina properties are determined then, depending on the detail required in the case model, laminate properties must be calculated. For filament wound cases the fibre angle changes with radial position, and in fact changes continuously along dome contours. Effectively this requires a material definition that varies as a function of position. Common practice, for use in codes that cannot explicitly handle position dependent material properties, is to pre-calculate the material properties for each finite element along the case contour. Additionally, if more than one lamina is included within each element, the material properties are averaged through the element in the direction normal to the case contour.

### 3.3.3 Insulation/Inhibitor (Rubber/Polymeric) Materials

When it is necessary to separately model the insulation (and/or inhibitor) then depending on the required accuracy and solution procedure either a hyperelastic rubber material law is used, requiring nonlinear material characterisation, or elastic material properties are used. Additionally, the use of a hyperelastic material law implies large deformations and therefore requires use of a non-linear solution procedure. The required material characterisation tests needed to determine the hyperelastic parameters can be significant and will include the need to perform at least some biaxial tests. The recorded stress/strain (load/displacement) data will then need to be represented as strain energy density plotted against the strain invariants (for use with the Mooney-Rivlin model, for example) or as stress versus the principal stretches (used in the Ogden model). This data will in turn be used to characterise the chosen material model (see section 3.8.2.5 for example problems).

### 3.3.4 Propellant Grain

The constitutive model for the propellant grain can be considered in a variety of forms. The simple approach, and one which leads to the most rapid solution, is to use the effective modulus representation (see section 3.7.1). For a time-varying solution, a linear viscoelastic material definition can be used. This type of model requires the least amount of time and temperature-dependant input data. For more accurate predictions, a nonlinear viscoelastic material definition may be used. However, adopting a nonlinear viscoelastic model may require a significant amount of characterisation testing.

If the propellant grain material is modeled using some appropriate viscoelastic model then the relaxation modulus data will be required in a form suitable for input to the chosen structural analysis code. Usually the input takes the form of fitted curves to the master relaxation data and the time-temperature shift data (usually the WLF representation as given in Equation 3.9). Frequently the relaxation modulus is represented by a Prony series. A Prony series fit to the modulus data can easily be obtained by determining an appropriate set of coefficients which are based on the following expression and illustration (Fig 3.10).

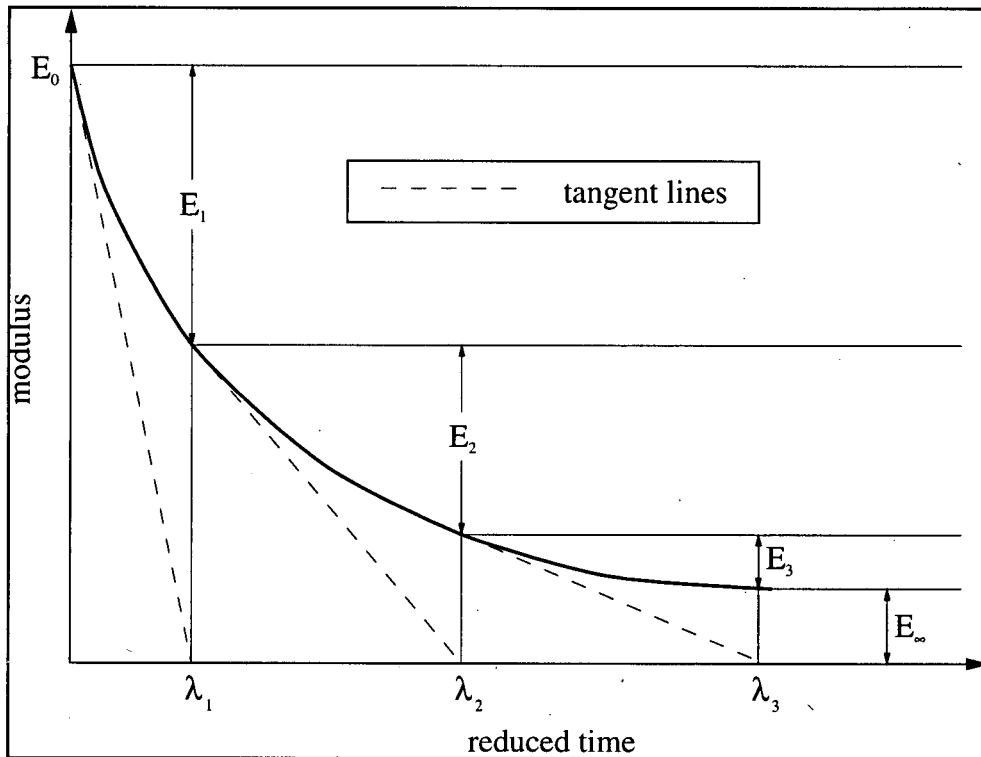


Figure 3.10 - Illustration of Prony series terms for modulus representation

$$E(\xi) = E_{\infty} + \sum_{i=1}^n E_i \cdot \exp\left(-\frac{\xi}{\lambda_i}\right) \quad (3.11)$$

where  $E_{\infty}$  is the equilibrium modulus,  $E_i$  are the relaxation coefficients, and  $\lambda_i$  are the relaxation times (in the form of reduced time, e.g.  $\lambda_i = t/a_T$  for isothermal loading).

For material models that separately treat the bulk behaviour and allow for compressibility some definition of the propellant dilatational behaviour is required. The representation of this data is highly dependant on the model used, but in general some material testing will be required to measure volume change for both compressive and tensile loading conditions.

### 3.4 LOAD DEFINITION

Implementation of the actual loading conditions into the finite element model requires additional assumptions. For example, it is often necessary to assume that the dynamics of the actual loading condition are negligible compared to the magnitude of the static loading. Also, complexities arise when attempting to model combined loading conditions. For example, a combined thermal cooldown and ignition pressurisation is a loading condition that typically must be considered. The following sections discuss some common practices used for various loading conditions.

#### 3.4.1 Ignition Pressurisation

The load induced by rapid pressurisation due to ignition of a solid propellant grain is typically modeled as a static load. This static load is taken as the initial maximum pressure obtained either through an internal ballistics prediction or from data collected from a static firing. Common practice is to include an initial stress state in the grain model to account for any prior grain loading history (e.g. thermal cooldown).

A potential complexity arises for motors with large length to diameter ratios. For these motors it is important to consider the pressure drop that occurs down the length of the grain. This pressure drop can induce a deformation in the propellant grain that causes a change in the motor ballistics. This change in ballistics results in a change in the pressure drop which can lead to an unstable condition commonly referred to as structural/ballistic interaction. Recent studies have attributed structural/ballistic interaction to several failures of both large solid rocket boosters as well as for tactical rocket motors.

#### **3.4.2 Thermally Induced Loads**

A critical loading condition (especially for end bonded grains) is the load induced by a cooldown from the propellant cure temperature. A thermal strain, for an unconstrained sample, may be computed simply as the thermal coefficient of linear expansion (TCLE) multiplied by the temperature change from a reference temperature (typically the "stress-free temperature"). If the actual material is unconstrained then no stress is induced, however, for case bonded systems the propellant grain may be highly constrained and therefore a potentially significant stress can develop at the case/grain interfaces. Additionally, solid rocket motors may experience thermal cycling during the service life of the motor. This thermal cycling can also produce significant bondline stresses. For thermally cycled motors it is important to consider the viscoelastic behaviour of the propellant material (i.e. use of a viscoelastic material model, for the propellant, is highly recommended).

An important parameter required for calculating the thermally induced loads is the reference temperature. Typically, a propellant stress-free (or strain-free) temperature for the grain is assumed as the reference temperature and is used throughout the grain model. However, in reality the stress-free (or strain-free) temperature may not be constant throughout the propellant grain. Typically the choice between using a stress-free or strain-free temperature is governed by the type of failure criteria used. Given a lack of an experimentally determined stress/strain-free temperature the grain cure temperature is usually assumed. It should be noted that in reality the stress-free and strain-free temperatures do not necessarily coincide.

#### **3.4.3 Acceleration**

The load induced by axial acceleration during launch may also be considered. This load is not usually found to be the critical loading condition since significant grain burnback can occur before any critical load, due to acceleration, can be reached. However, it is important to include the acceleration load when the complete propellant grain structural integrity needs to be analysed (e.g. for failure analysis or risk assessment).

#### **3.4.4 Vibration**

In some systems where significant transportation loads are expected, an analysis of the effect of vibration on the solid propellant grain structure may be appropriate. Additionally, vibration due to air carry can be significant and must be considered.

#### **3.4.5 Slump (Storage)**

For long term storage it is important to consider the effect of propellant "slump". For large rocket motors this loading condition can be critical especially if the motor is stored horizontally. It may also be important to consider the long time (low rate) creep behaviour of the propellant material.

#### **3.4.6 Air Carry Reaction Loads**

For air launch missile systems loads induced into the missile propulsion system can be significant due to possible high transverse accelerations.

#### **3.4.7 Aerodynamic Heating**

For tactical systems, heating of the external surface can cause an extreme thermal differential thus inducing a significant load on the bondline of the system (for case bonded systems).

#### **3.4.8 Combined Loads**

To accurately reflect true loading conditions or to model worst case scenarios it is often necessary to include the effects of combined loads. A common approach used to model combined loads is to sum

the results from the analysis of each separate load condition. For example, a combined thermal cooldown and ignition pressurisation can be analysed by first computing the stresses and strains induced by the thermal cooldown and ignition pressurisation separately using effective moduli appropriate to the separate loading conditions. The results obtained from these two analyses may then be superposed to obtain the stresses and strains for the combined loading condition. This approach produces valid numerical values only when linear elastic (or viscoelastic) material behaviour is assumed (i.e. the principle of superposition applies). Note that it is not valid to sum the results of analyses that were modelled with any material nonlinearities. To analyse a combined loading condition with a nonlinear material law it is required that a material constitutive law be chosen that contains appropriate terms to handle the multiple loads.

### **3.5 SOLUTION PROCEDURE**

The following paragraphs discuss implied assumptions (and the consequences) and any special considerations required to utilise various solution procedures.

#### **3.5.1 Linear (small displacement)**

If the solution to a particular problem is known to not contain any significant displacements (including rotation) then a simple linear solution procedure may be used. Basically, the implied assumption is that the maximum displacement at any node is sufficiently small so that the second order terms in the strain-displacement equations may be ignored. It should be noted that large displacements can occur without incurring large (finite) strains. For example, the rotating beam and simple cantilever problems, discussed in section 3.8.2.6, illustrate possible large sources of error if the linear solution is used incorrectly. For most practical problems localised large displacements (and rotations) may not be so readily identifiable. If, for example, a solid rocket motor design contains an unbonded flap it is possible that large localised rotations can occur, especially around the flap termination. This would result in artificially high stresses being calculated in a critical region of the rocket motor grain. However, the deformations may not appear to be inaccurate leading the analyst to believe the stress values are valid.

#### **3.5.2 Non-linear (large displacement)**

If the solution is believed to contain large displacements (irrespective of the expected strains) then a nonlinear solution procedure should be used. A nonlinear solution procedure iterates on the solution (starting, in fact, with the linear solution) until either the maximum residual displacement (the change in displacement between iterations) or the maximum residual force (the difference between the applied nodal load and the calculated reactive load) fall below set convergence criteria. Usually one or both of these tolerances may be specified. In some problems convergence to a solution may be slow (requires many iterations) whilst for other problems the solution may fail to converge. Convergence problems may occur for many different reasons, but a common solution is to increment the applied load in steps, iterating between steps to compute interim solutions. The simple cantilever beam problem discussed in section 3.8.2.6 illustrates an example of load stepping. Most finite element codes will handle load stepping internally, requiring only that the user specify the load increment (as a fraction of the total load). Additionally, most codes will also perform automatic load/time step control which will adjust the load increment to aid in convergence.

#### **3.5.3 Path Dependent**

For problems where the expected response is not only nonlinear but also unstable (i.e. the induced load and/or displacement may decrease with increasing external load/displacement application) a path dependent solution procedure may be required to converge on a solution. A popular choice, available in most commercial finite element codes, is the Modified Riks method [22].

### **3.6 RESULTS INTERPRETATION**

The post-processing of the solution to produce usable results requires consideration of the desired accuracy and possible failure modes (which may be dependent on location and material behaviour). Additionally, the solution may be used to determine possible geometric effects of loading or as a check for quality of the solution itself. It is also possible to utilise the solution from one analysis as input to

another. For example, a heat transfer analysis could be performed to calculate the temperature distribution which in turn could be used as an input for the structural analysis computations of the thermal strains (and associated stresses).

### 3.6.1 Accuracy

The accuracy of the computed results can depend greatly on the location within each element where the solution is evaluated. For the solution itself (e.g. displacements, temperature, etc.) the nodes are the natural choice for evaluation since the solution procedure is nodal based. To obtain solution values anywhere else within the element requires interpolation and hence introduces some inaccuracy (which is lessened through the use of higher order shape functions). For results derived from solution derivatives (e.g. stresses, strains, fluxes, etc.) the natural choice for evaluation are the points defined by the Gaussian quadrature rule associated with the order of the element shape function. These points lie in the interior of the element and, therefore, any results computed at the nodes tend to be the greatest in error. As an example, a structural analysis of a simple internally pressurised thick-walled cylinder modeled with nearly incompressible material resulted in the computed radial stresses shown in Fig. 3.11. These stresses were normalised using the known exact solution and plotted against the radial location. The nodes for the model are located at the grid lines. The stresses, obtained from the finite element solution, were found by interpolating within each element utilising the element shape functions. It can be readily seen that significant error occurs in elements near the bore of the cylinder at the element nodes. Even averaging the stresses at the element boundaries will still result in significant errors. However, as it turns out, the finite element solution is equal to the exact solution at precisely two locations within each element. These locations are in fact the Gaussian quadrature points. This example may be considered somewhat of an extreme, because of the nearly incompressible nature of the material, but for solid propellant rocket motor grains it is representative. It is possible to extrapolate results, computed at the Gaussian quadrature points, to the nodes for elements that use a quadratic or higher order shape function. In any case, it is advisable to check the finite element code documentation to fully understand how results are interpolated.

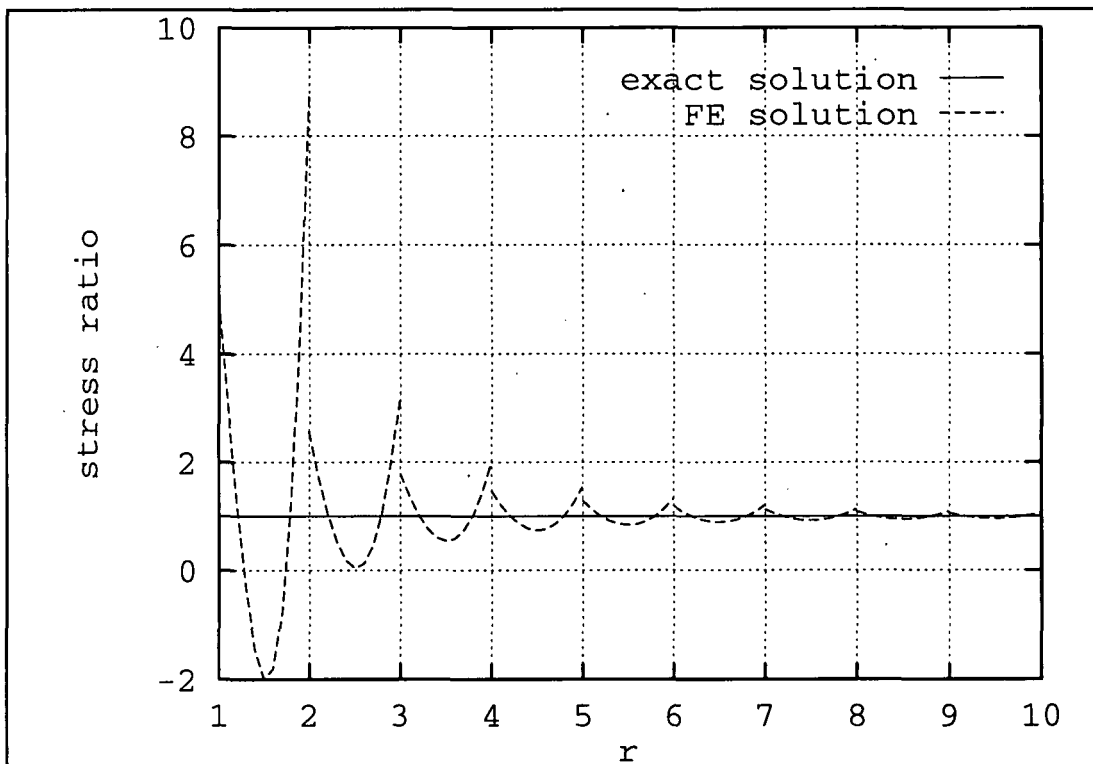


Figure 3.11 - Result comparison for internally pressurised cylinder

### 3.6.2 Solution Interpretation

Displaying the solution in a graphical form can offer some insight into the structure behaviour as well as to qualitatively check the solution validity. For a displacement solution an obvious way to display the solution is to plot the finite element mesh with the displacements applied to the nodal coordinates. Other kinds of solution values, such as temperatures, may be shown graphically as contours (e.g. isotherms).

### 3.6.3 Result Computations

List of symbols used in this section:

$\sigma_1, \sigma_2, \sigma_3$  - principal stress components

$\sigma_y$  - stress at yield

$\sigma_{eff}$  - von Mises stress

Results based on solution values or derivatives may also be calculated as a post-processing function. For example, stress and strain combinations may be computed from the solution derivatives. Typical stress and strain combinations used in the structural assessment of solid propellant rocket motors will be discussed in the following paragraphs. The stresses and strains referenced to the global reference frame were discussed previously.

#### 3.6.3.1 Principal Stress and Strain

Principal stresses and strains are components transformed such that the resulting values are a maximum and minimum normal value or a maximum shear value. These values are used in some failure theories or at least are the basis for other stress/strain combinations.

#### 3.6.3.2 Hydrostatic Stress

The average of the normal stress components is often referred to as the hydrostatic stress. This value is a measure of the equi-triaxial stress that a material undergoes and it is in fact a stress invariant (does not vary with coordinate transformation). It is a useful quantity for problems involving nearly hydrostatic loading conditions such as internal pressurisation of a solid rocket motor.

#### 3.6.3.3 Deviatoric Stress

This stress combination is simply the maximum principal stress with the hydrostatic stress removed. This stress combination is typically used in failure theories for solid propellants undergoing nearly hydrostatic loading.

#### 3.6.3.4 von Mises Stress

This stress combination is tied to the von Mises yield criterion which states that a material yields when the maximum distortional energy at the point in question reaches a critical value. This criterion can be illustrated as a stress yield surface (envelope) described by the following (in terms of the principal stresses),

$$\frac{1}{6}[(\sigma_1 - \sigma_2)^2 + (\sigma_2 - \sigma_3)^2 + (\sigma_3 - \sigma_1)^2] = \frac{1}{3}\sigma_y^2 \quad (3.12)$$

where  $\sigma_y$  is the stress at yield found from a simple uniaxial test.

The von Mises stress is defined simply as,

$$\sigma_{eff} = \sqrt{\frac{1}{2}[(\sigma_1 - \sigma_2)^2 + (\sigma_2 - \sigma_3)^2 + (\sigma_3 - \sigma_1)^2]} \quad (3.13)$$

### 3.6.4 Example Result Plots

The following figures show some example result plots. Fig. 3.12 shows a filled contour plot of the maximum principal strain with the deformed geometry superimposed for a simple axisymmetric geometry (pressure load applied internally along bore and end surfaces). Fig. 3.13 shows a vector plot of thermal flux indicating both direction and magnitude (vector colour).

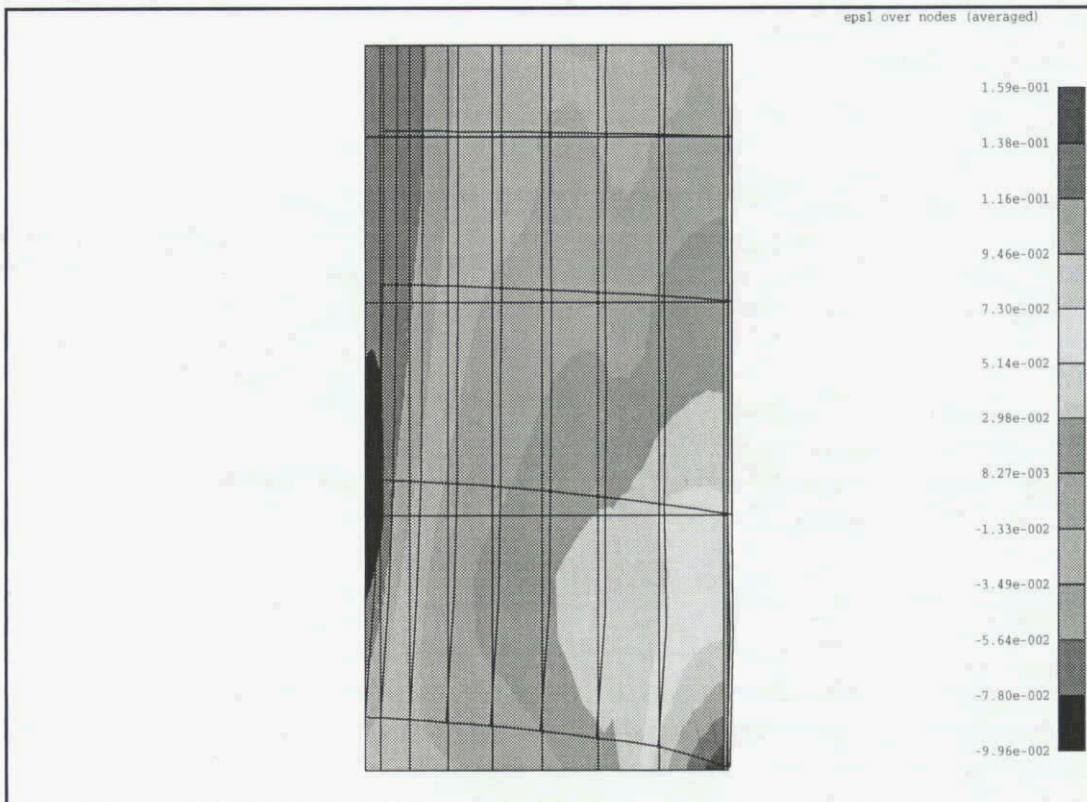


Figure 3.12 - Example filled contour with deformations

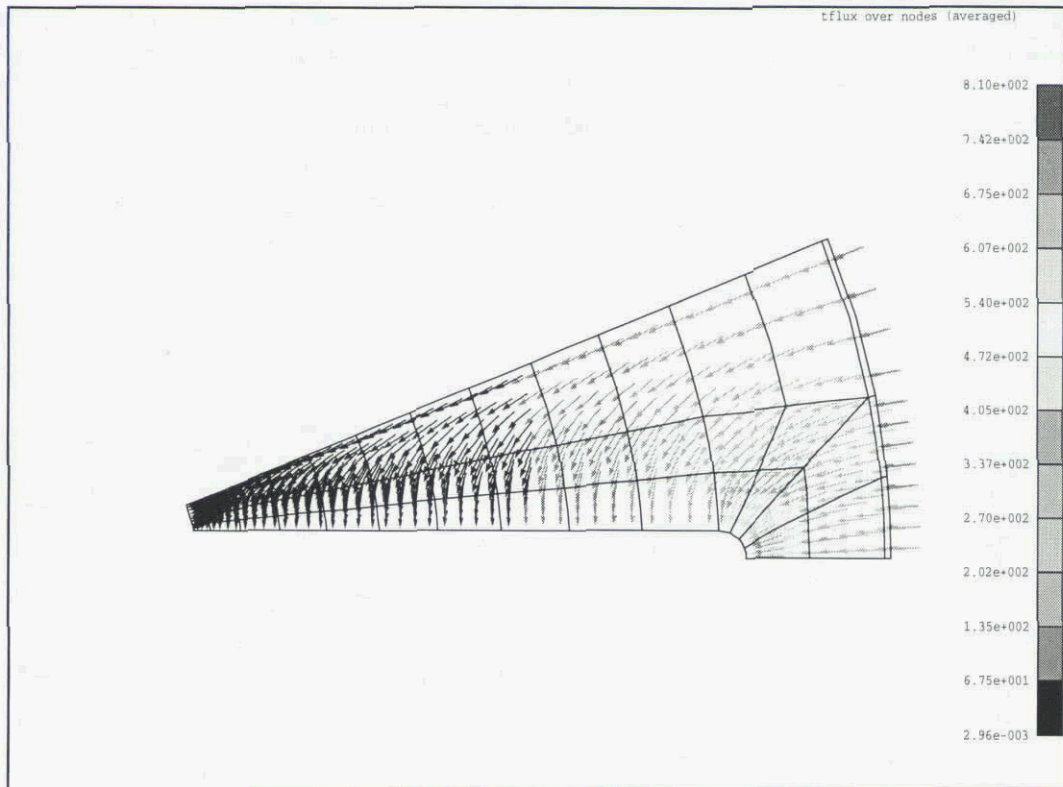


Figure 3.13 - Example vector plot

### 3.7 PRELIMINARY ANALYSES

During the preliminary or conceptual design phase for SRM propellant grains it may not be possible to perform a detailed structural analysis due to the lack of detailed data and the urgency of providing a solution. Preliminary structural analysis of an SRM propellant grain, including the case, can easily be performed by using simplified solutions. Assuming axisymmetry and given the field equations relating stress to strain and strain to displacements, the equations of equilibrium, and the compatibility conditions, with properly defined boundary conditions, closed form solutions may be derived for simple composite cylinders (case and grain). The GALCIT 101 report, "Fundamental Studies Relating to Systems Analysis of Solid Propellants" [23], gives complete derivations of closed form solutions for many possible problems involving simple cylindrical port grains with and without a case. For the analysis of more complicated geometries, such as slotted ports, some post-processing of the simple closed form solution may be used. For example, for slotted ports, a stress concentration factor may be applied to the closed form bore stresses to compute stresses at the slot tips [24].

Additionally, for a preliminary analysis it may be necessary to assume effective elastic material properties for the propellant grain. The next section describes an approach to calculating an effective modulus given an arbitrary strain history.

#### 3.7.1 Stress Response and Effective Modulus Calculation

Given an arbitrary strain history at a single point (either within a rocket motor or analogue) the viscoelastic stress response may be calculated using fairly simple calculations (requiring at most the computational power of a programmable calculator or small computer). Once the stress response is computed an effective modulus may then be calculated at any time in the loading history. This effective modulus may then be used as input to a linear elastic structural analysis of a full motor grain model to produce results throughout the grain at a single time instant. An example procedure is described in the following paragraphs.

##### 3.7.1.1 Basic Assumptions

To describe this procedure the basic assumptions used to develop this procedure are outlined below.

Assumption 1 - The propellant is a linear viscoelastic material and the problem to be solved involves no finite deformations. As a consequence, superposition (including time-temperature superposition) applies.

Assumption 2 - The Moreland-Lee hypothesis (Equation 3.8) applies.

Assumption 3 - The shift factor,  $a_T$ , can be represented in the following power law form,

$$a_T = w^{-m} \quad (3.14)$$

where

$$w = \frac{(T+C)}{(T_o+C)} \quad (3.15)$$

Assumption 4 - The relaxation modulus has one of the following two forms,

$$E_R = E_1 \left( \frac{t}{a_T} \right)^{n1} + E_\infty \quad (3.16)$$

or

$$E_R = E_1 \left( \frac{t}{a_T} \right)^{n1} + E_2 \left( \frac{t}{a_T} \right)^{n2} \quad (3.17)$$

For convenience, we refer to Equation 3.16 as the "modified power law" form and to Equation 3.17 as the "dual power law" form.

Assumption 5 - The temperature history may be closely approximated by

$$\frac{dT}{dt} = \frac{Rw^{-p}}{(1-p)} \quad (3.18)$$

in a piecewise-continuous fashion (i.e. R and p are constant over each interval). Note that the case of  $p=0$  corresponds to a simple linear temperature history.

Assumption 6 - The strain history is independent of the propellant modulus and is given by

$$\text{strain} = \text{mechanical strain} + \text{thermal strain} \quad (3.19)$$

and

$$\text{thermal strain} = K_\epsilon [(\alpha_p - \alpha_c)(T - T_s) + \alpha_c (T_c - T)] \quad (3.20)$$

where  $\alpha_p$  and  $\alpha_c$  are, respectively, the propellant and case thermal coefficients of linear expansion,  $T$  is the propellant temperature,  $T_s$  is the stress-free temperature, and  $T_c$  is the case temperature.

Assumption 7 - The strain history may be approximated by a piecewise linear function (or, equivalently, by a sum of linear ramp functions) in reduced time. The stress history is then obtained (from assumption

1) by superposition of the stress responses to the individual strain ramps.

### 3.7.1.2 Primary Relationships

From the assumptions stated above, we obtain a number of primary relationships which are used in the stress response and effective modulus calculation. These are discussed below.

Over a piecewise-continuous interval, the real time and the reduced time are related by

$$t = t_i + \left( \left( \frac{R \cdot (1-p+m)}{(1-p)(T+C)} \cdot \xi + w^{(1-p+m)} \right)^{\frac{(1-p)}{(1-p+m)}} - w_i^{(1-p)} \right) \left( \frac{T_o + C}{R} \right) \quad (3.21)$$

if the temperature is varying, and

$$t = t_i + \xi \cdot w^{-m} \quad (3.22)$$

if the temperature is constant.

At all times, the temperature is given by

$$T = w \cdot (T_o + C) - C \quad (3.23)$$

For a complex strain history composed of a finite number of piecewise linear segments, the strain  $\varepsilon$  and strain rate  $\dot{\varepsilon}$  are respectively given by

$$\varepsilon = \sum_{i=1}^n (\varepsilon(\xi))_i \cdot [\xi - (\xi_o)_i] \quad (3.24)$$

$$\dot{\varepsilon} = \sum_{i=1}^n (\dot{\varepsilon}(\xi))_i \quad (3.25)$$

while the stress  $\sigma_x$  is given by

$$\sigma_x = \sum_{i=1}^n (\sigma_x)_i \quad (3.26)$$

where  $(\xi_o)_{i+1} > (\xi_o)_i$  and  $n$  is the largest value of  $i$  such that  $\xi > (\xi_o)_i$ . For each linear ramp strain history component,

$$\sigma_{x_i} = [E_{\text{sec}} \cdot \varepsilon]_{x_i} \cdot K_\sigma = \left[ \int_{\xi_o_i}^{\xi} E_R \cdot \left( \frac{d\varepsilon_x}{d\xi} \right) d\xi \right] \cdot K_\sigma \quad (3.27)$$

For the assumed modulus functions, we get

$$\sigma_{x_i} = \left[ \left[ \dot{\varepsilon}_{x_i}(\xi) \right] \left[ E_1' \cdot (\xi - \xi_{o_i})^{n1'} + E_2' \cdot (\xi - \xi_{o_i})^{n2'} \right] + E_{\infty} \cdot \varepsilon_{x_i} \right] \cdot K_{\sigma} \quad (3.28)$$

where  $K_{\sigma}$  is a "geometry factor", which is obtained from a structural analysis model ( $K_{\sigma} = 1$  for a uniaxial load), and where

$$\varepsilon_{x_i} = \dot{\varepsilon}_{x_i}(\xi) \cdot (\xi - \xi_{o_i}) \quad (3.29)$$

and

$$E_1' = \frac{E_1}{n1'}, \quad n1' = 1+n1$$

$$E_2' = \frac{E_2}{n2'}, \quad n2' = 1+n2 \quad (3.30)$$

Note that in Equation 3.28 either  $E_2' = 0$  or  $E_{\infty} = 0$ , depending on which modulus representation is chosen.

Once the stress histories for each linear ramp strain history are found then the total stress history may be obtained by summing the ramp responses (Equation 3.26). With the calculated stress history and the strain history an effective modulus may be computed at any time within the loading history.

### 3.8 SELECTED MATERIAL MODEL EQUATIONS

The following sections discuss, in more detail, the mathematics behind some of the material models referenced in previous sections of this chapter.

#### 3.8.1 Linear Elastic Material Models

##### 3.8.1.1 Equations for Plane Stress/Strain

List of symbols used in this section:

- $E$  - Young's modulus
- $\nu$  - Poisson's ratio
- $\lambda$  - Lamé material constant
- $\mu$  - Lamé material constant
- $\sigma$  - stress tensor (displayed in contracted form)
- $\sigma_x$  - x component of the stress tensor
- $\sigma_y$  - y component of the stress tensor
- $\sigma_z$  - out-of-plane component of stress
- $\tau_{xy}$  - in-plane shear component of the stress tensor
- $\varepsilon$  - strain tensor (displayed in contracted form)
- $\varepsilon_x$  - x component of the strain tensor
- $\varepsilon_y$  - y component of the strain tensor

- out-of-plane component of strain
- $\varepsilon_z$  - in-plane shear component of the strain tensor
- $D$  - Derivative operator
- $\mathbf{u}$  - Displacement vector
- $u_x$  - x component of the displacement
- $u_y$  - y component of the displacement

The equations used to describe linear elastic (Hookean) material behaviour restricted to the plane (either assuming the out-of-plane stress or strain are zero) are presented here.

$$\boldsymbol{\sigma} = \begin{bmatrix} \sigma_x \\ \sigma_y \\ \tau_{xy} \end{bmatrix} = \mathbf{E}\boldsymbol{\varepsilon} \quad \boldsymbol{\varepsilon} = \begin{bmatrix} \varepsilon_x \\ \varepsilon_y \\ \gamma_{xy} \end{bmatrix} = \mathbf{D}\mathbf{u} \quad \mathbf{u} = \begin{bmatrix} u_x \\ u_y \end{bmatrix} \quad (3.31)$$

where:

$$\mathbf{D} = \begin{bmatrix} \frac{\partial}{\partial x} & 0 \\ 0 & \frac{\partial}{\partial y} \\ \frac{\partial}{\partial y} & \frac{\partial}{\partial x} \end{bmatrix} \quad \mathbf{E} = \begin{bmatrix} (\lambda+2\mu) & \lambda & 0 \\ \lambda & (\lambda+2\mu) & 0 \\ 0 & 0 & \mu \end{bmatrix} \quad (3.32)$$

$$\text{and } \lambda = \frac{E\nu}{(1+\nu)(1-2\nu)} \quad (\text{plane strain}),$$

$$\text{or } \lambda = \frac{E\nu}{(1-\nu^2)} \quad (\text{plane stress}),$$

$$\mu = \frac{E}{2(1+\nu)}$$

and  $E$  and  $\nu$  are the engineering material constants Young's modulus and Poisson's ratio respectively.

The out-of-plane stress/strain components may be computed after the solution is found through the following equations:

For plane strain:

$$\begin{aligned} \varepsilon_z &= 0 \\ \sigma_z &= \nu(\sigma_x + \sigma_y) \end{aligned} \quad (3.33)$$

For plane stress:

$$\begin{aligned}\sigma_z &= 0 \\ \varepsilon_z &= -\frac{\nu}{E}(\sigma_x + \sigma_y)\end{aligned}\tag{3.34}$$

### 3.8.1.2 Equations for Axisymmetry

List of symbols used in this section:

$E$  - Young's modulus

$\nu$  - Poisson's ratio

$\lambda$  - Lamé material constant

$\mu$  - Lamé material constant

$\sigma$  - stress tensor (displayed in contracted form)

$\sigma_r$  - radial component of the stress tensor

$\sigma_z$  - axial component of the stress tensor

$\sigma_\theta$  - hoop component of the stress tensor

$\tau_{rz}$  - in-plane shear component of the stress tensor

$\varepsilon$  - strain tensor (displayed in contracted form)

$\varepsilon_r$  - radial component of the strain tensor

$\varepsilon_z$  - axial component of the strain tensor

$\varepsilon_\theta$  - hoop component of the strain tensor

$\gamma_{rz}$  - in-plane shear component of the strain tensor

$D$  - Derivative operator

$u$  - Displacement vector

$u_r$  - radial component of the displacement

$u_z$  - axial component of the displacement

The equations used to describe linear elastic (Hookean) material behaviour are presented here in cylindrical coordinates and assuming rotational symmetry (no variation in the theta direction.)

$$\sigma = \begin{bmatrix} \sigma_r \\ \sigma_z \\ \sigma_\theta \\ \tau_{rz} \end{bmatrix} = E\varepsilon \quad \varepsilon = \begin{bmatrix} \varepsilon_r \\ \varepsilon_z \\ \varepsilon_\theta \\ \gamma_{rz} \end{bmatrix} = Du \quad u = \begin{bmatrix} u_r \\ u_z \end{bmatrix}\tag{3.35}$$

where:

$$\mathbf{D} = \begin{bmatrix} \frac{\partial}{\partial r} & 0 \\ 0 & \frac{\partial}{\partial z} \\ \frac{1}{r} & 0 \\ \frac{\partial}{\partial z} & \frac{\partial}{\partial r} \end{bmatrix} \quad \mathbf{E} = \begin{bmatrix} (\lambda+2\mu) & \lambda & \lambda & 0 \\ \lambda & (\lambda+2\mu) & \lambda & 0 \\ \lambda & \lambda & (\lambda+2\mu) & 0 \\ 0 & 0 & 0 & \mu \end{bmatrix} \quad (3.36)$$

$$\text{and } \lambda = \frac{E\nu}{(1+\nu)(1-2\nu)}, \quad \mu = \frac{E}{2(1+\nu)}$$

and  $E$  and  $\nu$  are the engineering material constants Young's modulus and Poisson's ratio respectively.

### 3.8.2 Nonlinear Elastic Material Models

#### 3.8.2.1 The Deformation Gradient

In general, the deformation of a solid can be represented by  $\mathbf{dx} = \mathbf{F}d\mathbf{X}$  where  $\mathbf{F}$  is defined as the mapping (or transformation) between the reference (undeformed),  $\mathbf{dX}$  and current (deformed),  $\mathbf{dx}$  configurations. This operator is commonly referred to as the deformation gradient. In general, for arbitrary deformation fields, this mapping operator is not diagonal nor symmetric, but is positive definite and invertible (i.e. there is a one-to-one correspondence between the reference and current configurations.) Furthermore, through the use of the polar decomposition theorem, the deformation gradient can be decomposed into pure rotation and pure stretch transformations giving the following,

$$\mathbf{F} = \mathbf{\Lambda} \mathbf{R} \quad (3.37)$$

where  $\mathbf{\Lambda}$  is the stretch tensor and  $\mathbf{R}$  is the rotation tensor. Additionally, it can be shown that,

$$\mathbf{B} = \mathbf{F}\mathbf{F}^T = \mathbf{\Lambda}\mathbf{\Lambda}^T \quad (3.38)$$

which is referred to as the left Cauchy-Green deformation tensor and is a measure of large strain referenced to the current (or deformed) configuration.

The deformation gradient is illustrated in Fig. 3.14.

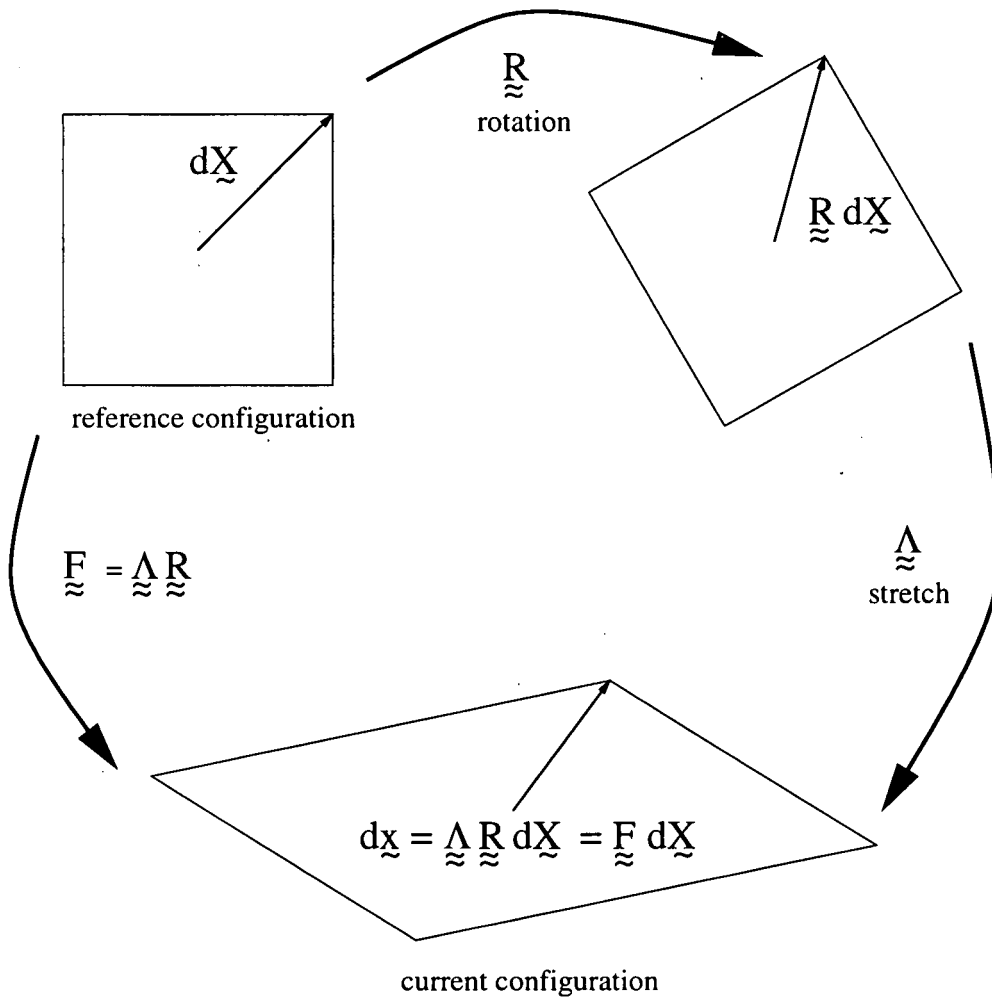


Figure 3.14 - The deformation gradient

### 3.8.2.2 Strain Energy Density

Energy is a convenient quantity to utilise in the development and description of material constitutive laws. A very common energy term is strain energy density which is used to represent the material response to strain input. Fig. 3.15 graphically defines the strain energy density.

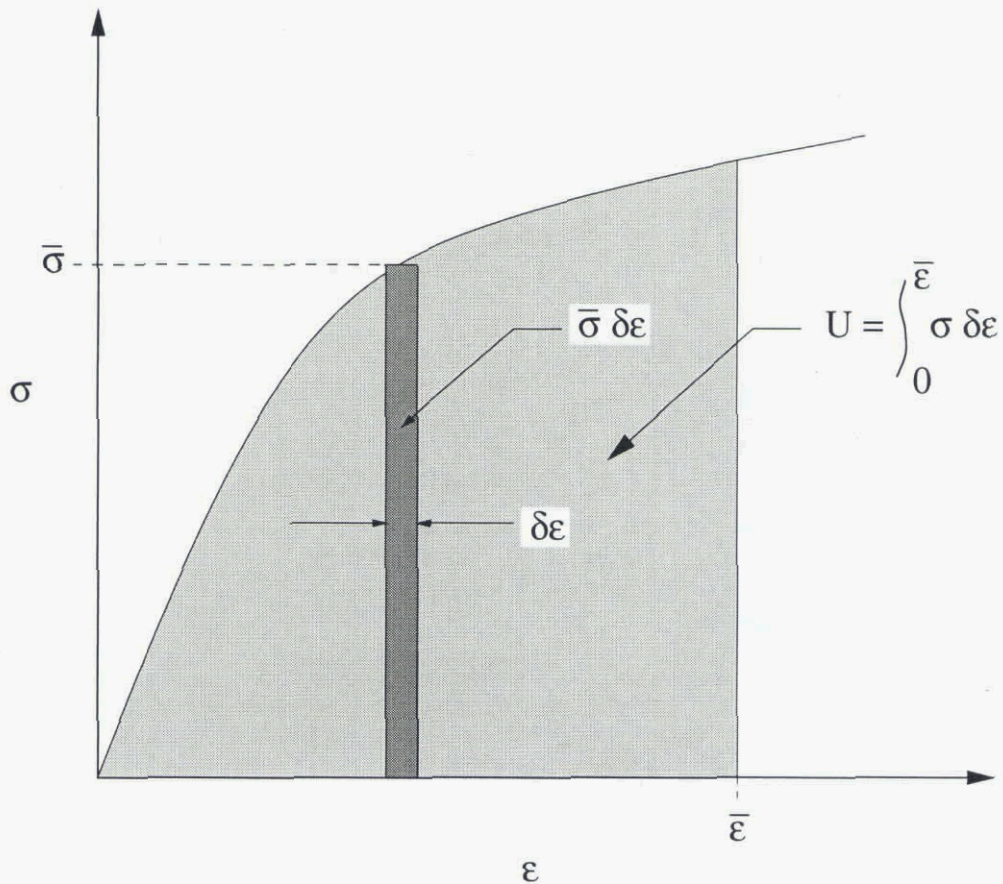


Figure 3.15 - Strain energy density

Strain energy density is defined as the area under the stress-strain curve as a function of the strain. Given a strain energy density function stress can then be written as,

$$\sigma = \frac{\partial U}{\partial \epsilon} \quad (3.39)$$

Various material models have been proposed based on some form of the strain energy density function some of which are discussed in the following sections.

### 3.8.2.3 Mooney-Rivlin Material Models

List of symbols used in this section:

$U$  - strain energy density

$C_{ij}$  - Rivlin polynomial constants

$I_1, I_2, I_3$  - strain invariants

$\lambda_1, \lambda_2, \lambda_3$  - principal stretches

$\sigma$  - stress

$p$  - hydrostatic pressure

A common material model used to represent rubber elasticity relates the strain energy density to the strain invariants (strain combinations that do not vary with transformation). For example, Mooney [25] proposed a simple two term (polynomial of degree one) representation of the following form (valid for

sufficiently small deformations), written in terms of strain energy density as a function of the strain invariants,

$$U = C_1(I_1 - 3) + C_2(I_2 - 3) \quad (3.40)$$

Higher degree polynomials may be used to better represent the observed material behaviour. Rivlin [26] observed that any smooth function of  $I_1$  and  $I_2$  can be approximated by,

$$U = \sum_{i,j=0,\dots} C_{ij} (I_1 - 3)^i (I_2 - 3)^j \quad C_{00} = 0 \quad (3.41)$$

Note that incompressibility is assumed and that compressibility can be modeled through an additional bulk term (such as  $K(J - 1)$  where  $J = I_3$ ). Given the strain energy density as a function of the strain invariants the principal (Cauchy) stresses can be written in the following form,

$$\sigma = 2 [(U_1 + U_2 I_2) \mathbf{B} - U_2 \mathbf{B}^2] + U_3 \mathbf{I} \quad (3.42)$$

where  $U_i = \frac{\partial U}{\partial I_i}$

$$I_1 = \text{trace} \mathbf{B} = \lambda_1^2 + \lambda_2^2 + \lambda_3^2 \quad (3.43)$$

$$I_2 = \Sigma \text{ sub det of } \mathbf{B} = \lambda_1^2 \lambda_2^2 + \lambda_1^2 \lambda_3^2 + \lambda_2^2 \lambda_3^2 \quad (3.44)$$

$$I_3 = \det \text{ of } \mathbf{B} = \lambda_1^2 \lambda_2^2 \lambda_3^2 \quad (3.45)$$

For incompressibility  $I_3 = 1$  and  $U_3 = p = \text{const}$  (hydrostatic pressure). This additional unknown must be solved for separately making use of the incompressibility constraint.

#### 3.8.2.4 Ogden Material Model

Alternatively, a material model may be chosen that relates the strain energy density to the principal stretches. Ogden [27] proposed the following form for incompressible hyperelastic materials,

$$U = \sum_{i=1}^3 \sum_{j=1}^m \frac{c_j}{b_j} (\lambda_i^{b_j} - 1) \quad (3.46)$$

with the principal stresses written in the following form,

$$\sigma_i = \lambda_i \frac{\partial U}{\partial \lambda_i} + p \quad (\text{no sum}) \quad (3.47)$$

### 3.8.2.5 Classical Problems in Hyperelasticity

The following is a discussion of a sample of problems involving simple deformations of hyperelastic materials. The problems considered are uniaxial tension (and compression) for compressible and incompressible materials, pure shear, and equi-biaxial tension. These problems are suitable for verifying hyperelastic material constitutive law implementation.

#### Uniaxial Tension and Compression (Incompressible)

From incompressibility,  $I_3 = \det \mathbf{F} = \lambda_1 \lambda_2 \lambda_3 = 1$ , therefore, for uniaxial tension (or compression) setting  $\lambda_1 = \lambda$  then,  $\lambda_2 = \lambda_3 = 1/\sqrt{\lambda}$ . The deformation gradient can then be written,

$$\mathbf{F} = \begin{bmatrix} \lambda & 0 & 0 \\ 0 & 1/\sqrt{\lambda} & 0 \\ 0 & 0 & 1/\sqrt{\lambda} \end{bmatrix}$$

and the Cauchy-Green deformation tensor becomes,

$$\mathbf{B} = \begin{bmatrix} \lambda^2 & 0 & 0 \\ 0 & 1/\lambda & 0 \\ 0 & 0 & 1/\lambda \end{bmatrix}$$

therefore, the strain invariants and principal stress are found as follows.

$$I_1 = \lambda^2 + \frac{2}{\lambda} \quad (3.50)$$

$$I_2 = 2\lambda + \frac{1}{\lambda^2} \quad (3.51)$$

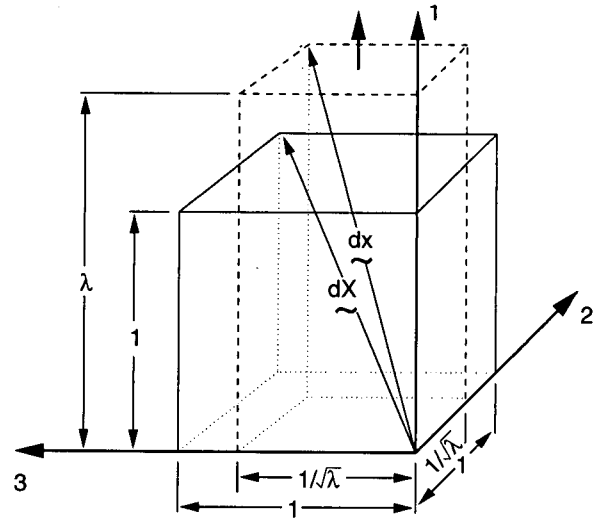
$$\sigma_1 = 2[(U_1 + (\lambda^2 + \frac{2}{\lambda})U_2)\lambda^2 - U_2\lambda^4] + p \quad (3.52)$$

$$\sigma_2 = 2[(U_1 + (\lambda^2 + \frac{2}{\lambda})U_2)\frac{1}{\lambda} - U_2\frac{1}{\lambda^2}] + p \quad (3.53)$$

Note that since  $\sigma_2 = 0$  the unknown constant,  $p$ , can be solved for. Substituting this expression for  $p$  into the equation for  $\sigma_1$  we obtain,

$$\sigma_1 = 2[(U_1(\lambda^2 - \frac{1}{\lambda}) + U_2(\lambda - \frac{1}{\lambda^2}))] \quad (3.54)$$

To demonstrate, the following problem was used to verify results obtained from a non-linear finite element code. Given the strain energy density,  $U = 100(I_1 - 3) + 10(I_2 - 3)$  then the following equations are obtained,



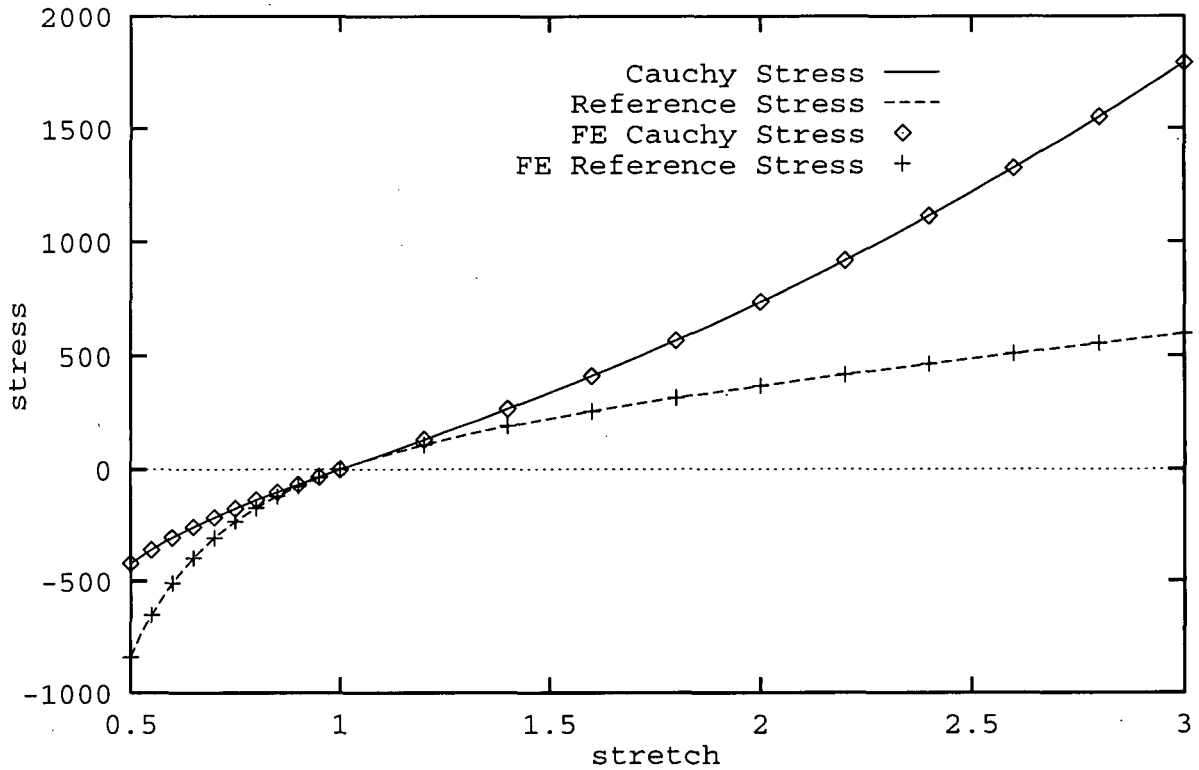


**Figure 3.16** - Analytical and FE results for uniaxial tension (and compression) based on Mooney-Rivlin model

$$U_1 = \frac{\partial U}{\partial I_1} = 100, U_2 = \frac{\partial U}{\partial I_2} = 10 \quad (3.55)$$

$$\sigma_1 = 200\left(\lambda^2 - \frac{1}{\lambda}\right) + 20\left(\lambda - \frac{1}{\lambda^2}\right) \quad (3.56)$$

Additionally, the reference (first Piola-Kirchoff) stress is defined by  $S = I_3 \sigma F^{-T}$  (for incompressibility,  $I_3 = 1$ ). Therefore,

$$S_1 = \sigma_1 \frac{1}{\lambda} = 200\left(\lambda - \frac{1}{\lambda^2}\right) + 20\left(1 - \frac{1}{\lambda^3}\right) \quad (3.57)$$

Fig. 3.16 shows a plot of the axial stresses along with results obtained from the finite element code using a single quadratic quadrilateral, plane stress element. The material was modeled as a rubber material with a Rivlin polynomial of degree one (i.e. the simple Mooney two term form as discussed above) to represent the strain energy density.

To demonstrate the verification of a material described using the Ogden form a similar approach is taken. For uniaxial tension (and compression) the axial stress in terms of the principal stretches reduces to,

$$\sigma_i = \sum_{j=1}^m c_j (\lambda_j^{b_j} - \lambda^{-b_j/2}) \quad (3.58)$$

For example, using a three term representation with the following coefficients,

$$\begin{aligned}
 c_1 &= 29.8223 & b_1 &= 1.3 \\
 c_2 &= 0.05680 & b_2 &= 5 \\
 c_3 &= -0.4734 & b_3 &= -2
 \end{aligned}
 \tag{3.59}$$

the stresses obtained are plotted along with the results from the finite element code (using the Ogden rubber material model) in Fig. 3.17.

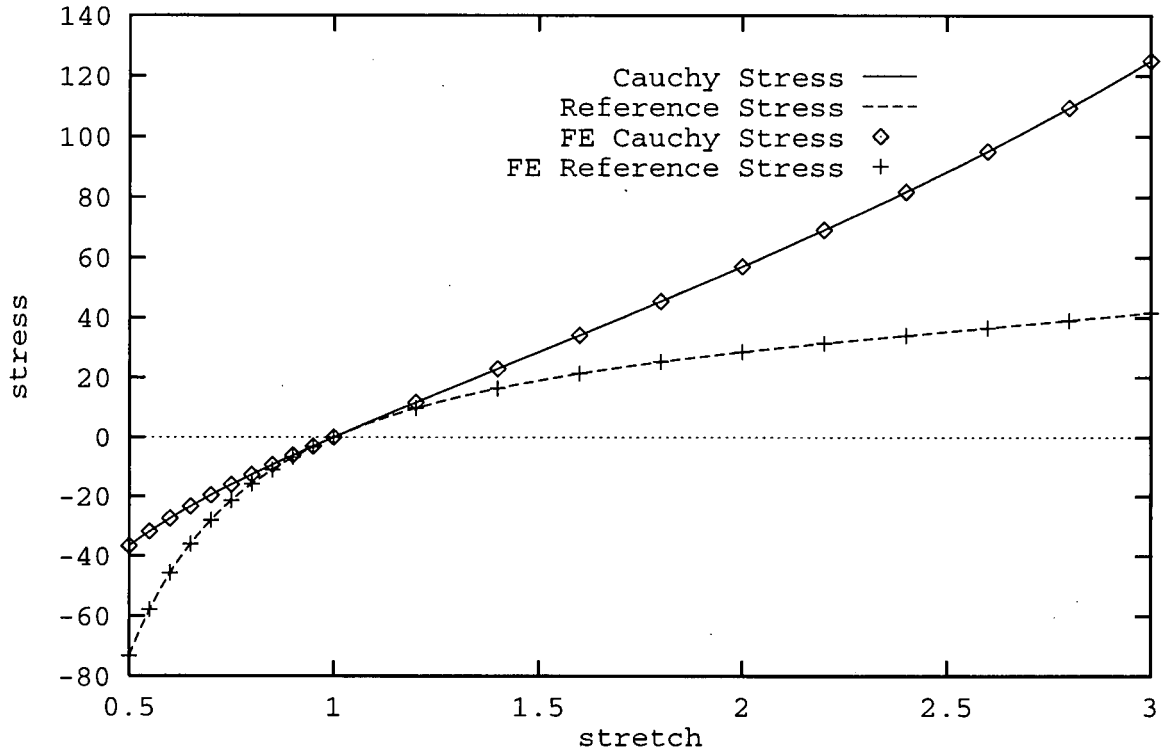


**Figure 3.17** - Analytical and FE results for uniaxial tension (and compression) based on Ogden model

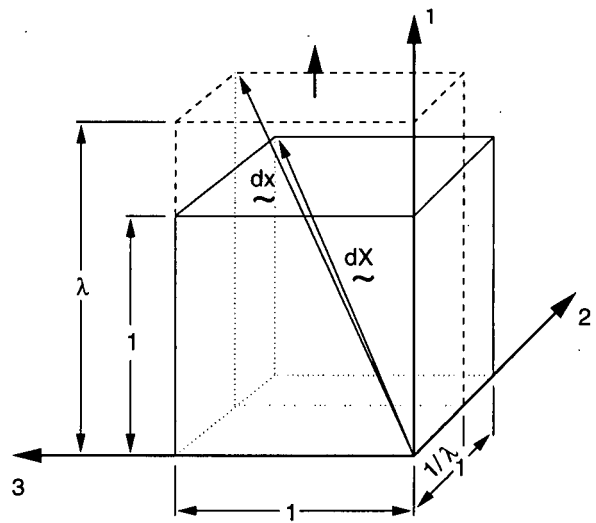
### Pure Shear

As illustrated, for pure shear we set  $\lambda_1 = \lambda$ ,  $\lambda_3 = 1$  and note that  $I_3 = \det|\mathbf{F}| = \lambda_1 \lambda_2 \lambda_3 = 1$  (for incompressibility), therefore,  $\lambda_2 = 1/\lambda$ . The deformation gradient can then be written,

$$\mathbf{F} = \begin{bmatrix} \lambda & 0 & 0 \\ 0 & 1/\lambda & 0 \\ 0 & 0 & 1 \end{bmatrix}$$

and the Cauchy-Green deformation tensor becomes,

$$\mathbf{B} = \begin{bmatrix} \lambda^2 & 0 & 0 \\ 0 & 1/\lambda^2 & 0 \\ 0 & 0 & 1 \end{bmatrix}$$



therefore, the strain invariants and principal stress are found as follows.

$$I_1 = I_2 = 1 + \lambda^2 + \frac{1}{\lambda^2} \quad (3.62)$$

$$\sigma_1 = 2[(U_1 + (1 + \lambda^2 + \frac{1}{\lambda^2})U_2)\lambda^2 - U_2\lambda^4] + p \quad (3.63)$$

$$\sigma_2 = 2[(U_1 + (1 + \lambda^2 + \frac{1}{\lambda^2})U_2)\frac{1}{\lambda^2} - U_2\frac{1}{\lambda^4}] + p \quad (3.64)$$

$$\sigma_3 = 2[(U_1 + (1 + \lambda^2 + \frac{1}{\lambda^2})U_2) - U_2] + p \quad (3.65)$$

Note that since  $\sigma_2 = 0$  the unknown constant,  $p$ , can be solved for. Substituting this expression for  $p$  into the equations for  $\sigma_1$  and  $\sigma_3$  we obtain,

$$\sigma_1 = 2(U_1 + U_2)(\lambda^2 - \frac{1}{\lambda^2}) \quad (3.66)$$

$$\sigma_3 = 2[U_1(1 - \frac{1}{\lambda^2}) + U_2(\lambda^2 - 1)] \quad (3.67)$$

To demonstrate, the same problem was used as in the uniaxial case. The resulting equations for the axial stress and the shear stress are,

$$\sigma_1 = 220(\lambda^2 - \frac{1}{\lambda^2}) \quad (3.68)$$

$$\tau_{max} = \frac{1}{2}(\sigma_1 - \sigma_2) = 110(\lambda^2 - \frac{1}{\lambda^2}) \quad (3.69)$$

Additionally, the reference shear stress is defined by,

$$T_{max} = J_s \tau_{max} \quad (3.70)$$

where  $J_s$  is the shear area ratio (the ratio of the area, on the shear plane, in the current configuration to the corresponding area in the reference configuration) which in the case of pure shear is,

$$J_s = \sqrt{\frac{2}{1/\lambda^2 + \lambda^2}} \quad (3.71)$$

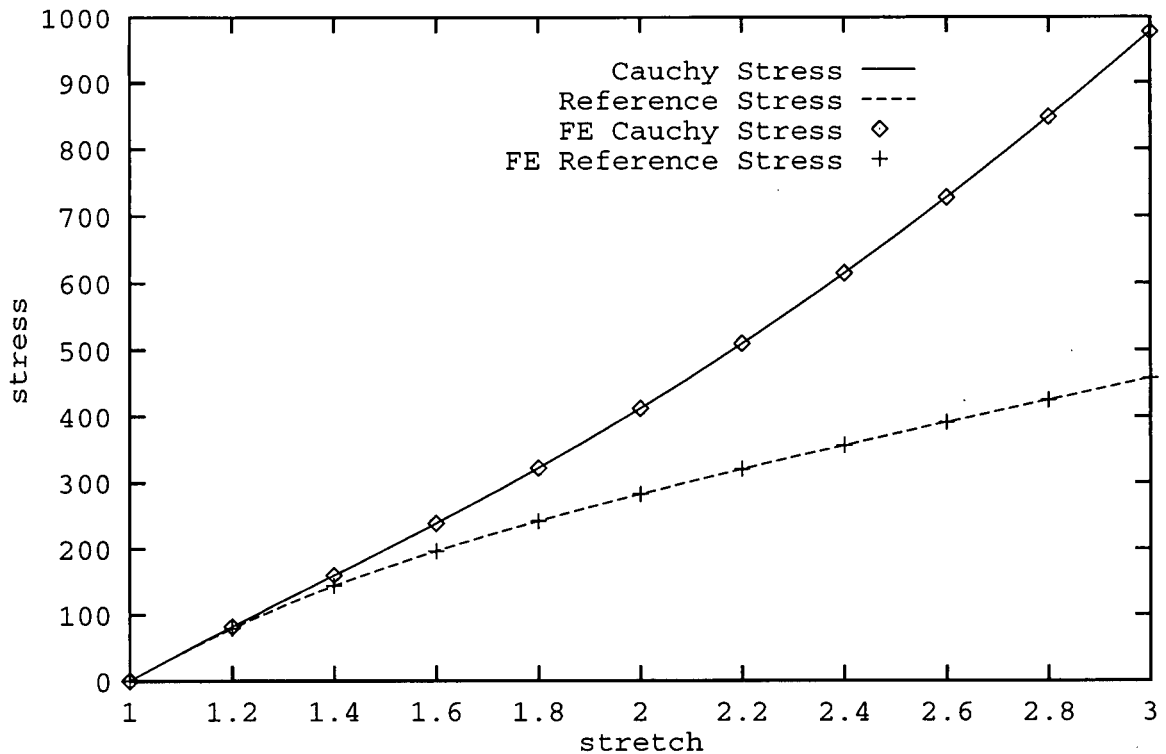


**Figure 3.18** - Analytical and FE results for pure shear based on Mooney-Rivlin model

Fig. 3.18 shows a plot of the shear stresses along with results obtained from the finite element code using a single quadratic quadrilateral, plane stress element. The material was modeled as a rubber material with a Rivlin polynomial of degree one (i.e. the simple Mooney two term form as discussed above) to represent the strain energy density.

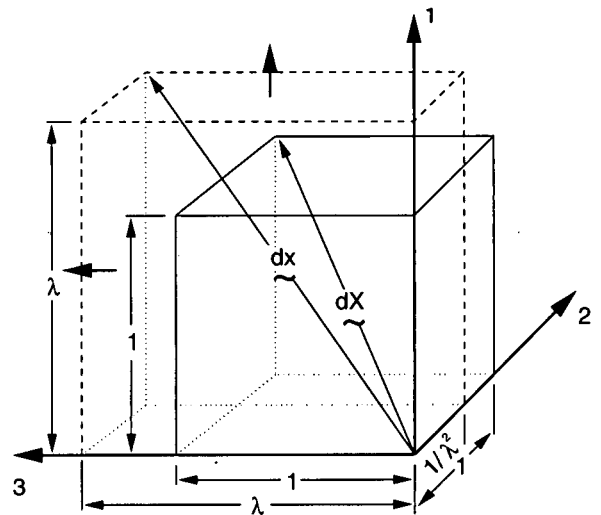
### Equi-Biaxial Tension

For equi-biaxial tension we set  $\lambda_1 = \lambda_3 = \lambda$  and note that  $I_3 = \det|\mathbf{F}| = \lambda_1 \lambda_2 \lambda_3 = 1$  (for incompressibility), therefore,  $\lambda_2 = 1/\lambda^2$ . The deformation gradient can then be written,

$$\mathbf{F} = \begin{bmatrix} \lambda & 0 & 0 \\ 0 & 1/\lambda^2 & 0 \\ 0 & 0 & \lambda \end{bmatrix}$$

and the Cauchy-Green deformation tensor becomes,

$$\mathbf{B} = \begin{bmatrix} \lambda^2 & 0 & 0 \\ 0 & 1/\lambda^4 & 0 \\ 0 & 0 & \lambda^2 \end{bmatrix}$$



therefore, the strain invariants and principal stress are found as follows.

$$I_1 = 2\lambda^2 + \frac{1}{\lambda^4} \quad (3.74)$$

$$I_2 = \lambda^4 + \frac{2}{\lambda^2} \quad (3.75)$$

$$\sigma_1 = \sigma_3 = 2[(U_1 + (2\lambda^2 + \frac{1}{\lambda^4})U_2)\lambda^2 - U_2\lambda^4] + p \quad (3.76)$$

$$\sigma_2 = 2[(U_1 + (2\lambda^2 + \frac{1}{\lambda^4})U_2)\frac{1}{\lambda^4} - U_2\frac{1}{\lambda^8}] + p \quad (3.77)$$

Note that since  $\sigma_2 = 0$  the unknown constant,  $p$ , can be solved for. Substituting this expression for  $p$  into the equation for  $\sigma_1$  we obtain,

$$\sigma_1 = \sigma_3 = 2[(U_1(\lambda^2 - \frac{1}{\lambda^4}) + U_2(\lambda^4 - \frac{1}{\lambda^2})] \quad (3.78)$$

To demonstrate, the same problem was used as in the uniaxial tension case. The resulting equations for the axial stress and the shear stress are,

$$\sigma_1 = 200(\lambda^2 - \frac{1}{\lambda^4}) + 20(\lambda^4 - \frac{1}{\lambda^2}) \quad (3.79)$$

Additionally, the reference stress is defined by,

$$S_1 = \sigma_1 \frac{1}{\lambda} = 200(\lambda - \frac{1}{\lambda^5}) + 20(\lambda^3 - \frac{1}{\lambda^3}) \quad (3.80)$$

Fig. 3.19 shows a plot of the stresses along with results obtained from the finite element code using a single quadratic quadrilateral, plane stress element. The material was modeled as a rubber material with a Rivlin polynomial of degree one (i.e. the simple Mooney two term form as discussed above) to represent the strain energy density.

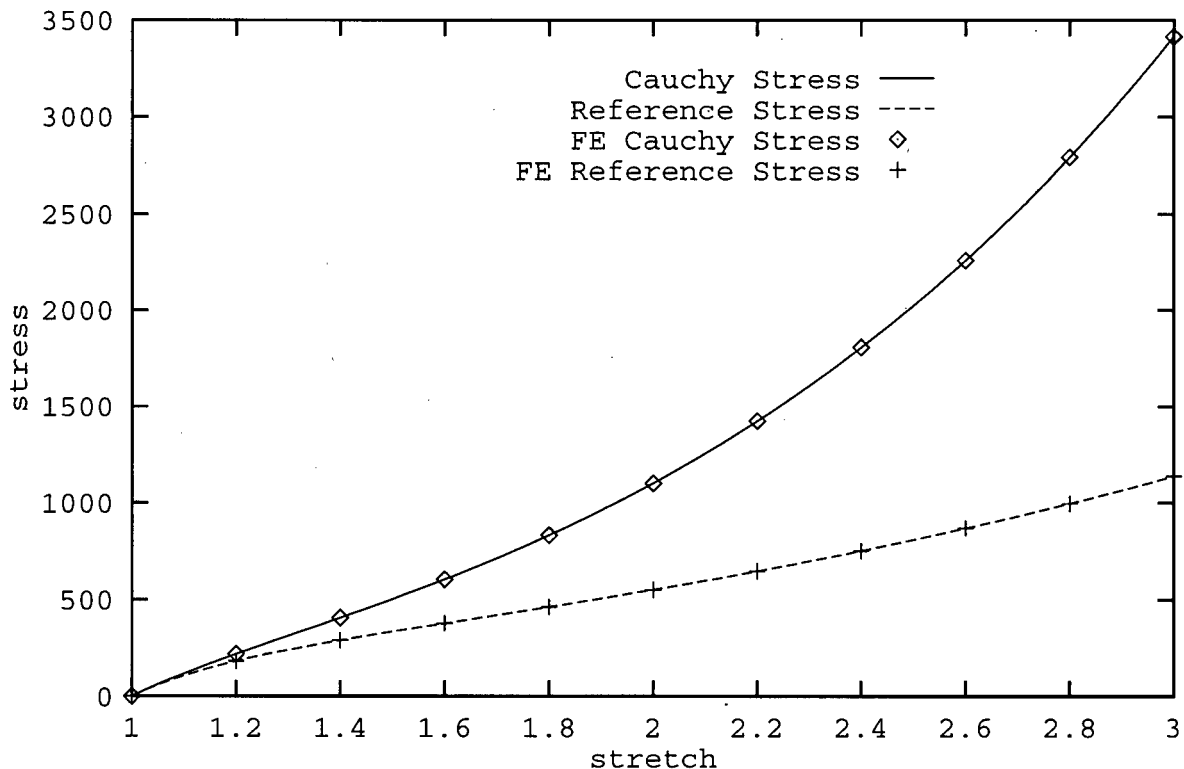


Figure 3.19 - Analytical and FE results for equi-biaxial tension based on Mooney-Rivlin model

### 3.8.2.6 Classical Geometrically Non-Linear Problems

A class of elasticity problems where large displacements (including rotations) are expected, but small strains can still be assumed can be handled as strictly geometric nonlinear problems. Simple problems with known solutions, that fall into this category, can be used to check a code's ability to converge to the correct solution. Two such problems are presented here.

#### The Rotating Beam

This problem consists of a beam subjected to displacements such that the resulting deformation be pure rotation. The applied displacements were large to ensure an adequate test of the large displacement formulation. While correct solution of this problem represents a necessary requirement it should be noted that it is not a sufficient test of the accuracy (or correctness) of the formulation.

The beam was modeled as a ten inch long, one half inch thick beam consisting of a single row of twenty linear quadrilateral (four node) elements. Displacements were applied to the lower left node (in both the x and y directions), to pin the beam, and to the upper right node to produce a 45 degree rotation.

The resulting displacements obtained from a computer code are shown in Fig. 3.20. Both the displacements found from the linear solution (the first iteration) and the nonlinear solution (the last iteration) are shown for comparison.

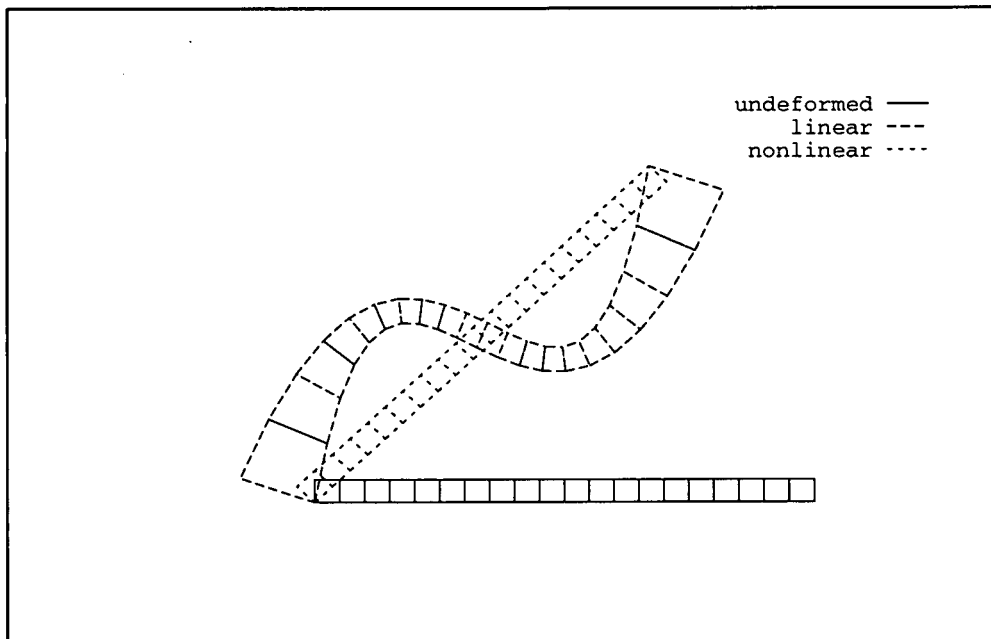


**Figure 3.20** - Nonlinear beam rotation

### The Cantilever Beam

This problem consists of a simple slender (length-to-thickness = 10) cantilever beam clamped at one end and loaded vertically at the other. The beam was modeled with a single row of ten quadratic quadrilateral (eight node) elements. The material was assumed to linear elastic with the Poisson's ratio set to zero (which gives equivalent results as simple beam theory). The applied load was incremented from 50 to 800 in load steps of 50 each.

The resulting displacements, at selected load steps, are shown in Fig. 3.21.

The deflections calculated at the loaded tip of the beam were compared with the deflections calculated analytically by Bisshopp and Drucker [28] and are shown in Fig. 3.22 along with the corresponding linear solution. Table 3.2 contains tabulated values, at selected loads, of the tip displacements obtained from the analytical solution.

The slight difference between the finite element results and the analytical results is most likely attributable to the fact that the analytical solution assumes that the beam is inextensible whereas the finite element model makes no such assumption.

**Table 3.2** - Tip displacements obtained from analytical solution

$\frac{PL^2}{EI}$	$\frac{(L-\delta_h)}{L}$	$\frac{\delta_h}{L}$
0.0	1.000	0.000
0.2	0.997	0.066
0.4	0.990	0.131
0.6	0.978	0.192
0.8	0.962	0.249
1.0	0.944	0.302
1.5	0.892	0.411
2.0	0.839	0.493
3.0	0.746	0.603
4.0	0.671	0.670
5.0	0.612	0.714
6.0	0.565	0.745
7.0	0.527	0.767
8.0	0.495	0.785
9.0	0.468	0.799
10.0	0.445	0.811
15.0	0.365	0.848
$\infty$	0.000	1.000

Large Deflection of a Cantilever Beam

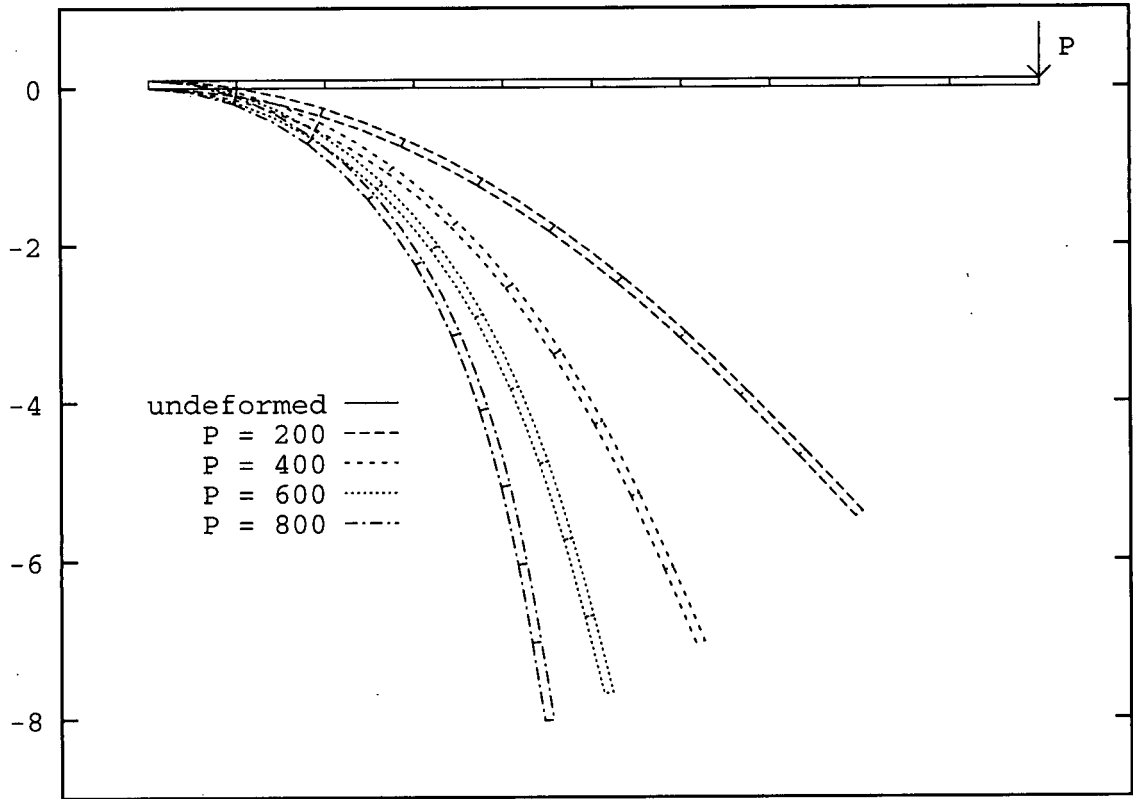


Figure 3.21 - Beam deflection with increasing load

Tip Displacement of a Cantilever Beam

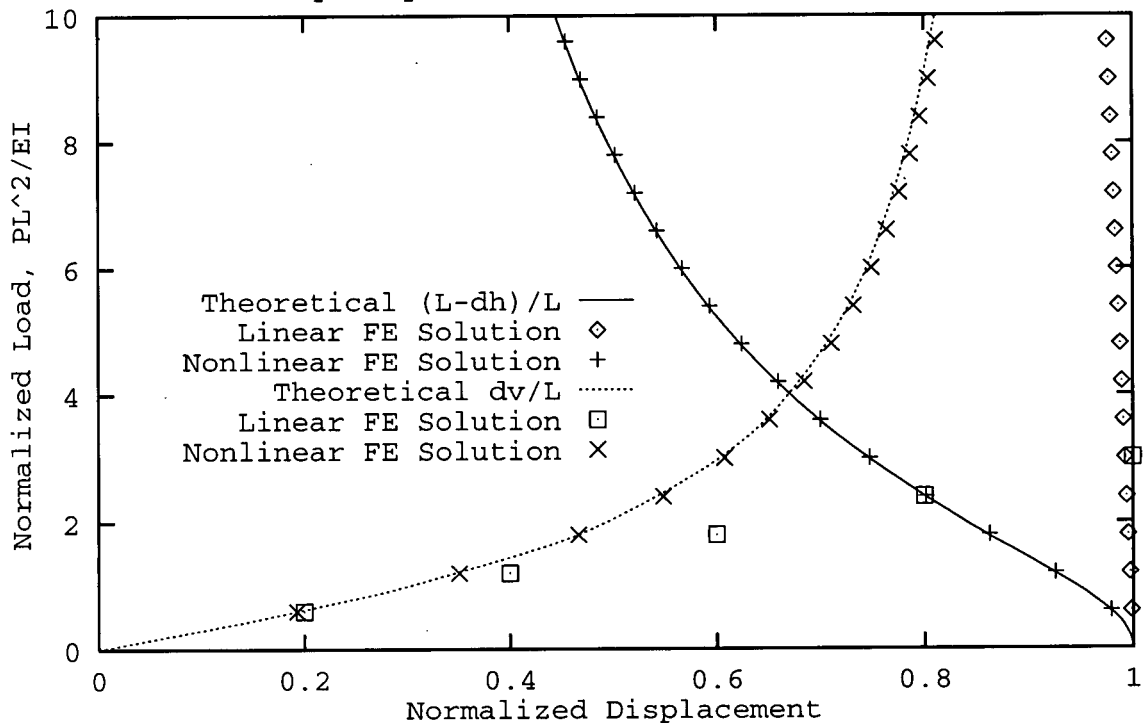


Figure 3.22 - Solution comparison

### 3.9 FINITE ELEMENT CODES

The following is a partial list of codes specifically used to assess SRM structural integrity. Listed with each code are specific features of interest for SRM analysis.

ABAQUS	Commercial general purpose finite element code (HKS, Inc. [29]). - Large element library including reformulated elements (for near-incompressibility) - User defined subroutine allowing incorporation of external material models
CAMILLE	SNPE in-house finite element code. - Reformulated elements - "Skin" elements to directly calculate stress/strain at free surfaces
MARC	Commercial general purpose finite element code - Large element library including reformulated elements (for near-incompressibility) - User defined subroutine allowing incorporation of external material models
ONDINE	SNPE in-house finite element code - Large displacement, large strain - Additional material laws (hyperelasticity, viscoelasticity, etc) - Damage model included
TEXGAP	USAF limited distribution finite element codes (2D and 3D). - Approximate 3D model features (2D code) - Fracture elements - Reformulated elements
TEXLESP	USAF limited distribution finite element code. - Large displacement, large strain - Compressible/incompressible rubber elasticity - Reformulated elements - Riks solution procedure (path-independent)
TEXNLVE	USAF limited distribution finite element code. - Update to TEXLESP code - Additional material laws (Swanson, Simo)
TEXPAC	Commercial finite element code (Mechanics Software, Inc. [30]). - Incorporates most features of TEXNLVE - Large selection of material laws (Rubber elasticity, Swanson, Peng, Park, Özüpek, etc.)

### 3.10 CONCLUSIONS

It has been recognised by this working group that the current predictive capability of the stress-strain response in a solid rocket propellant grain and associated bondline system, when subjected to its storage and service loads, lacks acceptable precision and in many situations is highly inaccurate. It is strongly recommended that attention is focused on the improvement of the current constitutive modelling capability. It is proposed that constitutive models be developed which will account for material non-linearity by considering the evolution of damage of the microstructure as a function of the applied loading history. Furthermore, these constitutive models should accurately describe combined mechanical and thermal loading conditions. *These non-linear thermo-viscoelastic constitutive models must be capable of giving a good correlation with uniaxial behaviour (under all forms of combined loading conditions) and, furthermore, be capable of extension to the multiaxial stress state.* The constitutive models should be computationally efficient because the finite element solution requirements for the storage and operational loading conditions will be computationally intensive. Although constitutive modelling has in the past been a graveyard for theoreticians there are grounds for optimism. Significant advances have recently been made in this theoretical field and this has been accompanied by important advances in the development of accurate stress measuring devices. The time is right in many respects to take on this challenge.

### 3.11 REFERENCES

- [1] Davenas, A., et al., **Solid Rocket Propulsion Technology**, Pergamon Press, 1993, pp. 215-302
- [2] Various, *Design Methods in Solid Rocket Motors*, **AGARD Lecture Series No. 150, AGARD-LS-150 (Revised)**, 1988
- [3] Zienkiewicz, O.C., Taylor, R.L., **The Finite Element Method, Vol. 1-2**, McGraw-Hill, 1989
- [4] Becker, E.B., Carey, G.F., and Oden, J.T., **Finite Elements; An Introduction, Vol. 1**, Prentice Hall, 1981
- [5] Cook, R.D., Malkus, D.S., and Plesha, M.E., **Concepts and Applications of Finite Element Analysis**, 3rd Ed., John Wiley, 1989
- [6] Farris, R.J., and Schapery, R.A., **Development of a Solid Rocket Propellant Nonlinear Viscoelastic Constitutive Theory, Vol. 1-2**, Aerojet Solid Propulsion Company, AFRPL-TR-73-50, June 1973
- [7] Francis, E.C., et al., **Propellant Nonlinear Constitutive Theory Extension: Preliminary Results**, United Technologies, Chemical Systems Division, AFRPL-TR-83-034, August 1983
- [8] Francis, E.C., et al., **Propellant Nonlinear Constitutive Theory Extension**, United Technologies, Chemical Systems Division, AFRPL-TR-83-071, January 1984
- [9] Lee, Y.T., *Coupled Thermomechanical Effects in High Solids Propellant*, **AIAA J.**, Vol. 17, 1979, pp. 1015-1017
- [10] Francis, E.C., *Nonlinear Material Considerations and Motor Instrumentation for Service Life Evaluation*, **12th Meeting of TTCP WTP-4, Vol. 2**, 1986, pp. 1-26
- [11] Cost, T.L., *Calculation of Transient Thermal Stresses in Solid Rocket Motors*, **AIAA/SAE/ASME 18th Conf.**, June 1982, Paper No. AIAA 82-1098
- [12] Swanson, S.R. and Christensen, L.W., *A Constitutive Formulation for High Elongation Propellants*, **J. Spacecraft**, Vol. 20, 1983, pp. 559-566
- [13] Simo, J. C., *On a Fully Three-Dimensional Finite-Strain Viscoelastic Damage Model: Formulation and Computational Aspects*, **Computer Methods in Applied Mechanics and Engineering**, Vol 60, 1987, pp. 153-173
- [14] Özüpek, S., **Constitutive Equations for Solid Propellants, PhD Dissertation**, The University of Texas at Austin, August 1995
- [15] Schapery, R. A., *A Theory of Nonlinear Thermoviscoelasticity based on Irreversible Thermodynamics*, Proceedings Fourth U.S. National Congress of Applied Mechanics, **The American Society of Mechanical Engineers**, 1966, pp. 511-530
- [16] Schapery, R. A., *A Micromechanical Model for Nonlinear Viscoelastic Behavior of Particle-Reinforced Rubber with Distributed Damage*, **Engineering Fracture Mechanics**, Vol 25, 1986, pp. 845-867
- [17] Schapery, R. A., *A Theory of Mechanical Behavior of Viscoelastic Composites with Growing Damage and Other Changes in Structure*, **J Mech Physics Solids**, Vol 38, 1990, pp. 215-253

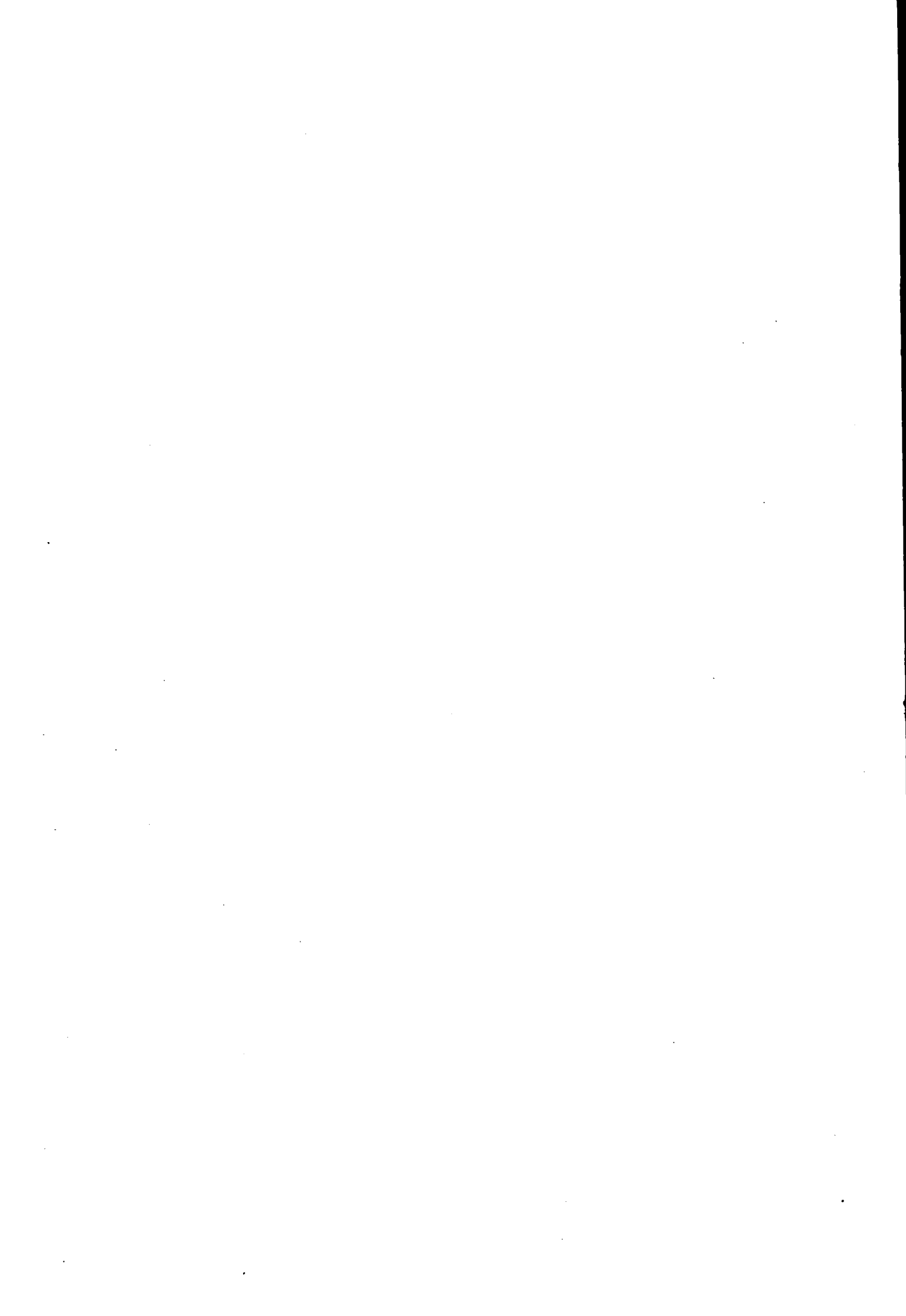
- [18] Schapery, R. A., *Simplifications in the Behavior of Viscoelastic Composites with Growing Damage*, **Proceedings of the IUTAM Symposium on Inelastic Deformation of Composite Materials**, May 29-June 1, 1990
- [19] Park, S., **Development of a Nonlinear Viscoelastic Constitutive Equation for Particulate Composites with Growing Damage**, **Dissertation**, The University of Texas at Austin, December 1994
- [20] Tsai, S.W., Hahn, H.T., *Introduction to Composite Materials*, **Technomic Publishing**, 1980
- [21] Jones, R.M., *Mechanics of Composite Materials*, **Hemisphere Publishing**, 1975
- [22] Anonymous, *ABAQUS Version 5.5 Theory Manual*, **Hibbitt, Karlsson and Sorensen, Inc.**, 1995, sec. 2.3.2
- [23] Williams, M.L., Blatz, P.J., and Schapery, R.A., *Fundamental Studies Relating to Systems Analysis of Solid Propellants*, **Guggenheim Aeronautical Laboratory, California Institute of Technology**, GALCIT 101, DTIC AD-256905, February 1961
- [24] Leighton, R.A., *Quick-Look Structural Analysis Techniques for Solid Rocket Propellant Grains*, **Air Force Rocket Propulsion Laboratory**, AFRPL-TR-81-80, May 1982
- [25] Mooney, M., **J. Appl. Phys.**, Vol. 11, 1940, pp. 582
- [26] Rivlin, R.S., **Phil. Trans. A**, Vol. 243, 1951, pp. 251
- [27] Ogden, R.W., *Large Deformation Isotropic Elasticity*, **Proc. Roy. Soc., Lond.** A328., 1972
- [28] Bisshopp, K.E., and Drucker, D.C., *Large Deflection of Cantilever Beams*, **Quarterly of Applied Mathematics**, Vol. 3, 1945, pp. 272-275
- [29] Anonymous, *ABAQUS Version 5.5 Users Manual*, **Hibbitt, Karlsson and Sorensen, Inc.**, 1995
- [30] Becker, E. B., Miller, T., *User's Manual for the TEXPAC Computer Code*, **Mechanics Software, Inc.**, 1989

# CHAPTER 4

## MATERIAL CHARACTERISATION

### TABLE OF CONTENTS

<b>4.1</b>	<b>INTRODUCTION</b>	<b>4-1</b>
<b>4.2</b>	<b>PROPELLANTS</b>	<b>4-1</b>
4.2.1	Material Tests to Determine Input Parameters for Structural Analysis	4-2
4.2.1.1	Stress-Strain Behaviour	4-2
4.2.1.2	Poisson's Ratio or Bulk Modulus	4-7
4.2.1.3	Density	4-9
4.2.1.4	Coefficient of Linear Thermal Expansion	4-9
4.2.1.5	Thermal Conductivity	4-9
4.2.2	Material Tests to Determine Failure Data	4-9
<b>4.3</b>	<b>INERT MATERIALS</b>	<b>4-14</b>
<b>4.4</b>	<b>DEVIATIONS FROM LINEAR BEHAVIOUR</b>	<b>4-14</b>
<b>4.5</b>	<b>REFERENCES</b>	<b>4-18</b>
<b>APPENDIX 4-1</b>	<b>Stress Relaxation Test</b>	<b>4-19</b>
<b>APPENDIX 4-2</b>	<b>Uniaxial Tensile Test</b>	<b>4-21</b>
<b>APPENDIX 4-3</b>	<b>Dynamic Mechanical Analysis</b>	<b>4-22</b>
<b>APPENDIX 4-4</b>	<b>Thermochemical Analysis</b>	<b>4-23</b>



## Chapter 4

# MATERIAL CHARACTERISATION

### 4.1 INTRODUCTION

Characterisation and modelling of the material behaviour of solid propellants is indeed a very difficult task. The response of such materials to loads is in a complex way dependant on the load conditions (direction, magnitude and speed), on environmental conditions (temperature, pressure, humidity) and on loading history.

As was indicated in the previous chapter, material models used in structural analyses of solid propellant rocket grains are simplifications of the real behaviour, ranging from linear elastic to non linear visco-elastic models. At present the introduction of more complex material models in computerised structural analysis is no longer limited by computer hardware. The problem is to find the correct mathematical description of the material behaviour in a material constitutive law.

With regard to the characterisation of the material by means of mechanical testing there are practical and cost limitations. A complete characterisation would lead to an enormous number of tests with a large variety of samples and test conditions. It is clear that a characterisation for all possible loading combinations would become very costly to perform. Thus, in the material characterisation phase the structural analyst is obliged to use data from relatively simple tests. In the case of very detailed analyses in problem areas specially designed tests may be used.

It is normal practice when performing the material characterisation of propellants to regard the propellants as a linear visco-elastic material satisfying conditions of homogeneity and the Boltzmann superposition principle of time and temperature [1]. This means in practice that short duration tests for one specific loading condition when performed at several temperatures will produce data for a larger time and loading domain. This will be illustrated for the case of the relaxation test in the next section.

In this chapter an overview is presented of tests that are currently used by the solid propellant rocket motor community to characterise the material behaviour for the purpose of performing a structural analysis.

The propellant characterisation tests may be divided into tests that generate the input data for the structural analysis (section 4.2.1) and tests that produce the failure data of the materials that can be used in the failure models described in chapter 5 (section 4.2.2).

For the bondline system materials are chosen with large capabilities to withstand the loads imparted by the solid propellant grain. Because no failure of these materials is assumed except in bonded interfaces only the input data and interface failure data are determined.

### 4.2 PROPELLANTS

In recent years a working group of Sub Group 1 of NATO AC 310 has made an inventory of all parameters needed for the qualification and documentation of explosive materials which includes solid propellants. Obviously in such a list the material properties used in structural analysis of solid propellant rocket grains are very prominent, although the description of the use of the parameters in structural analyses was beyond the scope of the working group.

The essential parameters list, test comparisons and data exchange formats that were produced by this working group have been recorded in the AOP-7 manual, Annex 1, Volume 1, Section 102.01, [2]. In the same section also a number of (draft) STANAG's have been introduced for which the working group has agreed on a standard procedure to perform certain tests.

So far the standardised tests and procedures are:

- Uniaxial compressive test
- Uniaxial tensile test
- Stress relaxation test in tension
- Thermo Mechanical Test for determining the Coefficient of Linear Thermal Expansion
- Dynamic Mechanical Analysis test to measure the Glass Transition Temperature
- Shifting Procedure for the determination of Master Relaxation curves

Where applicable, reference will be made to the comprehensive description of the test procedures in the AOP-7 Manual.

#### **4.2.1 Material Tests to Determine Input Parameters for Structural Analysis.**

Various characterisation tests are required firstly to define the stress-strain response of the propellant and secondly to determine other key material properties, all of which are essential to perform the structural analysis of a solid propellant rocket grain.

The material properties that have to be determined in order to generate the input parameters for the structural analysis computations are:

- Stress-strain relationship
- Poisson's ratio or bulk modulus.
- Density
- Coefficient of linear thermal expansion
- Thermal conductivity

Tests to determine these quantities are described in the following paragraphs. For a comprehensive description of test procedures reference is made to the above mentioned AOP-7 manual.

##### **4.2.1.1 Stress-Strain Behaviour**

There are a number of different test methods which may be selected to determine the stress-strain behaviour of solid propellants. The most common of these test procedures are the stress relaxation test in uniaxial tension, the uniaxial tensile test and the Dynamic Mechanical Analysis test procedure.

All three test methods have been introduced as (draft) STANAG's. For this reason only relatively short descriptions will be given here

##### *Stress relaxation test in uniaxial tension (STANAG 4507)*

In this type of test a constant strain of typically 1 to 5% is applied to a test sample and the relaxation of the force required to maintain this strain is measured. The recommended strain level in this test is the average strain level of the design which is being analyzed.

For this test end bonded samples are used if the strain measurement is performed by means of the cross-head displacement of the tensile machine. For cases where an untabbed is used a direct strain measurement method is mandatory. When such a method is applied special care should be taken that the measurement equipment does not influence the result of the measurement.

Typical sample geometries and the associated measurement results are respectively shown in Fig. 4.1 and Fig. 4.2.

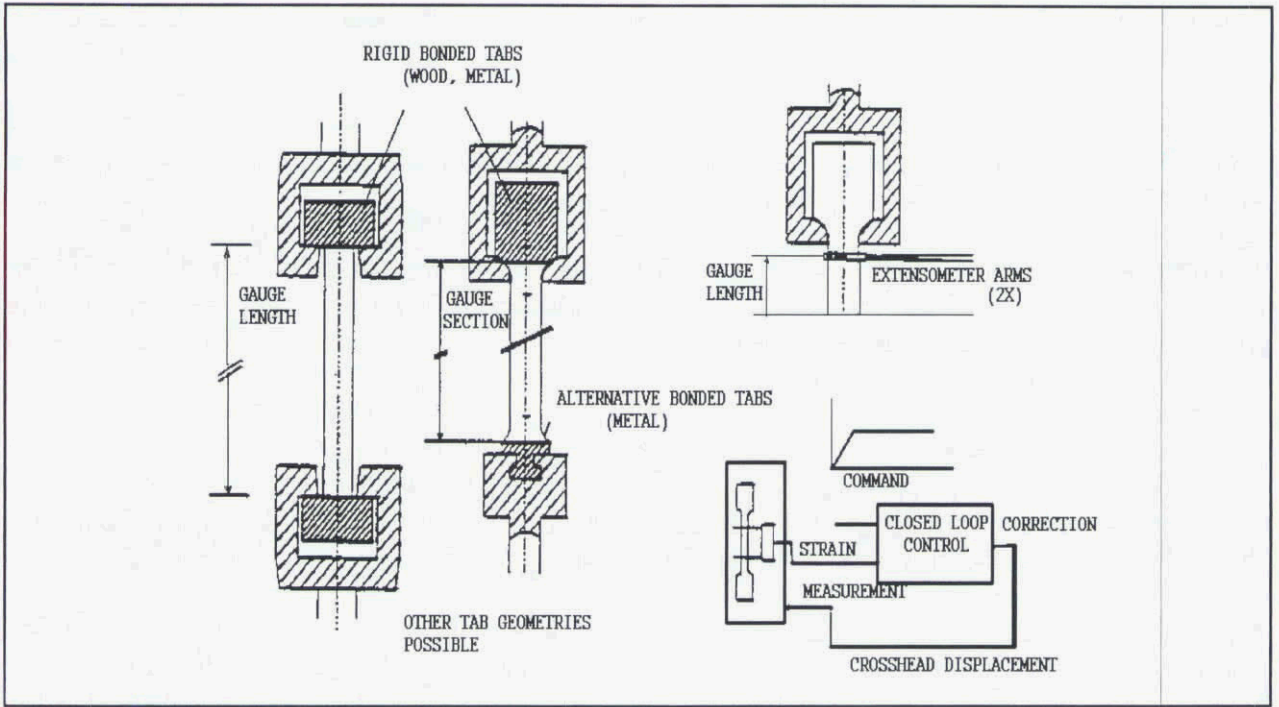


Figure 4.1: Typical test sample geometry for relaxation tests

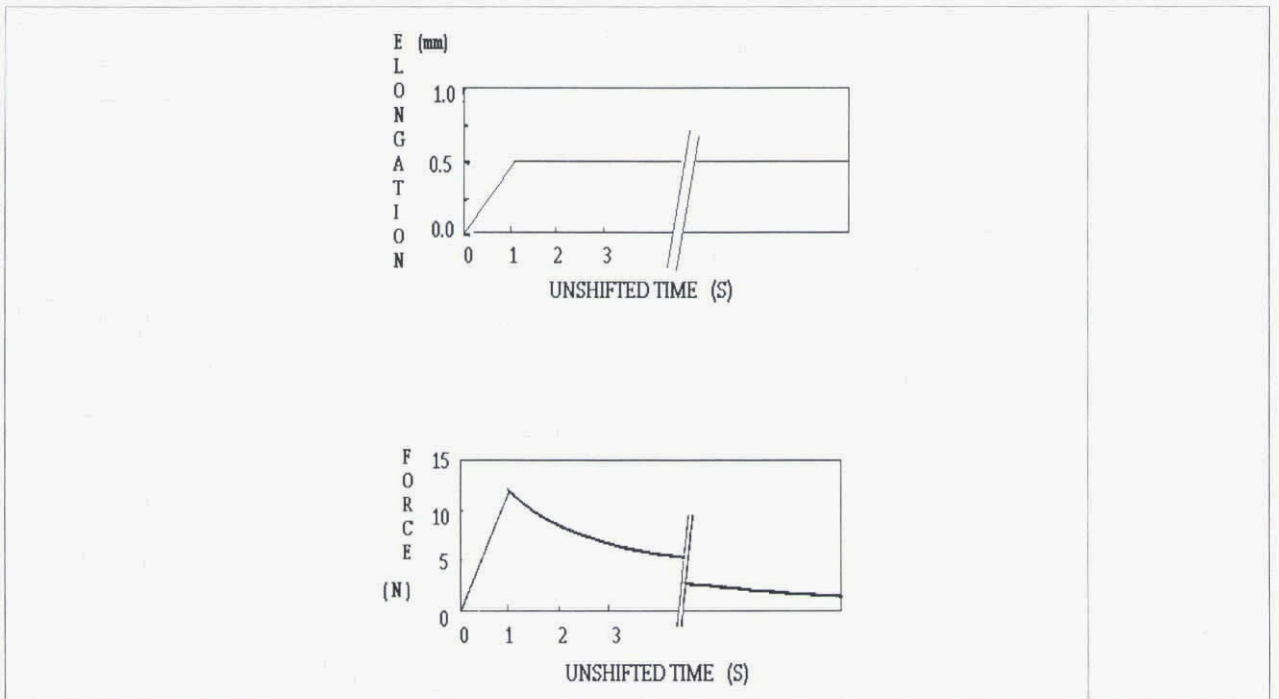


Figure 4.2: Typical measurement results for stress relaxation tests.

Assuming a linear visco-elastic material behaviour from the test results the Relaxation Modulus is calculated

$$E(t) = \sigma(t)/\epsilon$$

and plotted versus time on logarithmic scales. An example of the result of a relaxation test in the data exchange format of NATO AOP-7 is shown in appendix 4.1 (2 pages)

Performing the tests at different temperatures produces a set of relaxation moduli curves. In order to determine an Isothermal Relaxation Modulus the modulus is first multiplied by a factor  $T_0/T$  after which the Modulus curve can be shifted along the logarithmic time axis in order to generate a so-called Master Relaxation Curve. Shifts can be either manual or calculated from linear visco-elastic theory using the WLF shift factor:

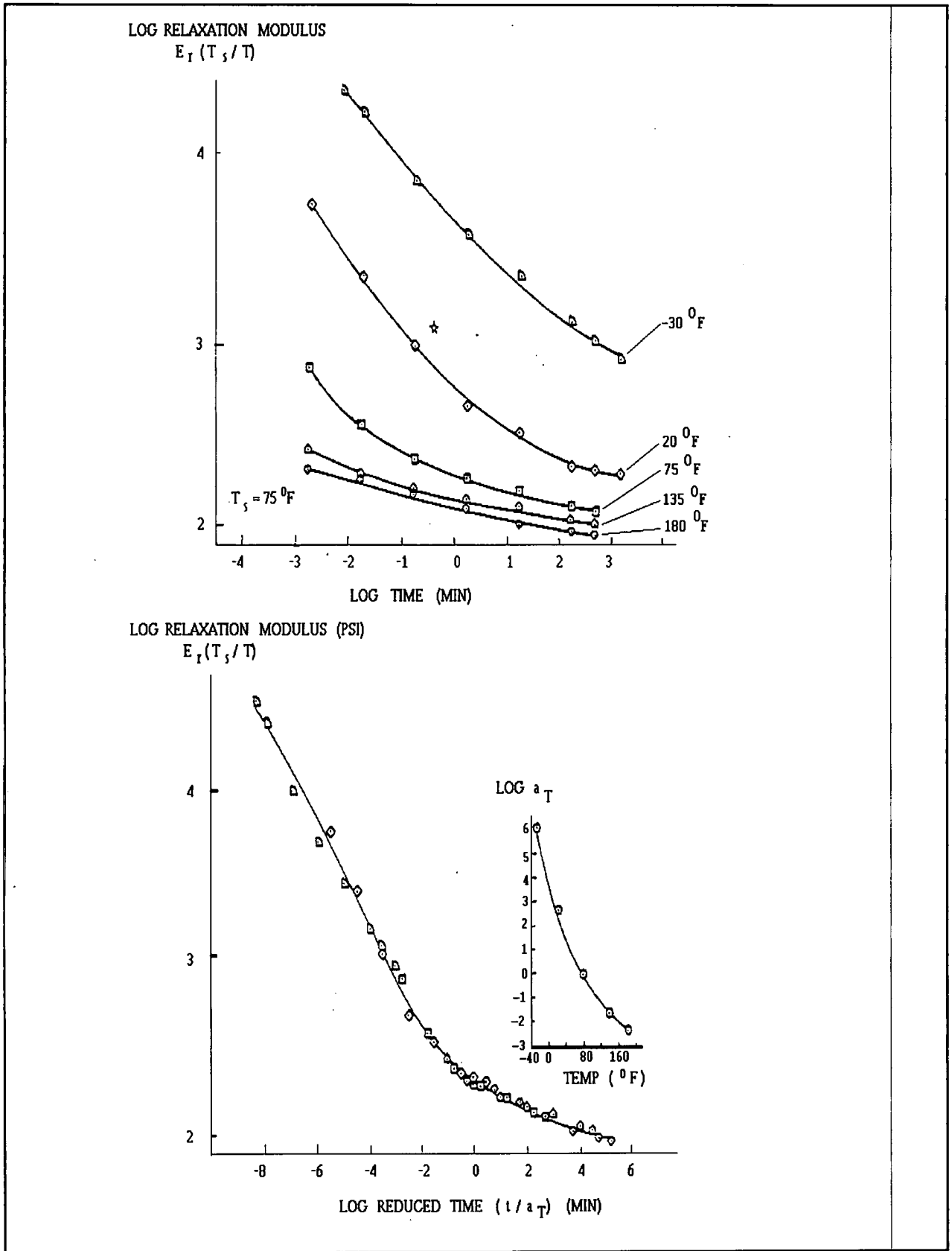
$$\log a_T = -C_1(T-T_0) / (C_2 + T-T_0) \quad T_0 = \text{reference temperature}$$

In this way a Relaxation Modulus can be generated for a large time and temperature domain. An example of a manually shifted set of curves is shown in Fig. 4.3.

The manner in which the relaxation modulus can be used as an input for the stress-strain behaviour of the propellant in the structural analysis depends on the constitutive material model selected for the propellant.

In the case of a linear elastic model an effective modulus value may be determined at an appropriate time and temperature which is representative of the given load case.

When adopting a visco-elastic model it is usual to define the relaxation modulus mathematically deduced from a curve fit analysis of the relaxation curves, as input for the material behaviour. Relaxation data are used as input for the stress-strain behaviour where the response to slowly varying processes are being analyzed. A typical example is the slow cooldown of a rocket motor. The data reduction procedures to determine effective moduli and mathematical curve fits are described in Chapter 3.



Reference Temperature  $T_0$  is represented as  $T_s$

**Figure 4.3:** Example of manually shifted Isothermal Relaxation moduli, producing a Relaxation Master curve (Courtesy NAWC)



### Dynamic Mechanical Analysis (Draft STANAG)

A test method used for the determination of the glassy moduli of Double Base propellants is the Dynamic Mechanical Analysis (DMA) test. A sample, usually a rod or rectangular bar, is subjected to a cyclic, usually sinusoidal, deformation with the stress and strain being recorded continuously. The stress and strain information is analyzed to produce the two moduli  $E'$  and  $E''$  (or  $G'$  and  $G''$  in case of shear deformation). It is normal to measure these parameters as a function of deformation frequency and temperature. The temperature range is often very large ( $-100^{\circ}\text{C}$  to  $+80^{\circ}\text{C}$ ) as the test is also used for the determination of the glass transition temperature. In a manner similar to that discussed previously for the relaxation moduli the  $\text{Log } E'$  versus  $\text{Log Frequency}$  can be shifted over the frequency axis in order to gain a mastercurve similar to the relaxation mastercurve. The modulus information so gathered is in any case an extension of the relaxation modulus data for short time phenomena.

The test procedure was introduced in a (draft) STANAG and the data exchange format of NATO AOP-7 is shown in appendix 4.3. It should be noted however that the data represented are those used for the determination of glass transition temperatures.

#### 4.2.1.2 Poisson's Ratio or Bulk Modulus

A very important parameter used in the structural analysis of solid rocket propellant grains is the compressibility of the material expressed either as a Poisson's ratio or a Bulk Modulus. Measurement of these parameters however is very difficult and no standard tests have so far been defined. For convenience analysts use values ranging from 0.5 to 0.49 for the Poisson's ratio but in many cases no measurement is performed. In some instances Poisson's ratios are determined from the measurements of volume dilatation during uniaxial tensile tests using a double cavity gas dilatometer. In this way the Poisson's ratio can be determined as a function of strain for the uniaxial load situation. A typical result for the dilatation measurement is shown in Fig. 4.5. The precision of the measurements of the Poisson's ratio are not accurate enough to determine whether the Poisson's ratio is 0.49 or 0.495 although such a small difference may influence the results of the structural analysis especially in those cases where geometrical constraints are dominant.

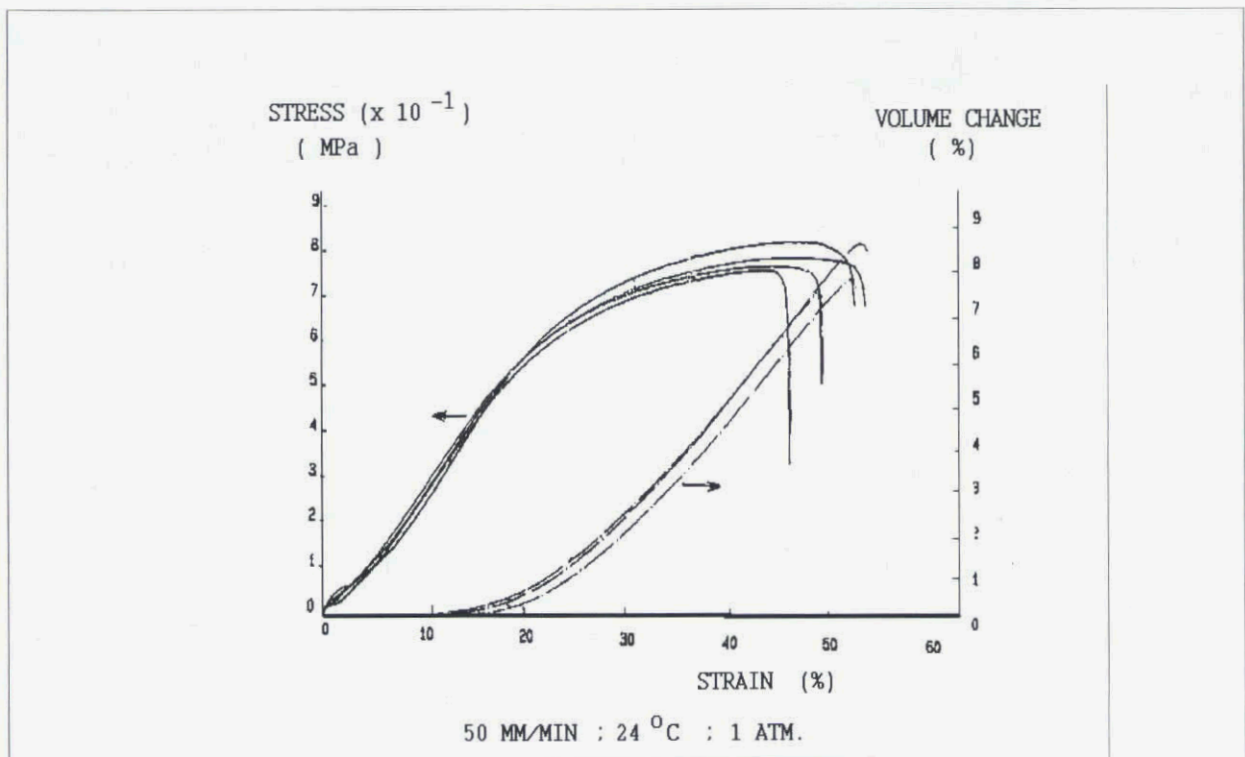


Figure 4.5: Typical results of dilatation measurements during uniaxial tensile tests.  
(Courtesy SNPE)

Another way of determining the compressibility of the propellant is by means of a Bulk Modulus measurement, like the one illustrated in Fig. 4.6. As before, no standard measurement procedure has been defined for the evaluation of this material property.

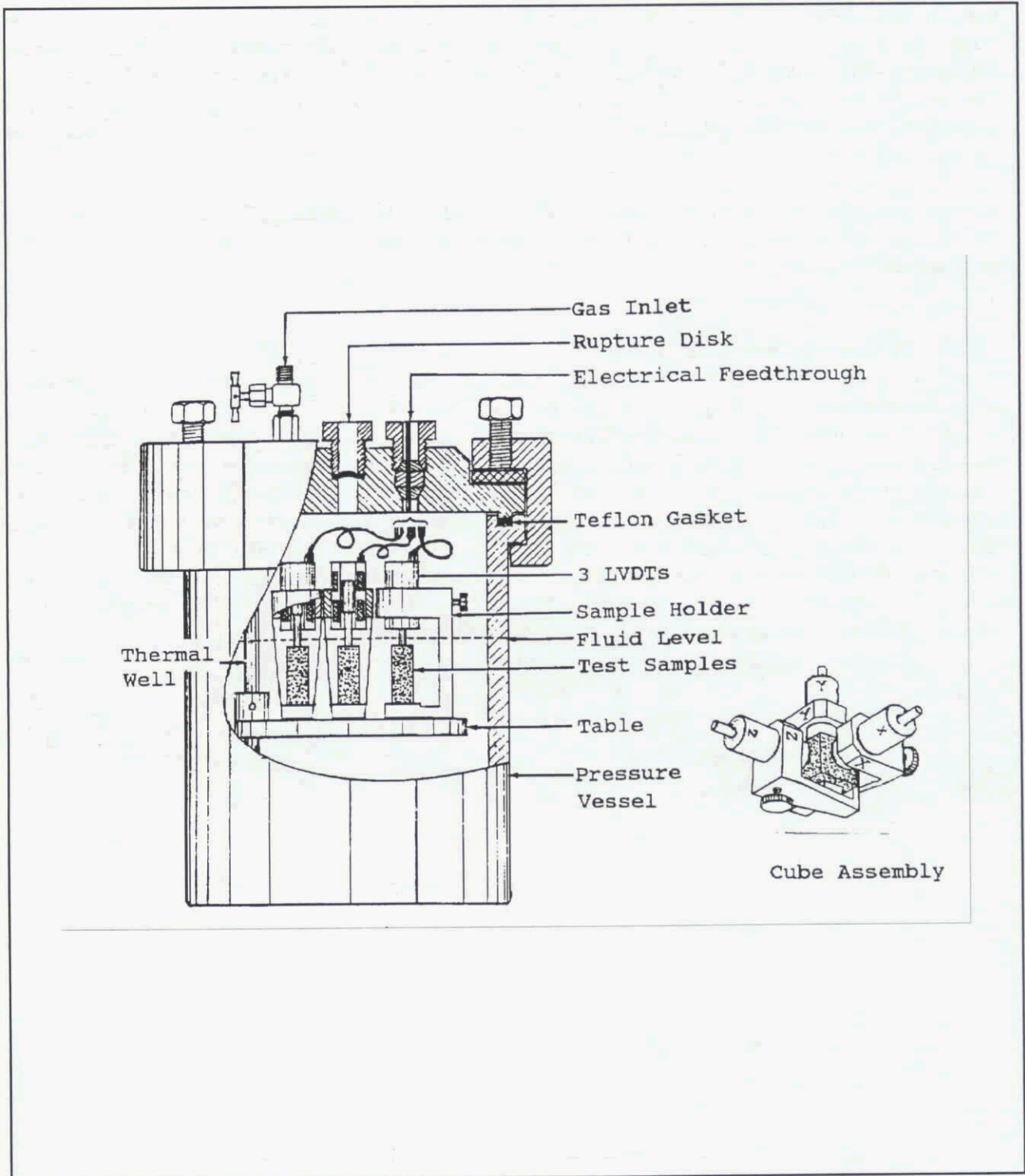


Figure 4.6: Bulk modulus measurement setup (Courtesy NAWC).

#### 4.2.1.3 Density

Densities for solid propellants are determined by immersion of propellant samples in suitable liquids like silicon oil in a so-called pycnometer, which is a glass vessel with an accurately defined volume. Masses are determined for the propellant sample, the empty pycnometer, the pycnometer filled with oil and the pycnometer filled with the sample plus oil. From the accurately defined volume of the pycnometer the density of the sample can be easily calculated. Another way of accurately measuring the density of a sample is through the use of a Helium densitometer. For the density measurement no (draft) STANAG is available at present.

#### 4.2.1.4 Coefficient of Linear Thermal Expansion

The coefficient of linear thermal expansion is measured via the change of length of a test sample with temperature. This so-called Thermo Mechanical Analysis or TMA is standardised in a (draft) STANAG by the AC310 working group. A typical result is shown in appendix 4.4 in the NATO AOP-7 data exchange format. Some companies determine expansion coefficients from Structural Test Vehicles or Analog Motors

#### 4.2.1.5 Thermal Conductivity

The thermal conductivity of propellant samples is derived from the temperature versus time measurements of two plates around a disk of propellant, with a heat source on one of the plates. Samples range for example from 5 mm thickness to 25 mm thickness. No (draft) STANAG is available for the thermal conductivity measurement at present.

### 4.2.2 Material Tests to Determine Failure Data.

Additional to the tests to determine the input data for the structural analysis that were described in the previous sections, tests also need to be performed to determine the failure properties of the propellant. Application of the failure prediction methodologies used in a structural integrity analysis of a solid rocket propellant grain is a complicated task involving many factors such as load conditions, loading history, previous damage and inherent material variability. These considerations will be reviewed in the chapters 5 and 6. Here the test methods are described which are used to determine propellant failure data that is used as a basis for performing the failure analysis. It is generally recognised that the failure properties critically depend on the load situations and these have an influence on the failure prediction. For reasons of economy the analyst usually has to rely on test data obtained under uniaxial or biaxial conditions. Using the so-called multi-axiality factors (see chapters 5 and 6) this failure data is modified to represent the actual multi-axial load situation. For very detailed analyses in critical areas or for trouble shooting purposes special multi-axially loaded samples may be used to generate the specific data.

#### *Uniaxial tensile test (STANAG 4506)*

Besides its use for the determination of stress-strain behaviour the already described uniaxial tensile test is also used to determine failure properties for the uniaxial tensile load case. Stress-strain curves are measured at various strain rates (between 0.01 /min. and 100 /s) and temperatures (as required, typically between -50° C and +60° C). Tests under hydrostatic pressure are also performed for the analysis of the ignition pressurisation condition. An example of uniaxial tensile test results under hydrostatic pressure is shown in Fig. 4.7.

The failure properties usually evaluated for use in the structural integrity analysis are the strain at maximum stress and the maximum stress. These quantities are obtained as a function of log reduced strain rate (i.e. strain rate multiplied by the shift factor  $a_T$ , determined from relaxation tests). An example of such a graph is given in Fig. 4.8.

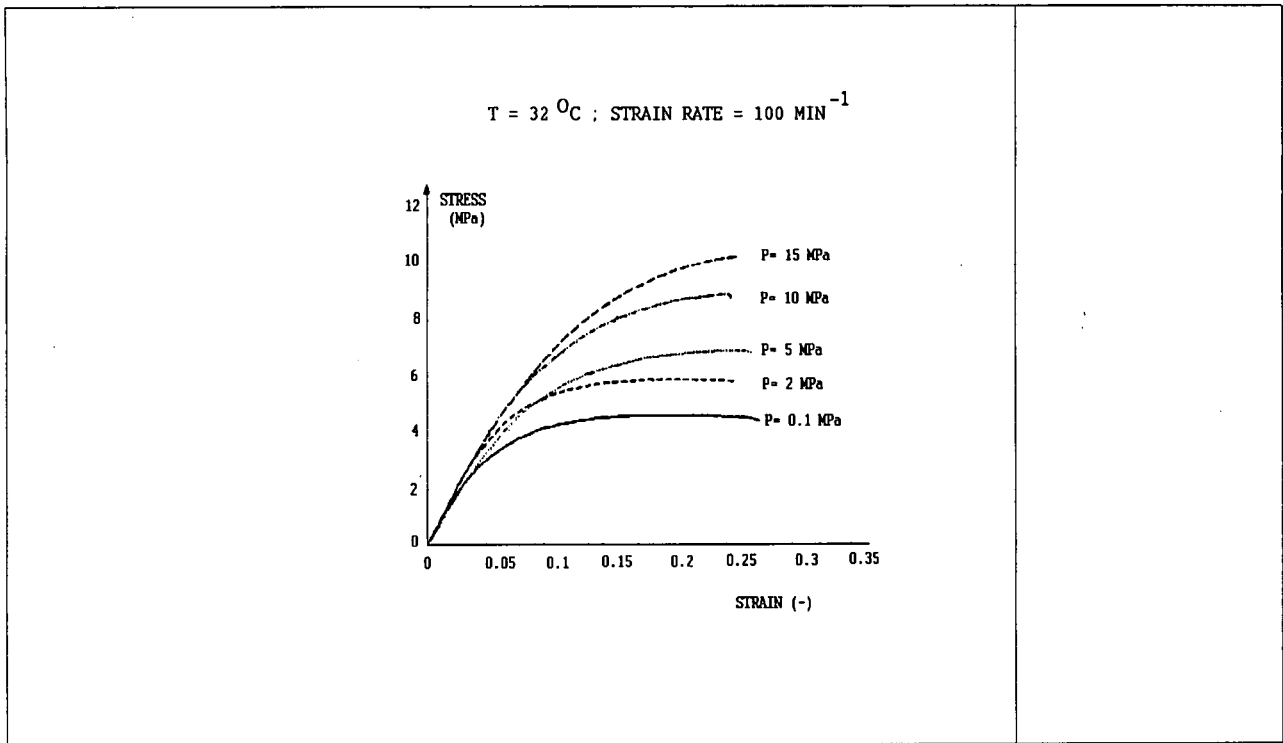


**Figure 4.7:** Example of uniaxial tensile test results under hydrostatic pressure.  
(Courtesy SNPE)

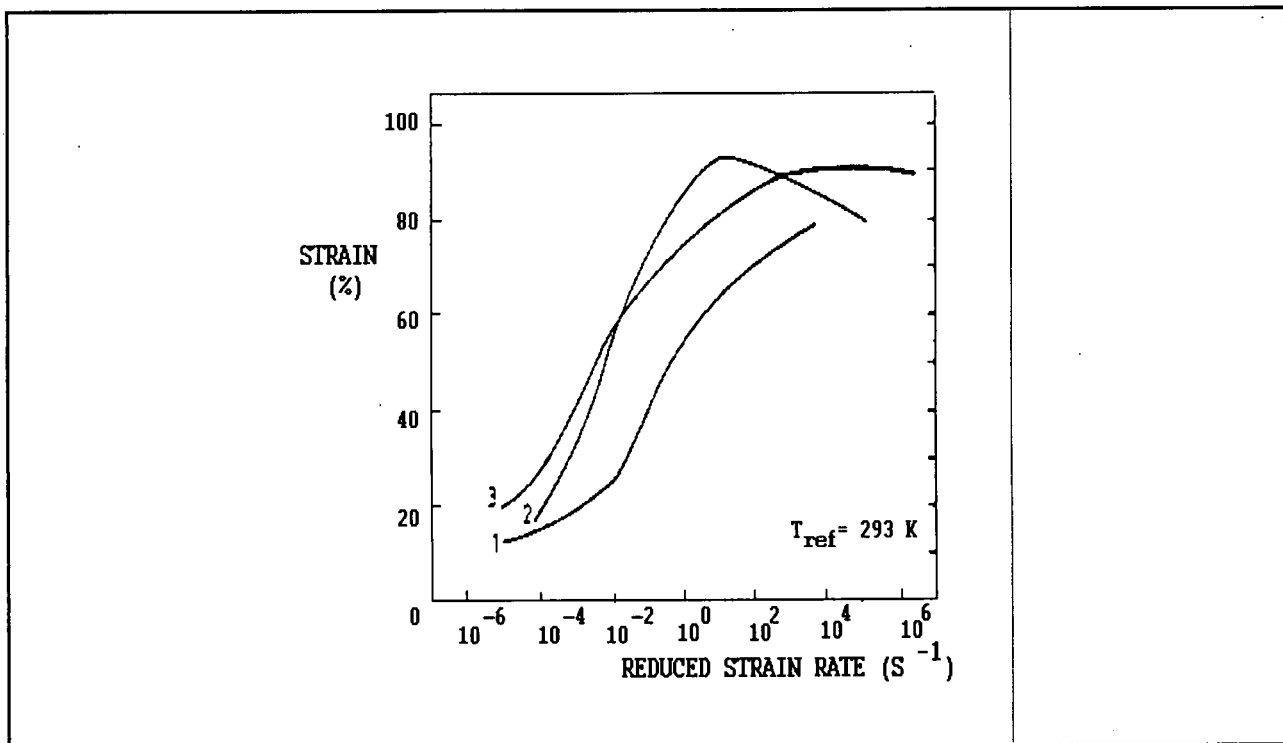


**Figure 4.8:** Strain at max. stress vs. reduced strain rate for three propellant batches  
(Courtesy TNO-PML)

### Strip biaxial test

The strip biaxial (tension-tension) test approximates the strain situation found at the inner bore of a cylindrical port motor under thermal cooling conditions or during pressurisation. The data obtained are therefore directly applicable to failure prediction in these cases. Use of this test has shown for many propellants that the biaxial failure strain data are smaller than those measured in uniaxial tension. This suggests that the performance of biaxial or multi-axial failure tests is necessary in order not to be optimistic in the Margin of Safety determination. The use of knockdown factors for multi-axial loading situations is described in chapters 5 and 6.

The strip biaxial test is a widely used experiment, but no standard has been reached. The test is usually performed at a constant crosshead speed and the load versus crosshead displacement is recorded for further treatment in the Margin of Safety determination. Tests are performed at various temperatures and displacement rates. A typical specimen configuration is shown in Fig. 4.9.

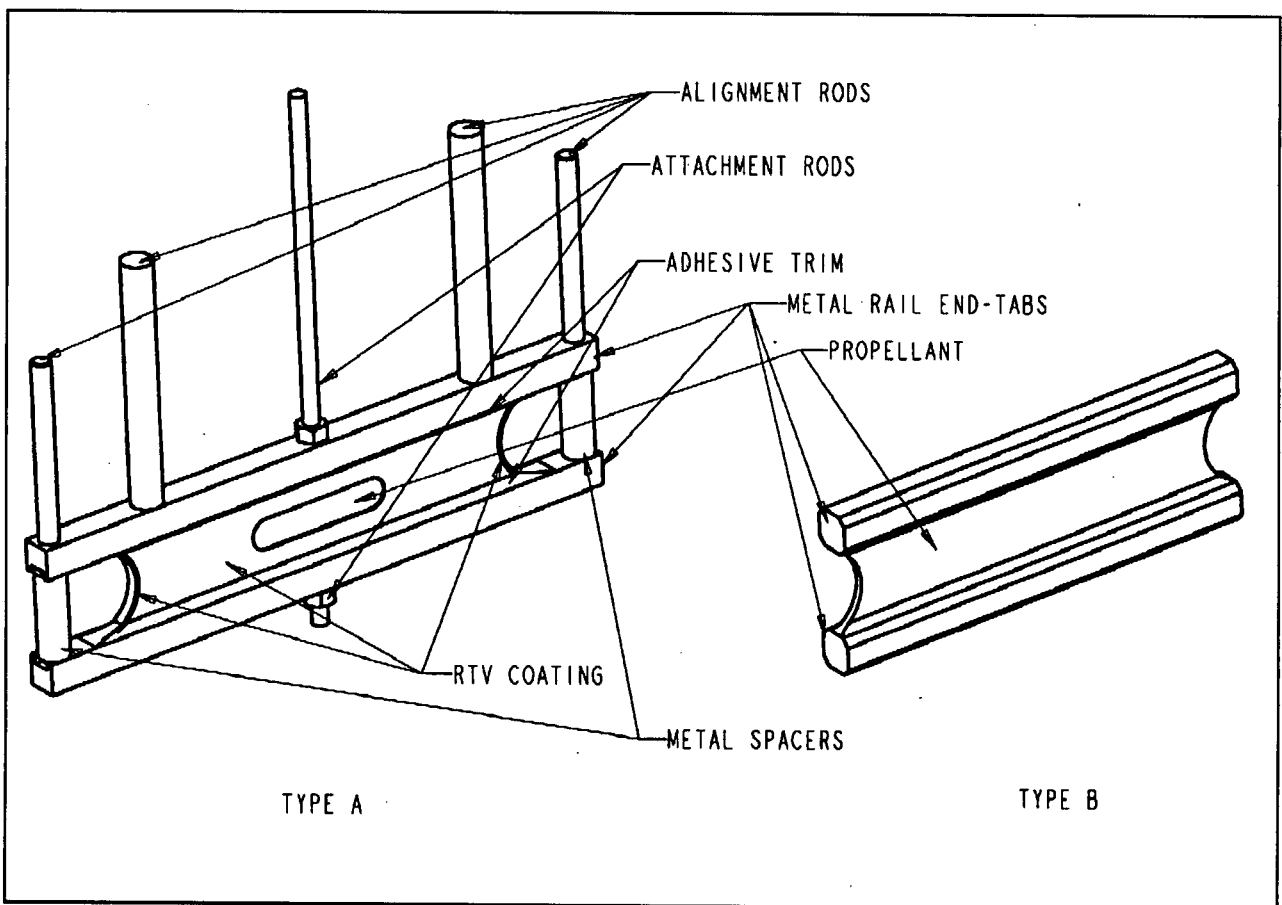


**Figure 4.9:** Pre-milled biaxial specimen post-bonded to aluminium end rails. Propellant surfaces are coated to achieve failure near the middle of the sample (type A) (Courtesy NAWC)

### Multi-axial tests

In order to be able to evaluate failure properties under multi-axial loadings and/or combined shear loads a wide variety of test samples are available from which a few are shown in Fig. 4.10. Although companies and government agencies have often standardised their own procedures internally, no universal standards have been achieved in this area. For the multi-axial test configuration the experimental tests are usually performed in a tensile test machine using a constant crosshead displacement speed. Force-displacement curves are recorded for further treatment in the Margin of Safety determination. Tests may be performed at various temperatures and displacement rates.

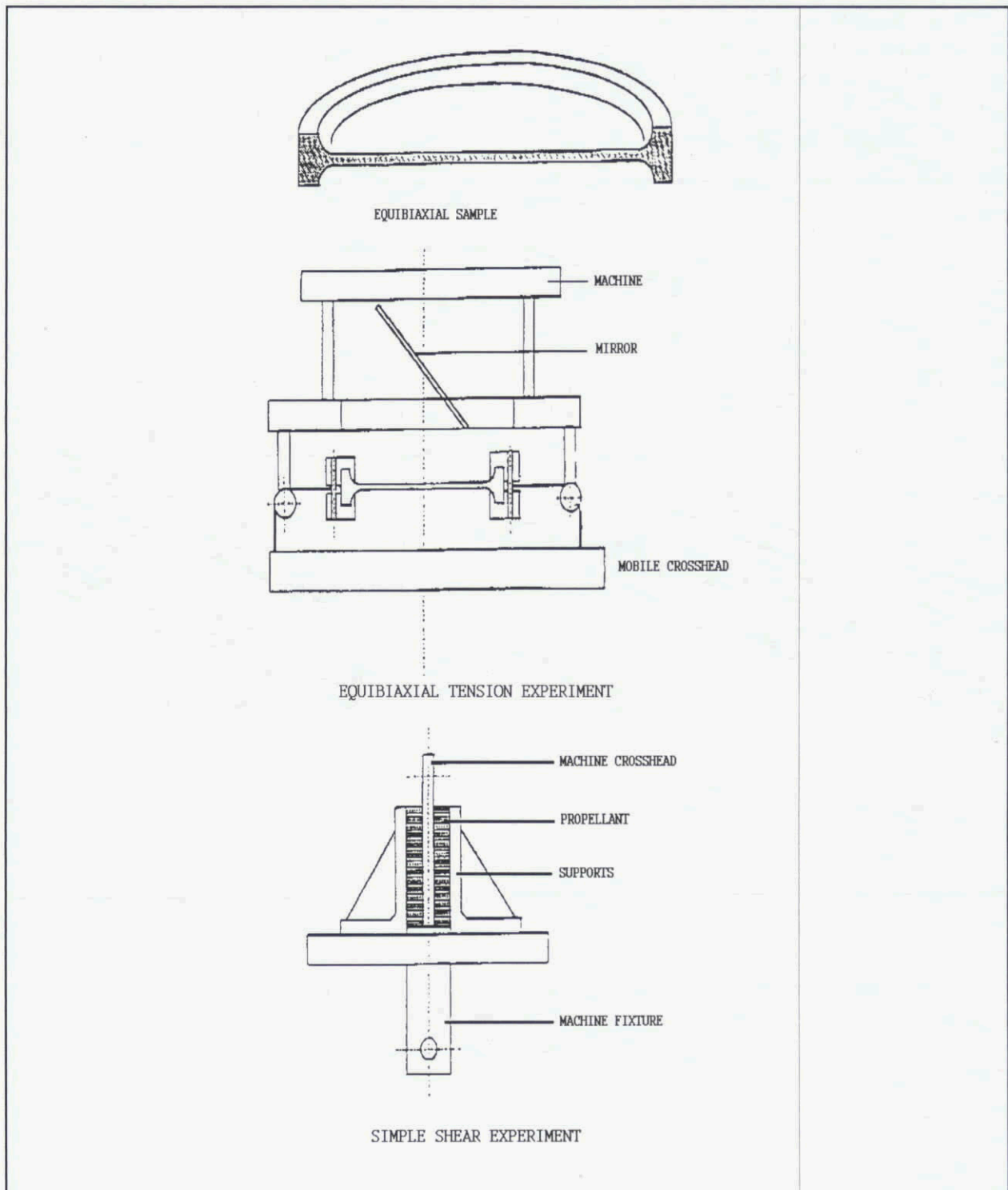


**Figure 4.10:** Examples of multi-axial and shear sample test specimen (Courtesy SNPE).

### Bond and Peel sample tests

Bonded area's of propellant, liners, insulators and casing material are of a special concern to the solid propellant rocket motor engineer. Problems in such area's are common failure modes for the complete motor. Knowledge of the bond strengths is therefore mandatory for the structural integrity analyst. In common with some of the previously discussed tests no standard has been reached so far for the bond and peel tests. Two typical examples of tensile bond samples are shown in Fig. 4.11. Samples are tested in a tensile machine usually at constant crosshead displacement rate. Load-displacement curves are recorded for further treatment in the Margin of Safety determination.

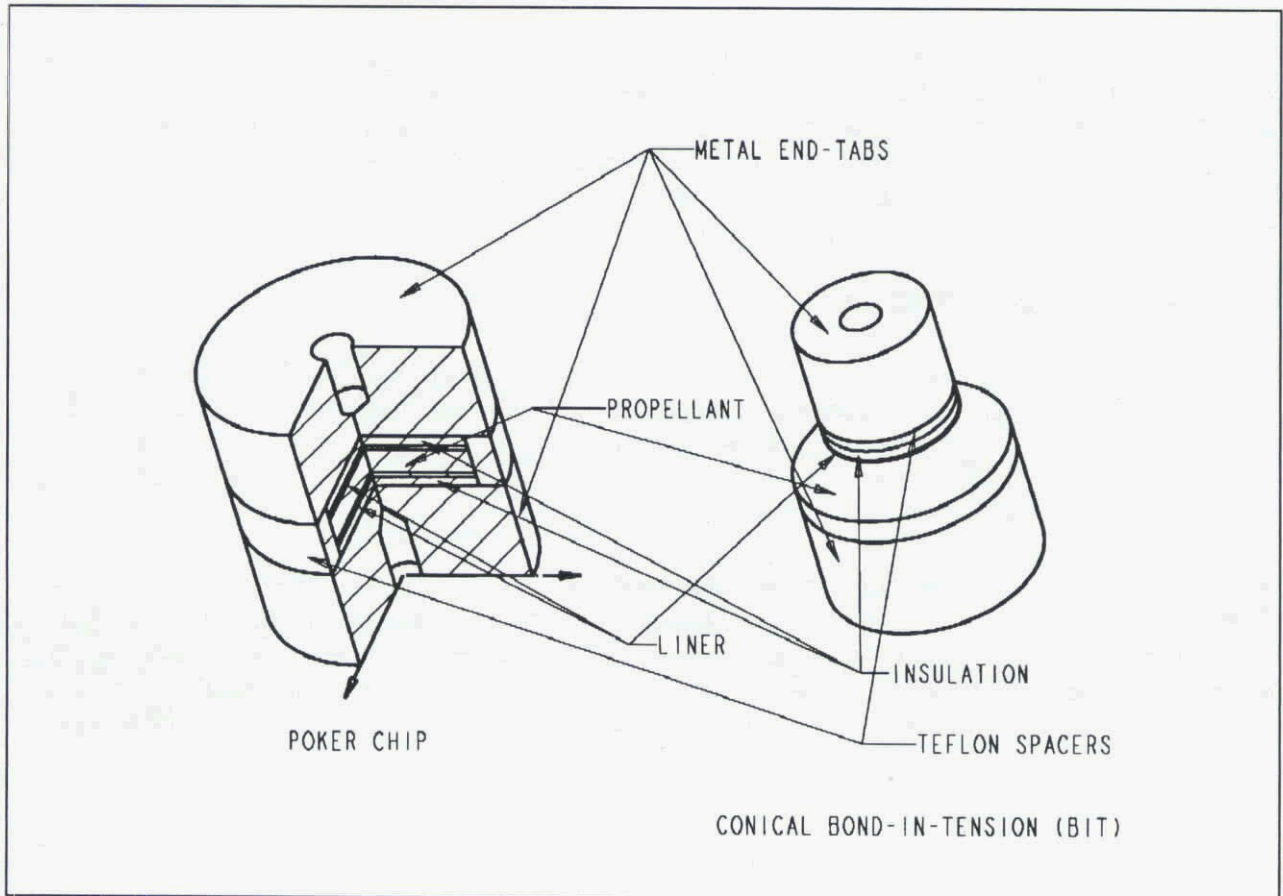


**Figure 4.11:** Conical Bond in Tension and Poker Chip test specimen (Courtesy NAWC).

### Endurance tests

As an alternative or in addition to the uniaxial tensile test at constant strain rate strain endurance tests may be performed in order to determine the strain capability of propellants at low deformation rates. A series of uniaxial tensile test samples is strained to a constant strain with an increasing level for each sample. Tests are performed at ambient temperature and the duration of the test is two weeks. The endurance strain is the lowest strain for which no failure of a sample has occurred. No standard has been reached for this test.

### 4.3 INERT MATERIALS

The stress-strain behaviour of inert materials used in a solid rocket motor play an important role in the response of the propellant grain to thermal and pressurisation loads. The same parameters mentioned previously in section 4.2.1 (stress-strain behaviour, Poisson's ratio, density, thermal expansion coefficient and thermal conductivity) have to be known in order to evaluate the deformation response of these materials using a structural analysis.

In the case of rubbery liner or insulation materials and metal case materials characterisation tests are often performed according to national or international standards. The ASTM handbook is a well known and widely used collection of such standards. In many instances the analyst may have to rely on handbook or manufacturer data.

A similar situation also exists for composite lamina motor cases. Material properties of fibres and polymeric matrix materials are determined using ASTM standard test procedures [3,4]. A micromechanical approach is used to determine the mechanical properties of the composite materials. Tests may also be performed using lamina / laminate coupons to directly determine the composite material properties. In such a case tests should be performed using the appropriate ply layups, as determined by the case design.

### 4.4 DEVIATIONS FROM LINEAR BEHAVIOUR

The assumption of linear visco-elastic behaviour in the material characterisation analysis, as used by most solid propellant rocket grain analysts, is known to be a simplification of the real propellant response. Non-linearities commonly observed in solid propellants [5] are the following:

- *Variation of Modulus with strain*

Fig. 4.12 shows nonlinear relaxation modulus data over the strain range of 1% to 20% at -50 °C. There is almost a 50% modulus change in going from the low strain data to the high strain data. Thermal strains in a solid propellant grain vary from almost zero at the case wall to 20% or higher at the bore regions (or star / slot tip regions). The effect of this strain variation is to induce a large modulus variation from the case wall to the high strain propellant regions. This variation can cause deviations from expected stresses at bond or bore regions.

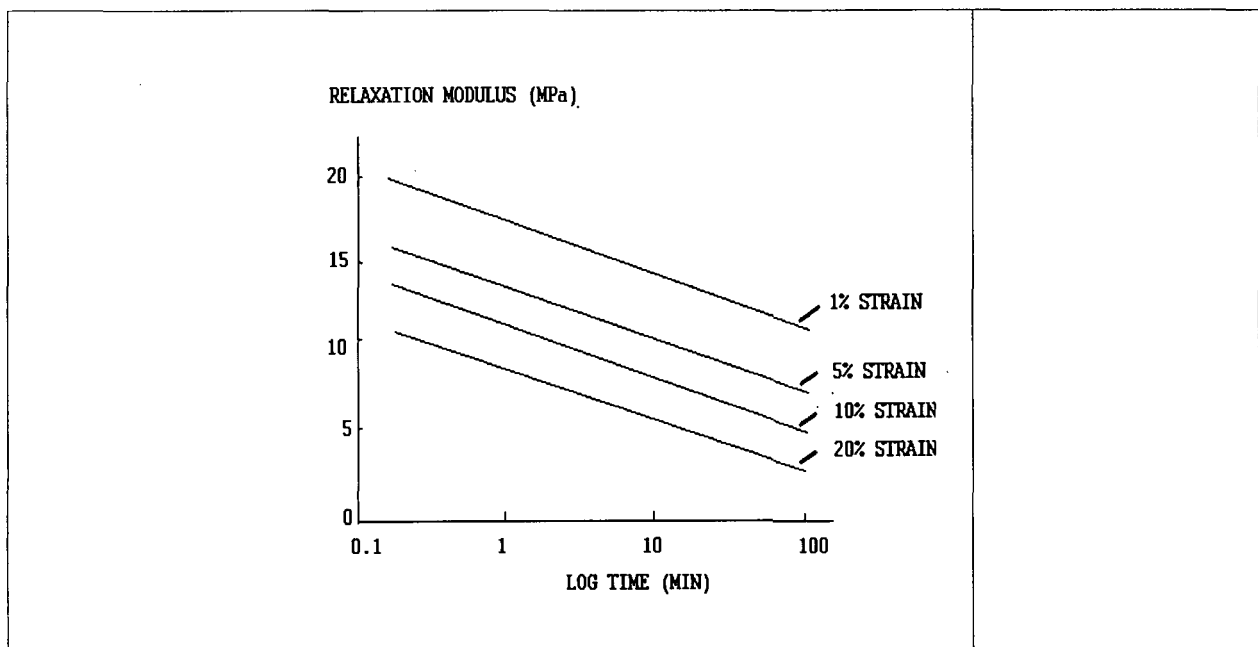


**Figure 4.12:** Solid propellant relaxation modulus data at different strain levels.  
(Courtesy E.C. Francis)

- *Variation of compressibility (volume change) with strain, dewetting*

Solid propellants routinely exhibit volume change during testing such as illustrated before in Fig. 4.5. This volume change has been attributed to dewetting or breakdown of the oxidiser-binder bond. This may partially be responsible for the modulus sensitivity, but the largest modulus changes occur before measurable uniaxial volume change is detected (less than 5% strain) as was already shown in Fig. 4.12

- *Combination of thermal and mechanical loads (not rheologically simple)*

For many solid propellants the result of a combination of thermal and mechanical loads is not easily predicted. Experimental verification is often needed to evaluate the response under such a combination of loads.

- *Change of Modulus by history (damage and rehealing)*

Solid propellants typically exhibit damage effects where unloading and reloading curves are significantly below the initial loading curve. Fig. 4.13 shows this effect for a bonded-end tensile bar exposed to a sawtooth strain history. Each time the strain history is reversed the stress (or modulus) response is only a fraction of the initial value. Each time the strain history exceeds the previous maximum strain level, the propellant tends to return to the virgin or undamaged curve. Some portion of the reduced modulus may be recovered if stored at an elevated temperature (Fig. 4.14) or it may tend to become a permanent set if stored in the strained state for a long period.

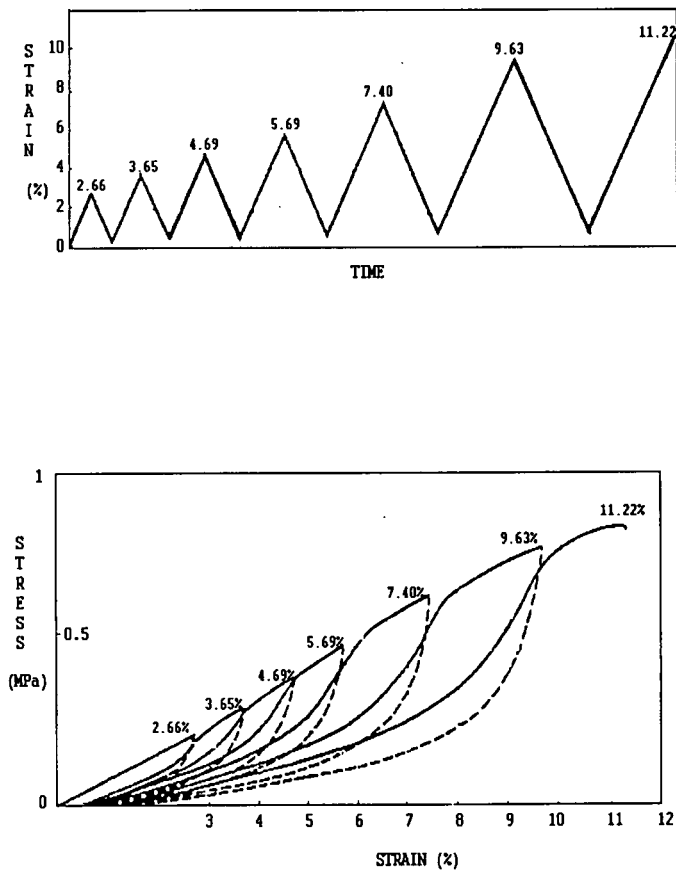


Figure 4.13: Stress-strain response showing damage effects for sawtooth strain history. (Courtesy E.C. Francis)

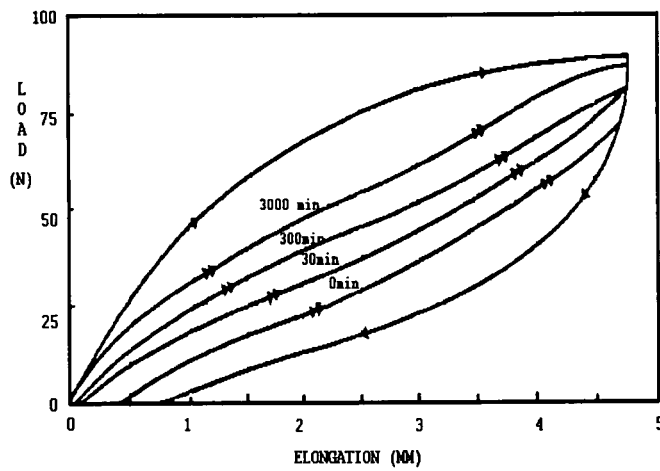
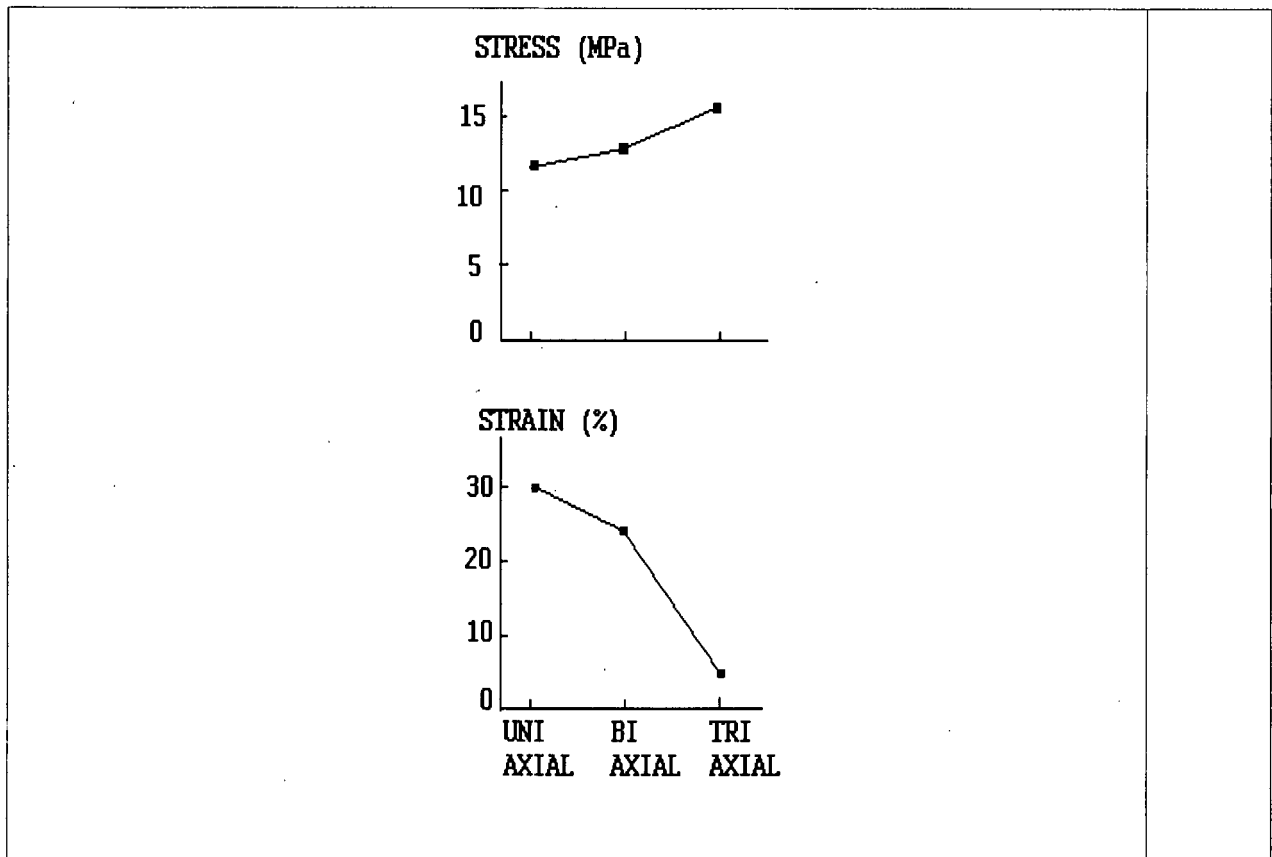


Figure 4.14: Healing effect for solid propellant (Courtesy E.C. Francis).

The stress axiality in solid rocket propellant grains is nearly always triaxial instead of uniaxial. Triaxial poker chip tests exhibit a much higher modulus than uniaxial or biaxial laboratory tests. Failure properties tests presented in Fig. 4.15 show a significant drop off in triaxial strain capability (4% versus 30%) for a composite solid propellant. Although the axiality effect itself is not a material non-linearity effect it is noticed that the effect of non-linear material behaviour is exaggerated by axiality.



**Figure 4.15:** Comparison of example propellant uni-, bi- and tri-axial tension failure data. (Courtesy E.C. Francis)

Although analysts are quite aware of the non-linearities mentioned, compensations are usually made in the form of knockdown factors to the results of calculations or measurements. The observed deviations from linear behaviour are such that it seems worthwhile to consider extending the scope of existing test methods and standards for the measurement of non-linearities. Already mentioned is the measurement of Poisson's ratio as a function of strain using double cavity dilatometers. The test equipment is readily available in the propellant industry and research laboratories but no standard approach to the use of data is defined. Special equipment for simultaneous cooling and straining was designed by some solid propellant manufacturers but again no universal approach appears to have been adopted. The same applies to the investigations of damage and strain level influence, load and unload tests and cyclic loading tests, which have not been advanced beyond the research stage.

It is recommended by the AGARD Working Group 25 that test standards for describing the non linear material behaviour of solid rocket propellants should be pursued. The results of such characterisations can either be used for a better evaluation of linear elastic or linear visco-elastic analysis or for the input of yet to be qualified non-linear analyses methods.

## 4.5 REFERENCES

- [1] Ferry, J. D.: **Visco-elastic properties of polymers**, J. Wiley 3rd edition (1980)
- [2] *Qualification and Documentation of Explosive Material for Military Use, Annex I, Section 102.01, Physical (including Mechanical) Properties Tests* , **Allied Ordnance Publication No. 7 (AOP-7)**
- [3] *Test for tensile properties of oriented fibre composites*, **ASTM D3039**
- [4] *Standard test method for compressive properties of unidirectional or crossply fibre resin composites*, **ASTM D3410**
- [5] Francis, E. C.;Thompson, R. E.: *Non linear structural modelling of solid propellants*. AIAA 84-1290.

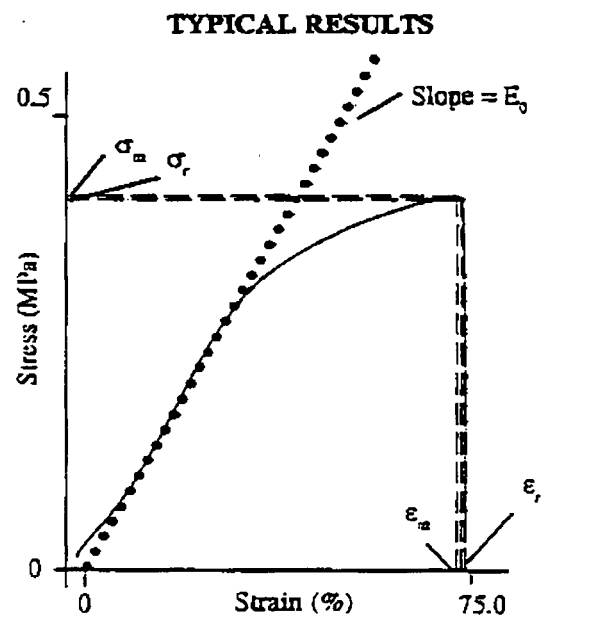
APPENDIX 4.1

NATO AOP-7 DATA EXCHANGE FORMAT																	
Report Reference Number: JM001	Stress Relaxation Test <i>(Sample Sheet)</i>																
Page <u>1</u> of <u>2</u> Page(s)																	
<b>TEST SITE INFORMATION</b> Laboratory: PML-TNO Date: 23/05/91 Test Procedure: Uniaxial Tensile Stress Relaxation NATO Test Procedure Number: 102.01.003 Date Tested: 26/03/91	<b>TEST CONDITIONS</b> Temperature (°C): -40 Relative Humidity (%): <30 Strain Rate (s <sup>-1</sup> ): 0.01      Strain (%): 10 Machine Type: Zwick 1445      Active Strain Control Grip Type: NA      Yes <input type="checkbox"/> No <input checked="" type="checkbox"/>																
SPECIMEN INFORMATION																	
Dimensions: Length (Gage Length): 50.0 (mm)      Width: 8.82 Thickness (Diameter): 12.81 X-Sectional Area (mm <sup>2</sup> ): 113.0  Form: Untabbed Dogbone Preparation Method: Milling Manufacturing Method: Cast Source: PML-TNO Lot or ID Number: CK-3025-38-4 Conditioning Period: 1 hr	Name: MX-B5 Composition: <table style="width: 100%; border-collapse: collapse;"> <thead> <tr> <th style="text-align: left; border-bottom: 1px solid black;">Component</th> <th style="text-align: left; border-bottom: 1px solid black;">Percent</th> </tr> </thead> <tbody> <tr> <td style="border-bottom: 1px solid black;">AN</td> <td style="border-bottom: 1px solid black;">69</td> </tr> <tr> <td style="border-bottom: 1px solid black;">Fillers</td> <td style="border-bottom: 1px solid black;">12</td> </tr> <tr> <td style="border-bottom: 1px solid black;">MTPB</td> <td style="border-bottom: 1px solid black;">12</td> </tr> <tr> <td style="border-bottom: 1px solid black;">IDP</td> <td style="border-bottom: 1px solid black;">7</td> </tr> <tr> <td style="border-bottom: 1px solid black;">Total</td> <td style="border-bottom: 1px solid black;">100</td> </tr> <tr> <td style="border-bottom: 1px solid black;"> </td> <td style="border-bottom: 1px solid black;"> </td> </tr> <tr> <td style="border-bottom: 1px solid black;"> </td> <td style="border-bottom: 1px solid black;"> </td> </tr> </tbody> </table>	Component	Percent	AN	69	Fillers	12	MTPB	12	IDP	7	Total	100				
Component	Percent																
AN	69																
Fillers	12																
MTPB	12																
IDP	7																
Total	100																
TYPICAL RESULTS																	

APPENDIX 4.1

NATO AOP-7 DATA EXCHANGE FORMAT						
Report Reference Number: JM001		Stress Relaxation Test <i>(Sample Sheet)</i>			Page <u>2</u> of <u>2</u> Page(s)	
Test ID: RE - 910326-02						
Data Disk ID:		File ID:		Format:		
Options: $E_t = \frac{\sigma}{\epsilon}$ or <del><math>E_t = \frac{\sigma}{\epsilon}(1 + e)</math></del> $t' = t - \underline{0.5 s}$						
Comments: One Specimen Only.						
Shifted Time (s) vs Relaxation Modulus (MPa)						
t' (s)	Specimen 1	Specimen 2	Specimen 3	Specimen 4	Specimen 5	Average
0	-					
1	-					
10	27.0					
20	23.0					
50	21.4					
100	19.9					
200	18.9					
500	17.0					
600	16.5					
Data Sent to: Rob Lieb, AMSRL-WT-PE Aberdeen Proving Ground, MD 21005-5066 USA						

APPENDIX 4.2

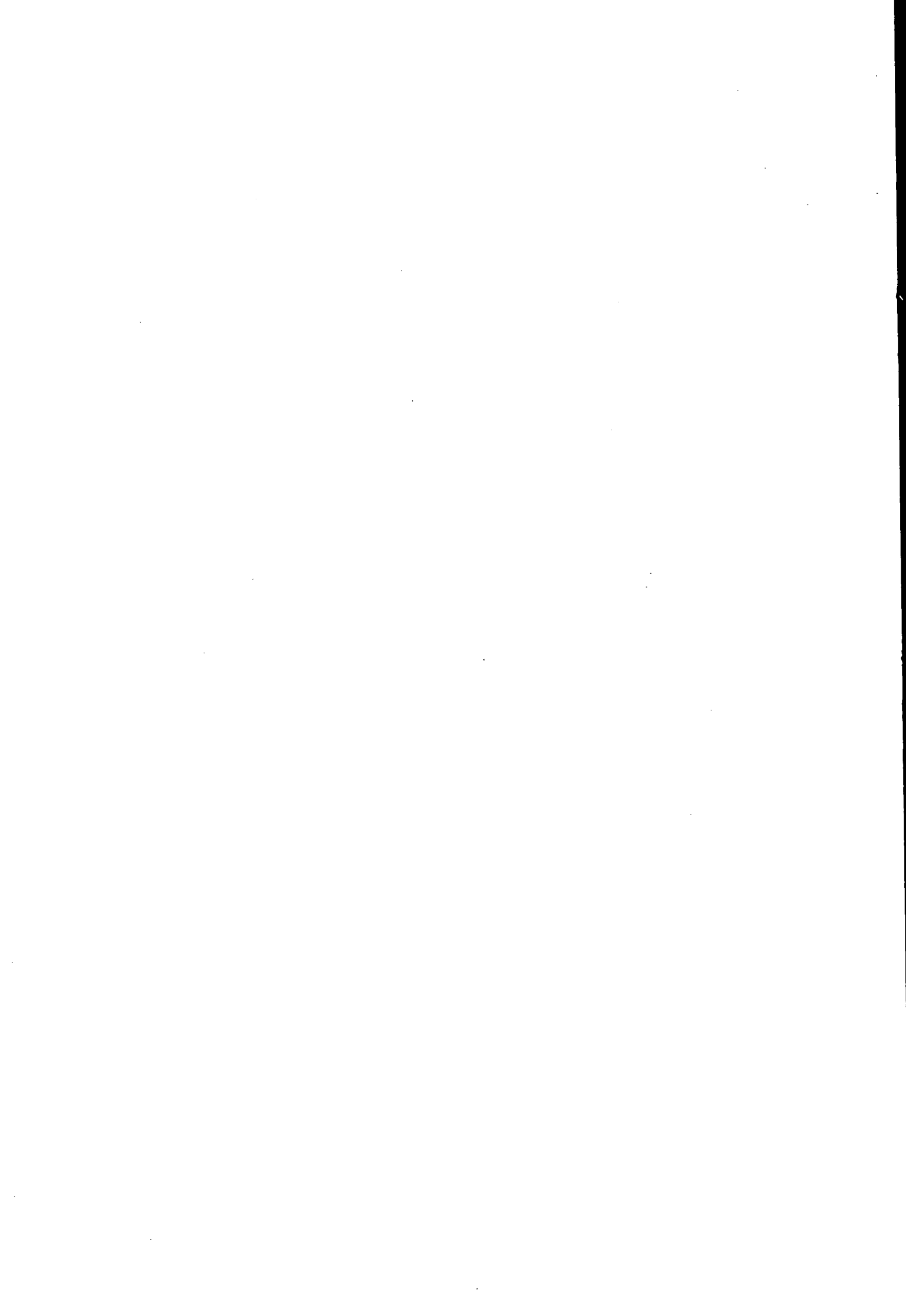
NATO AOP-7 DATA EXCHANGE FORMAT																							
Report Reference Number: AGE-1			Uniaxial Tensile Test <i>(Sample Sheet, Tensile)</i>					Page <u>1</u> of <u>1</u> Page(s)															
<b>TEST SITE INFORMATION</b> Laboratory: Naval Ordnance Station Date: 5 Nov 90 Test Procedure: Uniaxial Tensile Test NATO Test Procedure Number: 102.01.001 Date Tested: 31 Aug 89 POC: Frank Tse						<b>TEST CONDITIONS</b> Temperature (°C): 23.9      Extensometer Relative Humidity (%): 50      Yes <input type="checkbox"/> No <input checked="" type="checkbox"/> X-Head Speed (mm/sec): 0.847 Machine Type: Instron AMT System v4.05a Grip Type: JANNAF Dogbone Machine Stiffness (kN/mm): 257																	
<b>SPECIMEN INFORMATION</b> Dimensions: Length (Gage Length): 68.58 (mm)      Width: 8.46 Thickness (Diameter): 12.57 X-Sectional Area (mm <sup>2</sup> ): 106.34 Form: JANNAF Class C Dogbone Preparation Method: Stamped Manufacturing Method: Cast Source: NOSIH Lot or ID Number: DVT-1 Conditioning Period: None Composition: MK-6 <table style="width:100%; margin-top: 10px;"> <tr> <td style="width: 50%;">Component</td> <td style="width: 50%;">Percent</td> </tr> <tr> <td>Not Available</td> <td>_____</td> </tr> <tr> <td>_____</td> <td>_____</td> </tr> <tr> <td>_____</td> <td>_____</td> </tr> <tr> <td>_____</td> <td>_____</td> </tr> <tr> <td>_____</td> <td>_____</td> </tr> </table>						Component	Percent	Not Available	_____	_____	_____	_____	_____	_____	_____	_____	_____	<b>TYPICAL RESULTS</b> 					
Component	Percent																						
Not Available	_____																						
_____	_____																						
_____	_____																						
_____	_____																						
_____	_____																						
Test ID	Specimen T      A <sub>n</sub> (°C)    (mm <sup>2</sup> )		ε (s <sup>-1</sup> )	σ <sub>m</sub> (MPa)	ε <sub>m</sub> (%)	σ <sub>r,orp</sub> (MPa)	ε <sub>r,orp</sub> (%)	E <sub>0</sub> (MPa)	ε <sub>m</sub> (Direct) (%)	ε <sub>r,orp</sub> (Direct) (%)	E <sub>0</sub> (Direct) (MPa)												
1	24	104.5	0.012	0.394	65.2	0.392	66.8	1.08															
2	24	106.3	0.012	0.403	67.1	0.401	67.8	1.17															
3	24	107.4	0.012	0.437	63.6	0.429	65.4	1.32															
4	24	106.5	0.012	0.415	67.2	0.406	67.8	1.13															
5	24	105.8	0.012	0.403	69.7	0.397	71.2	1.10															
Average			0.012	0.410	66.5	0.405	67.8	1.16															
(σ <sub>(σ-1)</sub> )				0.016	2.34	0.015	2.2	0.10															
Data Sent To: Bernard Gondouin, SNPE 6 Boucher 91710 Vert le Petit, France						Comments:																	

## APPENDIX 4.3

NATO AOP-7 DATA EXCHANGE FORMAT																					
Report Reference Number: RL00A1		Dynamic Mechanical Analysis (Sample Sheet)			Page 1 of 1 Page(s)																
<b>TEST SITE INFORMATION</b> Laboratory: USA Ballistic Research Laboratory Date: 28 Oct 88 Test Procedure: Dynamic Mechanical Analysis AOP-7 Test Procedure Number: 102.01.025 Date Tested: 28 Jul 86				<b>TEST CONDITIONS</b> Initial/Final Temperature (°C): -60/35 Iso Temperature & Time (°C & min): NA & Osc Amp (mm): 0.20 Frequency(Hz): 62/43 Temperature Rate (°C/min): 2 Machine Type: DuPont 982 Grip Type: Notched V Test Type: Flexure																	
<b>SPECIMEN INFORMATION</b> Dimensions: Length: 38.53 (mm) Width: _____ Thickness (Diameter): (4.29) Length Correction: 0.72 Form: Solid Stick Preparation Method: Diamond Saw Manufacturing Method: Solvent Extrusion Source: Radford Army Amunition Plant Lot or ID Number: RAD81E001S110 Conditioning History: NA Composition: JA2 <table border="1" style="width: 100%; margin-top: 5px;"> <thead> <tr> <th>Component</th> <th>Percent</th> </tr> </thead> <tbody> <tr> <td>Nitrocellulose</td> <td>59.5</td> </tr> <tr> <td>Nitroglycerin</td> <td>14.9</td> </tr> <tr> <td>DEGDN</td> <td>24.8</td> </tr> <tr> <td>Akardit II</td> <td>0.70</td> </tr> <tr> <td>_____</td> <td>_____</td> </tr> <tr> <td>_____</td> <td>_____</td> </tr> </tbody> </table>				Component	Percent	Nitrocellulose	59.5	Nitroglycerin	14.9	DEGDN	24.8	Akardit II	0.70	_____	_____	_____	_____	<b>RESULTS</b> 			
Component	Percent																				
Nitrocellulose	59.5																				
Nitroglycerin	14.9																				
DEGDN	24.8																				
Akardit II	0.70																				
_____	_____																				
_____	_____																				
T (°C)	E' (GPa)	E'' (GPa)	G' (GPa)	G'' (GPa)	Tan δ	f (Hz)	Comments:														
-60	3.79	0.71			0.008	62.3															
-50	3.71	0.75			0.010	61.5															
-40	3.55	0.87			0.020	60.4															
-30	3.26	1.23			0.044	58.3															
-20	2.95	1.35			0.068	56.0															
-10	2.66	1.55			0.086	53.6															
0	2.38	1.35			0.064	51.2															
10	2.14	1.24			0.052	48.8															
20	1.94	1.16			0.036	45.9															
30	1.77	1.05			0.015	44.9															
Data Sent To: Bernard Gondouin, SNPE 6 Bouchet 91710 Vert le Petit, France					T <sub>g</sub> = -10 °C at 53.6 Hz																

APPENDIX 4.4

NATO AOP-7 DATA EXCHANGE FORMAT																		
Report Reference: Number: RL00A1		Thermomechanical Analysis <i>(Sample Sheet)</i>		Page <u>1</u> of <u>1</u> Page(s)														
<b>TEST SITE INFORMATION</b> Laboratory: USA Ballistic Research Laboratory Date: 9 Nov 90 Test Procedure: Thermomechanical Analysis AOP-7 Test Procedure Number: 102.01.060 Date Tested: 28 Jul 86		<b>TEST CONDITIONS</b> Initial Temperature (K): 150 Final Temperature (K): 350 Temperature Rate (K/min): 5 Machine Type: DuPont TA 942 Probe Mass (g): 2 g Probe Type: Flat																
<b>SPECIMEN INFORMATION</b> Dimensions: Length: 8.70 (mm) Width: Thickness (Diameter): (8.70) T (K): 295 Form: TMP Preparation Method: Diamond Saw - L/D=1 Manufacturing Method: Solventless Extrusion Source: Radford Army Amunition Plant Lot or ID Number: RAD81E001S110 Preconditioning: NA Conditioning Period: NA Composition: JA2 <table style="width:100%; margin-top: 10px;"> <tr> <td style="text-align: left;">Component</td> <td style="text-align: right;">Percent</td> </tr> <tr> <td><u>Nitrocellulose</u></td> <td style="text-align: right;"><u>59.5</u></td> </tr> <tr> <td><u>Nitroglvcerin</u></td> <td style="text-align: right;"><u>14.9</u></td> </tr> <tr> <td><u>DEGDN</u></td> <td style="text-align: right;"><u>24.8</u></td> </tr> <tr> <td><u>Akardit II</u></td> <td style="text-align: right;"><u>0.70</u></td> </tr> <tr> <td>_____</td> <td>_____</td> </tr> <tr> <td>_____</td> <td>_____</td> </tr> </table>		Component	Percent	<u>Nitrocellulose</u>	<u>59.5</u>	<u>Nitroglvcerin</u>	<u>14.9</u>	<u>DEGDN</u>	<u>24.8</u>	<u>Akardit II</u>	<u>0.70</u>	_____	_____	_____	_____	<b>RESULTS</b> 		
Component	Percent																	
<u>Nitrocellulose</u>	<u>59.5</u>																	
<u>Nitroglvcerin</u>	<u>14.9</u>																	
<u>DEGDN</u>	<u>24.8</u>																	
<u>Akardit II</u>	<u>0.70</u>																	
_____	_____																	
_____	_____																	
T (K)	ΔT (K)	$\times 10^{-2}$ $\Delta L/L_0$	$\times 10^{-4}$ $\alpha$ (K <sup>-1</sup> )	Comments:														
250		1.13	8.03	Unknown transition between 210 and 250 K.														
260	10	1.86	8.27															
270	20	2.68	8.39															
280	30	3.46	8.70															
290	40	4.46	8.63															
300	50	5.33	8.65															
310	60	6.10	8.69															
320	70	7.07	8.68															
Data Sent To: Bernard Gondouin, SNPE 6 Bouchet 91710 Vert le Petit, France			$\bar{\alpha} = 8.65 \times 10^{-4} \text{ K}^{-1}$		$280 < T < 320 \text{ K}$													

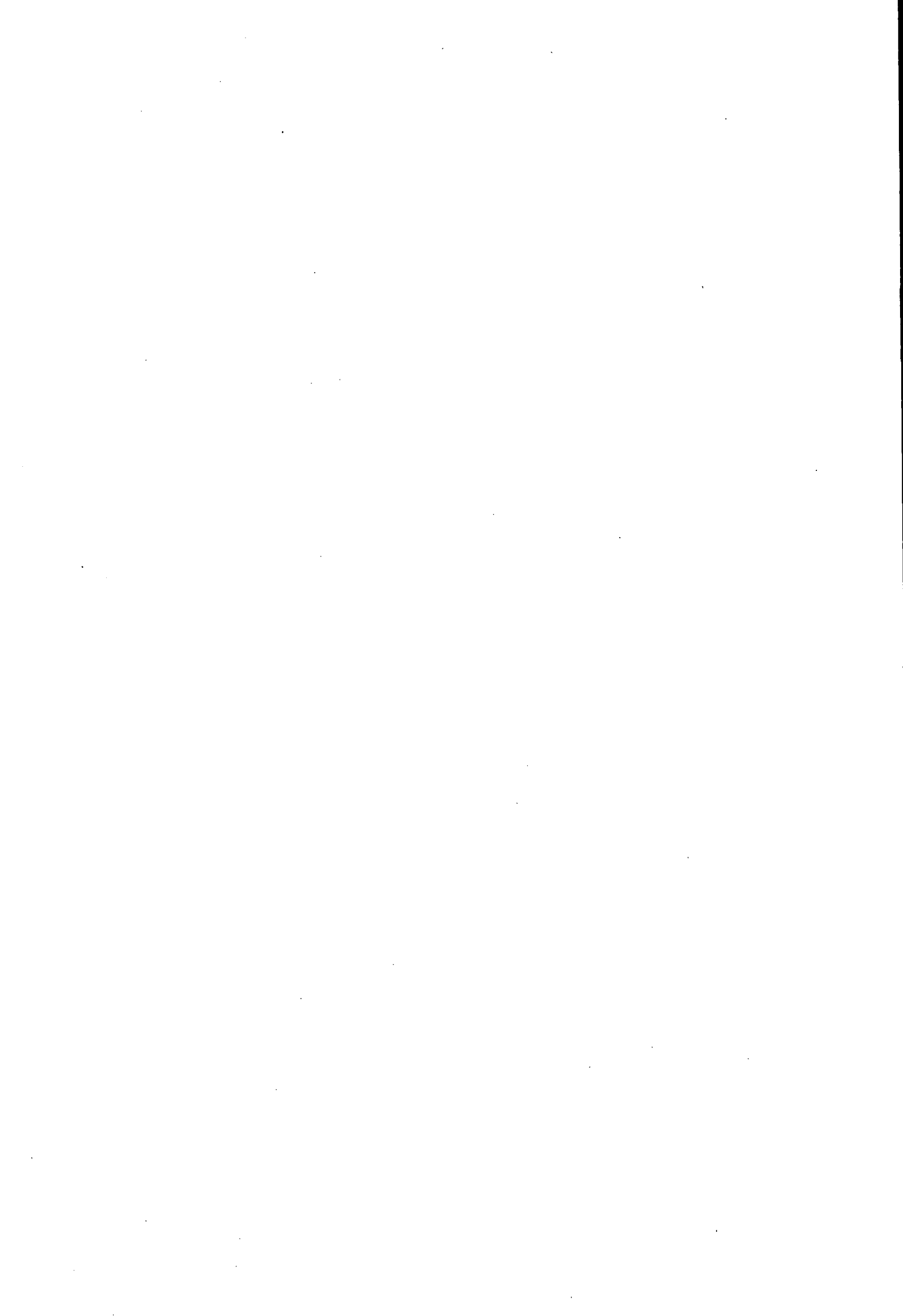


# CHAPTER 5

## FAILURE CRITERIA

### TABLE OF CONTENTS

<b>5.1</b>	<b>INTRODUCTION</b>	<b>5-1</b>
<b>5.2</b>	<b>FAILURE TYPES</b>	<b>5-2</b>
5.2.1	Surface Macro-Cracks	5-2
5.2.2	Debonding of Interfaces Propellant/Liner/Insulator/Case	5-4
5.2.3	Dewetting (Dilatation)	5-6
5.2.4	Excessive Deformation	5-7
<b>5.3</b>	<b>FAILURE CRITERIA AND THEIR APPLICATIONS</b>	<b>5-8</b>
5.3.1	General Definitions	5-9
5.3.2	Maximum Principal Strain Criterion	5-11
5.3.3	Effective Strain Criterion	5-12
5.3.4	Maximum Normal Stress Criterion	5-13
5.3.5	Effective Stress Criterion	5-13
5.3.6	Maximum Deviatoric Stress Criterion	5-13
5.3.7	Strain Energy Criterion	5-14
5.3.8	Stassi/Mises Failure Envelope	5-14
5.3.9	Smith Failure Envelope	5-16
5.3.10	Endurance Strain Based Criteria	5-16
5.3.11	Comparison of Application Profiles for Various Failure Criteria	5-17
<b>5.4</b>	<b>MULTI-AXIALITY (STRESS STATE) CONSIDERATIONS</b>	<b>5-17</b>
<b>5.5</b>	<b>SUCCESSIVE LOADING (DAMAGE)</b>	<b>5-18</b>
<b>5.6</b>	<b>FRACTURE MECHANICS</b>	<b>5-19</b>
5.6.1	Brittle Fracture Mechanics	5-19
5.6.2	Inelastic and Viscoelastic Crack Propagation	5-20
<b>5.7</b>	<b>REFERENCES</b>	<b>5-22</b>
	<b>APPENDIX A</b> Comparison of Some Failure Criteria for Double Base Propellants	<b>5-24</b>



## Chapter 5

### FAILURE CRITERIA

#### 5.1 INTRODUCTION

Any structural malfunctioning which deters the solid propellant rocket grain from performing its mission can be named as *failure of the solid propellant rocket grain* [1]. One important intermediate step of the structural integrity analysis of solid propellants is to determine whether failure will occur and, if not, how far the given state of the propellant grain is from a failure state. Ordinarily, this question is answered for a specific environmental condition (i.e., for a given *instant* of time in the life of the motor) and usually for simple loading. In this case, it is assumed that the capacity of the propellant is specified. On the other hand, advance applications require to answer the above question over a range of time (varying environmental conditions), for instance, to predict the service life of the solid propellant. Although, the prediction and evaluation of some failure types is rather straight-forward, some important failure modes like fracture require so-called *failure criteria* (for the prediction of onset of failure) or *failure theories* (for the modelling of crack-propagation) for this purpose. For given instants of time, the margin of safety (Chapter 6: Margin of Safety) is computed based on these failure criteria (theories) using the induced (predicted) state of the propellant as determined from the structural analysis (Chapter 3: Structural Analysis) and the ultimate states (capacity) of the propellant at given times (Chapter 4: Material Characterization). Service life estimation requires additionally the consideration of long-term aging of material properties as well as combined and successive loading effects (topic not addressed within the scope of this report). All evaluations can be performed *deterministic* (specifying a certain number like the margin of safety) or *probabilistic* (specifying a level of reliability).

The aim of this chapter is to discuss the basic failure theories and their applications which are commonly used by the NATO countries contributing to this report. Firstly, the different types of failure will be covered in Section 5.2. In Section 5.3, various failure criteria will be given together with the parameters required from the structural analysis as well as the ultimate material properties as required from material characterization tests. Detailed description of the experimental tests to gather failure data has been already covered in Chapter 4 (Material Characterization). It must be emphasized that the application of failure criteria depends on various factors, Fig. 5.1:

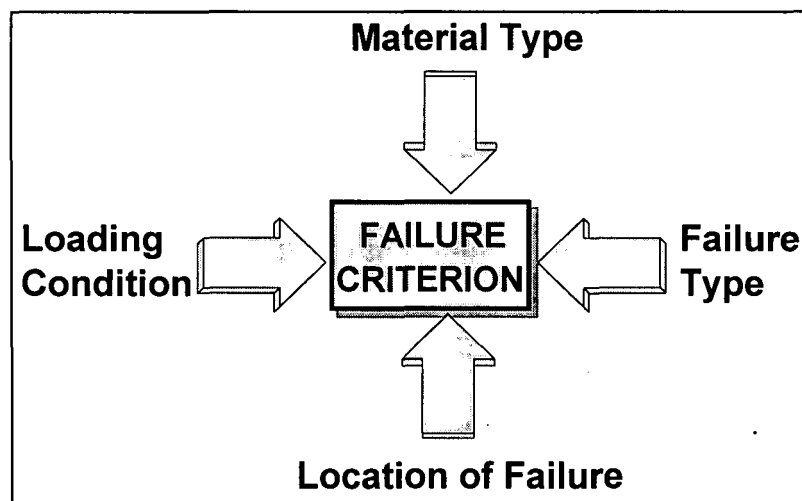


Figure 5.1: Principle factors effecting the selection of the failure criterion

After specifying the failure type and the loading conditions, the failure criterion is selected according to whether the bondline system (liner/insulator/inhibitor/etc.) or the propellant itself is considered and also according to the location of interest. The incorporation of additional aspects such as multi-axiality, for

instance, is the subject of Section 5.4. Cumulative damage and fracture mechanics is covered in Sections 5.5 and 5.6, respectively.

## 5.2 FAILURE TYPES

Failure may be described in several ways. An operational description might involve any deviation from the required motor ballistic performance such as motor pressure, total burn time, burning rate, etc. Several abnormalities may be related directly to grain structural integrity. Obviously, a crack or debond of sufficient size, which is exposed to the hot combustion gases, may result in a catastrophic pressure increase or premature burn-through to the case wall. However, it is quite possible for small changes in burn rate or minor pressure fluctuations to cause mission failure. These may be caused by small cracks or deformation of the propellant grain or even by debonding of liner/propellant interfaces. In some cases, the interaction of the gas dynamics in the rocket motor chamber coupled with the resonant modes of the propellant grain may lead to such a failure. Other descriptions of failure might include: the first visual crack which forms, sample rupture into two or more pieces, the maximum stress point on a stress-strain curve, a maximum acceptable volume increase, or perhaps a large modulus change resulting in grain slump or case bond release [2].

Basically there are four elementary types of failure (Fig. 5.2) which are discussed in detail in the following sections:

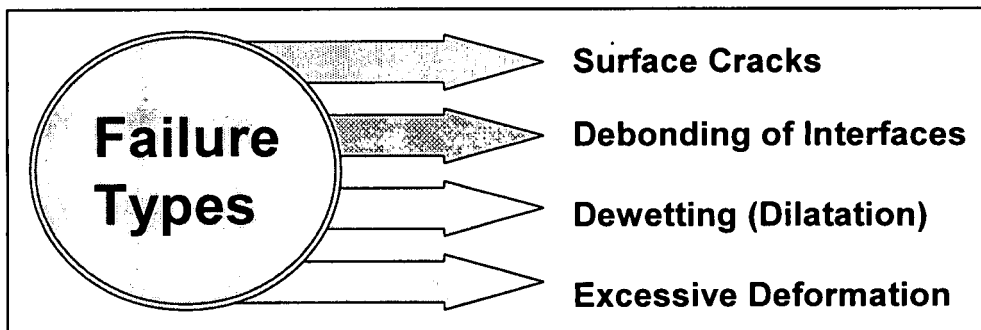


Figure 5.2: Basic elementary types of failure for solid propellant rocket motors

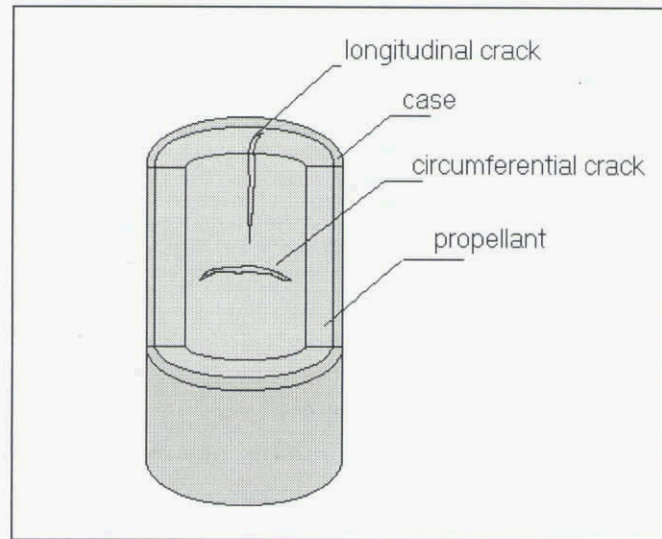
### 5.2.1 Surface Macro-Cracks

Cracks in the grain start at areas where the load exceeds a level the material can withstand. Originating at locations of stress concentration, micro-cracks may grow depending on the load history to macroscopic dimensions (see Fig. 5.3). As a consequence, the effective burning surface of the grain is unintentionally increased during motor operation which may result in an abnormal pressure and thrust history. The pressure time history for two low temperature firings is given in Fig. 5.4. Obviously, one of the motors exhibits an abnormal pressure increase due to crack formation in the propellant. In the worst case, the pressure rise is high enough to exceed the burst pressure of the case or particles of the grain detach from the residual structure and block the nozzle throat, causing fatal malfunction.

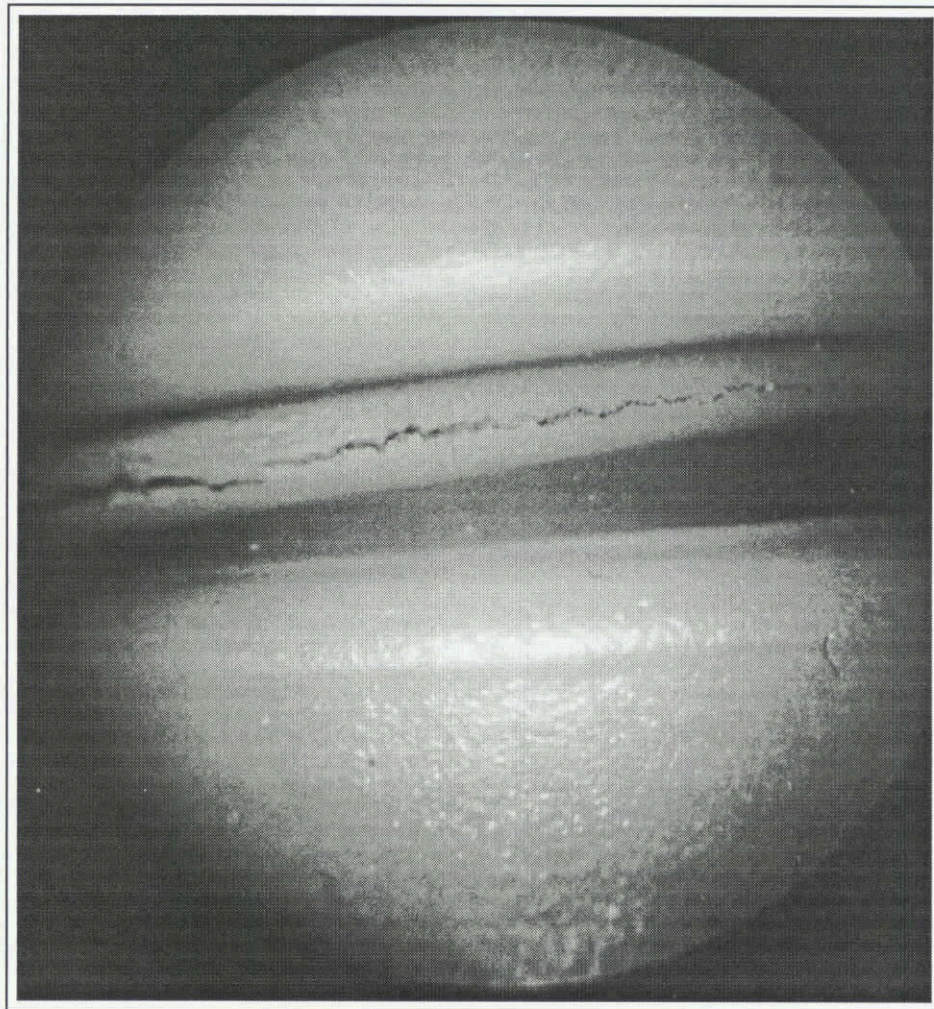
The type of failure described above is sometimes also named as *cohesive fracture*. Rupture of propellants can be "brittle" (at low temperatures and high strain rates) or "ductile" (at high temperatures and low strain rates). "Ductile" fracture occurs after high strains. Therefore, this type of fracture is preceded by dewetting (see Section 5.2.3) of the propellant, which makes its prediction more difficult.

Cracks occur usually at the bore surface of the propellant grain in case bonded motors as a result of cure shrinkage during and after cure (post curing), propellant fatigue due to thermal cycling during long term storage (cumulative damage), thermal shocks to low temperatures, ignition pressurization, and degradation in material properties due to moisture contamination (composite propellants are particularly sensitive). Moisture contamination is usually moisture condensing on the surface of the grain due to high humidity from atmosphere through sealings and large changes in temperature. Depending on the type of propellant used, this can result in increasing the post curing process of a particular propellant

formulation and decreasing the propellant's strain capabilities, increasing the possibility of cracks on the surface of the grain. Therefore, respective material properties have to be determined for analysis purposes.



(a) Schematic sketch



(b) Experimentally observed crack (Courtesy Royal Ordnance)

**Figure 5.3:** Crack development in the bore of a propellant grain

The occurrence of a crack is not always considered as a failure in solid propellant rocket technology. In more advanced applications, the existence of cracks is often taken for granted and only the unstable growth (without crack arrest) is considered as failure (see Section 5.6, Fracture Mechanics).

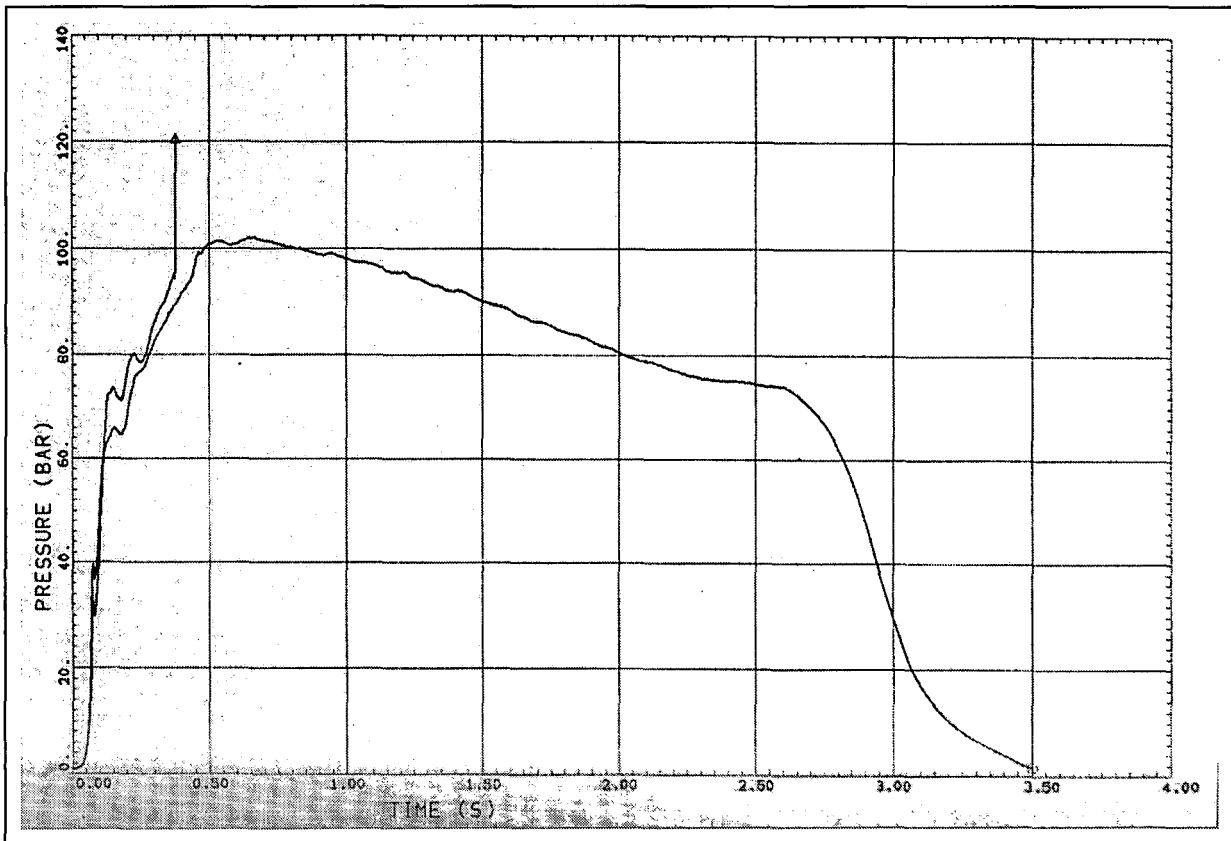
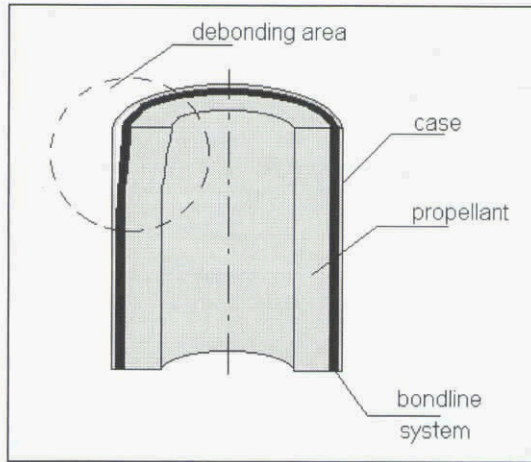


Figure 5.4: Pressure-time curve during two low temperature firings (Courtesy Royal Ordnance)

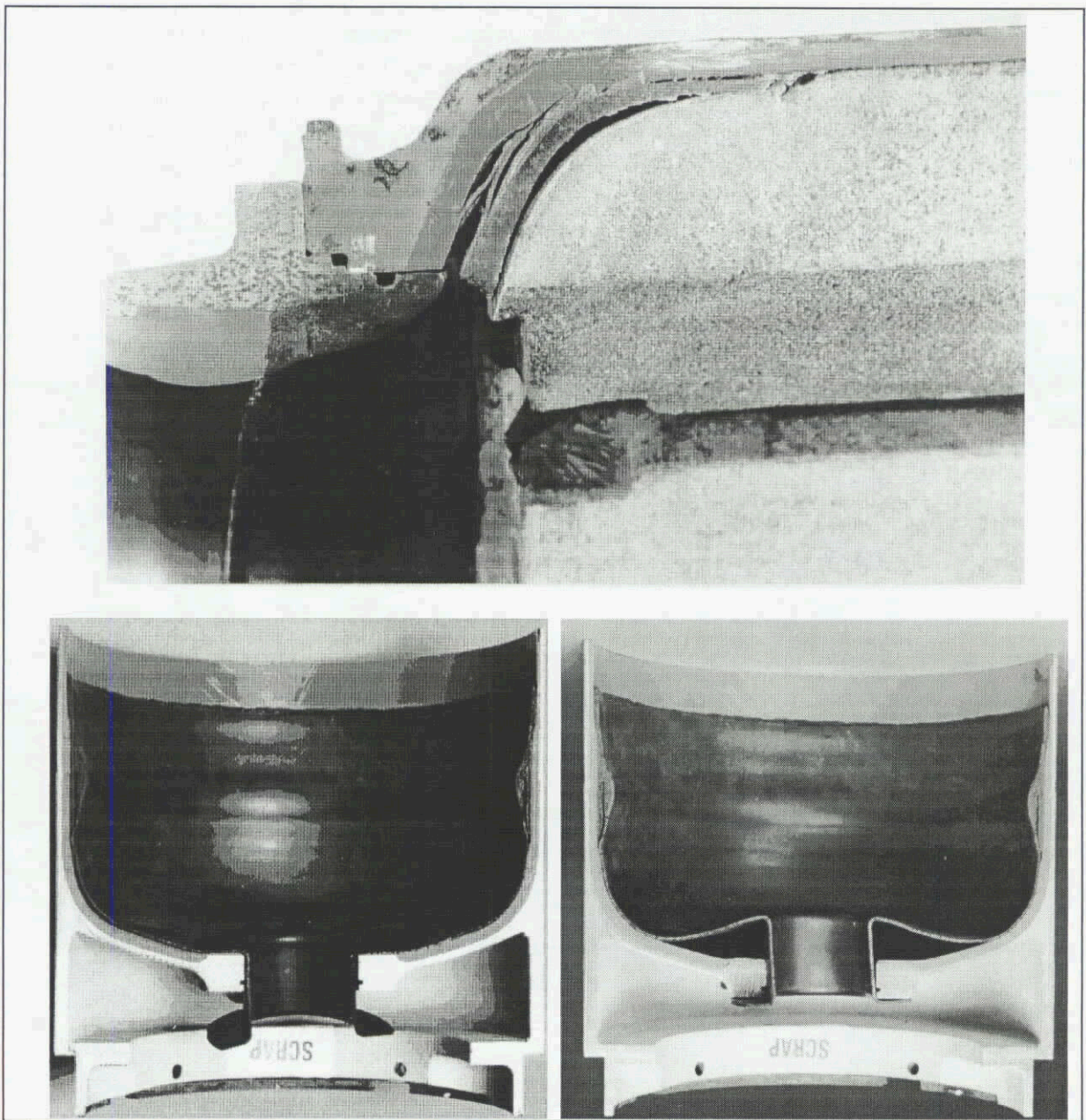
### 5.2.2 Debonding of Interfaces Propellant/Liner/Insulator/Case

The interface region between the case and the propellant consisting of various layers such as liner, insulator, inhibitor, etc. is subjected to stresses during thermal and mechanical loading for most types of case bonded and cartridge loaded grains. Thermal loading, such as in the case of cool-down during curing, produces high shear and normal stresses in the interface region since thermal expansion coefficients of the case and the propellant are significantly different ( $\alpha_{\text{steel}} = 12 \mu\text{mm}/\text{mm}/^{\circ}\text{C}$ ,  $\alpha_{\text{propellant}} = 85 \mu\text{mm}/\text{mm}/^{\circ}\text{C}$ , for instance). Similarly, interface stresses due to inertial loads on the grain during launch, carriage and transport have to be sustained by the interface. If, however, these kind of stresses exceed the capability of the interface materials (bond), separation of propellant and case may occur. This phenomenon is named *debonding* of the propellant/liner interface or sometimes even *adhesive bond fracture*, see for instance Fig. 5.5. In some cases, the debonded area can offer a path for hot gases to attack the unprotected case leading to a possible burn through.

Debonding results inherently from weak case bond systems, poor control of motor manufacturing, chemical degradation (due to human and moisture contamination, and liquid diffusion into or away from the region of the bond) and bond fatigue. Bond and flap terminations are always suspected regions for failure to occur.



(a) Schematic sketch



(b) Debonding in a real application (top photo) and stress relieving *boot* (lower photos)  
(Courtesy Royal Ordnance)

**Figure 5.5:** Typical debonding and stress relief system at the propellant/bondline/case interface

The use of stress relieving devices such as rubbery *boots* bonded to the liner through a hinge or radial slots which allow the propellant grain to expand and contract freely, greatly reducing the possibility of a debond-failure (see also Chapter 1).

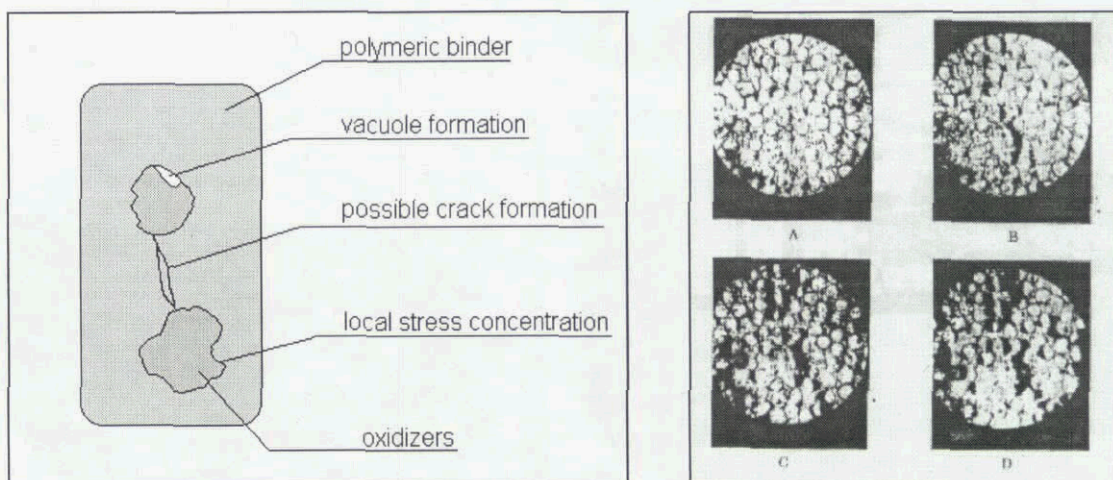
As is the case for certain types of crack failure, not all debonds have to be regarded as a failure; in some cases a thorough analysis of the debond regarding its rate of growth and effect on the performance of the motor is conducted.

### 5.2.3 Dewetting (Dilatation)

For propellant systems in which binders and fillers are used, dewetting, or dilatation, is defined as the microscopic process of debonding of the interface between the harder oxidizers and the embedding softer polymeric binder. Loading of the composite structure produces stress concentrations around the oxidizers which may lead to the breakdown of the binder and pull it away from the solids causing microvoids, or vacuoles (*vacuum-holes*) to form. As the grain begins to harden due to post curing and it begins to see a large thermal and/or mechanical cyclic loading condition, the voids may begin to tear at their weakest link and propagate, forming micro-cracks or crazing on the surface of the grain (as well as, throughout the bulk of the grain). With continuing loading, different vacuoles merge with adjacent ones producing macro-cracks and finally cause the ultimate failure, see Fig. 5.6. Dewetting is always accompanied by an increase in propellant volume.

Dewetting always precedes propellant fracture and can be, therefore, considered as a separate failure mode. Because of this property of dewetting, the phenomenon can be thought of as *yielding* in analogy to metal behaviour. From the stand point of motor performance, dewetting tends to increase the effective burning surface.

Another important issue related to dewetting is that the natural variability of the adhesive bond between binder and oxidizer is believed to be the primary source of the variability encountered in mechanical properties measurements and failure test data [3].



(a) Schematic sketch

(b) Experimentally observed dewetting [2]

Strains for A:5%, B:10%, C:15%, D:25%

**Figure 5.6:** Dewetting failure mode

### 5.2.4 Excessive Deformation

Excessive grain deformation (see Fig, 5.7) is a failure mode if the shape of the grain is changed such that the performance of the motor is affected unacceptably. Excessive deformation of the grain may occur under high acceleration during launch or captive flight, under long-term storage (slump), as a result of vibration, or, if a differential pressure drop exists along the length of the grain (specially true for loose grains). This failure mode is critical for any low modulus propellant. Also under pressurization, propellants especially in composite casings, which deform more than metallic ones, may exhibit large deformations, which have to be handled with special caution.

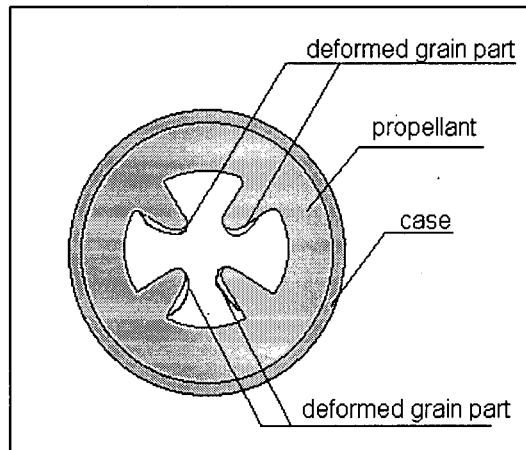


Figure 5.7: Deformation of propellant grain

Besides changing the burning surface geometry causing erosive burning effects to occur in the motor and causing an abnormal thrust history, this type of grain deformation can also result in a more serious problem called *port blockage (obduration)*. In case of port blockage, the grain or grain segments deforms enough to restrict the flow of hot gases generated by the burning propellant, causing the pressure differential to increase along the length of the grain. This increases in turn the grain deformation, which will increase further the pressure gradient. The interaction will continue until the pressure inside the motor reaches the burst pressure of the case, resulting in a catastrophic failure. This type of interaction may be referred to as *structural ballistic interaction*. A comprehensive example for the analysis of such an interaction is given in [4].

In situations where systems are gun launched, deformation of cartridge loaded grains (i.e. end-burners) upon ejection can become another serious structural problem. Upon ejection, the rocket motor will be exposed to very high acceleration loads which, depending on the hardness and toughness of the grain, can result in extruding the grain through the nozzle(s), possibly pre-igniting the grain in the gun barrel or failing upon motor ignition. Now, any type of failure mode (i.e. dilatation or chemical degradation) that causes void evolution to occur in any critical regions of the grain, could result in a pre-ignition of the grain due to hydro-dynamic compression, which will result in a catastrophic failure as the motor leaves the barrel, compromising the structural integrity of both the muzzle-end of the gun barrel and the rocket motor's case wall. Deformation of grains can also happen due to lateral acceleration, for instance, during lateral ejection or capture flight.

Slump or distortion can also be a factor in both case bonded and cartridge loaded designs. In cartridge loaded grains, it is quite temperature dependent since the size of the annulus around the grain and the inhibitor, and the stiffness of the column vary considerably with temperature. At low temperatures, the grain stiffness is sufficient to transmit all of the load to the support at the end of the grain. At high temperatures, the propellant can expand out to case wall, essentially creating a quasi-case bonded unit. However, at intermediate temperatures, a sufficient gap size can exist to create a differential pressure drop, which because of the temperature soften condition of the propellant it can lead to phenomena called grain buckling. Slumping can also occur in case bonded grains as well, especially for both high and intermediate temperatures depending on how much the grain soften through time. This phenomena

is a special concern in vertical-launch systems, where the grain can slump onto or into the nozzle, resulting in a catastrophic failure upon ignition.

### 5.3 FAILURE CRITERIA AND THEIR APPLICATIONS

Propellant deformations are calculated by means of finite element models utilizing viscoelastic material behaviour for large strains and the magnitude of the predicted deformation is used with the advice of a ballisticians to decide if a failure due to restricted gas flow is possible. Hence, there is a joint effort of the structural analyst and the ballisticians necessary, which consists usually of iterative loops. There is, however, no generally agreed approach of evaluating this type of failure, so that, these aspects are usually considered in the *margin of safety* (see Chapter 6: Margin of Safety) concept.

On the other hand, cracking of the propellant or the bond as well as dewetting of these materials can not be predicted in such a straight forward manner. After having determined analytically the response of the propellant under given loads, a statement is required whether the propellant is able to withstand the stresses and strains corresponding to the computed response. Such a statement, which relates the physical state at which failure occurs to some measured material parameters, is called a *failure criterion*. The criterion for failure permits a prediction of design margins expected under motor operation and handling, and defines the acceptable loading regimes.

Since the response behaviour of solid propellant and loading conditions are very complex, there is unfortunately, no unique universal failure criteria which can lead satisfactorily to the statement mentioned above. For this reason, following a pragmatic phenomenological approach, distinct failure criteria are constructed and applied for different application profiles characterized by the:

- Material (propellant versus bondline material)
- Loading-type (thermal, pressure, dynamic, gravity)
- Loading-nature (single static loading, successive loading, combined loading, cyclic loading)
- Superimposed pressure (this usually increases the stress capability and may increase or decrease the strain capability)
- State of stress or strain (uni-axial, bi-axial, tri-axial)
- Environmental effects (temperature history, humidity, aging, etc.)

Because of this pragmatic phenomenological approach, the application of any failure criteria conceals a significant amount of experience based on extensive experimental work. This leads also to distinct uses of the same criterion in different countries and even in different companies of the same country. It must be emphasized that these criteria have limited or conditional ranges of validity, which will be highlighted if possible in this text. For solid propellants, the failure criteria can be used reliably only for small extrapolations from test conditions underlying the criterion [5].

A rather widely accepted classification of failure criteria is given in Fig. 5.8. The basic categories are characterized according to the presence or lack of an initial flaw (usually a crack) in the material under consideration. When pre-existing flaws are not large enough to influence fracture classical approaches to predict failure are used; however, when the pre-existing flaws will influence fracture significantly, a fracture-mechanics or damage approach is required. This distinction is illustrated in Fig. 5.9. The difference between discrete and envelope type of failure criteria is that the discrete criteria use only a *single* material parameter and are usually *load path independent*, whereas envelope type of criteria use a *family* of material data, i.e. an *envelope of data*, and, therefore, can consider *load path dependence*.

In the forthcoming sections, basic formulation and place of application of the most widely used classical criteria for unflawed propellants (criteria in dashed box of Fig. 5.8) will be described in detail. Criteria for flawed propellants will be covered in Sections 5.7 and 5.8. Furthermore, most classical failure relationships have been based on a single loading history or initial loading conditions.

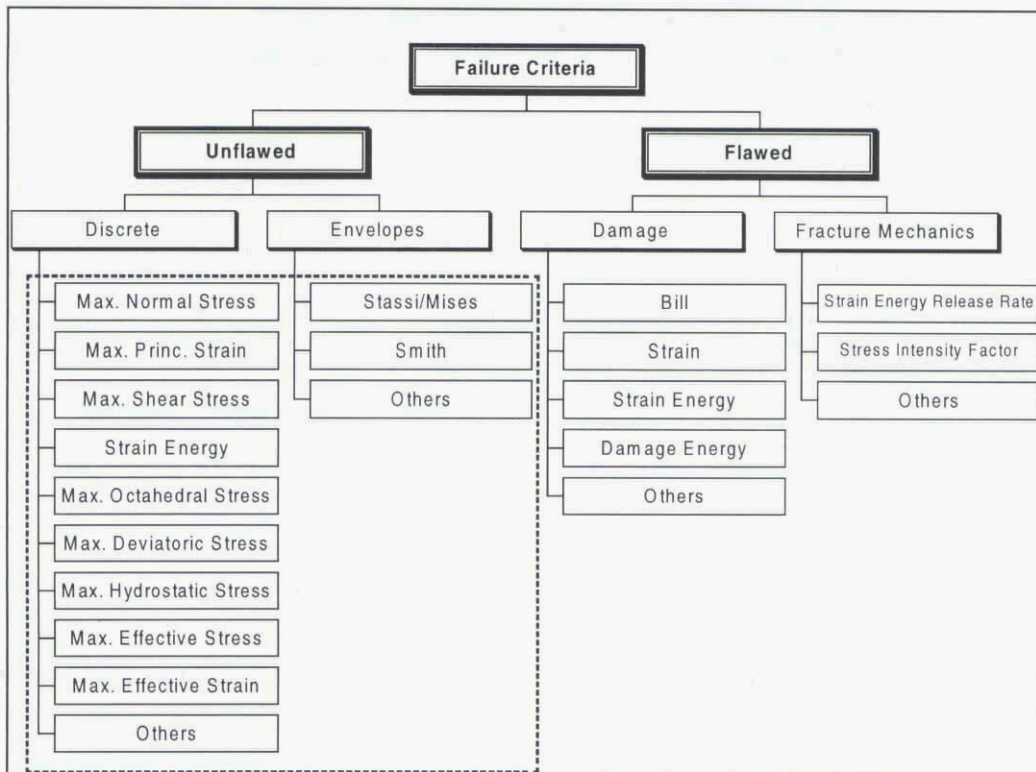


Figure 5.8: Classes of Failure Criteria

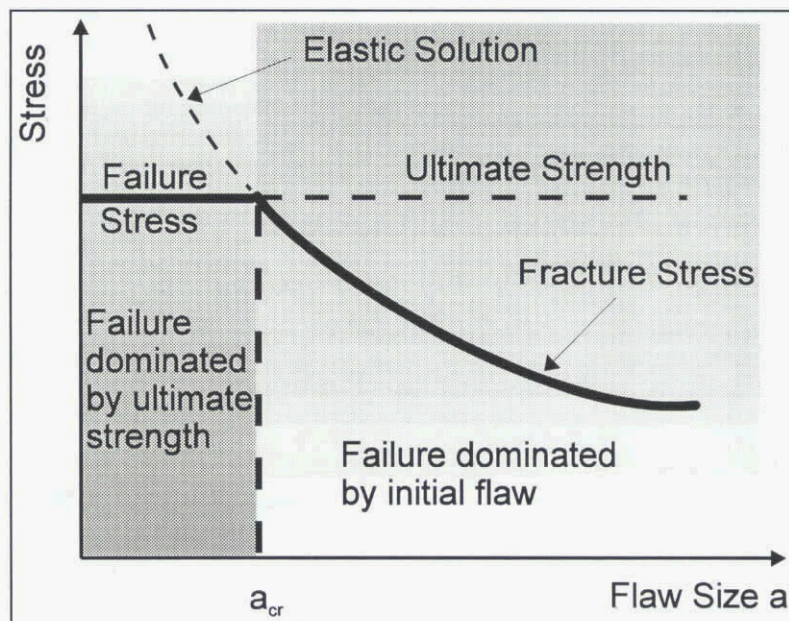


Figure 5.9: Conceptual relation between flaw size and type of failure

### 5.3.1 General Definitions

There are some basic considerations which apply to almost all of the following failure criteria, so that they will be introduced in this section.

**Engineering (I. Piola-Kirchhoff) Stress Components:** This type of stress components is obtained from the applied (current) loads and the initial (load-free) geometric configuration of the body. In the simple tension test, the engineering normal stress component in axial direction is simply obtained as the ratio of the applied tensile load by the original cross-sectional area of the test specimen.

**True (Cauchy) Stress Components:** Here, the stress is computed from the applied loads and the current (deformed) geometric configuration. In the simple tension test, the true normal stress component in the axial direction is obtained as the ratio of the applied load by the current (deformed) cross-sectional area of the test specimen. The true stress in simple tension can be obtained from the engineering stress by assuming incompressibility as:

$$\sigma_{true} = \sigma_{engineering} * (1 + \epsilon) \quad (5.1)$$

where  $\epsilon$  is the engineering axial normal strain. The term in parenthesis is named also as the stretch ratio  $\lambda$ .

**Temperature Corrected Stress:** Any stress value, which is considered as a material property, is *temperature corrected*, i.e. it is modified by the ratio of the reference temperature  $T_0$  and the current temperature  $T$  as:

$$\sigma_{corrected} = \sigma * \frac{T_0}{T} \quad (5.2)$$

**Engineering Infinitesimal Strain Components:** These strains measure pure deformation only for infinitesimal strains and displacements. However, in the simple tension test, they can be used to indicate level of deformation. The engineering normal strain component in axial direction is computed as the ratio of axial displacement by the original length over which this displacement is assumed to be occurring uniformly.

**True Strain:** In continuum mechanics true strain is defined as the natural logarithm of the ratio of the current length to the original length of a specimen in simple tension. Hence, the true strain is simply equal to  $\ln(1+\epsilon)$ , where  $\epsilon$  is the engineering normal strain as described above. On the other hand, sometimes, the term *true strain* is used incorrectly to describe the *engineering* normal strain determined by using a *gage* length on the test specimen over which the straining takes place uniformly in order to distinguish it from an engineering strain that would be measured, for instance, using the clamp displacements of the test machine.

**Reduced Strain-Rate Parameter  $R^*a_T$ :** The reduced strain-rate parameter is an artificial time which is used to correlate ultimate material properties obtained at different temperatures and strain-rates.  $R$  designates the constant strain-rate at which the property is defined and  $a_T$  is the shift factor corresponding to the constant temperature at which the property is obtained with respect to the reference temperature.

**Master Uniaxial Strain Curve:** The master uniaxial strain curve is the plot of the maximum strain  $\epsilon_m$  (corresponding to the maximum true stress  $\sigma_m$  during a uniaxial tensile test conducted at a given constant strain rate  $R$  and temperature  $T$ ) versus  $\log(R^*a_T)$ . This concept is illustrated in Fig. 5.10. The stress-strain curve for the propellant at the critical condition should be examined to see if there is a significant difference between strain at maximum engineering stress and strain at maximum true stress. Should differences in the values be found, which may lead one to believe that the analysis is not conservative, additional data confirming propellant failure should be generated.

**Master Uniaxial Stress Curve:** Similar to the master uniaxial strain curve,  $\sigma_m$  is plotted versus reduced strain-rate parameter.

**Reduced Time Parameter  $t^*/a_T$ :** Similar to the reduced strain-rate parameter, the reduced time is a temperature neutralized time measure making use of the superposition principle valid for rheologically simple materials.  $t^*$  is here the time to failure. Sometimes it is more convenient to express this parameter in terms of  $\epsilon_m/(R^*a_T)$ , which is equivalent to  $t^*/a_T$  if  $R$  is constant during straining. In certain applications, such as long term loadings, the master curves for stress and strain are obtained with respect to the reduced time parameter.

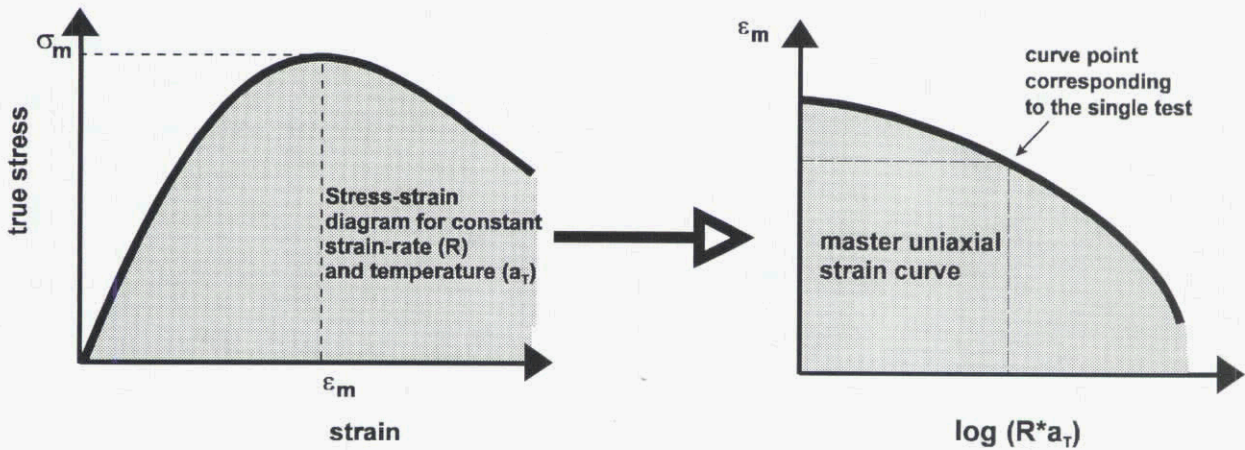


**Figure 5.10:** Construction of the master uniaxial strain curve from uniaxial tension data

In real motors, the highest stresses usually occur at discontinuities such as the grain bondline termination point, and the highest strains occur on the bore surface either in the middle of a long circular section or at discontinuities in the geometry [6]. Therefore, in practice usually strain based criteria are used for failure in propellants and stress based criteria are used for bond-failures. In the forthcoming sections, firstly strain based discrete failure criteria will be discussed. After presenting the important stress based criteria, envelope-type criteria will be covered. Finally, a summary of the application profiles for all discussed failure criteria will be given.

### 5.3.2 Maximum Principal Strain Criterion

The maximum principal strain criterion states that if the computed (predicted) maximum principal strain at the critical location of the propellant,  $\epsilon_{1,computed}$  exceeds the measured strain corresponding to the maximum true stress in the uniaxial tension test, failure will occur, or, in other terms:

$$\text{If } \epsilon_{1,computed} < \epsilon_m (R \cdot a_T) \text{ no failure is expected} \quad (5.3)$$

The measured strain value  $\epsilon_m$  is obtained from the master uniaxial strain curve for the respective strain-rate and temperature. In case of thermal loading, the strain-rate  $R$  is computed as

$$R = \frac{\text{total computed maximum principal strain}}{\text{time taken to reach this strain}} \quad (5.4)$$

and the temperature shift factor  $a_T$  is taken at the respective operating temperature, for instance,  $-40^\circ\text{C}$ . In case of pressurization loads, the time used for the computation of the strain-rate  $R$  is simply the time at maximum internal pressure, and the time shift factor is taken at the environmental temperature at time of firing.

Generally speaking, the maximum principal strain criterion is used for predicting surface crack formation with catastrophic failure. Some companies apply the criterion also within the grain. The criterion is applied usually for composite type of propellants and sometimes also for double base ones. The family of loads, for which the maximum principal strain criterion is used include thermal, pressure and spin loading. Finally, it must be emphasized that the criterion is rather conservative for composite propellants and very conservative for double based propellants as demonstrated in Table 5.1 for a series of HTPB propellants [7]. In this data, OUZEL II is a six-slotted charge containing aluminised cast composite propellant. OUZEL III is a four-slotted charge and contains also aluminised propellant. STM is exactly the same geometry of OUZEL III but contains non-aluminised propellant.

**Table 5.1:** Low temperature firing data (by Faulkner and Tod [7])

MOTOR	FIRING TEMP. in °C	PREDICTED SAFETY FACTOR	RESULT
OUZEL II	-73	0.46	FAIL
	-68	0.76	PASS
	-62	1.00	PASS
	-60	1.07	PASS
	-58	1.12	PASS
	-58	0.66	PASS
	-53	0.88	PASS
	-53	1.23	PASS
OUZEL III	-66	0.50	FAIL
	-66	0.54	PASS
	-63	0.55	PASS
	-58	0.66	PASS
STM	-53	0.62	PASS
	-53	0.62	PASS
	-56	0.61	PASS
	-57	0.61	PASS
	-57.5	0.60	FAIL
	-58	0.60	FAIL
	-58	0.60	FAIL

Note: Safety factor here is defined as in United Kingdom (see Table 6.1)

The results of the maximum principal strain criterion, may get even more conservative if tensile tests under pressure are applied. It is known that material properties such as ultimate stress, ultimate strain and dewetting strain tend to increase at the existence of superimposed pressure (see also Section 5.4.4). One reason for the conservative results could be however the multi-axiality effect (see also Section 4.2.2).

To account for multi-axiality a correction factor can be used:

$$\varepsilon_m^{\text{modified}} = \varepsilon_m (R \cdot a_T) * \left( 1 - \nu \frac{\sigma_3}{\sigma_1} \right) \quad (5.5)$$

$\sigma_1$  and  $\sigma_3$  are the larger and smaller principal stresses, respectively, and,  $\nu$  is the Poisson's ratio. Obviously, for a uniaxial stress field the correction factor is unity.

### 5.3.3 Effective Strain Criterion

The effective strain criterion states:

$$\text{If } \varepsilon_{\text{eff}}^{\text{computed}} < \varepsilon_m (R \cdot a_T) \text{ no failure is expected} \quad (5.6)$$

where the effective strain is defined as

$$\varepsilon_{\text{eff}} = \frac{\sqrt{2}}{3} \sqrt{(\varepsilon_1 - \varepsilon_2)^2 + (\varepsilon_2 - \varepsilon_3)^2 + (\varepsilon_3 - \varepsilon_1)^2} \quad (5.7)$$

and  $\varepsilon_1, \varepsilon_2, \varepsilon_3$  are the principal strains. The measured strain is obtained from the master uniaxial strain curve as already described above.

The effective strain criterion is used for predicting crack formation with catastrophic failure. The criterion is applied for composite type of propellants. The family of loads, for which the effective strain

criterion is used include thermal and pressure loading. This criterion is preferred by some countries as compared to the maximum principal strain criterion, since it is less conservative.

### 5.3.4 Maximum Normal Stress Criterion

The maximum *normal* stress criterion is basically used to predict debonding in the interface between propellant and casing. However, in some cases it is used also to predict propellant failure (in such cases, the criterion is referred as maximum *principal* stress criterion). The criterion states

$$\text{If } \sigma_n^{\text{computed}} < \sigma_m(R * a_T) \text{ no failure is expected} \quad (5.8)$$

where  $\sigma_m$  is the measured allowable stress value as determined for a reduced strain-rate  $R * a_T$  corresponding to an application temperature from a representative insulation-liner-propellant bond-in-tension (BIT) test, see also Chapter 4: Material Characterization. The computed stress  $\sigma_n^{\text{computed}}$  is the maximum normal bond stress at the respective location. In some cases, however, instead of the maximum normal bond stress, the maximum principal stress is used, which supplies more conservative results. The maximum normal stress criterion is applied under thermal, pressure and gravity loading. Some experts prefer to use this criterion for situations in which all stress components are tensile. From phenomenological point of view, microscopic voids within the propellant tend to proceed in the direction of maximum principal stress. In such an application, the allowable stresses are determined from tri-axial bond-in-tension (BIT) tests.

### 5.3.5 Effective Stress Criterion

The effective stress failure criterion is also basically used to predict debonding in the interface between propellant and casing. The criterion states that

$$\text{If } \sigma_{\text{eff}}^{\text{computed}} < \sigma_m(R * a_T) \text{ no failure is expected} \quad (5.9)$$

where the effective stress is defined as

$$\sigma_{\text{eff}} = \frac{\sqrt{2}}{2} \sqrt{(\sigma_1 - \sigma_2)^2 + (\sigma_2 - \sigma_3)^2 + (\sigma_3 - \sigma_1)^2} \quad (5.10)$$

and  $\sigma_m$  is determined similar as described in the previous criterion from tests with BIT specimens. Notice that the  $\sigma_m$  does not correspond to  $\sigma_{\text{eff}}$ , so that the criterion gets more conservative. Caution is required in cases of equi-triaxial stress states, where the effective stress goes to zero. The effective stress criterion is applied basically under thermal and pressure loading.

### 5.3.6 Maximum Deviatoric Stress Criterion

The maximum deviatoric stress criterion states that

$$\text{If } \sigma'_{1, \text{computed}} < \frac{2}{3} \sigma_m(R * a_T) \text{ no failure is expected} \quad (5.11)$$

The deviatoric stress is defined here as:

$$\sigma'_1 = \sigma_1 - \frac{\sigma_1 + \sigma_2 + \sigma_3}{3} \quad (5.12)$$

Similar to other stress based criteria, also this criterion is used basically for the failure considerations in the bond between propellant and case under thermal and/or pressure loads. Sometimes, however, this criterion is also applied for the failure of the propellant itself, where it yields too optimistic results.

### 5.3.7 Strain Energy Criterion

The strain energy failure criterion states that

$$\text{If } U_{\text{computed}} < U_m (R * a_T) \text{ no failure is expected} \quad (5.13)$$

where  $U_m$  is the measured allowable strain energy density value as determined for the reduced strain rate  $R * a_T$  from the master uniaxial strain energy density curve.

Here, strain energy is defined as work done, i.e. the area under the stress-strain curve

$$U = \int \sigma d\epsilon \quad (5.14)$$

At high strain levels the Cauchy stress and the logarithmic strain are used in the work expression.

### 5.3.8 Stassi/Mises Failure Envelope

The Stassi/Mises failure criterion consists of a three-dimensional surface in the space of either principal stresses or strains, which envelopes the region of no failure. Under various assumptions such as material isotropy and using the material indifference principle, the failure envelope can be reduced to a curve in the space of octahedral normal and shear stresses as defined by:

$$\sigma_{oct} = \frac{1}{3}(\sigma_1 + \sigma_2 + \sigma_3) \quad (5.15)$$

and

$$\tau_{oct} = \frac{1}{3} \sqrt{(\sigma_1 - \sigma_2)^2 + (\sigma_2 - \sigma_3)^2 + (\sigma_3 - \sigma_1)^2} \quad (5.16)$$

This curve is shown in Fig. 5.11. After a certain amount of superposed pressure, called the *saturation pressure*, the ultimate properties (stress or strain) remain unchanged for increasing pressure. This pressure is about 1.5 times the uniaxial fracture stress. Here, the envelope border is horizontal and is represented by the v. Mises equation:

$$\tau_{oct}^2 = \text{const.} \quad (5.17)$$

For lower pressures, on the other hand, the Stassi equation is used:

$$\tau_{oct}^2 + \alpha \sigma_{oct} = \beta \quad (5.18)$$

where,  $\alpha$  and  $\beta$  are material constants. For stress states corresponding to the interior of the curve no failure is expected. The excessive capacity can be defined for instance as by measuring orthogonal distances. Figs. 5.12 and 5.13 show typical failure curves for an HTPB propellant as obtained for 20°C and 60°C. If these results are normalized by the maximum stress (or, respectively, strain) obtained from an uniaxial tensile test at atmospheric pressure, it can be seen that they build a unique envelope as given in Fig. 5.11.

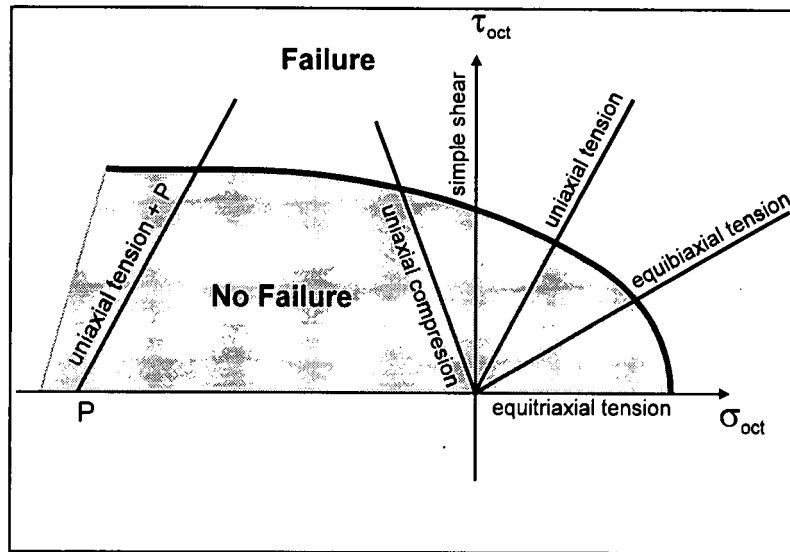


Figure 5.11: Stassi/Mises failure criterion

If the failure surface of a propellant is not identical for all stress-rates and temperatures tested, the failure criterion defined in this section must be determined experimentally under conditions similar to the operating ones (stress-rate, temperature, pressure) using multiaxial specimens [8].

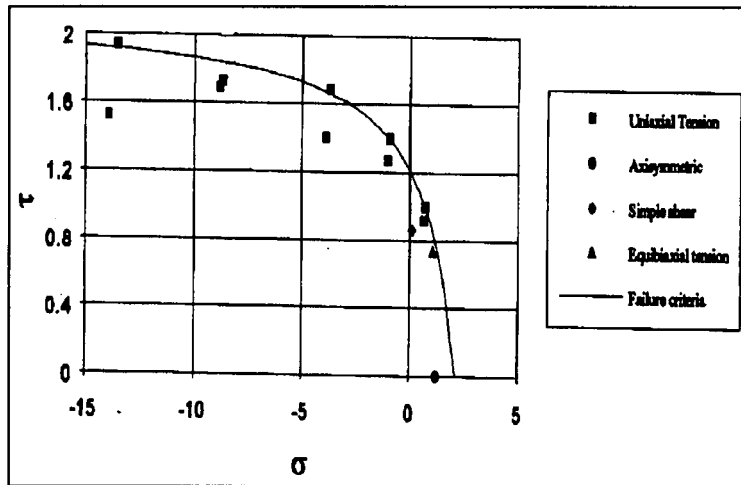


Figure: 5.12: Typical Stassi/Mises failure curves of an HTPB propellant obtained at 20°C (Courtesy SNPE)

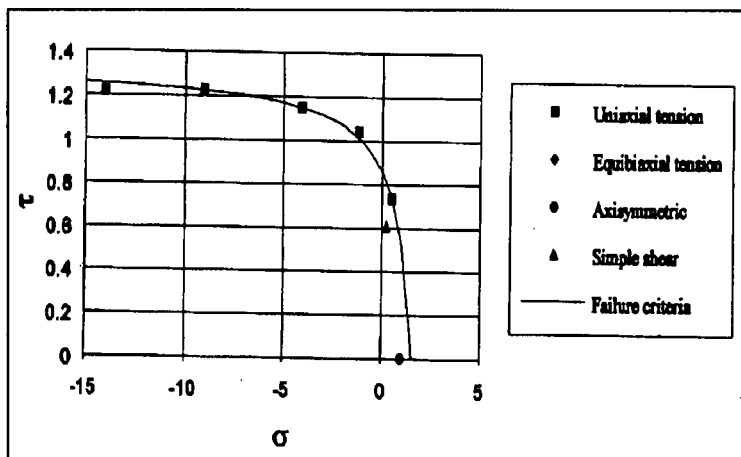


Figure: 5.13: Typical Stassi/Mises failure curves of an HTPB propellant obtained at 60°C (Courtesy SNPE)

The Stassi/Mises criterion is used for predicting crack formation with catastrophic failure. The criterion is applied both for composite and double base type of propellants. The family of loads, for which the Stassi/Mises criterion is used include thermal and pressure loading.

### 5.3.9 Smith Failure Envelope

The Smith failure envelope consists of a log-log plot of temperature reduced failure stress versus strain at break as obtained in uniaxial tension tests for various temperatures and strain-rates. A typical Smith envelope is given in Fig. 5.14. Here,  $\epsilon_b$  is the strain at break as found in the uniaxial tension test,  $\sigma_b$  is the *nominal* stress at break (*tensile strength*) in the uniaxial tension test (temperature corrected). In some cases, it is preferred to use the strain at maximum stress  $\epsilon_m$  instead of the strain at break, which is more likely to predict dewetting than rupture and is hence more conservative [2,9].

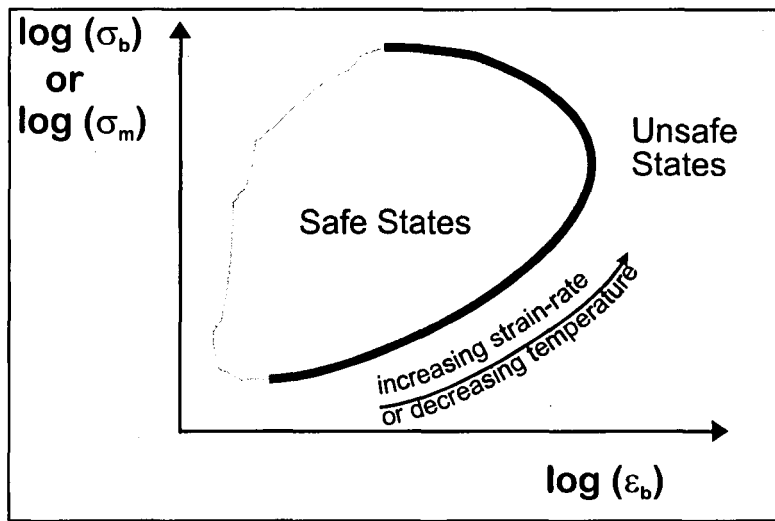


Figure 5.14: A typical Smith failure envelope

By assuming a path-independent criterion, the extremes of the failure envelope may be characterized using temperature-strain rate combinations which are convenient to the user.

The Smith criterion is also used for predicting crack formation with possible catastrophic failure. The criterion is applied basically for composite type of propellants. The family of loads, for which the Smith criterion is used include thermal and pressure loading. This criterion is sometimes used also for predicting the onset of dewetting.

For some propellants, the Smith failure envelope has been shown to coalesce data from a variety of laboratory test, including constant-rate uniaxial and biaxial tests, strain endurance tests, and stress endurance tests. When such results are obtained, the failure envelope can be very useful as a tool for selecting discrete failure criteria. For example, a very high loading rate would produce failure near the upper limits of stress on the failure envelope. Examination of Fig. 5.14 shows that the failure stress is relatively constant in this region, though the failure strain varies greatly. One would expect that a stress-based failure criterion would work best in this situation. On the other hand, an intermediate loading rate might produce a stress-strain trajectory that crosses the failure boundary at the *knee* of the curve, and a very low loading rate trajectory would cross the failure boundary near the strain endurance limit (low-stress end of the curve). These regions of the failure envelope show a much better definition of failure strain than of failure stress; strain-based failure criterion would appear to be the choice for these conditions [6].

### 5.3.10 Endurance Strain Based Criteria

For composite propellants under thermal loads sometimes endurance strain based failure criteria are employed. Here, the capability of the propellant is determined from strain endurance tests (see Chapter 4). This strain values are assigned to be the limiting values for the computed strains.

### 5.3.11 Comparison of Application Profiles for Various Failure Criteria

A comparison of the application profiles for various failure criteria is summarized in Table 5.2. The table reflects for each criterion the type of failure predicted, the material and loading type for which it is applicable, and some remarks about its usage. Finally, the name of the countries in which the respective criteria find common application is specified. It must be emphasized, that the supplied application profile is only a rough guideline and that exceptions are always given. Generally, it can be observed that strain based criteria are used for propellant failure detection, whereas stress based criteria are used for debonding type of failure.

**Table 5.2:** Application profiles for various failure criteria

Failure Criterion	Failure Type	Material	Loading	Remarks	Used by
<b>Maximum Principal Strain</b>	Surface crack formation	-Composite Propellants -Double Base Propellants	-Thermal -Pressure -Spin	-Rather conservative for composite propellants -Very conservative for double base propellants -Also used within the grain	UK, GE US, TU, NL
<b>Effective Strain</b>	Crack formation	Composite Propellants	-Thermal -Pressure	Preferred by some countries as compared to max. princ. strain criterion, since less conservative	GE, USA, TU
<b>Maximum Normal Stress</b>	Debonding of interface between propellant and case	insulation-liner-propellant interface	-Thermal -Pressure -Gravity	Sometimes also used for propellants directly to predict fracture within the grain	UK, GE USA, F, TU, NL
<b>Effective Stress</b>	Debonding of interface between propellant and case	insulation-liner-propellant interface	-Thermal -Pressure		UK, GE USA, F, TU
<b>Maximum Deviatoric Stress</b>	Debonding of interface between propellant and case	-insulation-liner-propellant interface -Composite Propellants -Double Base Propellants	-Pressure	Sometimes also used for propellants directly to predict fracture within the grain (too optimistic)	UK, GE USA, F, TU
<b>Strain Energy</b>	Crack formation	-Double Base Propellants -Composite Propellants	-Thermal -Pressure		UK, USA
<b>Stassi/Mises Envelope</b>	Crack formation with catastrophic failure	-Composite Propellants -Double Base Propellants	-Thermal -Pressure		F
<b>Smith Envelope</b>	Crack formation with catastrophic failure	-Composite Propellants	-Thermal -Pressure	Sometimes also used to predict dewetting	USA, TU
<b>Endurance Strain Based Criteria</b>	Crack formation	-Composite Propellants	-Thermal		USA

A comprehensive comparison of some failure criteria for double base propellants is performed by Amos [10]. An extensive summary of his results is given in Appendix A of this chapter. The critical issue of such comparisons is the fact that besides the failure criterion also the analysis method as well as the experimental method are involved. Therefore, a exclusive comparison of failure criteria is always rather complicated if not impossible.

## 5.4 MULTI-AXIALITY (STRESS STATE) CONSIDERATIONS

Phenomenological failure criteria have only a limited range of application due to the complex failure mechanisms of propellants as pointed out already earlier. One of the key issues which determines the successful failure prediction is the type of the stress state (also known as axiality) active at failure. The stress state can enter the strength analysis in two ways: Either stress state dependence is incorporated directly into the failure criterion or the failure ultimate data is measured in experiments exhibiting similar stress states as the real application. Unfortunately, none of these alternatives can supply the ultimate stress state invariance of the prediction. However, the determination of stress state dependent

failure data is currently the most widely applied solution. Accordingly, for instance, if case-bonded propellant grains show critical locations adjacent to the case bondline during exposure to thermal loads (like at cool-down after curing), the ultimate failure data should be determined from tri-axial tests, like the bond-in-tension (BIT) test, since the stress state at the mentioned locations are all in tension (almost a hydrostatic state of stress).

On the other hand, the inner-bore surface of the propellant grain during thermal loading, is under a two-dimensional stress state (biaxial stress state). During ignition, a pressure is superposed to this stress state resulting a three dimensional stress state. For the former case, biaxial test data is gathered (see Chapter 4), whereas in the latter case, pressurized simple tension or even biaxial tests are carried out.

Another alternative, to consider the effect of non-matching stress-states during experiments and real states, is the application of knockdown factors, which are determined mostly by applying the uniaxial failure data to known controlled multiaxial stress applications and comparing the failure stresses/strains leading to correction factors as the factors  $k_\sigma$ ,  $k_\epsilon$ , which are already mentioned in the previous sections (refer also to Section 6.4.2.3).

## 5.5 SUCCESSIVE LOADING (DAMAGE)

On occasion, cumulative damage methods are used to determine the structural integrity or life expectancy of a solid propellant grain (see also Section 5 of Chapter 6). A variation of the *Miner's Cumulative Damage Law* (see Equation 5.20) is used to derive the equations needed for the analysis. The law is expressed in general terms of time to failure under constant stress,

$$PD = P \sum D_i = \sum_{i=1}^n \frac{\Delta t_i}{t_{fi}} \quad (5.19)$$

where,  $P$  is the probability distribution observed during replicate failure characterisation tests;  $\sum D_i$  is the damage function;  $\Delta t_i$  is the time the specimen is exposed to the  $i$ th stress level; and  $t_{fi}$  is the mean time to failure if the specimen experienced only the  $i$ th stress level.

As for strain histories, a similar approach can be used involving a comparison between strain theories and predicted strains.

The equivalent of Equation 5.19 is

$$PD = \sum_{i=1}^n \frac{\Delta \epsilon_i}{\epsilon_{fi}} \quad (5.20)$$

where,  $\Delta \epsilon_i$  is the increment of strain at the  $i$ th rate and temperature  $T$ ; and  $\epsilon_{fi}$  is the mean strain at  $i$ th rate and temperature  $T$ . Note, the probability function,  $P$ , in this case is simply a ratio of time (or strain) at failure for a particular specimen to the average time (or strain) to failure for the population. Therefore, it represents the statistical spread of the failure data about the mean time (or strain).

Note, in applying the cumulative damage approach, the total stress or strain histories at the critical location is defined from a structural analysis. The stress (or strain) versus time curves are divided into increments. Since the stress over an increment of time is assumed constant in the stress-based cumulative damage theory and the strain rate is constant over the increment of time or strain with the strain-based theory, the division of the stress or strain curves must be such that variation of these parameters over a given increment is small.

The question of which stress or strain to be used in the respective cumulative damage theories is up to the analyst. However, most of the NATO countries uses maximum principal stresses or strains with

experimental failure data obtained from various mechanical property tests (ranging from uniaxial tensile to triaxial bond-in-tension tests - refer to Chapter 4). A detailed discussion about the application of damage theories in the context of margin of safety in the specific NATO countries is given in Chapter 6.

## 5.6 FRACTURE MECHANICS

Propellant grains frequently have flaws that either result from processing, form gas evolved from decomposition or from prior loads. If the flaws are larger than a critical value, it is appropriate to apply fracture mechanics to determine whether the flaws will grow during subsequent loading, see also Section 5.3. Although, fracture mechanics is an established discipline for brittle materials, research is still ongoing in field of viscoelastic fracture. Therefore, in this section only a summary of widely accepted fundamentals will be described and references for specific applications will be supplied. Since, most of the theories for the fracture behaviour of viscoelastic materials are modifications of the basic theories for brittle fracture, firstly, these theories will be described.

### 5.6.1 Brittle Fracture Mechanics

For perfectly brittle materials Griffith [11] proposed that existing cracks will propagate if the potential energy of the crack system reaches an unstable equilibrium state. Hence, if

$$\frac{dU}{da} = 0 \quad \text{and} \quad \frac{d^2U}{da^2} < 0 \quad (5.21)$$

are satisfied crack propagation will occur. Here,  $U$  is the total potential energy of the crack system and  $a$  is the crack length. The total potential energy of the crack system can be given as:

$$U = U_0 - U_a + U_\gamma \quad (5.22)$$

where,  $U_0$  is the potential energy before introducing the crack,  $U_a$  is the decrease in potential energy due to introducing the crack and  $U_\gamma$  is the increase in surface energy due to the new crack surface.

Application of Equations 5.21 (first) and 5.22 results:

$$\frac{dU_a}{da} = \frac{dU_\gamma}{da} \quad (5.23)$$

The left hand term in the above equation is named as the *strain energy release rate*,  $G$ , whereas, the right hand term is the *energy absorption rate* of the material,  $R$ . Hence, the Griffith criterion for unstable crack extension can be formulated as, *rapid extension of an existing crack takes place when the rate of elastic energy available ( $G$ ) exceeds the energy absorption rate of the material ( $R$ )*. Griffith related the energy absorption rate of the material to the *specific surface tension energy*  $\gamma$ , which is a material property and hence must be determined from laboratory experiments. For example, for an infinitely large plate under uniform biaxial tension  $\sigma_0$  with a central crack of initial length  $2a$ , the strain energy release rate can be derived as

$$G = \frac{\pi\sigma_0^2 a}{E} \quad (5.24)$$

where,  $E$  is the Young's modulus of the material and the energy absorption rate is given by

$$R = 2\gamma \quad (5.25)$$

Hence, using the Equations 5.23, 5.24 and 5.25 the critical applied stress prior crack propagation can be found as

$$\sigma_c = \sqrt{\frac{2E\gamma}{\pi a}} \quad (5.26)$$

As an alternative fracture criterion, Irwin [12], proposed, *if the stress intensity factor reaches a critical value, the crack will propagate*. The critical value of the stress intensity factor is named as the *fracture toughness*. Hence, for a mode I type of crack displacement, the criterion predicts onset of crack propagation, if:

$$K_I = K_{Ic} \quad (5.27)$$

where,  $K_I$  is the stress intensity factor for a crack deformation mode I and  $K_{Ic}$  is the fracture toughness for the same mode. Irwin, has shown also, that this criterion is equivalent for brittle materials to the strain energy release rate criterion. It can be shown, for instance, that for plane strain conditions and mode I crack displacements

$$G = \frac{K_I^2}{E} (1 - \nu^2) \quad (5.28)$$

where  $\nu$  is the Poisson's ratio.

Fatigue crack propagation is modeled by means of the Paris/Erdogan law [13],

$$\frac{da}{dN} = C (\Delta K_{eff})^n \quad (5.29)$$

Here,  $N$  is the number of cycles,  $\Delta K_{eff}$  the cyclic increment of the equivalent stress intensity factor, and  $C$  and  $n$  are material properties. By integration of the above equation, the total life of the specimen can be determined.

### 5.6.2 Inelastic and Viscoelastic Crack Propagation

A number of approaches are available to apply fracture mechanics to inelastic and viscoelastic crack propagation. The most commonly used methods are briefly outlined below:

#### **Crack Opening Displacement (COD) Method:**

In this approach, the "effective" defect parameter,  $a$ , is determined from the crack size and position. If the value of  $a$  is smaller than the tolerable defect parameter  $a_m$  calculated using the critical value of COD then the defect is regarded as acceptable. The tolerable defect parameter is calculated from the equation:

$$a_m = C(\delta_{crit} / \epsilon_y) \quad (5.30)$$

where  $C$  is a constant, dependent on stress,  $\delta_{crit}$  is the critical value of COD and  $\epsilon_y$  is the yield strain. A detailed assessment method is given in [14].

#### **J-Contour Integral Method:**

The J-integral [15], or crack extension force, can be defined by a path independent expression:

$$J = \int_{\Gamma} W dx_2 - \underline{T} \frac{d\mathbf{u}}{dx_1} d\Gamma_j \quad (5.31)$$

where  $W$  is the strain energy density,  $\underline{T}$  is the traction vector and  $\mathbf{u}$  is the displacement vector on the line element  $d\Gamma$  ( $\Gamma$  is the external boundary or perimeter).

The derivation of  $J$  is strictly only valid for linear and non-linear elastic materials where loading and unloading paths are the same. However, in a few instances, the J-contour integral has been used by a few workers for crack propagation in plastics [16,17].

**Fracture Energy Approach:**

This energy criterion for fracture is an extension of Griffith's theory, which can be also given by the following equation (refer also to Section 5.6.1):

$$\frac{\partial}{\partial a} (F - U) \geq \gamma \frac{\partial A}{\partial a} \quad (5.32)$$

where  $\partial A$  is the increase in surface area associated with an increment of crack growth  $\partial a$ ,  $F$  is the external force,  $U$  is the elastic energy stored in the bulk of the specimen and  $\gamma$  is the surface free energy. Assuming that the energy dissipation around the crack tip occurs in a manner independent of test geometry and loading conditions,  $2\gamma$  may be replaced by  $G_c$ , where  $G_c$  is the energy required to increase the crack by unit length.

The fracture energy approach can be readily extended to inelastic materials. Here fracture energy is the total amount of energy dissipated during crack growth and includes energy dissipated by plastic deformation and viscoelastic processes. The energy available for crack propagation is now taken as the input strain energy density minus the hysteresis (loss) energy. This approach has been applied by a number of workers to composite rocket propellants [18-20].

A generalised approach for inelastic behaviour taken by Andrews et al. [21,22] defines fracture energy by the equation:

$$G_c = G_0 \Phi(\dot{a}, T, \epsilon) \quad (5.33)$$

where  $G_0$  is the intrinsic failure energy and  $\Phi$  is a loss function which depends on the crack growth rate  $\dot{a}$ , temperature  $T$  and strain level  $\epsilon$ . The loss function is defined by:

$$\Phi = \frac{k_2(e)}{k_2(e) - \sum_{PU} h_r g \partial v} \quad (5.34)$$

where,  $h_r$  is the hysteresis ratio,  $\partial v$  is the volume element,  $g$  is a distribution function of the energy density  $W$  throughout the specimen,  $PU$  denotes summation over points which unload as the crack propagates and  $k_2$  is an explicit function.

**Linear Elastic Fracture Mechanics (LEFM) Corrected for Plastic Zone Size:**

To account for plasticity, the crack length is corrected by an amount equal to the radius of the plastic zone, such that the new crack length is  $a+r$  where

$$r = \frac{1}{2\pi} \left( \frac{K}{\sigma_y} \right)^2 \quad (\text{for plane stress}) \quad (5.35)$$

The plastic zone size must be small compared with the crack size and width of the specimen.

Further studies on viscoelastic fracture can be found in [23-25].

## 5.7 REFERENCES

- [1] Wang, D.T.; Shearly, R.N.: *A Review of Solid Propellant Grain Structural Margin of Safety Prediction Methods*. AIAA/SAE/ASME/ASEE 22<sup>nd</sup> Joint Propulsion Conference and Exhibition, June 16 - 18, 1986, Huntsville/Alabama, pre-print AIAA-86-1415, pp. 1-8.
- [2] Kelley, F. N.: *Solid Propellant Mechanical Properties. Testing, Failure Criteria, and Aging*. In: **Propellants Manufacture, Hazards, and Testing, Advances in Chemistry Series** (Ed. R. F. Gould), Washington, D.C.: American Chemical Society, 1969, pp. 188-243.
- [3] Bills, K.W.; Wiegand, J.H.: *Relation of Mechanical Properties to Solid Rocket Motor Failure*. AIAA-Journal, 1 (1963) 9, pp. 2116-2123.
- [4] N. N.: *Solid Propellant Grain Structural Integrity Analysis*. NASA Space Vehicle Design Criteria (Chemical Propulsion), NASA-SP-8073, 1973.
- [5] Trasher, D. I.; Empleo, P. R.: *Structural/Ballistic Instability Ageout Mechanism in the Sparrow Mark 52 SRM*. In: **Proceedings of the 87th Symposium on Service Life of Solid Propellant Systems, PEP/AGARD/NATO**, paper number 42, May 6-8, Athens (1996).
- [6] Trasher, D. I.: *State of the Art of Solid Propellant Rocket Motor Grain Design in The United States*. In: **AGARD Lecture Series No: 150, Design Methods in Solid Rocket Motors**, 1987, pp.9.1-9.21.
- [7] Faulkner, G. S.; Tod, D.: *Service Life Prediction Methodologies Aspects of the TTCP KTA-14 UK Programme*. In: **Proceedings of the 87th Symposium on Service Life of Solid Propellant Systems, PEP/AGARD/NATO**, paper number 7, May 6-8, Athens (1996).
- [8] Davenas, A.: **Solid Rocket Propulsion Technology**, Oxford: Pergamon Press, 1993.
- [9] Ferry, J. D.: **Viscoelastic Properties of Polymers**, 3. Edition, New York: John Wiley & Sons, 1980.
- [10] Amos, R. J.: *Viscoelastic Analysis of Cast Double Base Propellant Rocket Motor Grains*. AIAA/SAE/ASME/ASEE 29th Joint Propulsion Conference and Exhibition, June 28 - 30, 1993, Monterey/California, pre-print AIAA 93-2167, pp. 1-9.
- [11] Griffith, A. A.: *The Phenomena of Rupture and Flow in Solids*. **Phil. Trans. Royal Soc.**, A221 (1921), pp. 163-197.
- [12] Irwin, G. R.: **Fracture, Handbuch der Physik, Vol. IV**, (Editor: Flügge), Berlin: Springer-Verlag, 1958, pp. 551-590.
- [13] Erdogan, F.; Sih, G. C.: *On the Crack Extension in Plates Under Plane Loading and Transverse Shear*, **J. Basic Engineering**, 85 (1963), pp. 519-524.
- [14] BS5762 (British Standards): *Methods for Crack Opening Displacement (COD) and Testing*, 1979.
- [15] Rice, J.R.: *A Path Independent Integral and Approximate Analysis of Strain Concentration by Notches and Cracks*. **J. Applied Mechanics**, 35 (1968), pp. 379-386.
- [16] Plati, E.; Williams, J. G.: *Determination of Fracture Parameters for Polymers in Impact*. **Polym. Eng. Sci.**, 15 (1975) 6, pp. 470-477.
- [17] Hodgkinson, J. M.; Williams, J. G.: *J-Analysis and GC-Analysis of the Tearing of a Highly Ductile Polymer*. **J. Mater. Sci.**, 16 (1981) 1, pp. 50-56.
- [18] Kinloch, A. J.; Tod, D. A.: *A New Approach to Crack Growth in Rubbery Composite Propellants*, **Propell. Explos. Pyro.**, 9 (1984), pp.48-55.
- [19] Ho, S. Y.; Tod, D. A.: *Mechanical Failure Analysis of Rubbery Composite Propellants Using a Modified Fracture Mechanics Approach*, **Proceedings of the 21st ICT Conference**, Karlsruhe (1990).
- [20] Ho, S. Y.; Ide, K. M.; Macdowell, P.: *Instrumented Service Life Program for the Pictor Rocket Motor*, **Proceedings of the 87th Symposium on Service Life of Solid Propellant Systems, PEP/AGARD/NATO**, paper number 28, May 6-8, Athens (1996).
- [21] Andrews, E. H.: *Generalized Theory of Fracture Mechanics*. **J. Mater. Sci.**, 9 (1974) 6, pp. 887-894.
- [22] Andrews, E. H.; Fukahori, Y.: *Generalized Fracture Mechanics Prediction of Fracture Energies in Highly Extensible Solids*. **J. Mater. Sci.**, 12 (1977) 7, pp. 1307-1319.
- [23] Williams, M. L.: *Initiation and Growth of Viscoelastic Fracture*, **Int. J. Fracture Mechanics**, 1 (1965), p.4
- [24] Francis, E. C.; Carlton, C. H.; Lindsey, G. H.: *Viscoelastic Fracture of Solid Propellants in*

- Pressurization Loading Conditions, J. Spacecraft*, 11 (1974) 10, pp.691-696
- [25] Liu, C. T.: *Microstructural Damage and Crack Growth Behavior in a Composite Solid Propellant. Proceedings of the 87th Symposium Service Life of Solid Propellant Systems, PEP/AGARD/NATO*, May 6-8, Athens (1996).

**APPENDIX A:  
COMPARISON OF SOME FAILURE CRITERIA FOR DOUBLE BASE PROPELLANTS**

An illustrative comparative study about the performance of various failure criteria for cast double base (CDB) and elastomer-modified cast double base (EMCDB) propellants has been performed by Amos [10]. Table 5.3 gives an extract of the results for four different failure criteria: Strain energy (work done, i.e. sum of the dissipated and stored energies), maximum principal strain, maximum principal stress and Smith's envelope. Computations have been conducted with a commercial finite element code utilizing linear viscoelasticity assumption and considering finite strain kinematics. Experiments have been performed by means of a thermal structural test vehicle (STV), which comprises a heavyweight steel case and a case bonded grain with circular conduit, providing a range of values of grain radius ratio. The STV is cooled down from its cure temperature at a known rate and inspected at regular intervals until failure (surface cracks) is observed. The prediction of grain structural failure is based on the ratio predicted/measured capability. If this ratio exceeds unity failure is assumed to occur. The results given in Table A5.1 are found by assuming that loading all takes place at the temperature of the test. Amos supplies also results for simultaneous loading and cooling. No correction has been made for axiality in any of the methods considered.

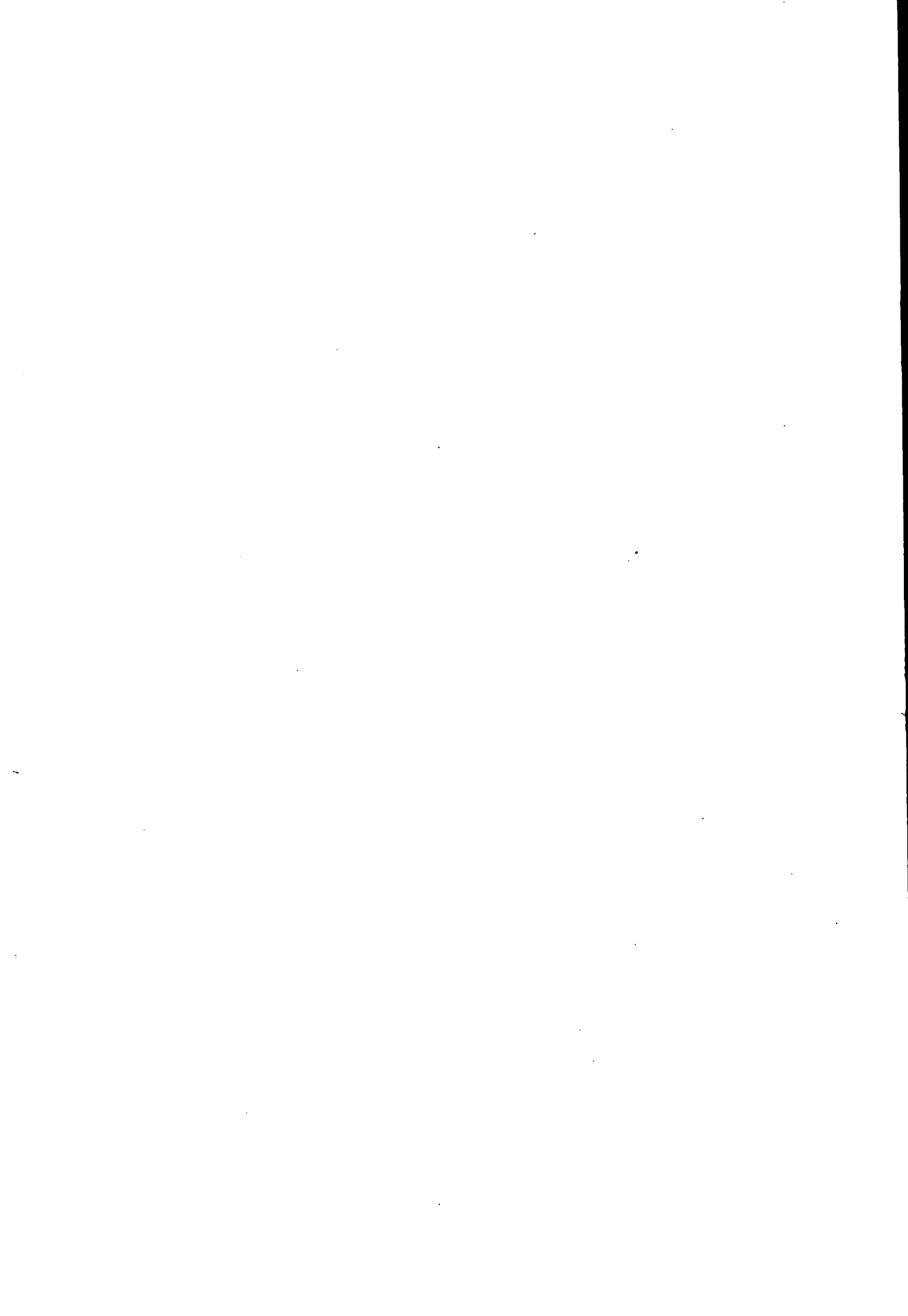
**Table A5.1: Measured and predicted failure temperatures [10]**

Propellant	Radius Ratio	STV Test Results at Failure		Predictions of Failure Temperature (°C)			
		Strain (%)	Temp (°C)	Strain Energy	Max. Principal Strain	Max. Principal Stress	Smith Envelope
EMCDB A	6.0	50.0	-58	-60	-32	-58	-46
	4.7	34.5	-56	-62	-42	-60	-53
	3.7	28.0	-63	-63	-46	-61	-55
EMCDB B	6.0	70.0	-55	-56	-27	-59	-48
	4.7	51.0	-55	-57	-36	-60	-54
	3.7	35.0	-62	-59	-43	-62	-58
EMCDB C	6.0	73.4	-53	-53	-33	-56	-47
	3.7	39.3	-59	-57	-42	-59	-55
EMCDB D	6.0	72.6	-51	-52	-22	-56	-42
	3.7	38.9	-58	-57	-36	-58	-52
CDB E	6.0	64.5	-34	-34	-12	-34	-
Mean Difference (+: prediction higher):				-0.55	21.18	-1.73	6.00
Standard Deviation:				2.38	4.79	2.49	3.20

Another interesting result of Amos [10] is related to low temperature pressurization tests. The tests consist of two series: non-destructive rapid pressurization using cold dry nitrogen gas (at rates and level similar during ignition) and motor firing. The results have been compared with the various failure criteria listed above, from which only the energy criterion results are given in Table A5.2. It is seen that the strain criterion is more conservative whereas the stress criterion is more optimistic for the propellants studied [10].

**Table A5.2: Pressurization Results [10]**

<b>Motor</b>	<b>Propellant</b>	<b>Conditioning Temperature °C</b>	<b>Rapid Pressurization Results</b>	<b>Firing Results</b>	<b>Prediction by strain energy</b>
1	B	-33 to -34	2 Passed 0 Failed	50 Passed 0 Failed	Pass
		-37 to -38	4 Passed 0 Failed	10 Passed 4 Failed	Marginal
		-40 to -41	0 Passed 5 Failed	25 Passed 1 Failed	Fail
2	A	-51	0 Passed 1 Failed	3 Passed 0 Failed	Fail
		-54	- -	2 Passed 0 Failed	Fail
3	C	-55	- -	5 Passed 0 Failed	Fail

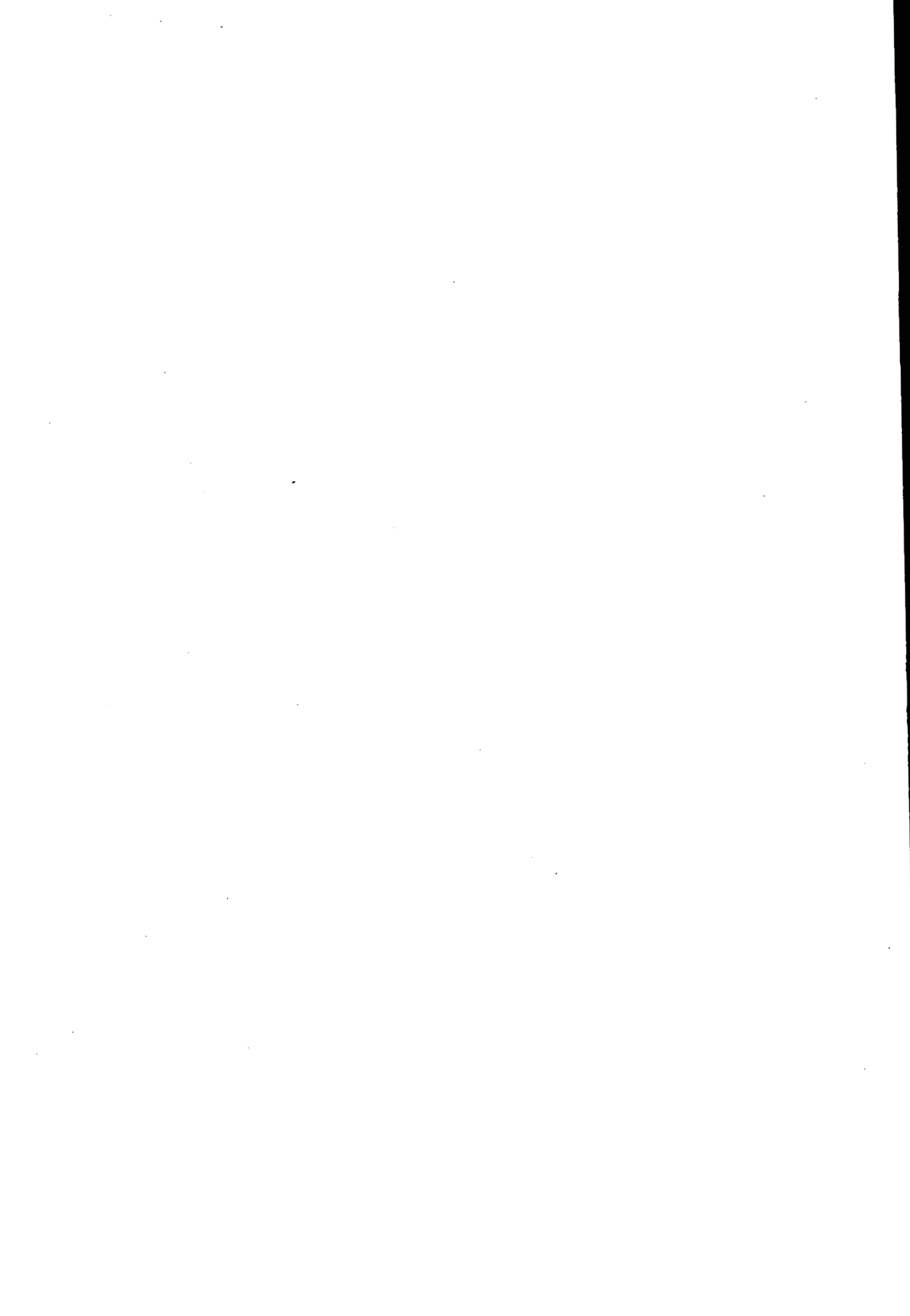


# CHAPTER 6

## MARGIN OF SAFETY DETERMINATION

### TABLE OF CONTENTS

<b>6.1</b>	<b>INTRODUCTION</b>	<b>6-1</b>
<b>6.2</b>	<b>DEFINITION</b>	<b>6-1</b>
<b>6.3</b>	<b>MINIMUM REQUIRED VALUES</b>	<b>6-3</b>
<b>6.4</b>	<b>DESIGN FACTORS AND KNOCKDOWN FACTORS</b>	<b>6-5</b>
6.4.1	Design Factors	6-5
6.4.2	Knockdown Factors	6-6
6.4.2.1	Aging	6-7
6.4.2.2	Variability	6-9
6.4.2.3	Multiaxiality	6-10
6.4.2.4	Compressibility	6-10
6.4.2.5	The De-wetting Strain and Break-Point Concept	6-10
<b>6.5</b>	<b>CUMULATIVE DAMAGE METHODS</b>	<b>6-11</b>
<b>6.6</b>	<b>MULTIPLE LOADING CONDITIONS</b>	<b>6-15</b>
<b>6.7</b>	<b>PROBABILISTIC METHODS</b>	<b>6-16</b>
<b>6.8</b>	<b>EXAMPLES</b>	<b>6-22</b>
6.8.1	Multiple Loading Example #1 - A "Quick-Look" Approach	6-22
6.8.1.1	Problem Statement	6-22
6.8.1.2	Solution	6-22
6.8.1.2.1	Thermal Cool-down	6-22
6.8.1.2.2	Ignition Pressurization	6-24
6.8.2	Multiple Loading Example #2 - A Detailed Deterministic Approach	6-26
6.8.2.1	Problem Statement	6-26
6.8.2.2	Solution	6-26
6.8.2.2.1	Thermal Cool-down	6-27
6.8.2.2.2	Ignition Pressurization	6-31
6.8.3	Multiple Loading Example #3 - The Probabilistic Approach	6-41
6.8.3.1	Problem Statement	6-41
6.8.3.2	Solution	6-41
6.8.3.2.1	Determination of $K_0$	6-41
6.8.3.2.2	Thermal Cool-down	6-42
6.8.3.2.3	Ignition Pressurization	6-43
6.8.3.2.4	Multiple Loading Conditions	6-44
<b>6.9</b>	<b>REFERENCES</b>	<b>6-45</b>



## Chapter 6

### MARGIN OF SAFETY DETERMINATION

#### 6.1 INTRODUCTION

The distinct differences that exist between the methods and terminology used among the various countries to describe a rocket motor's grain structural capability, are described in this chapter. The reader must read the chapter carefully to understand clearly how each country defines the terms Margin of Safety, Safety Ratio and Safety Factor before applying any of the equations in a strength analysis. These terms can have different meanings in different countries. It is the purpose of this chapter to fully define these differences.

After the structural analysis and selection of failure criteria, a strength analysis is the next step in determining the structural integrity of a solid propellant grain/bondline system within a rocket motor. The results are typically expressed in terms of Margin of Safety, Safety Ratio or Safety Factor as listed in Table 6.1. Determining a minimum required value demands consideration of ( a ) the statistical variations inherent in polymeric materials and their testing, ( b ) the loading conditions imposed on the propellant grain/bondline system ( e.g., thermal cool-down, ignition pressurization, acceleration, vibration, etc.); and ( c ) the inaccuracies inherent in the analysis methods, artificially introduced through simplifying assumptions. Values determined through proper consideration of these factors is an indication of the overall structural integrity of the propellant grain/bondline system. If these factors were precisely known there would be no real requirement for a Margin of Safety greater than zero, or a Safety Ratio greater than one. However, this is not the case. There are frequently instances where the analyst has to make assumptions or approximations to perform the analysis due to unavailable or ill-defined material property data by placing arbitrary restrictions on the minimum required value. These restrictions are reflected through either the Margin of Safety, Safety Ratio, Safety Factor, or uncertainty factors (i.e., Design and Knockdown Factors) associated with the structural analysis, loading environment, propellant grain/bondline behavior and failure criteria; constrained or set by the customer's mission requirements. This chapter will explain how these restrictions are calculated and used in the determination of a propellant grain/bondline system's structural integrity.

The various countries contributing to this document all use the same basic parameters in constructing expressions to describe structural integrity, but with some important differences in methodology and definition. This chapter will discuss these variations in methodologies including with how each country handles variability and aging, comparison of uniaxial material property data with a multiaxial loading environment, and multiple loading conditions in determining propellant grain/bondline system's Margin of Safety, Safety Ratio or Safety Factor. Also, this chapter will describe the various types of cumulative damage models each country uses to determine the aging capabilities of the propellant grain/bondline system and discuss the various types of probabilistic methods some countries are use to determine the reliability of propellant grain/bondline systems in meeting their service requirements.

#### 6.2 DEFINITION

The Margin of Safety (MS), Safety Ratio (K), and Safety Factor (SF) values are all measures of the excess propellant grain/bondline material capability over the design requirement. A value is calculated at each critical location in a rocket motor for various loading conditions, using the failure criteria discussed in Chapter 5. Table 6.1 provides a list of equations that each country uses to determine these quantities.

Table 6.1: Equations used by Various Countries.

COUNTRY	EQUATION	COUNTRY	EQUATION
Australia	$K = \frac{C}{S}$ $MS = \frac{C}{(DF)(S)} - 1$ $MS = \frac{1}{D} - 1$	The Netherlands	$MS = \frac{(KDF_{total})(C)}{S} - 1$
Canada	$MS = 1 - \frac{S}{C}$	Turkey	$MS = \frac{C}{(DF)(S)} - 1$
France	$K = \frac{C}{S}$ <p>(used in probability analysis)</p>	United Kingdom	$SF = \frac{1}{(D_i + D_p)}$ <p>Damage Factors:</p> $D_i = \frac{S_i}{C_i} \quad D_p = \frac{S_p}{C_p}$
Germany	$MS = \frac{C}{(DF)(S)} - 1$ $MS = \frac{1}{D} - 1$	United States	$MS = \frac{(KDF_{total})(Z_{allowable})}{(DF)(Z_{induced})} - 1$

where, DF= Design Factor

C = material's measured capability

S = stress or strain calculated from induced loads

Z = Failure Parameter

D = Damage Factor

KDF = Knockdown Factor

At first glance, these equations may appear to be very different from each another; however, upon a closer examination it can be shown that most of them follow the same relationship;

$$\frac{C-S}{S} \quad (6.1)$$

$$\frac{C}{S} - 1 \quad (6.2)$$

which can be simplified to

$$K - 1 \quad (6.3)$$

where,

$$K = \frac{C}{S} = \frac{Z_{allowable}}{Z_{induced}} \quad (6.4)$$

is the ratio of the material's capability or allowable response to induced loads called the Safety Ratio. In the United States, Z is considered a dummy variable representing the failure parameter in general terms; where  $Z_{allowable}$  is the corresponding value of the allowable parameter of the material, and  $Z_{induced}$  is the stress-strain value calculated from a finite element model subjected to the induced loads.

Though each equation given Table 6.1 uses essentially the same relationship, the differences lie in how the relationship is used. For instance, Canada divides the quantity, C minus S, by the material's measured capability, C, and not by the induced stresses and strains, S, as do some of the other countries. France uses the Safety Ratio and damage factor in combination with a probability analysis to determine the structural integrity of a propellant grain/bondline system. The United Kingdom uses the Safety Factor and a damage approach to assess the system's structural integrity for multiple loading conditions. These differences also lie in how each country handles aging effects of polymeric materials along with variability of material properties (i.e., lot-to-lot of raw materials, mix-to-mix, and experimental variability), relating uniaxial material properties to a multiaxial stress-strain fields, and multiple loading conditions.

### 6.3 MINIMUM REQUIRED VALUES

All of the participating countries agreed that for a rocket motor design to be considered structurally sound, the MS values should in theory be a positive number. Therefore, the minimum required value is zero. If we substituted zero into Equation 6.3, we can reduce the equation to reveal that the minimum required K value is one (see Equation 6.6):

$$K - 1 \geq 0 \quad (6.5)$$

reduced to

$$K \geq 1 \quad (6.6)$$

In the United States the practice is to allow a MS of zero only if a detailed analysis is completed using a minimum number of assumptions with well-characterized propellant and bondline mechanical property data. However, if a preliminary analysis is being conducted using closed-form solution(s) and with very little data then allowance must be made for uncertainty and the minimum required MS value could vary from 0 to 0.25 for strategic systems, all the way up to one for tactical systems (see Table 6.2). The chosen value is dependent upon the type of application, loading condition, and propellant grain/bondline system being evaluated. Along with a "degree" of confidence the analyst may have in the analysis due to the lack of data available.

As stated in Chapter 3, closed-form solutions have been used to give the analyst an initial assessment of the design's structural integrity, during the preliminary design phase. As a general rule, the United States uses a minimum required MS value of 1.0 based on lower three-sigma, unaged propellant property data that leads to an acceptable design: one standard deviation typically represents about a 10% variation. This coefficient of variation is frequently used when there are not enough data available on the proposed propellant grain/bondline system at the time of the analysis. However, the more information is obtained, the lower the minimum required MS becomes, such as, information on aging degradation that suggests the  $MS_{\min}$  should be reduced to a value between 0.25 and 0.50 for long term storage conditions. As the knowledge of the factors affecting the propellant grain/bondline system's structural integrity increases, minimum required Margins of Safety may approach values as low as 0.10. Therefore, to give the analyst (and the customer) a starting point for choosing a minimum required MS value, the United States have put together Table 6.2. This table lists various minimum required MS values the analyst can use during a preliminary analysis; only if his customer did not provide him with one or is unsure to what value to choose for his particular system he is analyzing. The table provides a range of typical values used for both the strategical and tactical-based systems, subjected to two separate loading conditions.

Before the analyst can begin evaluating the structural integrity of a rocket motor, using any of the equations listed in Table 6.1, he must ask himself the following questions:

- (1) What types of analytical method are going to be used in the analysis (preliminary or detailed -- refer to Chapter 3)?
- (2) What type of application and extreme loading conditions is the rocket motor designed for or intended to see in the field?
- (3) For each loading condition considered in the analysis, how well was the propellant and bondline mechanical properties characterized?

In answering these questions, the analyst can determine ( a ) what minimum required MS value should be used to quantify the results; and/or ( b ) the minimum Design and Knockdown Factors (refer to Section 6.4) needed in the MS calculation. The analyst must be careful when selecting the minimum required Margin of Safety, Design Factor, and Knockdown Factor values, and using these values together when determining the design's structural integrity. If the selection of values does not properly reflect the depth of the structural analysis and the accuracy of propellant data, then the results could be too conservative or too optimistic. For example, there have been instances where the structural integrity assessment predicted the propellant grain/bondline system to have negative margins (or safety ratios and safety factors below the chosen limit), showing that the design was structurally unsound. Yet, the rocket motor operated without any problems when tested under extreme conditions. These comments are particularly applicable to the United States' method of determining Margin of Safety that employs design and knockdown factors. Caution should be taken whenever using these values with the equations listed in Table 6.1.

**Table 6.2: Range of Typical Minimum Required MS Values used in the United States.**

Application (Propellant type)	Loading Condition	$MS_{\min}$
Strategical (C&HiE)	TC	0.0-0.25
	IP	0.0-0.25
Tactical ( C )	TC	0.0-1.00
	IP	0.0-0.50

C - Conventional  
HiE - High Elongation

TC - Thermal Cool-down  
IP - Ignition Pressurization

The difference of approach in France should be noted where the values of  $K$  (known as  $K_o$ ) are used as objective values for the design of a grain and are determined from reliability requirements for the solid rocket motor, refer to Section 6.7.

## 6.4 DESIGN FACTORS AND KNOCKDOWN FACTORS

Design and Knockdown Factors are used to build in some level of conservatism into a design in a formalised way. The determination of these factors depends on the type of analysis method used [preliminary or detail, see Chapter 3] and how well the propellant grain/bondline system's structural capabilities have been characterized using standardized test methods described in Chapter 4.

In the United States, the determination of both the Design Factor and the total Knockdown Factor is dependent on each other, the selection of the minimum required MS value (either by the customer or the analyst); and how well the propellant grain/bondline system has been characterized. For example, as the knowledge of the system's material responses grows, the lower the minimum required MS value can become and the closer some factors will reach unity. These values are very dependent upon what data is available for the strength analysis and the analyst's understanding of the problem. **Therefore, care should be taken when using this factors in a strength analysis. A clear understanding of the problem is required before using any factors in the analysis.**

### 6.4.1 Design Factors

Where the Design Factor (DF) is used it is a contingency factor multiplied to the induced stresses and strains generated from the analysis to account for unavailable or ill-defined propellant grain/bondline mechanical property data. Also, the factor is used to account for the generality of the analysis being conducted, whether it is preliminary or detailed in nature. Some countries multiply this factor to  $Z_{\text{induced}}$  (otherwise known as,  $S$ ), where as others rely solely on a specific minimum MS value. In the USA the Design Factor is determined using the following list of guidelines:

**Type 1:** If the propellant and bondline have been "well-characterized" with known aging and variability behavioral data, then the Design Factor can be either 1.0 or 1.25, depending on the type of method used in the analysis (detail or preliminary, respectively).

**Type 2:** If the propellant and the bondline are a derivative or a modification of Type 1, with sufficient experimentation performed to assure the similarity, then the Design Factor is 1.5.

**Type 3:** If the propellant and the bondline are virtually un-characterized, then a Design Factor of 2.0 is applied to the induced stresses and strains.

Table 6.3 shows a typical range of Design Factors used in the United States for different types of applications, loading conditions, and failure modes analyzed, primarily for surface cracking at the bore or de-bonding at the bondline.

In the United States, the MS calculation is sometimes based upon the statistical descriptions of the load and material properties, but usually a single value for each pertinent parameter is used in the analysis. Mean and lower three-sigma values selected from distribution curves are used in some extent by each country performing this type of calculation. The limits placed on data used in the analysis will influence the Design Factor. So, if "worst-on-worst" conditions are assumed throughout, and there is little uncertainty in the approach, a very low or no Design Factor value may be used. However, if average properties are used, then a higher Design Factor would be more appropriate. In fact, a MS,  $K$  or SF calculation based on average or mean properties does not indicate the structural integrity of a design, if the standard deviations are unknown.

Australia uses a Design Factor of 2.0 during the design phase, no matter how well the propellant has been characterized or what type analysis method was used.

**Table 6.3: A Typical Range of Design Factors used in the United States.**

Application (Propellant Type)	Loading Condition	Failure Mode	DF
Strategic ( C )	TC	SCB	1.0-1.5
		DB	1.0-2.0
	IP	SCB	1.0-2.0
		DB	1.0-2.0
Strategic (HiE)	TC	SCB	1.25
		DB	1.0
	IP	SCB	1.25
		DB	1.5
Tactical ( C )	TC	SCB/DB	1.0-1.25
		IP	1.0-1.25

C - Conventional  
HiE - High Elongation

DB - De-bond at Bondline  
SCB - Surface cracks in bore

TC - Thermal Cool-down  
IP - Ignition Pressurization

#### 6.4.2 Knockdown Factors

Knockdown Factors (KDF's) where they are used allow for such influences as:

- variability of material properties data (i.e., lot-lot of raw materials, mix-to-mix, and experimental variability),
- casting configurations,
- test specimens,
- mix scale-up,
- the "level of knowledge" related to the propellant bondline system's material properties,
- and, other factors, such as uncertainties during design phase concerning operating conditions (eg., thermal cycling definition), environmental loads (eg., humidity conditions), conversion of uniaxial material properties data to multiaxial loading conditions and compressibility, or when simply the data is unavailable.

These factors, derived from data obtained from other similar programs, are used during the preliminary design phase (i.e., proposals) of a rocket motor and should serve to build conservatism in the design. Consequently, the KDFs will change as the knowledge about material properties, capabilities, and variability increases during the design process. For instance, once the design has reached the development phase, zero time, accelerated (or compressed; materials aged at 32.22 °C for two to three years) and real-time aged mechanical property data are obtained for the propellant grain/bondline system. This data is used to obtain a better failure allowable value(s) for determining a realistic safety margin for the design, and the KDF for aging will default to one.

Obviously, the estimate of the KDFs depends strongly on the specifics of the design, as well as on the manufacturing process and the environmental conditions. Nevertheless, there are some "default" values in use that will be discussed in the following subsections. These subsections will describe what types of KDFs are used by the various countries to account for aging; variability of material property data (such as lot-to-lot of raw materials, mix-to-mix, and experimental variability), converting uniaxial material property data to a multiaxial loading condition, and compressibility (used only for very special cases, refer to Section 6.4.2.4). Also, the following subsections will describe how these values are obtained.

Equation 6.7 shows the relationship used to combine the various KDFs chosen for the structural integrity analysis;

$$KDF_{total} = (KDF_{aging})(KDF_{variability})(KDF_{multiaxiality})(KDF_{etc.})... \quad (6.7)$$

where,  $KDF_{etc.}$  represents any additional factor being considered in the analysis. The  $KDF_{total}$  is a product of all the factors combined.

The United Kingdom does not use KDFs in calculating a rocket motor's structural integrity. However, they do account for mix-to-mix variability in mechanical property data during production, by determining a "propellant minimum property specification" using statistical methods (i.e., the Monte Carlo method) when analyzing design responses to various loading conditions. The specification ensures that in production, no mix is accepted which falls below the critical acceptance values. Typically, one might specify strain capability, modulus and strength (along with other parameters such as burning rates,  $\pi_k$ , etc.) which need to be met in production. Therefore, it is important to note that the SF is calculated using these minimum values.

#### 6.4.2.1 Aging

Aging Knockdown Factors ( $KDF_{aging}$ ) can vary with propellant formulation and design life requirements. Table 6.4 provides a listing of typical default aging factors used in the United States in lieu of specific propellant data. The Netherlands refers to the  $KDF_{aging}$  as the damage factor that accounts for thermal cycling and long term storage (at low temperatures) of polymeric materials. They assume that for a preliminary analysis, all propellants and bondline systems age the same way and at a constant rate. Therefore, the Netherlands uses a general  $KDF_{aging}$  of 0.9 to account for aging effects of any polymeric material.

Germany however, uses a technique based on chemical aging simulated by the classical Arrhenius equation discussed in Section 6.5 to determine their aging knockdown factors used in the MS equations listed in Table 6.1.

Rather than applying a  $KDF_{aging}$  the United Kingdom allows for chemical aging of the propellant by performing the necessary aging characterization tests or by using a database of aging data for generic propellant types and applying a corrected value for S. The United Kingdom assesses the drop in the strain capability, or other applicable failure criterion, and determines the SF at the end of the desired life [as does every other country, in one form or another]. This is achieved by substituting aged failure data for fresh in the SF equation and recalculating the Damage Factors,  $D_t$  and  $D_p$  (thermal cool-down and ignition pressurization, respectfully). Only uniaxial data is used to generate the master curves; no biaxial or triaxial factors are applied. Although not rigorously correct, this method has been found to be very conservative in predicting SF.

In the United States, the hydroxy-terminated poly butadiene (HTPB) aging factors given in Table 6.4 have been developed using a combination of data from different formulations. Variables such as bonding agents, polymer grades, and other ingredients have been shown to affect both normal aging and "post curing" of these propellants. The surface versus bulk propellant aging may also differ. Therefore, the analyst is cautioned to review as much aging data pertinent to the specific formulation available to ensure consistency with the default factors. Also, these values are used for both thermal cool-down and ignition pressurization when conducting the analysis; however, they are to be used with caution. It has been proven that aging KDFs will vary from one loading condition to the next; therefore, once the design has reached its development phase, extensive aging studies are required better to characterize both the propellant's and the bondline's material responses to these different loading conditions.

**Table 6.4: Default Aging Knockdown Factors for Common Propellant Families used in the United States.**

Propellant Family		5 yrs	10 yrs	15 yrs	20 yrs	25 yrs
CMDB	$\sigma$	0.96	0.92	0.89	0.86	0.82
	$\epsilon$	0.98	0.95	0.93	0.90	0.88
XLDB	$\sigma$	0.92	0.84	0.77	0.71	0.65
	$\epsilon$	1.10	1.21	1.33	1.47	1.62
NEPE	$\sigma$	1.00	1.00	1.00	1.00	1.00
	$\epsilon$	1.02	1.05	1.07	1.09	1.12
HTPB	$\sigma$	1.10	1.12	1.14	1.16	1.18
	$\epsilon$	0.90	0.88	0.86	0.84	0.82

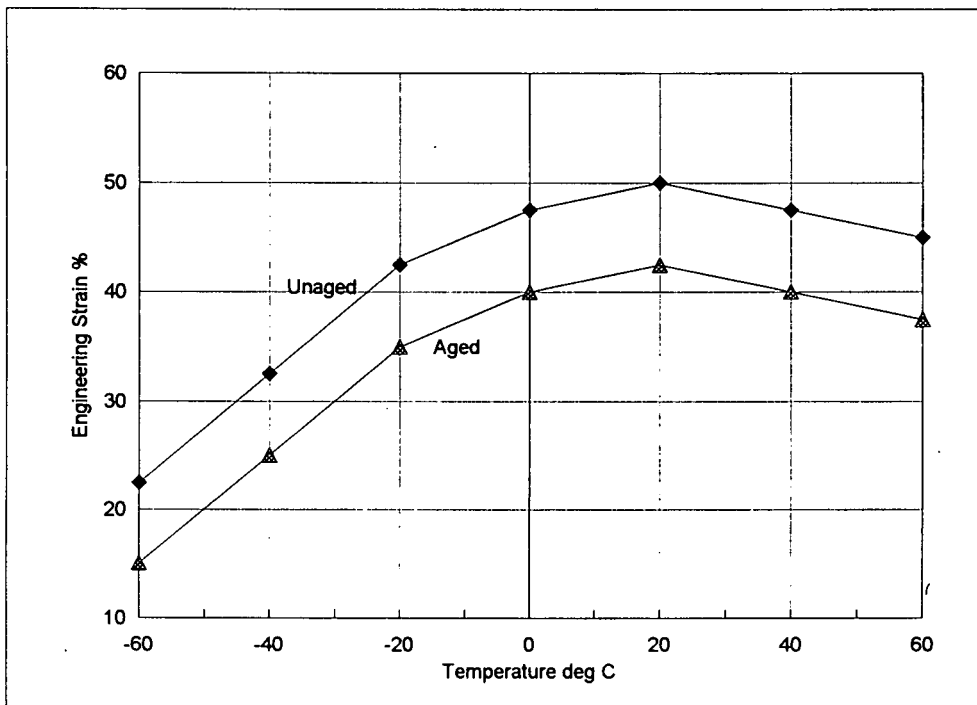


**Figure 6.1: Example Strain Curves used in the United Kingdom.  
(I) Strain Capability before Aging, (II) Strain Capability after Aging,**

Using these factors only on the allowable properties does not consider the changes in the applied loads due to modulus variation with age. Therefore, the use of these factors does not preclude performing a full-scale service life assessment that takes in to account both changes in applied loads and allowable properties.

#### 6.4.2.2 Variability

Knockdown factors for lot-to-lot of raw materials, mix-to-mix, and experimental variability are determined based upon the type of application, propellant and bondline system, and loading condition for both surface cracking and de-bonding. Material variability data is obtained from the same family of propellant and bondline systems, manufactured by similar processes. The Variability Knockdown Factor ( $KDF_{\text{variability}}$ ) can be calculated by using Equations 6.8 and 6.9,

$$\text{Variability} = \chi - \kappa(\sigma) \quad (6.8)$$

$$KDF_{\text{variability}} = 1 - \frac{\kappa(\sigma)}{\chi} \quad (6.9)$$

where,  $\chi$  is the material property of interest and  $\sigma$  is the standard deviation of the data retrieved. These  $\kappa$  values can vary for different types of loading conditions and applications as shown in Table 6.5. However,  $\kappa = 3$  is the value used most often in every country.

Both the Netherlands and the United States have found for most propellants. The  $KDF_{\text{variability}}$  will usually range between 0.7 and 0.8 depending on the type of propellant and property data available. Therefore, if the analyst finds himself without enough mechanical property data to determine a realistic  $KDF_{\text{variability}}$ ; then, he can use 0.7 as a default value. Note. The United States would always determine experimentally how much variability their particular design has by using similar test methods described in Chapter 4.

Table 6.5: Ranges of  $\kappa$  Values used in the United States.

Application (Propellant Type)	Loading Condition	$\kappa$
Strategical ( C )	TC	2.0-4.0
	IP	2.0-4.0
Strategical (HiE)	TC	3.0
	IP	3.0
Tactical ( C )	TC	3.0-4.6
	IP	2.0-4.6

C - Conventional  
HiE - High Elongation

TC - Thermal Cool-down  
IP - Ignition Pressurization

### 6.4.2.3 Multiaxiality

At the preliminary design and analysis phase, the Netherlands and the United States are the only countries that consider multiaxiality by way of knockdown factors in calculating MS for thermal cool-down. For France, the multiaxiality effects are taken into account when using Stassi/von Mises's failure envelope (see Chapter 5). The other countries account for multiaxiality in their structural integrity assessment by obtaining failure allowable values from various multiaxial tests (see Section 4.2.2), and using them to determine MS, K or SF through many phases of rocket motor's development. Only during a detailed analysis would the United States and the Netherlands account for multiaxiality this way; otherwise, knockdown factors are used.

Assuming the propellant is incompressible, the Netherlands uses a Multiaxiality Knockdown Factor ( $KDF_{\text{multiaxiality}}$ ) of 0.91 when translating uniaxial failure strain data to an induced multiaxial strain field (generated from finite analyses or closed-form solutions) within the propellant grain. For biaxiality, the United States have used a  $KDF_{\text{multiaxiality}}$  of 0.75 to relate uniaxial failure strain data to the induced biaxial strain field on the surface of the bore (or anywhere a biaxial strain field may exist). Experimental results indicated that this factor may vary from 0.65 to 0.85 depending on the type of propellant formulation used in the design. Therefore, the United States would most likely perform the necessary tests to determine the  $KDF_{\text{multiaxiality}}$  for their particular design, when performing a detail analysis. For relating uniaxial failure strain data to a triaxial strain field, the United States would conduct the multiaxial tests to determine the failure allowable values and set the  $KDF_{\text{multiaxiality}}$  to one.

### 6.4.2.4 Compressibility (only for special cases)

The compressibility Knockdown Factor ( $KDF_{\text{compressibility}}$ ) is a factor that considers the effects of pressure on the propellant grain during ignition pressurization, at thermal equilibrium. France and the United States have been known to use this when similitude data was unavailable during a preliminary analysis of a rocket motor design. Experience dictates that for most propellant formulations, the uniaxial failure strains obtained from a similitude test is double that of the "un-pressurized" case at temperatures above  $-17.78^{\circ}\text{C}$  and about 1.5 times as great at lower temperatures (i.e., a  $KDF_{\text{compressibility}}$  of 2.0 for temperatures above  $-17.78^{\circ}\text{C}$  and 1.5 for temperatures below  $-17.78^{\circ}\text{C}$ ).

France and the United States use the  $KDF_{\text{compressibility}}$  only in special cases when pressurized mechanical property data is unavailable. However, for a detail analysis both countries conduct the required tests to obtain actual stress-strain data and do not use this knockdown factor in the analysis.

### 6.4.2.5 The De-wetting Strain and Break-Point Concept

In some applications, one or more tensile specimens are tested at the critical storage condition. The resulting stress-strain curves are analysed to determine the strain at which de-wetting occurs and whether there is a shift in the onset of de-wetting relative to what would be expected by extrapolating the characterization data. This de-wetting strain is sometimes coupled with a combined KDF (known as  $KDF_{\text{total}}$ ) of 1.0 and included in the MS calculation. It is known that de-wetting occurs over a range of strains and that the stress-strain curve can be used as an indicator of de-wetting by observing its change-in-slope as shown in Fig. 6.2. Repeated strain cycling beyond the "breakpoint" of the stress-strain curve has been observed to induce surface cracking in the bore of analog motors. This maximum strain is less than the strain at maximum stress or the strain at rupture from tensile dog-bones. Similarly, strains in the center-port of the grain imposed by specific temperature cycles are evaluated based on maximum cycles that the grain can withstand before failing. Maximum cycles are experimentally determined from strain evaluation cylinders (SECs) or thermal analog motor tests (refer to Chapter 7).

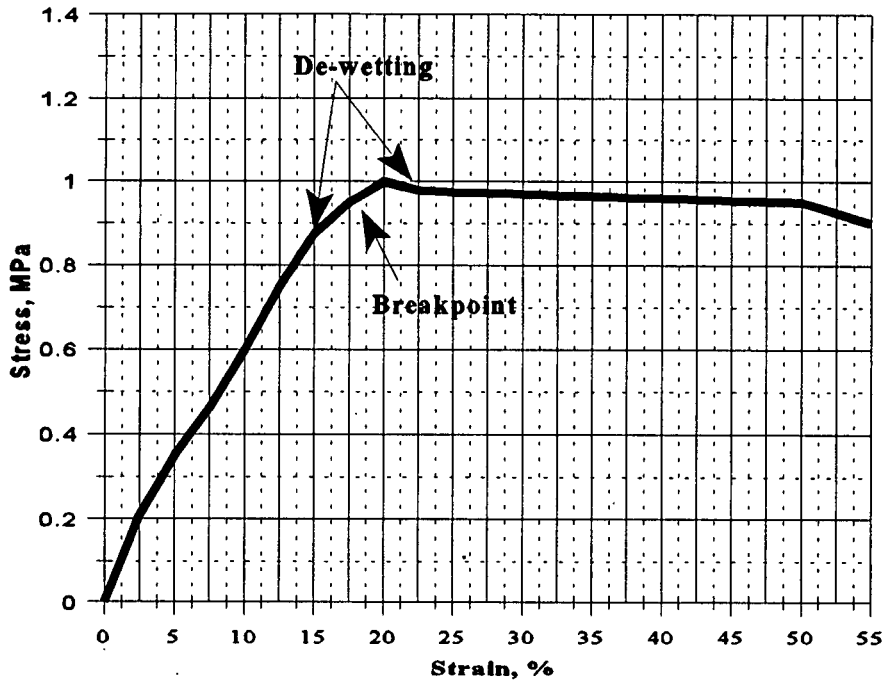


Figure 6.2: An example of a Propellant Grain's Critical Cold Storage Stress-Strain Curve showing De-wetting.

## 6.5 CUMULATIVE DAMAGE METHODS

Many countries have used cumulative damage methods to evaluate the structural integrity or "service life" of solid propellant grain/bondline systems. The basis for this analysis is Miners Cumulative Damage Law

$$D = \sum_{i=1}^n D_i = \sum_{i=1}^n \frac{\Delta t_i}{t_{fi}} \quad (6.10)$$

which relates the cumulative damage,  $D$ , to the incremental damages,  $D_i$ ,  $i = 1, 2, \dots, n$ . In the above equation the incremental damage,  $D_i$ , is the ratio of the time,  $\Delta t_i$ , that the specimen is exposed to the  $i^{\text{th}}$  stress level,  $\sigma_i$ , relative to the mean time to failure,  $t_{fi}$ , when the specimen is subjected only to the  $i^{\text{th}}$  stress level. To generalize the equation to a discrete stress history,  $\sigma_i$ ,  $i = 1, 2, \dots, n$ , acting for time durations  $\Delta t$ ,  $i = 1, 2, \dots, n$ , it is necessary to define a relationship between the "time-to-failure" and the applied stress. For this purpose the following relationship postulated by Bills, and derived from experimental observations, is extensively used

$$t_{fi} = t_0 a_T(T_i) \left( \frac{\sigma_0}{\sigma_i} \right)^\beta \quad (6.11)$$

Here,  $t_{fi}$  is the "time-to-failure" at the reference stress  $\sigma_i$ ,  $t_0$  is the "time-to-failure" at the reference stress  $\sigma_0$ ,  $\beta$  is the negative inverse slope of the log-log plot stress versus time, and  $a_T(T_i)$  is the shift factor at the temperature  $T_i$ . If we eliminate the "time-to-failure,"  $t_{fi}$ , between Equations 6.10 and 6.11, we would yield the cumulative damage law in terms of an arbitrary discrete stress state

$$D = \sum_{i=1}^n D_i = \sum_{i=1}^n \left[ \frac{\Delta t_i}{a_T(T(t_i))t_0} \left( \frac{\sigma_i}{\sigma_0} \right)^\beta \right] \quad (6.12)$$

For continuous stress histories  $\sigma(t)$ , Equation 6.12 can be generalized to

$$D(t) = \frac{1}{t_0 \sigma_0^\beta} \int_0^t \frac{\sigma(t)^\beta}{a_T(t)} dt \quad (6.13)$$

It follows from Equation 6.10, by setting  $\Delta t_i = t_i$  and  $n = 1$ , that failure occurs when the cumulative damage,  $D$ , equals unity which implies from Equation 6.13 that

$$D(t_f) = \frac{1}{t_0 \sigma_0^\beta} \int_0^{t_f} \frac{\sigma(t)^\beta}{a_T(t)} dt = 1 \quad (6.14)$$

Clearly, the damage index  $D(t)$ ,  $0 < t < t_f$  represents intermediate damage states up to failure and takes on values between zero and unity. An alternative damage function adopted by France is given by

$$D(t) = D_0 \left[ \int_0^t \frac{\sigma(t)^\beta}{a_T(t)} dt \right]^{\frac{1}{\beta}} \quad (6.15)$$

where,

$$\frac{1}{D_0} = \sigma_0 \left( \frac{t_0}{a_T(T_0)} \right)^{\frac{1}{\beta}} \quad (6.16)$$

For the above model failure occurs when  $D(t_f)$  equals unity. In terms of the above damage functions Margin of Safety (MS) and Damage Safety Factors ( $K_D$ ) can be defined as follows,

$$MS = \frac{1}{D(t)} - 1 \quad (6.17)$$

and,

$$K_D = \frac{1}{D(t)} \quad (6.18)$$

which respectively denote the of Margin of Safety and Safety Ratios used by the United States and France. Values of  $MS = 0$  and  $K_D = 1$  denote the failure condition (as discussed in Section 6.2).

In the United States, various facilities (governmental and private) have developed their own approaches to determine the structural integrity of aged solid propellant grain/bondline systems. Various analysis techniques have been adopted all of which rely to some extent on the use of accelerated or real-time aged material characterization data. This test data is frequently derived from pressurized and un-pressurized uniaxial tests, biaxial and equil-biaxial tests, analog wedge tests, stress and strain endurance tests, and bond-in-tension tests conducted on quality control cartons and/or dissected aged "in-service" rocket motors. Also, depending on the investigation, various types of analog motor tests have been used to determine the propellant grain/bondline system's aged structural capability related to a "full-scale" rocket motor. All of this data has been used in linear and nonlinear viscoelastic finite element models (see Chapter 3) to evaluate the projected long term stress and strain responses of a single rocket motor, deployed in various locations around the world. These responses are then compared with the rocket motor's structural capabilities and related to a population of motors (deployed in the same locations) using probabilistic methods and mathematical relationships to estimate when the motors will reach their "useful" life. A typical probabilistic methodology involves using strength distribution parameters in a three-parameter Weibull strength analysis, which have been obtained from statistical strength tests done on the aged propellant grain and bondline samples. Sometimes, analysts in the United States have been known to analyze the effects of degradation (i.e., mechanical and chemical) using the cumulative damage relationships detailed above and the Arrhenius equation given below

$$K' = A \exp\left(-\frac{E_a}{kT}\right) \quad (6.19)$$

In the above equation,  $K'$  is the rate of the reaction at temperature  $T$ ,  $E_a$  is activation energy (assumed constant),  $A$  is the Arrhenius constant, and  $k$  is the Boltman's constant.

For example, the United States government uses one approach that involves calculating the total cumulative damage index of a population of motors subjected to a long-term storage scenario. This calculation is based upon accelerated quality control data and the cumulative damage index of a single motor. The value is then used to determine the  $MS$  value for the whole population of motors from the same "lot" using a modified version of Equation 6.17 to account for aging; Equation 6.17 is modified as follows

$$MS = \frac{1}{D(AF)^\beta} - 1 \quad (6.20)$$

where,  $D$  is the cumulative damage index of a single rocket motor at a specific location and  $AF$  is the aging factor for that location (determined from quality control data), modified by the damage parameter,  $\beta$ .

The aging factor appearing in Equation 6.20 is obtained from accelerated property data, analyzed using an Arrhenius aging model, for each mechanical property used to characterize the aging process. This results in an aging relationship of the form

$$AF = \sum_{i=1}^n \Delta t_i R_i \quad (6.21)$$

where,  $R_i$  is the aging rate at aging temperature  $T_i$  and  $\Delta t_i$  is the time duration that the propellant is exposed to the temperature  $T_i$ . The aging rate,  $R_i$ , at the  $i^{\text{th}}$  temperature  $T_i$  is related to the aging rate,  $R_{i+1}$ , at the  $(i+1)^{\text{th}}$  temperature  $T_{i+1}$  through the following Arrhenius relationship, derived from Equation 6.19. Note that this aging model has been derived according to the kinetic theory of chemical reactions and does not account for cumulative damage effects due to thermal cycling.

$$R_i = R_{i+1} \exp \left[ \frac{E_a}{15.058 \frac{\text{kJ}}{\text{°C}}} \left( \frac{1}{T_{i+1}} - \frac{1}{T_i} \right) \right] \quad (6.22)$$

An Arrhenius model is also used by Germany to establish the aging properties of their solid propellant grain/bondline systems. The aging process is experimentally simulated by storing the systems at elevated temperatures thereby accelerating the natural aging phenomena, such as, degradation or chemical decomposition over a reduced period in time. The Arrhenius model used for this purpose is a simplification of equation 6.22 and is given by

$$t_{RT} = t_{ST} A_f \left[ \frac{(T_{ST} - T_{RT})}{10^{\circ\text{C}}} \right] \quad (6.23)$$

where,  $t_{RT}$  is the natural storage time at ambient temperature,  $t_{ST}$  is the storage time at accelerated conditions,  $T_{RT}$  is the ambient temperature at storage condition,  $T_{ST}$  is the temperature at accelerated conditions, and  $A_f$  is the Arrhenius acceleration factor. In the application of Equation 6.23, there does not appear to be a general consensus regarding the magnitude of  $A_f$  which should be used in the analysis. For example, Germany uses Arrhenius acceleration factors of 2.6 and 2.88 in most of their strength analyzes. The United States, on the other hand, used values ranging from 2.0 to 2.6 for composite propellants and 2.88 for double-base propellants, and used only when no experimental data is available to determine the value for each mechanical property. The United States believes that to conduct a proper service life assessment of a "lot" of production rocket motors. The analyst must use an Arrhenius model in conjunction with a cumulative damage model for each mechanical property, complete with Arrhenius factors obtained experimentally for each parameter used in the assessment. In some cases, nations (i.e., Germany, United Kingdom and the United States) have used an empirical model proposed by Layton

$$P(t_a, T_a) = P_0 + K(T_a) \log \left( \frac{t_a}{t_0} \right) \quad (6.24)$$

to determine the aged mechanical properties of the solid propellant grain/bondline system.

In this equation,  $t_a$  is the aging time,  $T_a$  is the aging temperature,  $t_0$  is the propellant's age at the start of the aging process,  $P$  is the propellant mechanical property (i.e., stress or strain),  $P(t_a, T_a)$  is  $P$  at aging time and temperature, and  $P_0$  is  $P$  at the start of aging time  $t_0$ . The parameter  $K$  is determined by the corresponding test procedure performed with an aged propellant grain/bondline system.

## 6.6 MULTIPLE LOADING CONDITIONS

France, the United States, the United Kingdom, and the Netherlands are the only countries involved in this study that considers multiple loading conditions when analyzing a rocket motor's structural integrity. Each country evaluates multiple loading conditions as a matter of course when required to model the loading situation as accurately as possible. A good example of this is modeling a rocket motor ignited at its extreme cold operating temperature or modeling thermal shock seen during captive-carry.

A definitive MS method used to combine individual loading conditions due to various environments (thermal, internal pressures, acceleration loads, etc.) into total applied stress and strains for a given motor condition has not yet been agreed upon in the United States. However, a very conservative approach involving superposition, as illustrated in Equation 6.25 (otherwise, known as the Damage Factor Approach or Method) is being used in the United States to evaluate tactical systems. This equation should be used with caution, and only when ( a ) certain test data (from variable-rate similitude, strain endurance, and thermal analog motor tests) is unavailable or ill-defined to characterize the propellant grain/bondline system properly; ( b ) it is necessary to do so due to the complexity of the loading condition (e.g., cold ignition during a high-G maneuver); or ( c ) the customer requires it so to build additional conservatism into the design. Otherwise, the United States would normally obtain the required data and evaluate the design's structural integrity based on each individual loading condition, using Equation 6.26. A variable-rate similitude test (i.e., A bi-rate stress/strain test) involves pressurizing a uniaxial tensile specimen and varying the crosshead rate during the longitudinal extension to simulate ignition pressurization (e.g., a specimen tested at 6.9 MPa with an initial crosshead rate of 0.254 mm/min and then increased to 2540 mm/min, after a 1 or 2% offset has been reached) and it is use as failure data in Equation 6.26.

$$MS_{total} = \left[ \sum \frac{(DF)_{lc} (Z_{induced})_{lc}}{(KDF_{total})_{lc} (Z_{allowable})_{lc}} \right]^{-1} - 1 \quad (6.25)$$

$$MS_{lc} = \frac{(KDF_{total})_{lc} (Z_{allowable})_{lc}}{(DF)_{lc} (Z_{induced})_{lc}} - 1 \quad (6.26)$$

where,  $lc$  denotes the individual loading condition being considered in the analysis (e.g.,  $tc$  or  $t$  for thermal cool-down,  $ip$  or  $p$  for ignition pressurization, etc.).

The United Kingdom uses a similar approach involving Equation 6.27. Here, the United Kingdom determines the total Safety Factor to define whether the rocket design is acceptable, rather than using safety margins. In a similar way Equations 6.25 and 6.27 both consider the level of damage each loading condition imposes onto the rocket motor using superposition:

$$SF = \frac{1}{\left( \frac{S_t}{C_t} + \frac{S_p}{C_p} \right)} \quad (6.27)$$

Where  $t$  and  $p$  denote thermal cooldown and pressurisation respectively.

In France, the most currently used approach for a multiple loading condition is the evaluation of the Safety Ratio as shown in Equation 6.28.

$$K = \frac{C}{S_{total}} \quad (6.28)$$

where,  $C$  is the capability of the propellant corresponding to the last induced load seen by the propellant grain/bondline system (obtained from a master curve). For example, in the case of ignition pressurization. The capability,  $C$ , corresponds to the reduced time at a specific temperature and ignition rate, and  $S_{total}$  is the total equivalent stress obtained when summarizing the stress tensors computed for each loading condition (e.g., thermal cool-down plus ignition pressurization). A worked example is given in section 6.8.3.

## 6.7 PROBABILISTIC METHODS

The Margins of Safety and Safety Ratio approaches used in the evaluation of the structural integrity of a solid propellant grain/bondline system are essentially deterministic techniques. Since, neither approach considers the variability of the induced loads and material capability in a rigorous statistical sense. The statistical variability of these quantities is embodied in some numerically defined constants used in the Margin of Safety and Safety Ratio calculations. For a quantitative reliability analysis of the propellant grain/bondline system, it is necessary to regard the material capability,  $C$ , and the induced loads (stress or strain response),  $S$ , as random variables. It then follows that the failure probability is the probability that the capacity random variable,  $C$ , is less than or equal to the loading random variable  $S$ , i.e.,

$$P_f = P(C \leq S) \quad (6.29)$$

Alternatively, the reliability can be defined which is the probability that the capacity random variable,  $C$ , is greater than the loading random variable,  $S$ , i.e.,

$$R = P(C > S) \quad (6.30)$$

The above reliability statement can be expressed in the following equivalent forms

$$R = P(C > S) = P\left(\frac{C}{S} > 1\right) = P\left(\frac{C}{S} - 1 > 0\right) \quad (6.31)$$

But, the Margin of Safety is given by

$$MS = \frac{C}{S} - 1 \quad (6.32)$$

which follows that if,  $C$  and  $S$ , are random variables, then  $MS$  is also a random variable. Therefore, from the above equations, the reliability is then given by

$$R = P(C > S) = P(MS > 0) \quad (6.33)$$

If the structural integrity is being evaluated using the Safety Ratio,  $K = C/S$ , then the reliability for a statistically varying Safety Ratio is given by

$$R = P(C > S) = P(K > 1) \quad (6.34)$$

In the discussions presented thus far, the distributional form of the random variables,  $C$  and  $S$ , have been unspecified. Defining distributional forms for  $C$  and  $S$  is now necessary, and to derive specific relationships that will allow the reliability to be evaluated in terms of the key parameters that define those distributions. Within the propulsion community that adopts the probabilistic approach, it is usual practice to assume that the random variables,  $C$  and  $S$ , are normally distributed. However, many statisticians would object to this for the following reasons. First, the observed distributions of  $C$  and  $S$  are frequently found skewed which rules out the use of the normal distributions that are symmetric about its mean value. The capacity and load variables,  $C$  and  $S$ , have minimum bounds that are positive and this is not accommodated for when the normal distribution is adopted. The normal distribution has a minimum bound at minus infinity. However, it is argued that representative reliability values can be obtained based on the assumption of normality, despite the previously mentioned inadequacies. An advantage of the normality assumption is the resulting simple closed-form solution that can be used for evaluating reliability.

If  $C$  and  $S$  are random variables from normal distributions with respective means,  $\mu_C$  and  $\mu_S$ , it can be shown that the difference distribution given by the random variable

$$D = C - S \quad (6.35)$$

is also normally distributed with mean  $\mu_D$  given by

$$\mu_D = \mu_C - \mu_S \quad (6.36)$$

It can also be shown that the standard deviations of the normal distribution of  $C$  and  $S$ , respectively denoted by  $\sigma_C$  and  $\sigma_S$ , are related to the standard deviation of the difference distribution  $D$  by

$$\sigma_D = \sqrt{\sigma_C^2 + \sigma_S^2} \quad (6.37)$$

Having established that the difference distribution,  $D$ , is normally distributed with mean,  $\mu_D$ , and standard deviation,  $\sigma_D$ , it can be shown that the reliability

$$R = P(C > S) = P(C - S > 0) = P(D > 0) \quad (6.38)$$

is simply given as

$$R = P(C > S) = P(D > 0) = \Phi\left(\frac{\mu_D}{\sigma_D}\right) \quad (6.39)$$

where  $\Phi(X)$  is the cumulative normal distribution function. Geometrically,  $\Phi(X)$  represents the area under the "frequency distribution" curve bounded by the random variable,  $X$ . The distribution function  $\Phi(X)$  is a tabulated quantity and is listed at the back of most text books on statistics.

It is now of interest to take the above probabilistic relationship given by Equation 6.39 and show how the deterministic Safety Ratio and Margin of Safety methodologies can be generalized for the probabilistic condition. For the purpose of illustration, reliability relationships will be derived for a probabilistic Safety Ratio analysis. The probabilistic Margin of Safety analysis can be developed in a similar manner. It is convenient to take the reliability relationship given by Equation 6.39 and express  $\mu_D$  and  $\sigma_D$  in terms of the means and standard deviations of  $C$  and  $S$ , using equations 6.36 and 6.37. The resulting reliability relationship is then obtained

$$R = P(C > S) = \Phi\left(\frac{\mu_C - \mu_S}{\sqrt{\sigma_C^2 + \sigma_S^2}}\right) \quad (6.40)$$

It is now necessary to take the argument of the above cumulative normal distribution function and express it in the following form, i.e.,

$$\left[\frac{\mu_C - \mu_S}{\sqrt{\sigma_C^2 + \sigma_S^2}}\right] = \left[\frac{\frac{\mu_C}{\mu_S} - 1}{\sqrt{\left(\frac{\mu_C}{\mu_S}\right)^2 \left(\frac{\sigma_C}{\mu_C}\right)^2 + \left(\frac{\sigma_S}{\mu_S}\right)^2}}\right] \quad (6.41)$$

Introducing the following definitions for the coefficients of variation for the random variables,  $C$  and  $S$ , together with the mean Safety Ratio, respectively denoted by

$$CV_C = \frac{\sigma_C}{\mu_C}, \quad CV_S = \frac{\sigma_S}{\mu_S}, \quad \bar{K} = \frac{\mu_C}{\mu_S} \quad (6.42)$$

it is a matter of simple substitution to show that

$$\left[ \frac{\mu_C - \mu_S}{\sqrt{\sigma_C^2 + \sigma_S^2}} \right] = \left[ \frac{\bar{K} - 1}{\sqrt{\bar{K}^2 CV_C^2 + CV_S^2}} \right] \quad (6.43)$$

from whence it can be deduced that

$$R = P(C > S) = P(K > 1) = \Phi \left( \frac{\bar{K} - 1}{\sqrt{\bar{K}^2 CV_C^2 + CV_S^2}} \right) \quad (6.44)$$

The probabilistic Equations 6.40 and 6.44 are used to perform a structural “reliability” analysis (i.e., service life assessments) of the solid propellant grain/bondline system. The industries within the United States, which have adopted the probabilistic approach, tend to use Equation 6.40 in determining the probability when a propellant grain or bondline will fail. For example, for a probabilistic bond failure analysis,  $\mu_C$  and  $\mu_S$  represents the mean bond strength and mean bond (induced) stress, respectively; where,  $\sigma_C$  and  $\sigma_S$  are the respective standard deviations. This equation is also used for the probabilistic bore failure analysis with the random variables associated with strain (i.e., a probabilistic strain-based failure analysis). Thus,  $\epsilon_C^m$  and  $\epsilon_S^m$  respectively denote the mean bore strain capability and mean induced bore strain, with  $\sigma_C$  and  $\sigma_S$  denoting the respective standard deviation; it follows that the failure probability is given by

$$P_f = P(\epsilon_C \leq \epsilon_S) = 1 - P(\epsilon_C > \epsilon_S) \quad (6.45)$$

i.e.,

$$P_f = 1 - \Phi \left( \frac{\epsilon_C^m - \epsilon_S^m}{\sqrt{\sigma_C^2 + \sigma_S^2}} \right) \quad (6.46)$$

Here,  $\Phi$  is the cumulative normal distribution that can be evaluated using statistical tables for the area under the normal distribution curves;  $\sigma_C$  represents the standard deviation of age-dependent material strain capability; and  $\sigma_S$  represents the standard deviation of age-dependent induced strain.

For time dependent loading conditions and time dependent strain capability degradation conditions, the above probability expression can be used to evaluate the probability of surface cracking in the bore as a function of time. In the United States, reliability analysis methods have not been fully used in a structural integrity analysis, except in predicting service life. In fact, service life prediction is the only area where probabilistic methods have been used to determine the probability of one out of a population of motors aging to a desired point in time.

The United States have been investigating the possibility of using probabilistic methods, instead of the MS equations, to determine a rocket motor's structural integrity. However, these methods have not been utilized nationwide due to uncertainties in stress analysis methods and failure criteria, and the high cost of obtaining pertinent data in sufficient quantities to support the statistical analysis.

France, being technically consistent with their deterministic Safety Ratio approach, uses the relationship given by Equation 6.44. In fact, France has extended the above methodology one step further. After applying Equation 6.44, the minimum Safety Ratio factors, evaluated for a specified reliability level for the propellant grain,  $\phi_1$ , and the bondline,  $\phi_2$ , are obtained by determining the value of the minimum Safety Ratio,  $K_{\min}$ , which satisfy the following relationship

$$\phi_{1,2} = \phi \left( \frac{K_{\min} - 1}{\sqrt{K_{\min}^2 CV_C^2 + CV_S^2}} \right) \quad (6.47)$$

It is important to note that the minimum Safety Ratio,  $K_{\min}$ , is evaluated from Equation 6.47 using a specified reliability level and coefficient of variation values for the capacity and induced load, respectively denoted by  $CV_C$  and  $CV_S$ ; these values are determined from tests conducted on a single batch of propellant. To take account of batch-to-batch variation of the propellant properties, extending the above probabilistic analysis is necessary. Starting from Equation 6.47, and having established the minimum Safety Ratio,  $K_{\min}$ , for a single batch of propellant, the next step involves the determination of the average value of  $K$ , denoted by  $K_0$ , of the whole family of propellant mixes. It can be shown by considering the reliability equation

$$R = P(K > K_{\min}) = P(C - SK_{\min} > 0) \quad (6.48)$$

by which the required probabilistic relationship for evaluating  $K_0$  is given

$$P(K_{\text{design}} > K_{\min}) = \phi \left( \frac{K_0 - K_{\min}}{\sqrt{K_0^2 CV_{2C}^2 - 2\rho K_0 K_{\min} CV_{2C} CV_{2S} + K_{\min}^2 CV_{2S}^2}} \right) \quad (6.49)$$

In Equation 6.49, it is usual practice to assign the probability value  $P(K_{\text{design}} > K_{\min})$  equal to the three-sigma value of 0.9986, which fixes the right-hand side of the equation. The quantities  $CV_C$  and  $CV_S$ , respectively denotes the coefficients of variation of the propellant capacity and induced load, taking into account the batch-to-batch variation,  $\rho$  is the correlation coefficient which accounts for the observed correlation between capacity and load. The quantity  $K_{\min}$  is the minimum Safety Ratio evaluated previously and  $K_0$  is the required mean Safety Ratio that can be evaluated in terms of all the other known parameters appearing in Equation 6.49. The resulting value of  $K_0$  that emerges from this analysis defines a target value of the Safety Ratio, which must be achieved for the design to be accepted. Additional margins or knockdown factors may be introduced, depending on the type of rocket motor and corresponding requirements set by the customer (e.g., operating conditions, service life, etc.).

In addition to the probabilistic procedures described above, which have been based on a classical statistical approach, techniques have been developed (by France in particular) to use prior information through the application of Bayesian statistics. The Bayesian approach has been used by France to improve the level of confidence associated with the reliability estimates derived from a limited number of over-tests. France's methodology is described with reference to the following study:

Seven over-tests were performed on solid propellant rocket motors to produce a situation where the anticipated Safety Ratio was close to unity and the anticipated reliability level was in the region of 0.5. For each over-test an increase in ignition pressure was achieved by reducing the throat diameter of the nozzle. Out of the seven tests performed, three failures were observed thereby confirming that the target reliability level of 0.5 was being achieved. At the end of each tests, a Bayesian analysis was applied to the results and the level of confidence associated with the reliability level evaluated.

At the end of the testing program, the estimated confidence level became progressively more accurate as more test data became available. The model was subsequently used to assess the reliability of the solid propellant grain/bondline system, ignited under normal operating conditions.

The application of probabilistic methods as an analytical tool for use in the evaluation of the structural reliability of solid propellant grain/bondline systems is receiving increasing attention, but these methodologies are not currently routinely used by all the countries. These techniques are used to varying degrees of sophistication by France and the United States, as mentioned in the preceding paragraphs. The United Kingdom is currently evaluating the use of probabilistic methodologies as a research tool; before possible implementation as a technique for evaluating the structural reliability of the solid propellant grain/bondline system, as part of a service life prediction. Though the investigation is still in the early stages of development, they have been using methods similar to those used in the United States. The strength variability of the propellant is first characterized using Weibull statistics. Then, a failure probability analysis is used to determine the probability that the statistically varying time dependent stress exceeds the statistically varying strength of the propellant. Finally, a time dependent failure growth relationship is used to determine the time taken for the failure probability to increase to a specified level.

In conclusion, France, the United States, the United Kingdom and Australia are the only countries developing or using some type of probabilistic method to determine the reliability and "level of confidence" of the propellant grain/bondline system: validating their estimate using various experimental methods. In fact, France is the only country that uses these methods to determine the reliability and confidence level of a grain design in a structural integrity analysis. Where the United States and the United Kingdom primarily use these methods to determine the design's service life. As for Australia, they are using probabilistic methods at the research level, but have yet to apply a method to determine the service life of "in-service" motors.

## 6.8 EXAMPLES

For the purpose of illustration, several examples are presented in this section to show how the various nations calculated safety margins and reliability for particular grain/bondline systems. Each example considers thermal cool-down, either for ambient conditions or another thermal state (i.e., the extreme "cold" temperature condition), and then deals with ignition pressurization. The first example shows how a "quick-look" analysis, which is based on a simplified analytical approach, can be used to determine the margin of safety when only limited data is available. The second example illustrates how the margin of safety is evaluated when a detailed structural analysis has been performed (i.e., finite element approach) and sufficient experimentation performed to classify this as a Type 2 problem as defined in section 6.4.1. The third and final example shows how a probabilistic approach can be applied to predict the structural reliability of the propellant grain/bondline design.

### 6.8.1 Multiple Loading Example #1: A "Quick-Look" Approach

#### 6.8.1.1 Problem Statement

It is a customer requirement that a 17.8 cm diameter rocket motor is produced which is capable of being exposed to a  $-40^{\circ}\text{C}$  lower temperature limit and subsequently fired. This is a feasibility study based on the limited information both in terms of design configuration and material property data. For the purpose of this example it is assumed that the propellant grain is made of an HTPB composite propellant and that the same material properties are assumed for the liner. Furthermore, it is assumed that the propellant is case-bonded to the rocket motor case and that the propellant grain design has a cylindrical bore (see Fig. 6.3). For this particular example it is assumed that the rocket motor case is infinitely rigid and the propellant is incompressible. For this given set of assumptions a definition of the propellant modulus is not required.

The "quick-look" method provides simple analytical relationships for evaluating the cool-down and pressurization strain response. However, it is perhaps worth noting that it is becoming increasingly common to use a finite element analysis to determine these strain levels since these models can be generated so quickly. In this example the United Kingdom safety factor methodology (see Table 6.1) is used to sum the damage factors associated with the thermal cool-down and pressurization loading conditions, regardless of the selected failure criterion.

#### 6.8.1.2 Solution

##### 6.8.1.2.1 Thermal Cool-down

Experience has shown that the cool-down time is approximately 24 hours (1440 min) for a 17.8 cm diameter rocket motor. For this example it is assumed that a 17.8 cm diameter motor is cooled down to  $-40^{\circ}\text{C}$  and the "strain-free" temperature is some  $6^{\circ}\text{C}$  higher than the cure temperature. The thermal strain can be assessed by using the following expression:

$$\epsilon = \ln(1 + 1.5k\lambda^2\alpha_r\Delta T)P_{arr} \quad (6.50)$$

where,  $k$  is the strain concentration factor,  $\lambda$  is equal to  $b/a$  (propellant grain outside diameter divided by the bore diameter) of the propellant grain,  $\alpha_r$  is the reduced coefficient of expansion ( $\alpha_p - 0.666(1 + \nu_c)\alpha_c$ ),  $\Delta T$  is the "strain-free" temperature minus the conditioning temperature, and  $P_{arr}$  is a correction factor obtained from various tables. The  $k$  value is usually calculated by hand; however, it can be obtained from a finite element analysis that would give a direct printout of the strain level at a critical location in the propellant grain. For a typical rocket motor with a cylindrical bore the strain concentration factor is equal to unity.

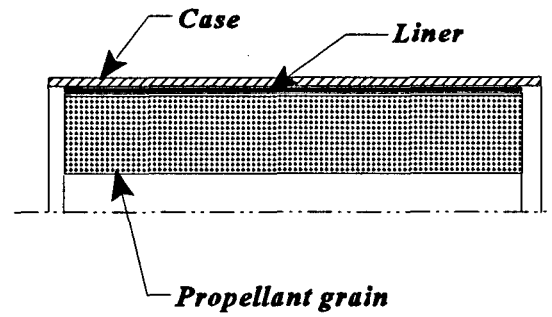


Figure 6.3: Typical Rocket Motor with a Cylindrical Bore.

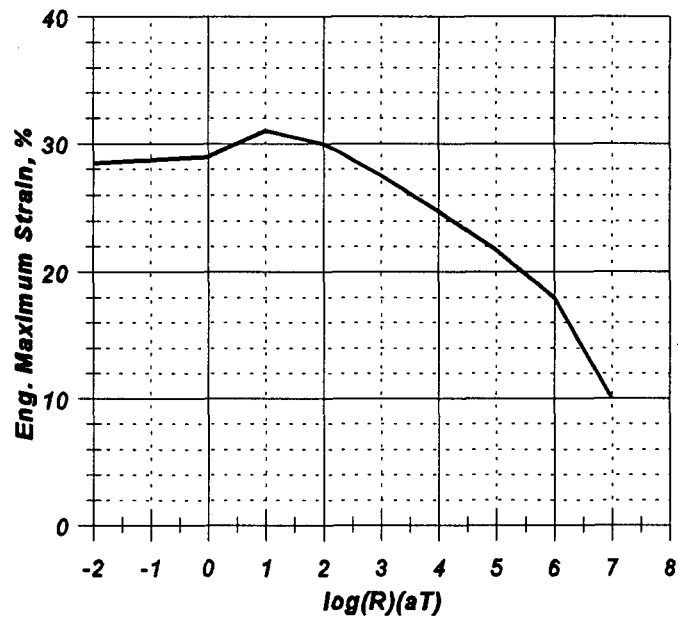


Figure 6.4: Strain Master-Curve.

If the strain level is calculated to be 10%, the analyst will need to determine the allowable to calculate the Thermal Damage Factor,  $D_T$  (see Table 6.1 and Section 6.7),

$$D_t = \frac{S_t}{C_t} \quad (6.51)$$

First calculate the effective cool-down rate based on a 24-hour period

$$Rate = R = \frac{\text{strain applied}}{\text{time taken (min)}} \quad (6.52)$$

$$R = \frac{0.10}{1440 \text{ min}} = 6.94 \times 10^{-5} \text{ min}^{-1} \quad (6.53)$$

and then evaluate,

$$\log_{10}(R) = -4.15 \quad (6.54)$$

Next determine the temperature-shift factor,  $a_T$ , for the propellant grain from actual mechanical property data. For this example the following assumed value is used

$$\log_{10}(a_T) = 5.00 \quad (6.55)$$

from whence it follows,

$$\log_{10}(Ra_T) = \log_{10}(R) + \log_{10}(a_T) \quad (6.56)$$

$$\log_{10}(Ra_T) = -4.15 + 5.00 = 0.85 \quad (6.57)$$

Using the strain master-curve given in Fig. 6.4, the analyst can determine the strain allowable value to be 30% for this propellant. Once the strain allowable is determined, the  $D_i$  can be calculated using Equation 6.58;

$$D_i = \frac{S_t}{C_t} = \frac{0.10}{0.30} = \underline{0.33} \quad (6.58)$$

#### 6.8.1.2.2 Ignition Pressurization

The pressurization strain can be approximated by the following expression,

$$\epsilon_p = R(1 - \nu^2)k\lambda^2 \frac{P}{hE_c} \quad (6.59)$$

where,  $\nu$  is Poisson's ratio for the case,  $R$  is the outer-radius of the grain,  $h$  is the case thickness,  $P$  is the motor's operating pressure at plus three-sigma level, and  $E_c$  is the Young's modulus of the case. For a conservative solution, the analyst should use the "full motor pressure."

Assuming a pressurization strain of 2% (based on an equilibrium temperature of  $-40^{\circ}\text{C}$ ), the strain rate (i.e., the strain generated over a given time interval) and  $\log_{10}(\text{Ra}_T)$  for the pressurization condition can be calculated using the rocket motor's pressure-time curve (see Fig. 6.5) and the propellant's temperature-shift curve; obtained from various pressurized mechanical property data on a similar system or from actual tests (see Section 4.2.2) conducted on the system being analyzed. Next, using propellant's failure data and the strain rate previously calculated, determine the propellant's allowable strain for pressurization. If the propellant's allowable strain was determined to be 10%, it follows that the Pressurization Damage Factor,  $D_p$ , given in the following equation is

$$D_p = \frac{S_p}{C_p} = \frac{0.02}{0.10} = \underline{0.20} \quad (6.60)$$

Substituting for  $D_p$  and  $D_t$  into Equation 6.27 gives the baseline safety factor for this multiple loading condition as

$$SF = \frac{1}{D_t + D_p} = \underline{1.88} \quad (6.61)$$

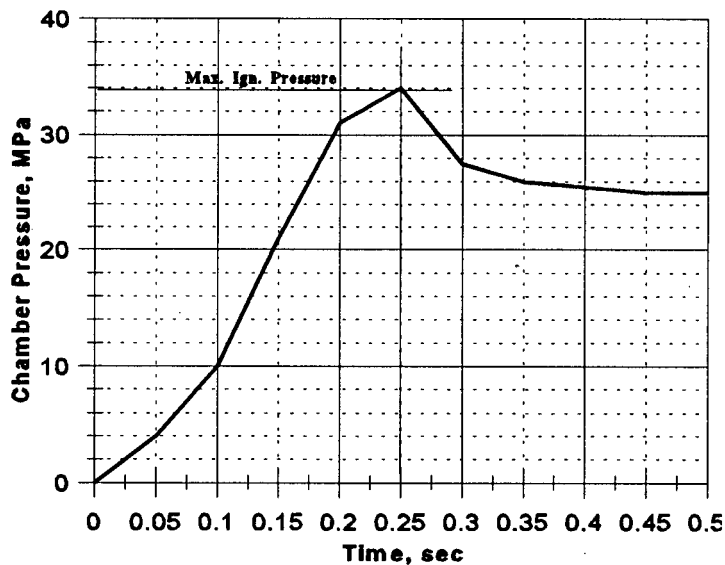


Figure 6.5: Typical Pressure-Time Curve.

## 6.8.2 Multiple Loading Example No 2 - A Detailed Deterministic Approach

### 6.8.2.1 Problem Statement

It is a customer requirement to determine the propellant grain's structural integrity, based on the Effective Strain Criterion, of a case-bonded 21.2 cm diameter "conventional" tactical test motor with an length to diameter ratio of 2.81. The rocket motor is assumed to have been cooled down to a thermal equilibrium of  $-40^{\circ}\text{C}$  within 48 hours and then pressurized to a "positive three-sigma plus nominal" operating pressure of 12.76 MPa in 50 msec.

The rocket motor (i.e., propulsion section) consists of the following components: the motor case, liner, insulator, split-boot, propellant, nozzle and igniter as shown in Fig. 6.6. The motor case is made of AISI 4130 steel, which has been insulated with an ethylene propylene diene monomer (EPDM) boot and insulator, and lined with a HTPB-based liner material. The propellant is made of the same HTPB material used in the liner, except being filled with various solids, mixed with an antioxidant, and cured with a different curing agent. The solid propellant has been cast into the lined case with a mandrel forming the desired ballistic profile, required for this design. The perforation is of a circular cylindrical, three-slotted finocyl design with a cone formed at the end of the propellant grain as shown in Fig. 6.6. The customer requires the propellant grain/bondline system to have a designed service life of 10 years, and the margins be calculated using Equation 6.25.

### 6.8.2.2 Solution

First, generate a two- or three-dimensional finite element model(s) of the motor with a commercial or in-house finite element analysis code of your choice. In the United States, two basic approaches involving two-dimensional modeling of three-dimensional geometries called "three-dimensional approximations," as well as, three-dimensional modeling techniques have been used to determine the induced stresses and strains within a propellant grain/bondline system. One involves generating two-dimensional axisymmetric and plane-strain models along the length of the motor, calculating shape factors to relate the models together in determining the induced strains at the tips of the fins and the induced stresses at the bondline. The other involves generating a two-dimensional axisymmetric model with reformulated and non-reformulated "time-to-failure," elements to account for fin and bondline geometries, simultaneously; only applicable if computer code can generate and use "slot" elements for compressible and incompressible materials, respectively. Clearly, the second two-dimensional method is far better in handling the three-dimensional effects that exist within a transition region and will be used in this example as shown in Fig. 6.7. Although this grain design is asymmetrical, the fin's are geometrically "simple" slots that gradually merge into the cylindrical section of the bore and the geometry is ideal for analyzing using "slot" elements, designed to model the width and shape of the longitudinal fin. For more complex grain geometries, the three-dimensional modeling technique is the selected method adopted in the United States. Three-dimensional finite element models based on linear-elastic, nonlinear-elastic, hyper-elastic and linear-viscoelastic constitutive theories are now more widely used in the United States, than the above mentioned three-dimensional approximation techniques. However, for this example a three-dimensional approximation technique will be used to evaluate the design's structural integrity and to simply illustrate a "detail deterministic" approach. Furthermore, if the motor case is made of a composite construction, then it is recommended to use a computer code that can model structural/ballistic interaction seen during ignition pressurization to obtain realistic induced stress-strain values (see Chapter 3).

For this investigation, the stress relaxation tests and (pressurized and un-pressurized) uniaxial tensile tests (see Section 4.2.2) were used to obtain the propellant's mechanical property and lower-three sigma failure data necessary to complete the analysis. Table 6.6 provides some initial mechanical property data for the critical components of the rocket motor to simplify the example. From time to time these default values are used when certain data are unavailable or ill-defined at the time of the analysis. For this example, the given default mechanical property data will be used to analyze the propellant grain for locations of high strain. These strains are due to one thermal cooling cycle to the equilibrium temperature ( $T_e$ ) of  $-40^{\circ}\text{C}$  in 48 hours followed by an ignition shock of 12.76 MPa applied in 50 msec at the equilibrium temperature. In this study, the forward polar boss was not modeled because the forward section is relieved by a split-boot (see Fig. 6.7). To simplify the analysis, the rocket motor case was considered rigid for both thermal and pressurization loading conditions.

It was also assumed that the propellant and liner were made of the same material. Thus, having the same mechanical properties, the propellant and liner could be modeled as one component. This is a valid assumption to make during an initial study of a design's structural integrity. Especially, when most liners are too thin (depending on the size of the system) to affect the induced stresses and strains levels calculated by the linear-elastic finite element computer code. For this analysis it was assumed that the motor case, propellant-liner ( p ), insulator ( I ) and split-boot ( b ) were all made from isotropic materials. Finally, for both the thermal cool-down and ignition pressurization loading conditions the Effective Strain Criterion given in Section 5.3.3 was used to determine the design's margin of safety.

#### 6.8.2.2.1 Thermal Cool-down

As a preliminary to the analysis, the propellant's "strain-free" temperature needs to be determined. Strain evaluation cylinders (SECs) are typically used for the purpose to determine the biaxial strain capability and "strain-free" temperature of a particular propellant formulation (refer to Chapter 7). However, sometimes when conducting a preliminary structural analysis this type of data is unavailable. Under these conditions, the propellant's "strain-free" temperature,  $T_{sf}$ , can be determined using the following relationship

$$T_{sf} = T_{cure} + T \quad (6.62)$$

where,  $T_{cure}$  is the cure temperature of the propellant, and  $T$  ranges between 8 and 11 °C that represent the spread of temperatures that exist between the "strain-free" temperature and the cure temperature for most composite propellants. This range was determined from actual SEC experiments conducted on various types of composite propellant, by selecting various cool-down rates and thermal profiles (including thermal cycling).

Knowing the propellant's cure temperature for this example is 60 °C and assuming a minimum temperature spread of 8 °C, the propellant's "strain-free" temperature is

$$T_{sf} = 60^{\circ}C + 8^{\circ}C = 68^{\circ}C \quad (6.63)$$

Once the "strain-free" temperature has been calculated and knowing the equilibrium temperature to be -40 °C, the coefficient of thermal expansion (a required input for the computer code),  $\delta$ , can then determine for all the components of the motor (considered in the analysis) using the following relationships:

$$\delta_p = -\alpha_p(T_{sf} - T_f) \quad (6.64)$$

$$\delta_{ib} = -\alpha_{ib}(T_{cure} - T_f) \quad (6.65)$$

$$\delta_c = -\alpha_c(T_{cure} - T_f) \quad (6.66)$$

The calculated  $\delta$  values for each component are listed in Table 6.6.

The propellant's initial modulus value used in the code's input is determined next using the temperature shift-factor and the stress relaxation modulus master curve given in Fig. 6.9. Given that the motor has been cooled to a thermal equilibrium of  $-40^{\circ}\text{C}$  for 48 hours (2880 min), we can use Fig. 6.8 to determine the temperature shift-factor at  $-40^{\circ}\text{C}$  to be

$$\log_{10}(a_T) = \underline{6.00} \quad (6.67)$$

The propellant's initial modulus can now be determined using Fig 6.9 after first obtaining the point on the horizontal axis

$$\log_{10}(t) - \log_{10}(a_T) = \log_{10}(2880) - 6.00 = 3.46 - 6.00 = -2.54 \quad (6.68)$$

and reading the value from the vertical axis

$$\log_{10}\left[E_o\left(\frac{T_s}{T}\right)\right] = 1.60 \quad (6.69)$$

to yield the required modulus value of

$$E_o \sim \underline{40.00\text{MPa}} \quad (6.70)$$

Note that this initial modulus can also be determined using the methodology explained in Section 3.3.

These values (along with the values listed in Table 6.6) are used as input data in the finite element model (see Fig. 6.7) to calculate the induce strains at locations A, B, C, and D, as shown in Fig. 6.6. The results of the computations are given in Table 6.7, where the effective strain,  $\epsilon_{\text{eff}}$ , for each location has been calculated using the following equation:

$$\epsilon_{\text{eff}} = \frac{\sqrt{2}}{3} \sqrt{(\epsilon_1 - \epsilon_2)^2 + (\epsilon_2 - \epsilon_3)^2 + (\epsilon_3 - \epsilon_1)^2} \quad (6.71)$$

The allowable strain values necessary to complete the structural integrity analysis are calculated from the unpressurized uniaxial tensile test results depicted in Figs. 6.10, 6.11, and 6.12.

It is necessary to first calculate (using the finite element model) the log of the effective cool-down (strain) rate based on a maximum  $\epsilon_{\text{eff}}$  of 3.1% at Location A (see Fig. 6.7), which took a total of 2880 min to reach a thermal equilibrium of  $-40^{\circ}\text{C}$ .

$$\text{Strain Rate} = \epsilon' = \frac{\text{strain applied}}{\text{time taken (min)}} \quad (6.72)$$

$$\epsilon' = \frac{0.031}{2880 \text{ min}} = 0.0000108 \frac{1}{\text{min}} \quad (6.73)$$

$$\log_{10}(\epsilon') = -4.97 \quad (6.74)$$

Using Fig. 6.10 the temperature shift-factor is then determined to be

$$\log_{10}(a_T) = 5.00 \quad (6.75)$$

from whence it follows after adding the above two values together that

$$\log_{10}(\epsilon') + \log_{10}(a_T) = -4.97 + 5.00 = 0.03 \quad (6.76)$$

The maximum allowable corrected stress and elongation at maximum corrected stress for the propellant can be readily deduced from Fig 6.11. Using the Williams, Landel, and Ferry (WLF) plot shown in Fig. 6.11, the maximum failure corrected stress allowable at an equilibrium temperature of  $-40^\circ\text{C}$  (i.e.,  $\log_{10}(\epsilon'a_T) = 0.03$ ) is given by

$$\log_{10}(\sigma_{corr \max}) = 0.67 \quad (6.77)$$

$$\sigma_{corr \max} = 4.68 \text{ MPa} \quad (6.78)$$

The elongation at maximum corrected stress is given graphically in Fig 6.11 as

$$\epsilon_{\max} = \underline{37.0\%} \quad (6.79)$$

As an alternative procedure, the strain allowable can be determined from Fig. 6.12 (the Smith Failure Envelope) by finding the strain corresponding to the  $\log_{10}(\sigma_{corr \max}) = 0.67$  value, which is

$$\epsilon_{\max} = \underline{37.0\%} \quad (6.80)$$

At this stage of the analysis it is now necessary to specify and evaluate the uncertainty factors (otherwise known as the Design and Knockdown factors). Based on the guidelines given in Section 6.4.1 the Design Factor (DF) required for this analysis is 1.5 (for this example, the propellant grain/bondline system is a Type 2). The total Knockdown Factor is calculated using Equation 6.7 (see Section 6.4.2)

$$KDF_{total} = (KDF_{aging})(KDF_{variability})(KDF_{multiaxiality}) \quad (6.81)$$

for biaxiality (regions of biaxial strain, i.e., the cylindrical bore - Location B; see Fig. 6.6)

$$(KDF_{total})_{tc, \text{biaxiality}} = (0.88)(0.76)(0.75) = 0.50 \quad (6.82)$$

for triaxiality (regions of triaxial strain, i.e., the termination flap, transition regions, and slot tips - Locations A, C, and D; see, Fig. 6.6)

$$(KDF_{total})_{tc, \text{triaxiality}} = (0.88)(0.76)(0.91) = 0.61 \quad (6.83)$$

The above numerical values assigned to the various knockdown factors are based on the following considerations.

(a) A 10-year aging requirement and the propellant grain/bondline system is made of an HTPB binder material, from whence it follows that  $KDF_{aging}$  is

$$KDF_{aging} = 0.88 \quad (6.84)$$

(b) A  $\kappa$  value of 3.0 for a "conventional" tactical propellant grain design exposed to a thermal cool-down environment, a standard deviation,  $\sigma$ , of 3% (obtained from the review of the uniaxial tensile data), and a failure strain of 37.0%, gives rise to the following  $KDF_{variability}$  knockdown factor (see Equation 6.9)

$$KDF_{variability} = 1 - \frac{\kappa(\sigma)}{\chi} = 1 - \frac{3(0.03)}{0.37} = 0.76 \quad (6.85)$$

(c) In Section 6.4.2.3, it was explained that the United States related the uniaxial tensile strain data to the biaxial strain fields located on the surface (e.g., Location B as shown in Fig. 6.6) of the bore by using a  $KDF_{multiaxiality}$  of 0.75. For any triaxial strain regions, the United States would conduct the appropriate multiaxial tensile tests to determine the failure allowable values and substitute a  $KDF_{multiaxiality}$  of 1.0 into Equation 6.7. However, for this example, the Netherlands' default value of 0.91 has been used to relate the uniaxial strain failure allowable values to the triaxial strain fields that exist at locations A, C, and D, shown in Fig. 6.6.

Once the  $KDF_{total}$  for both biaxial and triaxial regions location in the propellant grain and the DF have been determined, Equation 6.26 can then be used to determine the propellant grain's  $MS_{tc}$  for thermal cool-down at each location, i.e.,

$$MS_{tc} = \frac{(KDF_{total})_{tc} (\epsilon_{max})_{tc}}{(DF)_{tc} (\epsilon_{induced})_{tc}} - 1 > 0 \quad (6.86)$$

If the margin of safety is less than zero (refer to as the minimum required  $MS_{tc}$  value), the design requirements will not be satisfied.

Note. The minimum required  $MS_{tc}$  value, including the Design and Knockdown factors, was based on the following answers given to the questions listed in Section 6.3, assuming the motor was a "conventional" tactical rocket motor design being exposed to a thermal cool-down environment:

Q1. What types of analytical method are going to be used in the analysis (preliminary or detailed -- refer to Chapter 3)?

A1. *Detailed.*

Q2. What type of application and extreme loading conditions is the rocket motor designed for or intended to see in the field?

A2. *Typical operation requirements and loading conditions are going to be evaluated.*

Q3. For each loading condition considered in the analysis, how well was the propellant and the bondline mechanical properties characterized?

A3. *Type 2.*

The results of the analysis are given in Table 6.7 and shows that based on the Effective Strain Criteria the propellant grain has positive margins of safety for thermal cool-down. The critical location with the lowest MS of 3.31 was determined to be at Location B, halfway down on the surface of the cylindrical bore (refer to Figs. 6.6 and 6.13).

#### 6.8.2.2.2 Ignition Pressurization

For ignition pressurization, the problem under consideration is the evaluation of the margin of safety when the rocket motor is fired at a temperature of  $-40^{\circ}\text{C}$ . For this analysis it was assumed that ( a ) the internal combustion pressure was 12.76 MPa with an associated rise time of 50 msec; ( b ) the same initial mechanical property values as those detailed in Section 6.8.2.2.1 could be assigned for the rocket motor case, insulator and split-boot; and ( c ) the same undeformed model used in Section 6.8.2.2.1 (see Fig. 6.7) could again be used for the ignition pressurization analysis. Normally, the analyst would use a deformed finite element model of the rocket motor exposed to the thermal cool-down condition. However, for the purpose of illustration, the undeformed model shown in Fig. 6.7 was assumed to be the deformed prior to ignition.

Given that the motor has been cooled to an equilibrium temperature of  $-40^{\circ}\text{C}$  and is then ignited to a pressure of 12.76 MPa in 50 msec (0.0008333 min), determine the initial modulus value of the propellant for use in the finite element structural analysis. The required modulus is obtained using the same method described in Section 6.8.2.2.1. Using the temperature shift-factor plot and the relaxation modulus master curve given in Figs. 6.8 and 6.9 the following quantities are calculated at  $-40^{\circ}\text{C}$

$$\log_{10}(a_T) = \underline{6.00} \quad (6.87)$$

$$\log_{10}(t) - \log_{10}(a_T) = \log_{10}(0.000833) - 6.00 = -3.08 - 6.00 = -9.08 \quad (6.88)$$

$$\log_{10}\left[E_o\left(\frac{T_s}{T}\right)\right] = 2.34 \quad (6.89)$$

$$E_o \sim \underline{220.0\text{ MPa}} \quad (6.90)$$

These values (along with the ones listed in Table 6.6, minus the thermal coefficient of expansion values for each component) are used as inputs into the finite element model (see Fig. 6.7) to calculate the induced strains at locations A, B, C, and D. The results of the computations are given in Table 6.7 where the effective strain,  $\epsilon_{\text{eff}}$ , for each location has been calculated using Equation 6.71.

The next step in the analysis is to use the data obtained from pressurized uniaxial tensile tests and determine the strain allowable given that the equilibrium temperature is  $-40^{\circ}\text{C}$ ; the ignition "transient" time is 50 msec; and the maximum  $\epsilon_{\text{eff}}$  is 20.76% at Location D (see Fig. 6.6). After applying the same approach as described in Section 6.8.2.2.1, assuming the data was obtained, it can be shown that the elongation at maximum corrected stress is given by

$$\epsilon_{\text{max}} = \underline{15.0\%} \quad (6.91)$$

Based on the guidelines given in Section 6.4.1 the Design Factor (DF) required for this Type 2 analysis is 1.5. From Section 6.4.2 the total Knockdown Factor (see Equation 6.7) is given by

$$KDF_{\text{total}} = (KDF_{\text{aging}})(KDF_{\text{variability}}) \quad (6.92)$$

which for this problem under investigation yields

$$(KDF_{\text{total}})_{ip} = (0.88)(0.60) = 0.53 \quad (6.93)$$

The numerical values appearing in the above equation are based upon

( a ) A 10-year aging requirement and the assumption that the propellant grain/bondline system is made of an HTPB binder material. For these assumptions the  $KDF_{aging}$  is given by

$$KDF_{aging} = 0.88 \quad (6.94)$$

( b ) A  $\kappa$  value of 3.0 for a “conventional” tactical propellant grain design exposed to an ignition pressurization environment, a standard deviation,  $\sigma$ , of 2% (obtained from the review of the uniaxial tensile similitude data) and a failure strain of 15.0% gives (see Equation 6.9)

$$KDF_{variability} = 1 - \frac{\kappa(\sigma)}{\chi} = 1 - \frac{3(0.02)}{0.15} = 0.60 \quad (6.95)$$

Once the  $KDF_{total}$  and the DF have been calculated, Equations 6.25 and 6.26 can then be used to determine the propellant grain’s  $MS_{ip}$  and  $MS_{total}$  values at each location. The resulting margins of safety relationships are given by

$$MS_{ip} = \frac{(KDF_{total})_{ip}(\epsilon_{max})_{ip}}{(DF)_{ip}(\epsilon_{induced})_{ip}} - 1 > 0 \quad (6.96)$$

$$MS_{total} = \left[ \frac{(DF)_{tc}(\epsilon_{induced})_{tc}}{(KDF_{total})_{tc}(\epsilon_{max})_{tc}} + \frac{(DF)_{ip}(\epsilon_{induced})_{ip}}{(KDF_{total})_{ip}(\epsilon_{max})_{ip}} \right]^{-1} - 1 > 0 \quad (6.97)$$

which in turn can be reduced to

$$MS_{total} = \left[ \frac{1}{MS_{tc} + 1} + \frac{1}{MS_{ip} + 1} \right]^{-1} - 1 > 0 \quad (6.98)$$

The minimum required  $MS_{ip}$  and  $MS_{total}$  values, including the Design and Knockdown factors, were determined based on the same answers given to the questions listed in the previous thermal cool-down solution (see Section 6.8.2.2.1) and that the motor was a “conventional” tactical rocket motor design being exposed to cold ignition.

The results of the analysis given in Table 6.7, show that based on the Effective Strain Criteria, the propellant grain will experience negative margins of safety during cold ignition, with a  $MS_{total}$  value of -0.75 occurring at Location D (around the slot-tip, refer to Figures 6.6 and 6.14). The analysis reveals that this grain design will not meet the design requirement for the ignition condition, after being thermally soaked for 48 hours at -40°C. Therefore, the grain will have to be redesigned. One possible solution would be to extend the slot outward until the tips completely disappear into the insulation. Another option would be to design mu-strips into the insulation, running a quarter the way down along the length of the slot-tips (starting from the back surface of the propellant grain). Both solutions should reduce the high strains seen at the slot-tips, located at the back-end of the rocket motor.

In the United States, if proper material characterization data (i.e., variable-rate similitude data) were available for ignition pressurization at the time of the analysis, then the MS for each loading condition would be evaluated separately. Thus, cold ignition would be modeled with all the input parameters, including thermal coefficient of expansion to simulate thermal cool-down and ignition pressurization, simultaneously. Instead of modeling each loading condition separately and combining the MS values using Equation 6.25, the loading condition would be combined in one finite element model and evaluated separately using Equation 6.26. Sometimes evaluating the strains this way, may result in having positive margins; therefore, obtaining the proper data to evaluate the design is very important in creating an optimum design.

It is important to note that the same methodology applies when determining the structural integrity of the bondline. Except, here, the Effective Stress Criteria (see Section 5.3.5) and bond-in-tension data (used with uniaxial tensile data) are used for performing the margin of safety computations.

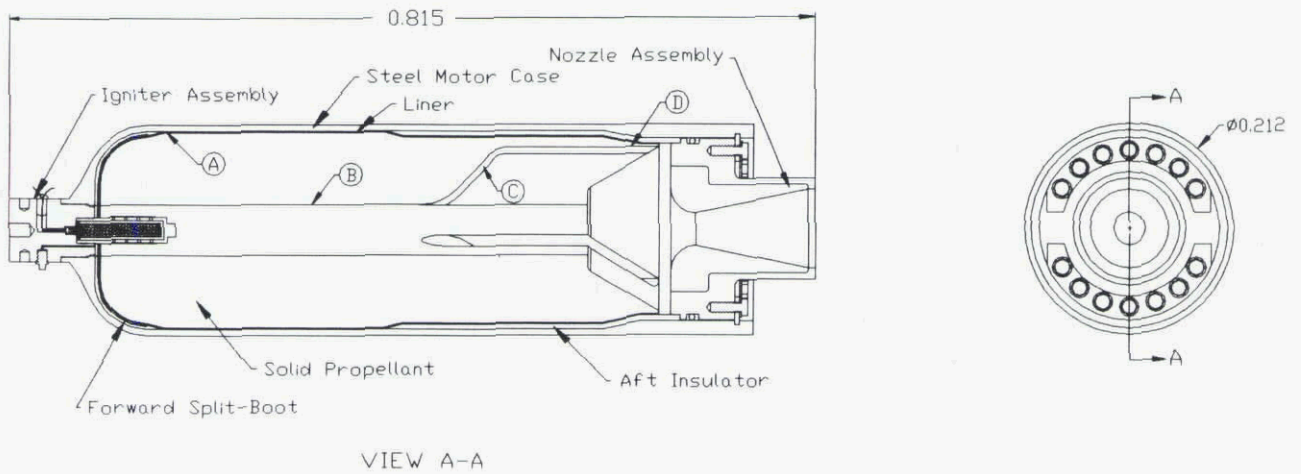


**Figure 6.6: A Typical Rocket Motor Design with a Circular Cylindrical/ Three-Slotted Finocyl (with a Conical-end Section) Propellant Grain.**

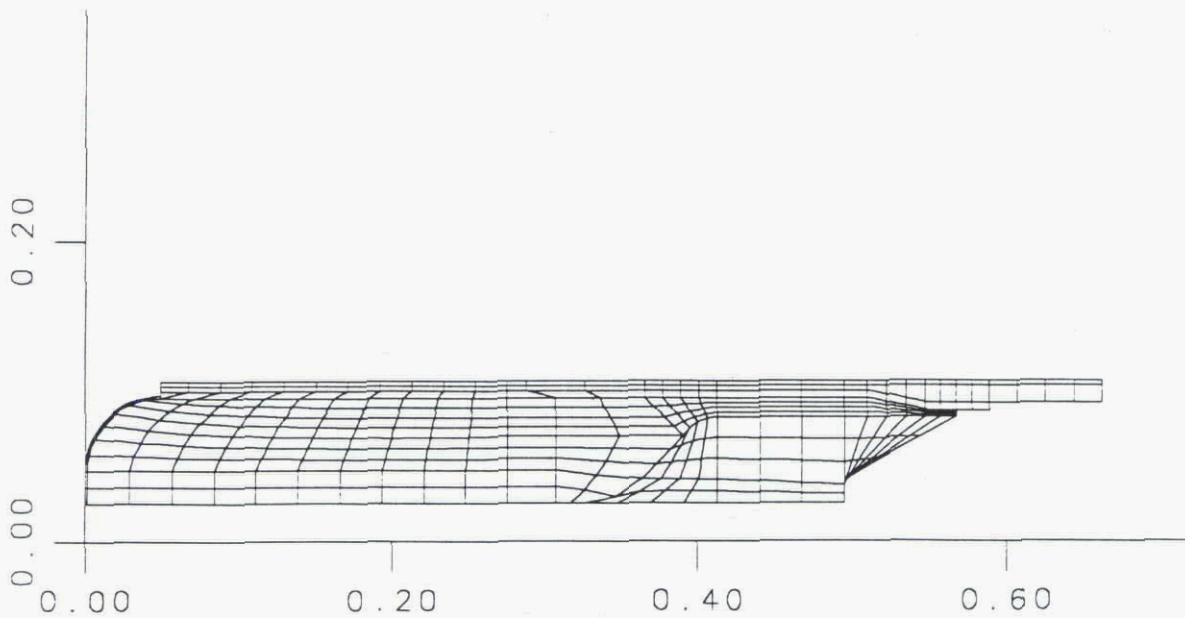


**Figure 6.7: A Typical Two-dimensional, Axisymmetric (Undeformed) Model of Example #2 Motor Design, using Reformulated Isotropic "Slot" Elements.**

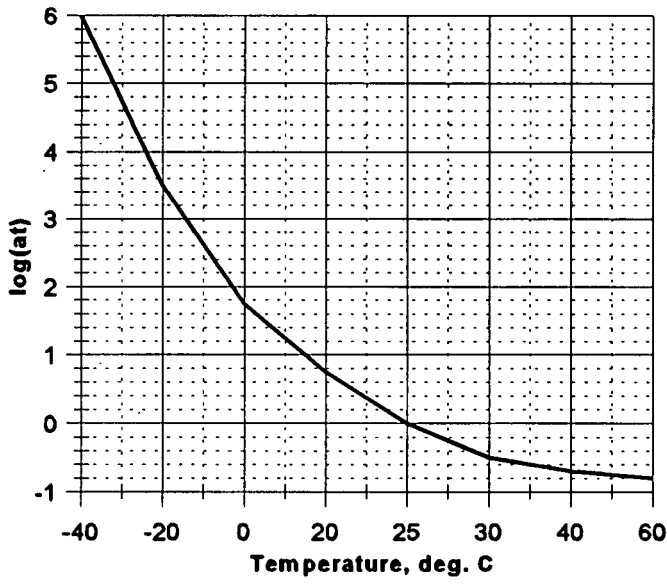


**Figure 6.8: Typical Temperature Shift-Factor Plot from Stress Relaxation Modulus Tests.**

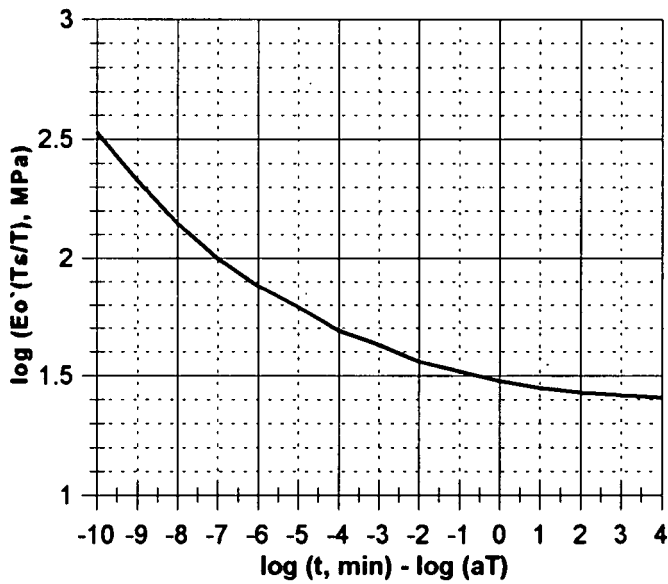


**Figure 6.9: Typical Stress Relaxation Modulus Master Curve (Smoothed) from Stress Relaxation Modulus Tests.**

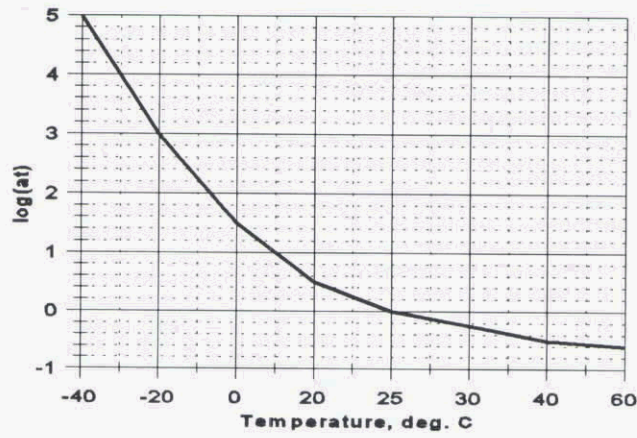


Figure 6.10: Typical Temperature Shift-Factor Plot from Un-pressurized Uniaxial Tensile Tests.

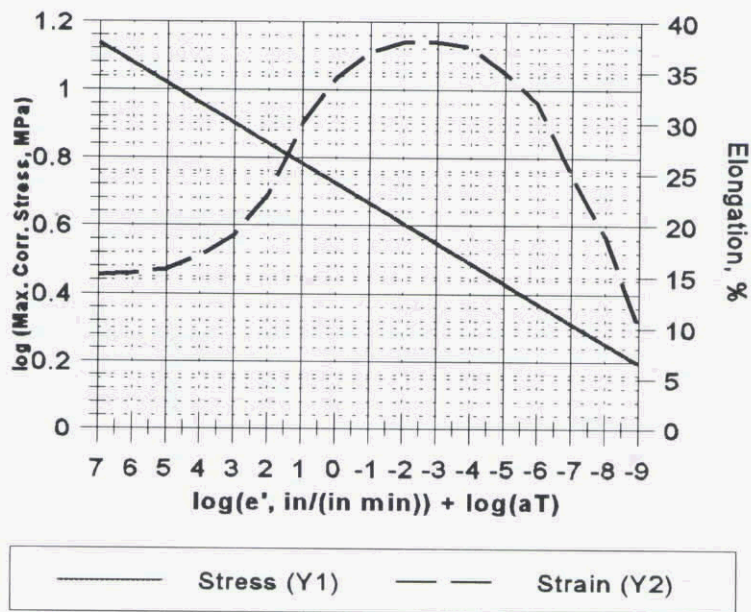


Figure 6.11: Typical WLF Corrected Stress and Elongation Plot (at  $-3\sigma$ ) from Un-pressurized Uniaxial Tensile Tests.

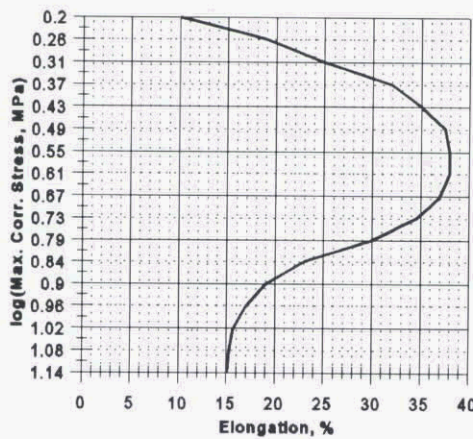


Figure 6.12: Typical Smith Failure Plot (at  $-3\sigma$ ) from Un-pressurized Uniaxial Tensile Tests.

Table 6.6: Initial Code Inputs of Material Property Data for Example No 2.

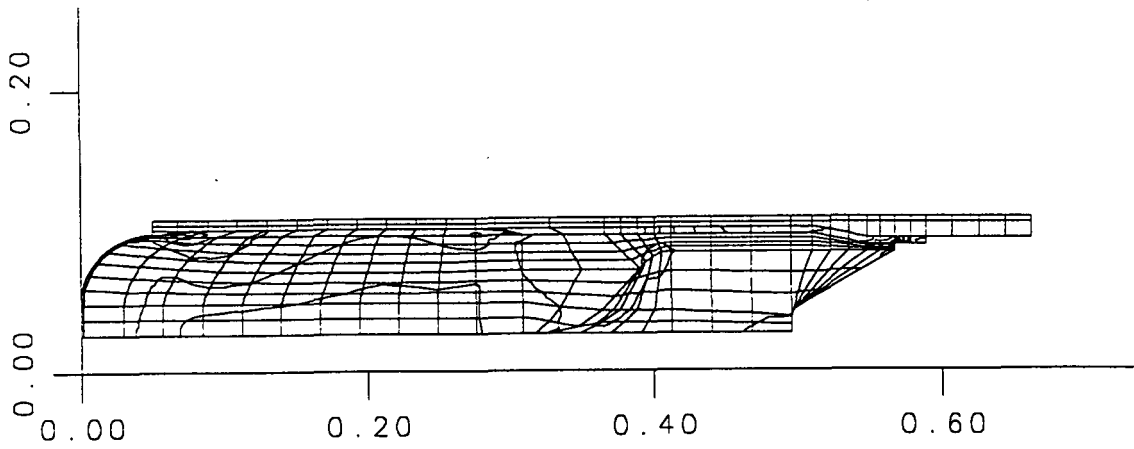
Property	Prop/ liner	Insul./Boot	Motor Case
$E_o$ , GPa	b	0.00552 <sup>a</sup>	200.0
$\nu$	0.4995 <sup>a</sup>	0.33	0.32
$\alpha$ , $\mu\text{mm}/\text{mm}^\circ\text{C}$	27.78	25.33	3.33
$\delta$ , mm/mm	-0.0030	-0.0025	-0.0003

a - assumed value

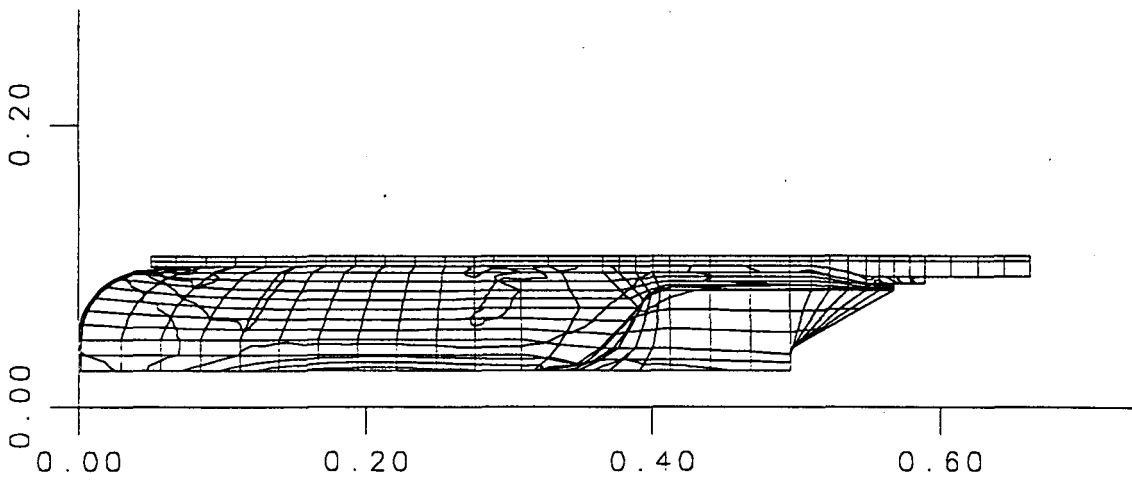
b - calculated from experimental data

Table 6.7: Results for Thermal Cool-down and Ignition Pressurization for Example No 2.

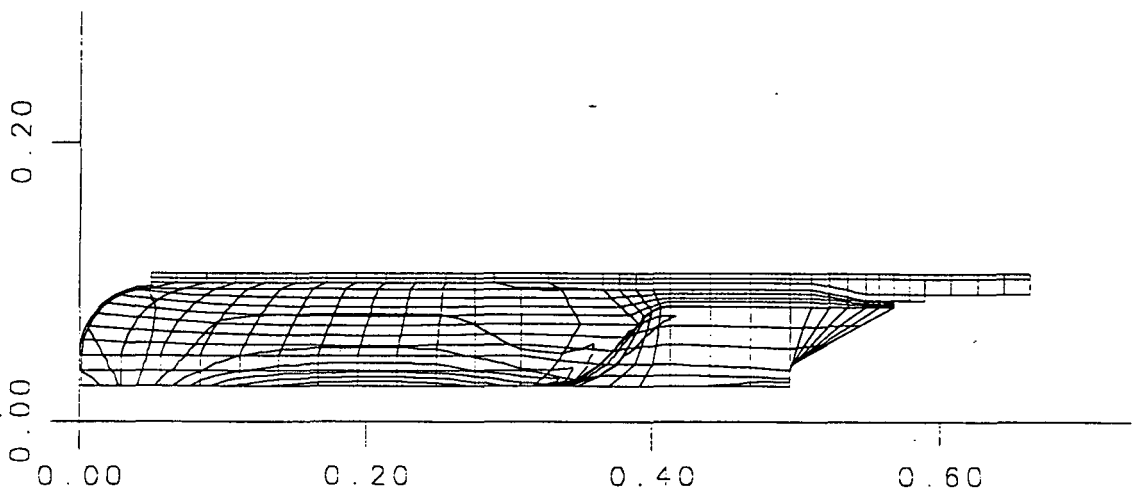
Location				
Thermal Cool-down 60 to -40°C	A	B	C	D
$\epsilon_1$ , %	2.56	-0.53	0.87	0.30
$\epsilon_2$ , %	-2.79	-2.17	-0.30	-0.61
$\epsilon_3$ , %	0.28	2.70	-0.40	0.35
$\epsilon_{\text{eff}}$ , %	3.10	2.86	0.82	0.62
$\epsilon_{\text{max}}$ , %	37.0	37.0	37.0	37.0
DF	1.5	1.5	1.5	1.5
$KDF_{\text{total}}$	0.61	0.50	0.61	0.61
$MS_{\text{tc}}$	3.85	3.31	17.35	23.27
Ignition Pressurization at -40°C	A	B	C	D
$\epsilon_1$ , %	2.67	0.35	3.63	1.29
$\epsilon_2$ , %	-2.13	-1.38	0.43	-18.35
$\epsilon_3$ , %	0.23	1.05	-2.05	17.56
$\epsilon_{\text{eff}}$ , %	2.77	1.44	3.29	20.76
$\epsilon_{\text{max}}$ , %	15.0	15.0	15.0	15.0
DF	1.5	1.5	1.5	1.5
$KDF_{\text{total}}$	0.53	0.53	0.53	0.53
$MS_{\text{ip}}$	0.91	2.68	0.61	-0.75
$MS_{\text{total}}$	0.37	0.99	0.48	-0.75



a. Plot showing the Location of High Principle Strain,  $\epsilon_1$ .

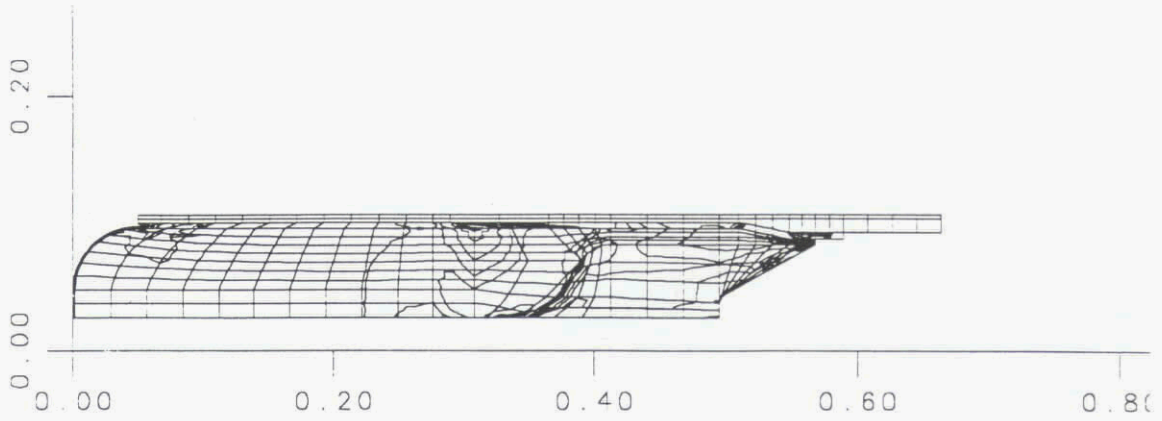


b. Plot showing the Location of High Principle Strain,  $\epsilon_2$ .

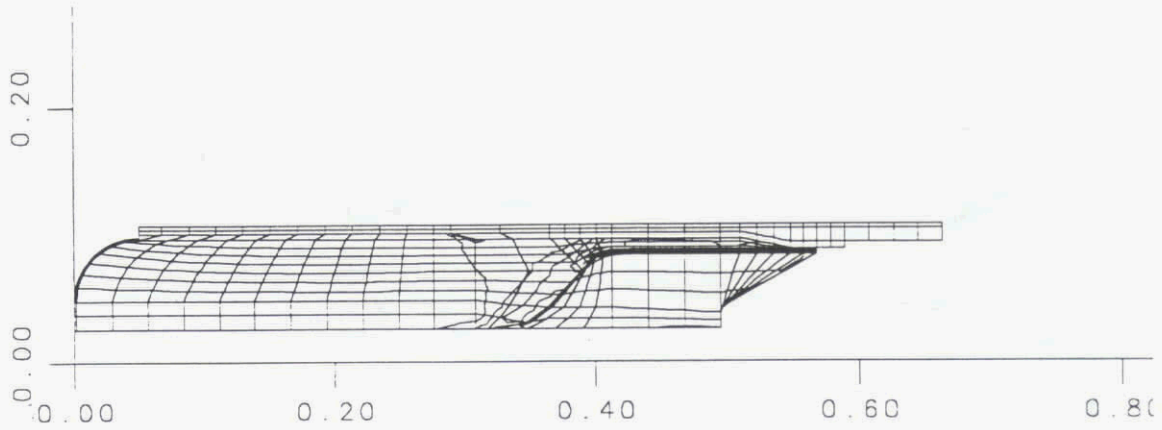


c. Plot showing the Location of High Principle Strain,  $\epsilon_3$ .

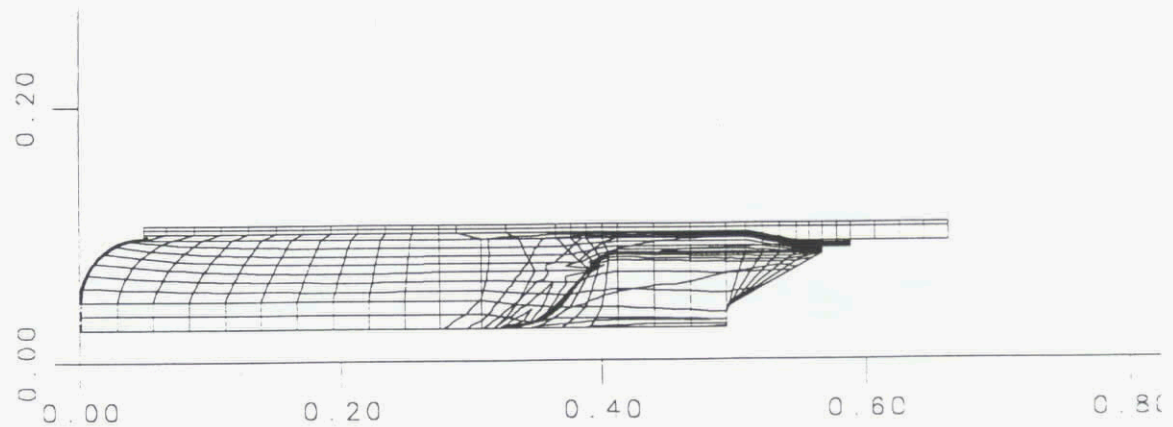
Figure 6.13: Contour Plots for Thermal Cool-down from 60 to  $-40^\circ\text{C}$ , for Example #2.  
 Note. The strain values are in m/m and the dimensions are in meters.



a. Plot showing the Location of High Principle Strain,  $\epsilon_1$ .



b. Plot showing the Location of High Principle Strain,  $\epsilon_2$ .



c. Plot showing the Location of High Principle Strain,  $\epsilon_3$ .

Figure 6.14: Contour Plots for Ignition Pressurization 12.76MPa at  $-40^\circ\text{C}$ , for Example #2.  
 Note. The strain values are in m/m and the dimensions are in meters.

### 6.8.3 Multiple Loading Example #3 - The Probabilistic Approach

#### 6.8.3.1 Problem Statement

In this final example, a probabilistic approach is used to determine whether or not a propellant grain design meets a given reliability limit. This limit is required for ignition after thermal cool-down, which is standard practice in the French rocket industry. It is assumed that the propellant grain is a star-shaped HTPB propellant grain bonded to a metallic case, as shown in Fig. 6.15. The required reliability for the grain is

$$\phi > 0.998 \text{ at a 60\% confidence level} \quad (6.99)$$

and the assumed motor operating temperature is  $-30^{\circ}\text{C}$ .

#### 6.8.3.2 Solution

##### 6.8.3.2.1 Determination of $K_0$ (objective value of Safety Ratio)

Starting from the required reliability level, Equation 6.47 is first used to determine the minimum required Safety Ratio for one grain with the following assumptions:

$$CV_{1C} = 3.5\% \quad (6.100)$$

$$CV_{1S} = 9.5\% \quad (6.101)$$

Making the appropriate substitutions into Equation 6.47 and solving the probabilistic equation for  $K_{\min}$  yields

$$K_{\min} = 1.3 \quad (6.102)$$

If there is more than one grain to be considered, manufactured from different mixes, then Equation 6.49 is used to calculate  $K_0$  that takes into account the mix-to-mix variations that exist in a production line.

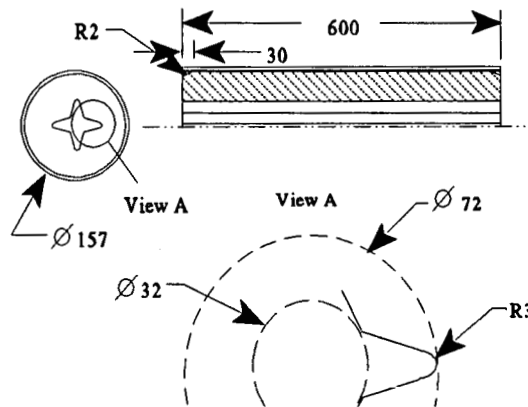


Figure 6.15: Typical Rocket Motor with a Star-shaped Bore.

For this example it is assumed that

$$CV_{2C} = 10\% \quad (6.103)$$

$$CV_{2S} = 13\% \quad (6.104)$$

$$\text{Correlation coefficient, } \rho = 0.8 \quad (6.105)$$

For the  $K_{\min}$  value of 1.3 calculated previously, and the coefficient of variation values given by Equation 6.103 and 6.104, the  $K_0$  value for the required reliability can be evaluated from Equation 6.49 of which takes the value

$$K_0 = 1.6 \quad (6.106)$$

The quantity  $K_0$  is defined to be the objective value of the Safety Ratio for the design.

#### 6.8.3.2.2 Thermal Cool-down

A three-dimensional finite-element model of the grain is mostly generated using a reliable computer code. For this problem it is assumed that the cool-down time of the grain is 24 hours plus 6 hours held at temperature to reach thermal equilibrium, the mechanical properties of the propellant are determined from the master curve with a reduced time,  $t/a_T$ , obtained as follows

$$t = 30 \text{ hrs} = 1800 \text{ min} \quad (6.107)$$

$$\log a_T(-30^\circ\text{C}) = 2.89 \text{ (for HTPB propellant)} \quad (6.108)$$

implying,

$$\frac{t}{a_T} = \underline{2.3 \text{ min}} \quad (6.109)$$

Other relevant input data used in the structural analysis code is given by

$$\Delta T = -90^\circ\text{C} \text{ (Cure temperature} = 60^\circ\text{C)} \quad (6.110)$$

$$E_{p+l} = 1.5 \text{ MPa}; \nu_{p+l} = 0.5 \text{ (for propellant + liner)} \quad (6.111)$$

$$E_c = 1.88 \times 10^5 \text{ MPa}; \nu_c = 0.3 \text{ (for case)} \quad (6.112)$$

The results of the finite element analysis computation giving the stress components at the star-tips are as follows

$$\sigma_r = 0 \quad (6.113)$$

$$\sigma_\theta = 3.45 \text{ MPa} \quad (6.114)$$

$$\sigma_z = 1.80 \text{ MPa} \quad (6.115)$$

### 6.8.3.2.3 Ignition Pressurization

The ignition pressurization analysis is performed using the same three-dimensional finite-element model of the grain generated to analyze the thermal cool-down loads. The applied loading conditions are

$$P_{ign} = 10 \text{ MPa} \quad (6.116)$$

$$T_{ign} = -30^\circ\text{C} \quad (6.117)$$

$$t_{ign} = 50 \text{ msec } (1.1 \times 10^{-6} \text{ min at } -30^\circ\text{C}) \quad (6.118)$$

with the additional strain displacement condition

$$\varepsilon_\theta = 2\% \text{ at } P_{ign} = 10 \text{ MPa (forced displacements on the case)} \quad (6.119)$$

The modulus value used in the finite element analysis is

$$E_p \left( \frac{t}{a_T} \right) = 48 \text{ MPa} \left( \frac{t}{a_T} = 1.1 \times 10^{-6} \text{ min for propellant} \right) \quad (6.120)$$

The results of the finite element analysis computations giving the stress components at the star-tips are as follows

$$\sigma_r = 0 \quad (6.121)$$

$$\sigma_\theta = 5.94 \text{ MPa} \quad (6.122)$$

$$\sigma_z = 3 \text{ MPa} \quad (6.123)$$

#### 6.8.3.2.4 Multiple Loading Conditions

For the multiple loading condition, the cool-down and ignition pressurization stress components are combined assuming linear superposition. Once the stress components for the combined loading condition have been determined, the Stassi/von Mises criteria (discussed in Chapter 5) can be used to compute the resulting equivalent stress,  $\sigma_0$ . The results of the analysis are as follows

$$S_{total} = \sigma_0 = 6 \text{ MPa} \quad (6.124)$$

$$C = 9 \text{ MPa} \quad (6.125)$$

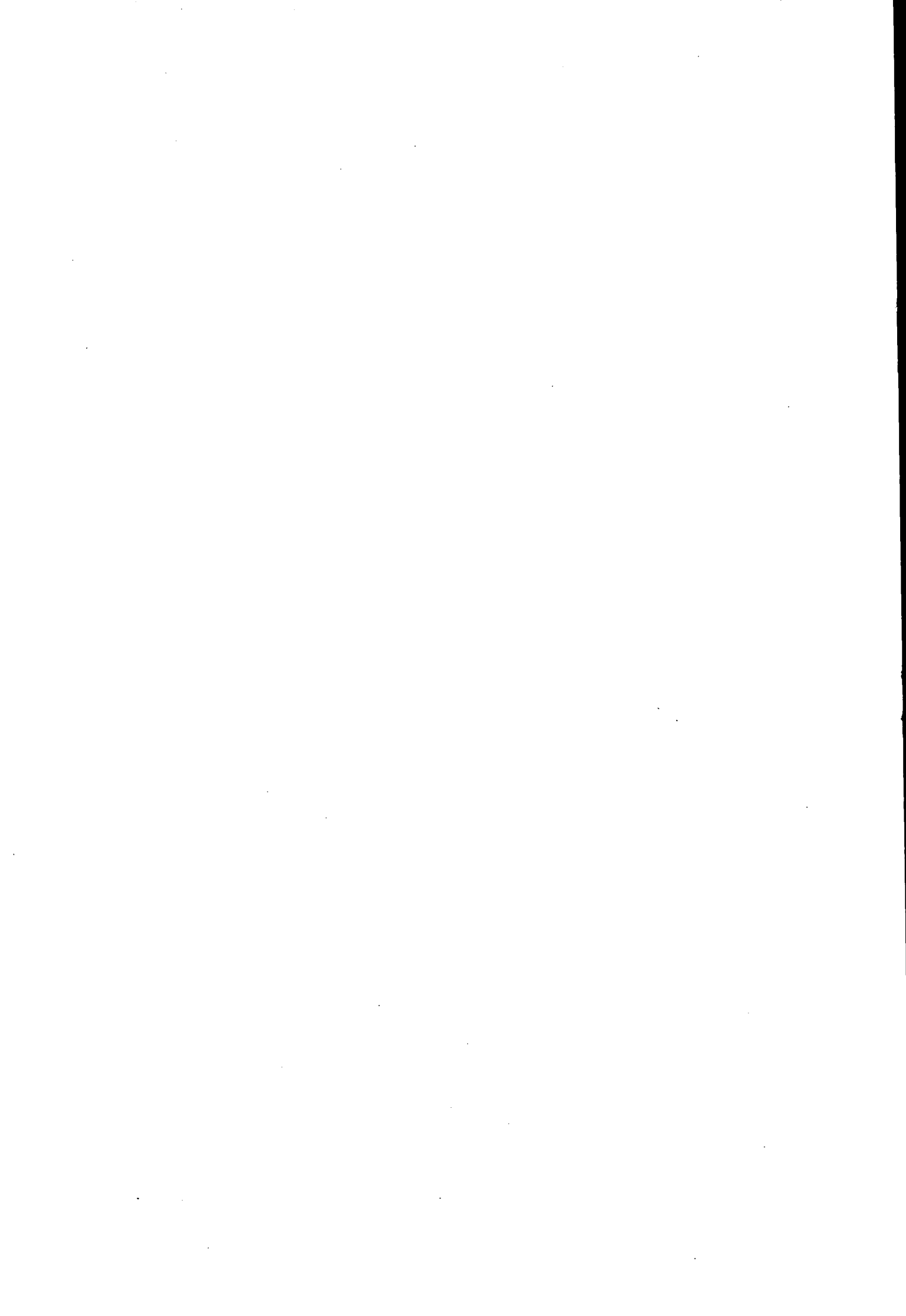
where  $S_{total}$  is obtained from the combined loading analysis and  $C$  is the maximum uniaxial strength capacity of the propellant. It therefore follows that the Safety Ratio for the design is given by

$$K = \frac{C}{S_{total}} = \frac{9}{6} = \underline{1.5} \quad (6.126)$$

The above value  $K = 1.5$  apparently does not exceed the objective (target) value of  $K_o = 1.6$ , which implies that the design requirements have not been satisfied for the specified level of reliability and hence a redesign if the grain will be necessary.

## 6.9 REFERENCES

- [1] Carden III, J.P.; *An Investigation of the Applicability of a Damage Failure Theory for Solid Rocket Propellants*, **AIAA-92-0132**.
- [2] Davenas, A.; **Solid Rocket Propulsion Technology**, Pergamon Press, 1993.
- [3] Meili, G.; Thepenie, J.; Pasquier, M.; Dubroca, G.; *Mechanical Design of Case-bonded CMDDB Grains by a Non-linear Viscoelastic Method*, **AIAA-80-1177**, Boston 1980.
- [4] Nahon, S.; Silvestrini, P.; Thepenier, J.; *Probabilistic Assessment for the Design of High Reliability Objects (> 0.999) such as Solid Propellant Grains*, **AIAA-92-3359**, Nashville 1992.
- [5] Wang, D.T.; Shearly, R.N.; *A Review of Solid Propellant Grain Structural Margin of Safety Predictions Methods*, **AIAA-86-1415**.

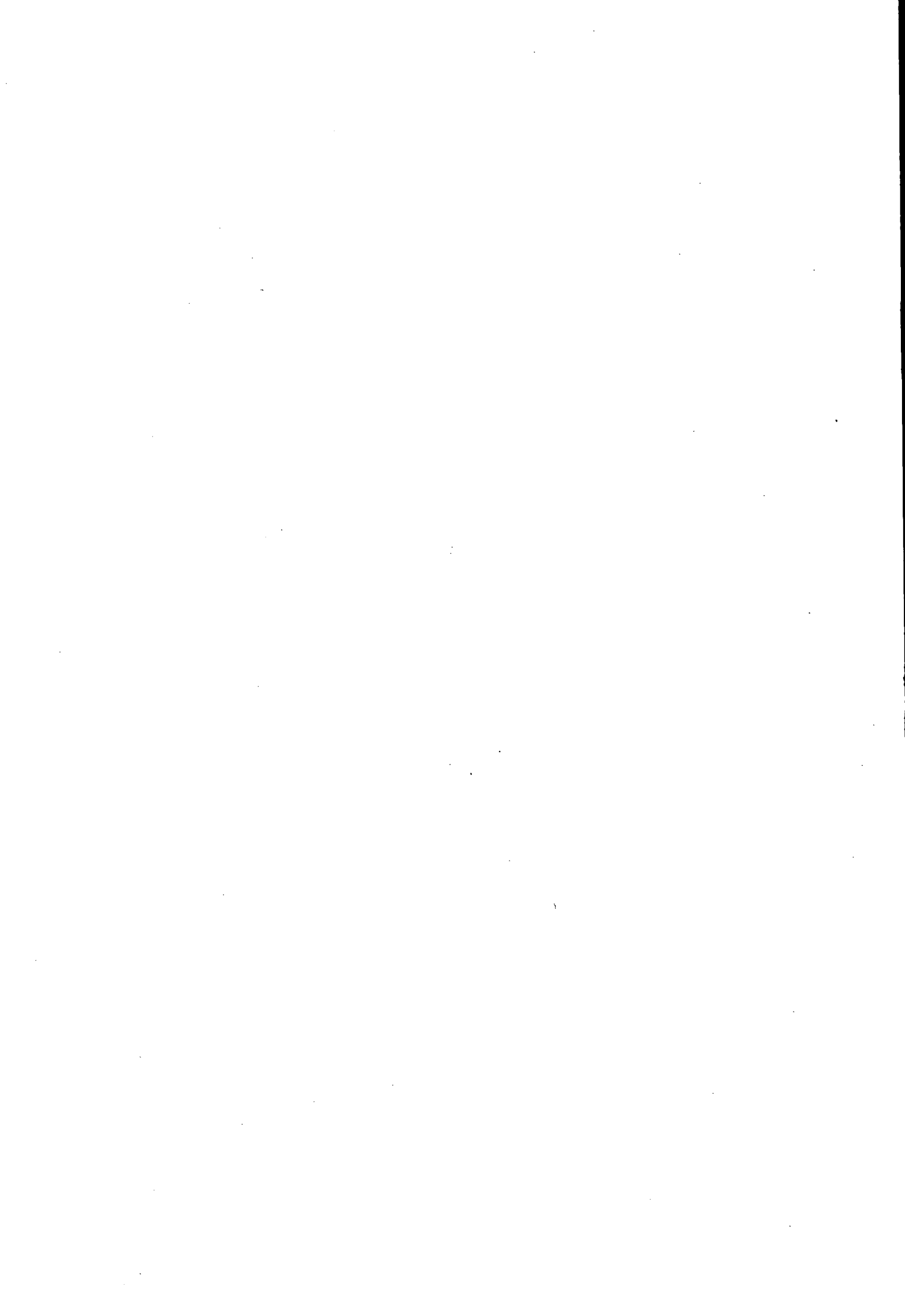


# CHAPTER 7

## VERIFICATION

### TABLE OF CONTENTS

<b>7.1</b>	<b>INTRODUCTION</b>	<b>7-1</b>
<b>7.2</b>	<b>OVERVIEW OF DIFFERENT VERIFICATION PHASES</b>	<b>7-2</b>
<b>7.3</b>	<b>VERIFICATION OF INPUT PARAMETERS</b>	<b>7-2</b>
	7.3.1 Literature and Database Surveys	7-2
	7.3.2 Laboratory Tests	7-2
<b>7.4</b>	<b>VERIFICATION USING ANALOGUES</b>	<b>7-3</b>
	7.4.1 Types of Analogue Motors	7-3
	7.4.1.1 SEC Analogue Motor	7-3
	7.4.1.2 Analogue Motor PHI	7-4
	7.4.1.3 Analogue Motor FIANICOL	7-5
	7.4.2 Associated Experiments and Measurements	7-5
<b>7.5</b>	<b>VERIFICATION USING SUB-SCALE MOTORS OR STV (Structural Test Vehicle)</b>	<b>7-8</b>
	7.5.1 Description of Types of STV	7-8
	7.5.2 Associated Experiments and Measurements	7-9
<b>7.6</b>	<b>VERIFICATION USING FULL-SCALE MOTORS</b>	<b>7-11</b>
	7.6.1 Final Design Verification Tests	7-11
	7.6.2 Environmental Tests	7-11
	7.6.3 Overtests	7-11
	7.6.4 Ageing Evaluation	7-11
	7.6.5 Associated Testing	7-12
<b>7.7</b>	<b>METHODS OF EVALUATION</b>	<b>7-12</b>
	7.7.1 Non Destructive Tests	7-12
	7.7.2 Destructive Tests	7-13
<b>7.8</b>	<b>REFERENCES</b>	<b>7-13</b>



## Chapter 7

# VERIFICATION

### 7.1 INTRODUCTION

The verification of the structural integrity of the solid rocket propellant grain is an essential phase of the structural integrity assessment process. It is necessary that the solid rocket propellant designer must demonstrate to the prime contractor (and the customer) that all the requirements have been satisfied in the sense that an acceptable Margin of Safety has been achieved or, alternatively, an acceptable reliability level has been established. An acceptable Margin of Safety or reliability is first demonstrated theoretically and then verified experimentally using sub-scale motors or other appropriate analogues. At the final qualification phase the structural integrity of the final design configuration of the solid propellant grain is verified using full scale tests on actual rocket motors. For reasons of economy and in order to conserve expensive rocket motors, the verification of the structural integrity of the solid propellant grain is, by necessity, carried out for a limited number of components because the solid rocket motor is a "one shot device" and each full scale test is a destructive test.

Although there is an obvious need for verification at the final qualification stage, it is worth noting that verification is an ongoing process which receives consideration during the evolution of the design of the solid rocket propellant grain (i.e. from the initial concept design to the final configuration). In the early phases of the design, for example in the outline design stage, one often has to make assumptions regarding the properties of the proposed propellant because extensive mechanical testing, of the nature required to perform a rigorous analysis, may not have been carried out on the propellant. At this stage the analyst may have to assume mechanical properties based on properties of similarly formulated propellants, past experience or even good engineering judgement. This situation frequently arises at the initial feasibility phase when the contractor (solid rocket motor designer) is proposing an outline design and the financial resources have not been made available for extensive mechanical property testing of the solid rocket propellant grain and associated materials. Once the detailed design (post contract award) is started, full scale testing of the propellant can commence and the detailed characterisation of the properties of the new propellant undertaken. Margin of Safety predictions can then be revised during the development stage, based on improved and newly acquired data, for the actual propellant. Assumptions made at the concept stage are confirmed or reassessed by verification.

Once the final propellant grain configuration has been established and a predicted Margin of Safety or a reliability level determined it is then necessary to verify these predictions through some development stage testing program. Sometimes actual motors can be used for this purpose when the solid rocket motor is relatively inexpensive. In other situations, for example when the solid rocket motor is large (e.g. a strategic missile or space vehicle, such as the Ariane 5 boosters) cost considerations necessitate the use of analogue motors (i.e. a motor specially designed to simulate specific features of the actual motor) or sub-scale replicas of the full size rocket motor. Whilst the previously mentioned verification tests are destructive in nature, other test procedures are carried out which are non-destructive - e.g. radiography, strain measurements, stress gauging, propellant penetrometer tests, etc. The tests using the analogue or sub-scale rocket motors give the solid rocket propellant design engineer a greater degree of confidence before proceeding with qualification testing on the final full scale rocket motor. The verification procedures discussed thus far are now described in detail in the following sections of this chapter.

## 7.2 OVERVIEW OF DIFFERENT VERIFICATION PHASES

The different verification phases which are invoked during the structural integrity process leading to the design and qualification of the solid propellant grain configuration are depicted in Fig. 7.1. The verification activities are focused on the critical areas of the design which are considered to be of high risk. Verification of the input parameters leading to the definition of the final design solution are also considered.

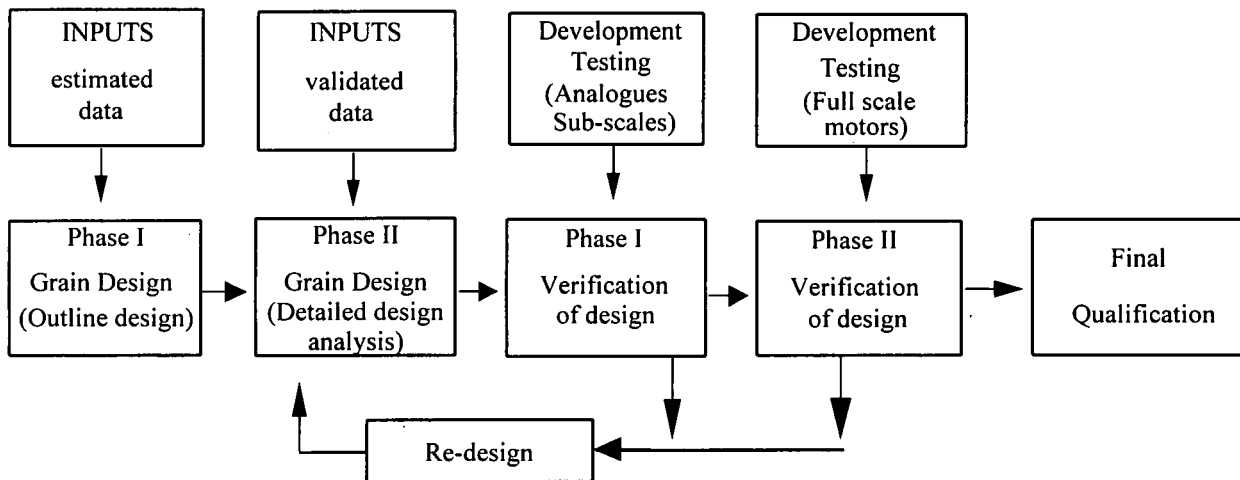


Figure 7.1 Structural integrity verification procedures

## 7.3 VERIFICATION OF INPUT PARAMETERS

### 7.3.1 Literature and Database Surveys

Although in-house mechanical testing will provide detailed information on the propellant properties required to perform a structural integrity analysis considerable information can be gained from external literature surveys and in-house databases. Information from previous work on other solid rocket motors, where similar propellant grain formulations have been used, will often provide useful information for future grain designs. These in-house databases are constructed during the development of each solid rocket motor project and, in particular, contain valuable rheology material property data (e.g. for liner, propellant, insulator materials etc.) including statistical information (e.g. average values and standard deviations) which describe the inherent variability of these materials. Other background information such as knockdown factors, which reflect uncertainties on analysis, ageing properties etc., are usually available to companies working in the solid rocket motor design field. These databases are used wherever possible when materials proposed for a solid rocket propellant grain and associated bondline system have not been entirely characterised for that specific application. In addition, it may be useful to examine the lessons learned and information gained from design studies and test results on other propellant and motor systems.

### 7.3.2 Laboratory Tests

Laboratory tests are performed in order to characterise the mechanical and physical properties of the different materials used in the solid propellant grain and associated bondline system. Appropriate tests are carried out for the range of conditions necessary (i.e. temperature and strain rates, etc.) to define the material properties (see chapter 4) which are required for use in the structural analysis, failure prediction and Margin of Safety calculations (see chapters 3, 5, 6) of the structural integrity assessment.

## 7.4 VERIFICATION USING ANALOGUES

Once a final design configuration of the solid propellant grain and associated bondline system has been established a very useful vehicle for achieving a first level verification of the design is through the use of an analogue motor. An analogue motor (as defined by the working Group) is "a tube filled with a simple propellant grain geometry or alternatively a specimen designed to simulate a specific motor feature". These analogue motors allow a significant number of tests to be performed due to the fact that they are usually relatively small in size and their production costs are low. Different types of analogues may be used and these depend on the type of loadings which are being considered (i.e. thermal cycling, ignition, etc.) or the critical design feature of the propellant grain (i.e. propellant bore, bondline system, etc.) which is being modelled. It is therefore desirable to design analogue motors that are small in size, simple to use and inexpensive with the ability of allowing the creation of induced stresses (strains) identical or representative to those occurring in full-scale solid propellant grains. It can be very useful to carry out a failure mode effects analysis (FMEA) to determine the critical areas of the grain which are to be verified.

### 7.4.1 Types of Analogue Motors

#### 7.4.1.1 SEC Analogue Motor

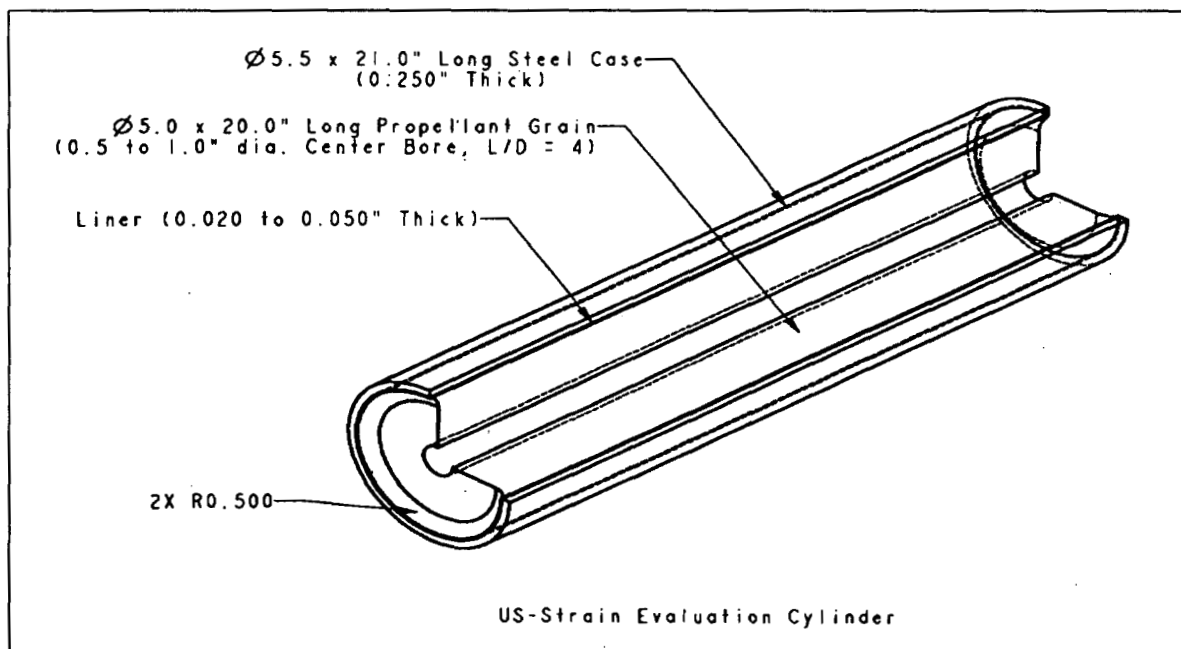


Figure 7.2 SEC analogue motor (Courtesy of NAWC)

An analogue motor commonly used in the many of the NATO countries, called the Strain Evaluation Cylinder and given the acronym SEC, is shown in Fig 7.2. The SEC analogue motor is used during various verification phases of the design of a solid propellant grain [1]. Some of the common applications of the SEC analogue are listed below

- a) A SEC simulating the length-to-diameter ratio and web fraction of the critical regions of the propellant grain may be used to validate the grain design.
- b) The SEC analogue can be placed in a temperature controlled oven and cycled to failure in order to perform overtest to determine the failure strain.
- c) The SEC can be used to compare observed and predicted failures in order to validate a new analytical tool.

### 7.4.1.2 Analogue Motor PHI

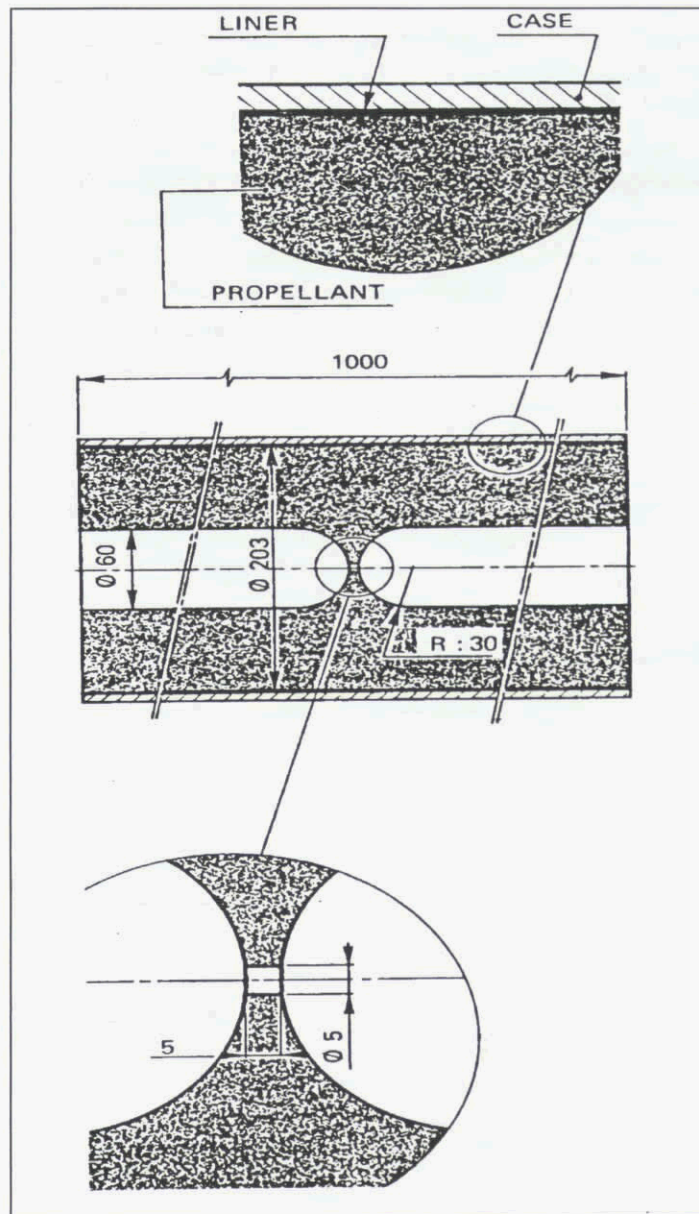


Figure 7.3 Analogue motor PHI (Courtesy of SNPE)

The PHI analogue motor, named because of the similarity to the French term for reliability (i.e. fiabilité), is shown in Fig 7.3. The PHI analogue motor can be used to achieve the same verification objectives as the previously described SEC analogue motor, but with obvious differences in the analysis reflecting the added complexity of the central region. The PHI motor offers distinct advantages over the SEC motor due to its extra degree of flexibility and control over the induced load levels. This is achieved in the PHI motor by simply modifying the following geometric parameters:

- 1) Inside diameter
- 2) Diameter of the hole in the membrane
- 3) Thickness of the membrane
- 4) Length of the motor

Clearly, the location of the most stressed point in the PHI motor is known. Furthermore, the volume of the propellant in the highest stressed region is small in comparison with the total volume of the propellant.

### 7.4.1.3 Analogue motor FIANICOL

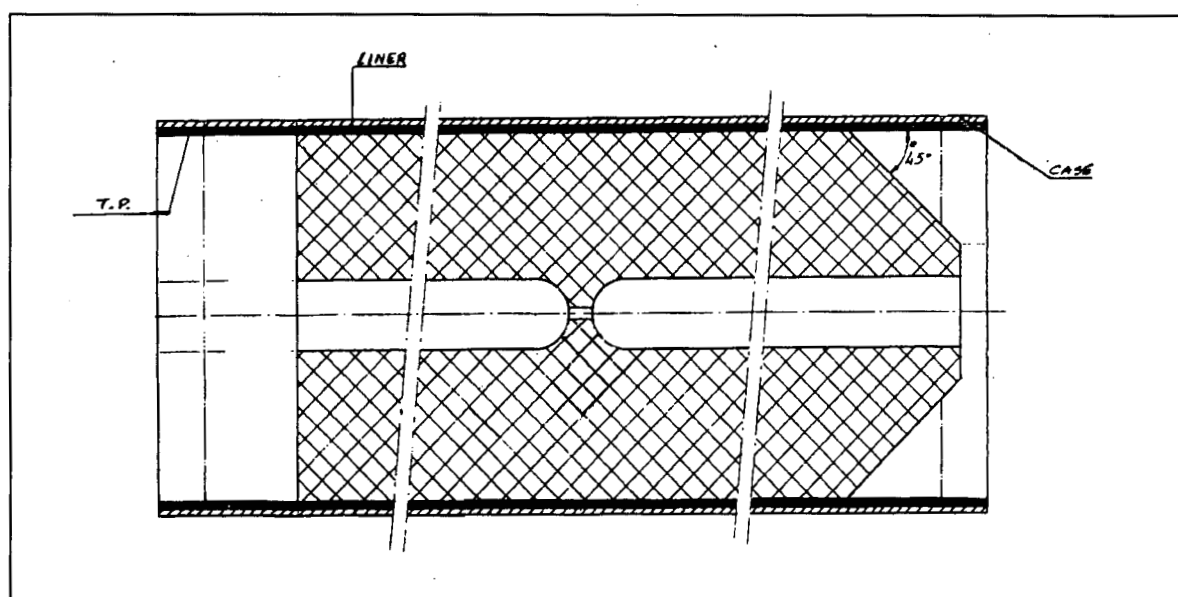


**Figure 7.4 Analogue motor FIANICOL (Courtesy of SNPE)**

A development of the PHI analogue motor, called the FIANICOL, has been made by the French to evaluate the structural reliability of the bond line system, as a function of ageing, when the motors are subjected to thermal cycling. The FIANICOL analogue motor is shown in Fig 7.4 and contains all the geometric features of that model with the exception of the additional 45° annular taper extending from the propellant to bond line interface.

### 7.4.2 Associated Experiments and Measurements

It has already been stated that the primary objective of the analogue motor is to simulate the various loading conditions, on a simple geometry grain designed to simulate a specific motor feature, and thereby evaluate the response of that feature in the actual solid propellant grain or associated bondline system. The verification experiments most commonly performed on these analogue motors are given in the following list:

- 1) Thermal shock tests.
- 2) Thermal cycling tests
- 3) Centrifuge tests to simulate acceleration loads
- 4) Cold gas pressurisation tests to simulate ignition
- 5) Combined loading tests such as thermal cycling followed by cold gas pressurisation.

The above analogue motor tests are selected to simulate the storage profile and ignition conditions. The tests are either performed under nominal conditions, that is close to the operating conditions of the actual solid rocket motor, or alternatively the above tests are carried out for a more severe set of conditions. The latter tests, called overtests, are sometimes designed to induce failures which in turn provides additional information from which a more accurate determination of the margin of safety can be determined.

A variety of different types of measurements are taken when tests are performed on these analogue motors. Typical measurements include:

- a) Temperature measurements at different locations in the outer and inner parts of the analogue using, for example, thermocouples.
- b) Displacement measurements using specially designed displacement gauges (see, for example the bore displacement gauge shown in Fig 7.5) or displacements measured by optical devices such as lasers.
- c) Bond stress measurements using specially designed bond stress transducers (based on miniature semi-conductor strain gauge technology).
- d) Determination of the occurrence of particular failures (e.g. crack initiation, debonds etc.) using various defect visualisation aides (e.g. endoscopy, ultrasonic, photography, X-ray, etc.). An example of crack visualisation in a PHI analogue motor [2] is shown in Fig 7.6.

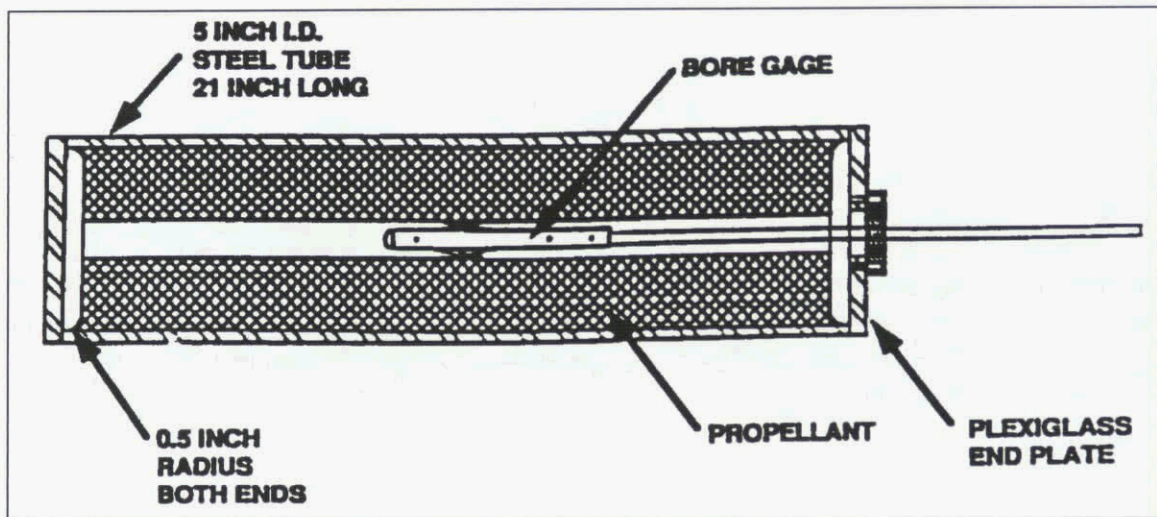


Figure 7.5 SEC with end-mounted bore gauge (Courtesy of NAWC)

Some destructive testing may be carried out on the propellant removed from these motors, e.g. for measurements of sol-gel.

An analysis of the test results obtained from experiments performed on these analogue motors provides a great deal of valuable information which leads to the following:

- a) Comparison of predicted and observed failures.
- b) Validation of calculations (i.e. thermal, structural etc.).
- c) Estimation of actual Margins of Safety for the solid rocket propellant grain.

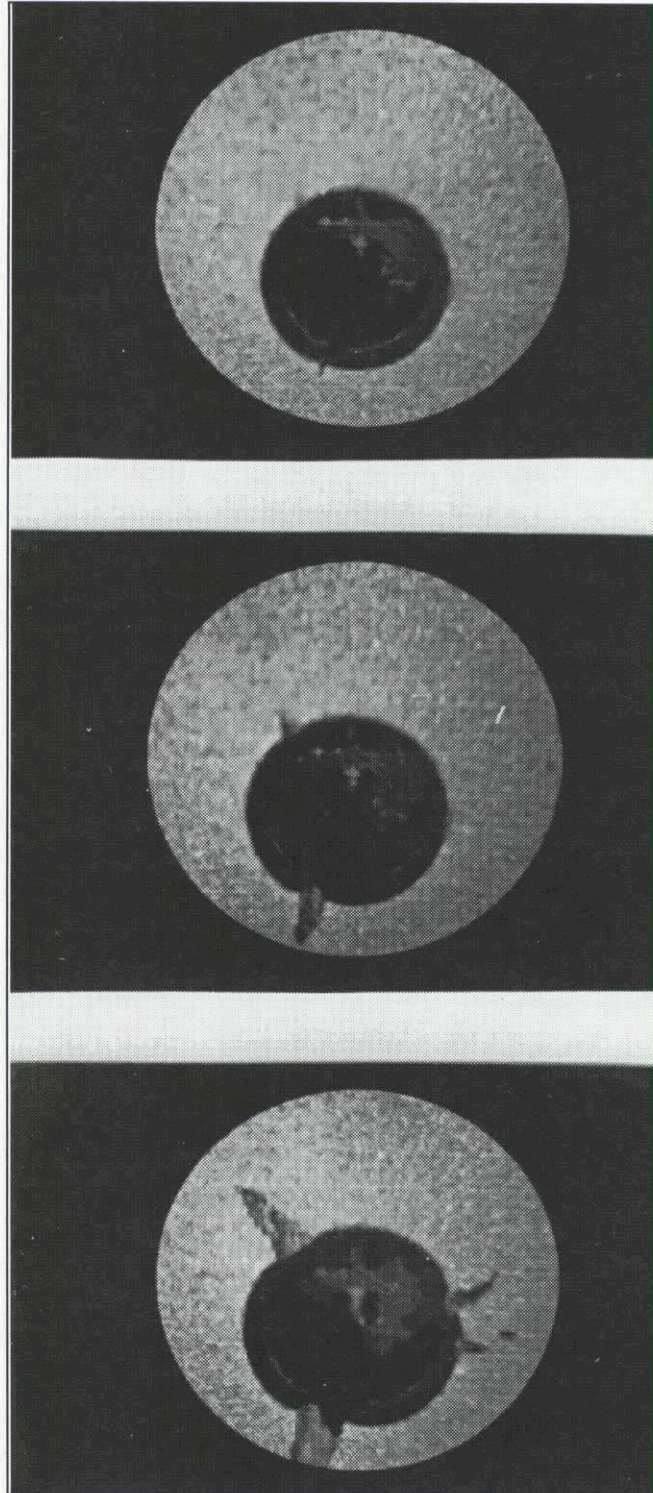


Figure.7-6 : Crack development in the bore of an analogue (Courtesy of SNPE)

**7.5 VERIFICATION USING SUB-SCALE MOTORS OR STV (Structural Test Vehicle )**

The verification of the structural integrity of the solid rocket propellant grain is also carried out using what are termed Structural Test Vehicles (STV) and sub-scale rocket motors. The STV is essentially a tube with a propellant grain designed to simulate the rocket motor response to complex loading. The sub-scale rocket motor is a tube filled with the same propellant and grain features as the full size rocket motor but of smaller size. Sub-scale rocket motors are mainly restricted to large solid rocket motor verification programmes and are used to address both the structural and ballistic concerns.

**7.5.1. Description of Types of STV**

An example of an STV that has been used in the United Kingdom is the Structural Test Motor, or STM for short, [Ref 5]. The STM was designed to be representative of a typical flightweight, case-bonded HTPB propellant motor. The motor case was constructed from 1mm thick monolithic steel. The liner material is also 1mm thick. The features of the grain are shown in figure 7.7 below. The grain is stress-relieved at the head end using a butyl boot. The propellant used in the STM was a non-aluminised, cast HTPB composite. The STM was instrumented using thermocouples and stress transducers which monitor the stress levels at the bondline between the propellant and the motor case. The instrumented version of the STM (called the Structural Test Instrumented Motor) was given the acronym STIM to differentiate it from the uninstrumented STM. A typical layout for the stress transducers and thermocouples is shown in figure 7.8. Temperature cycling was applied to represent service conditions and the stresses were monitored as a function of time and temperature. The resulting data has been used to verify the structural integrity analysis methodologies and to quantify cumulative damage effects.

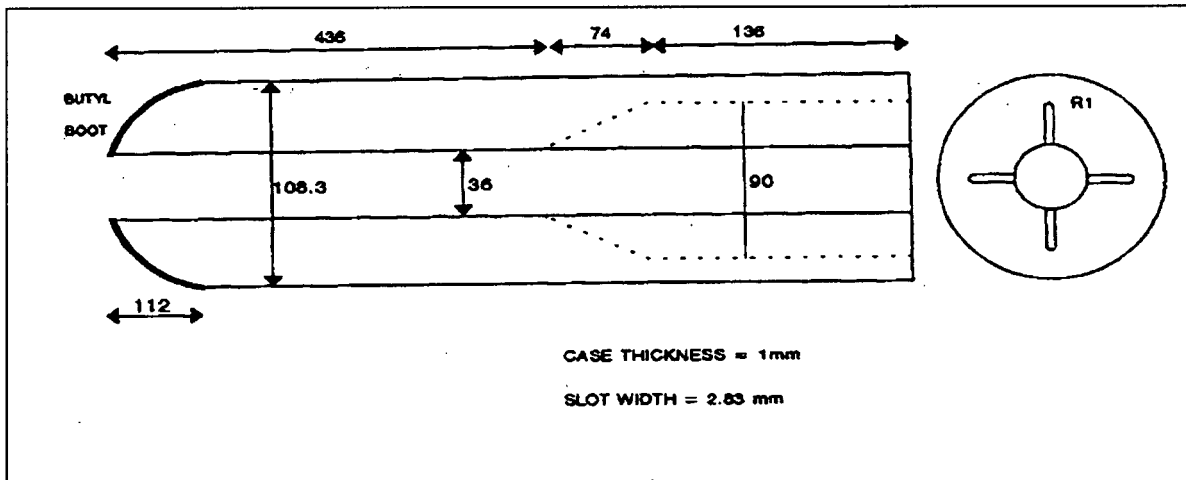


**Figure 7-7 : Example of STV (Courtesy of Royal Ordnance)**

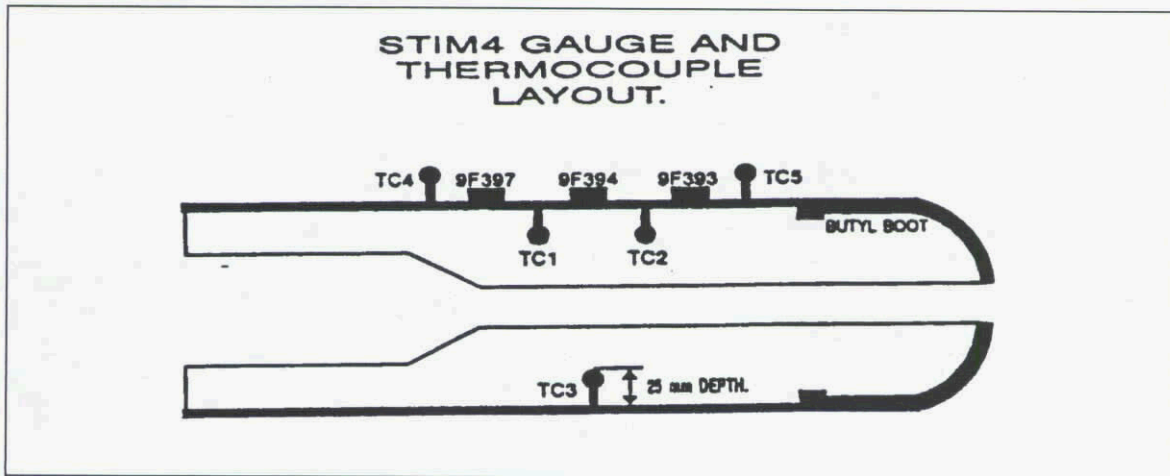


Figure 7-8 : Example of instrumented STIM motor (Courtesy of DRA)

An other example of an STV which has been developed for use in the United States is shown in fig 7-9. The analysis performed using that type of motor is described in ref [6].

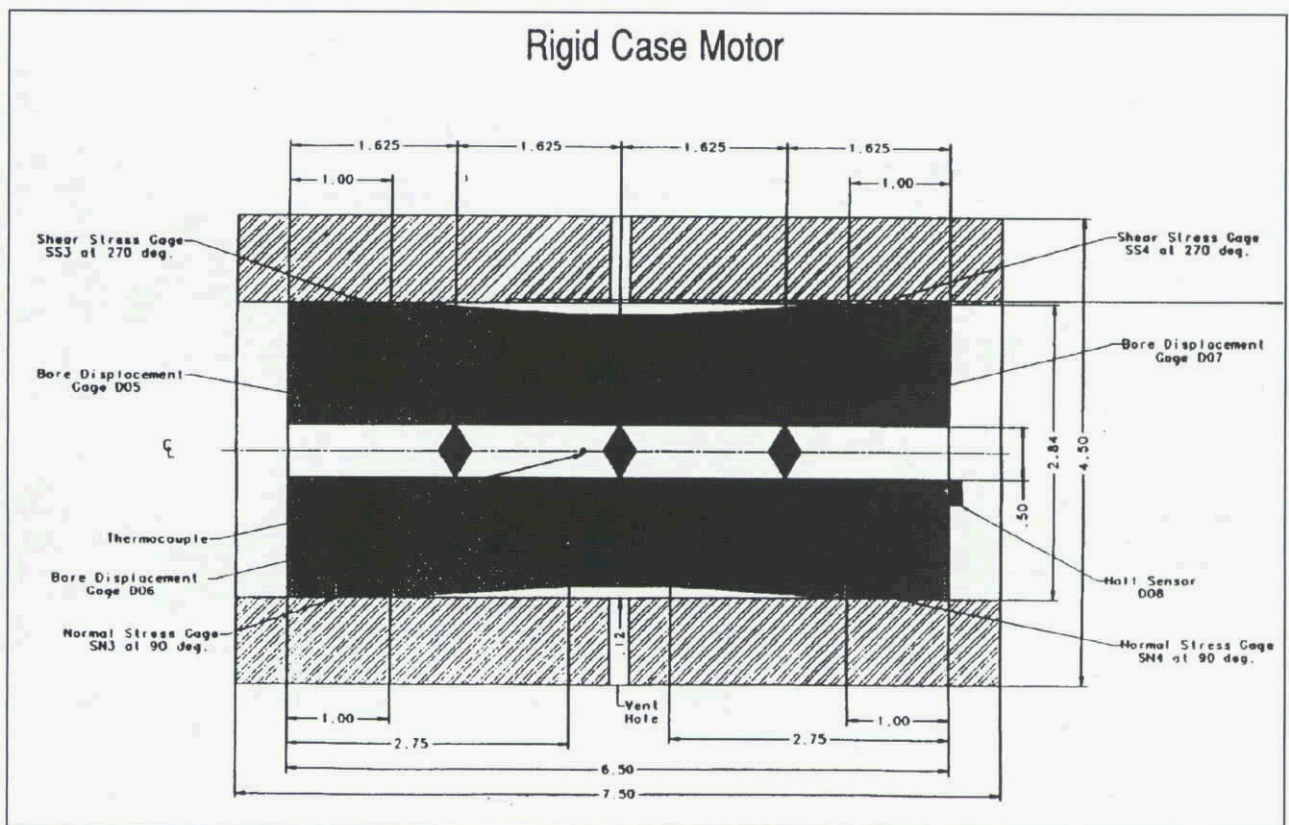


Figure 7-9 : Other type of instrumented STV ( Courtesy of Thiokol)

### 7.5.2. Associated Experiments and Measurements

Two types of thermal cycling tests were performed using the STM; the thermal shock cycle and the arctic cycle shown respectively in fig 7.10 and fig 7.11. The values of stress and temperature measured by the stress gauges and thermocouples were then able to be used to make comparisons with the theoretical predictions and to establish what was the best available predictive technique.

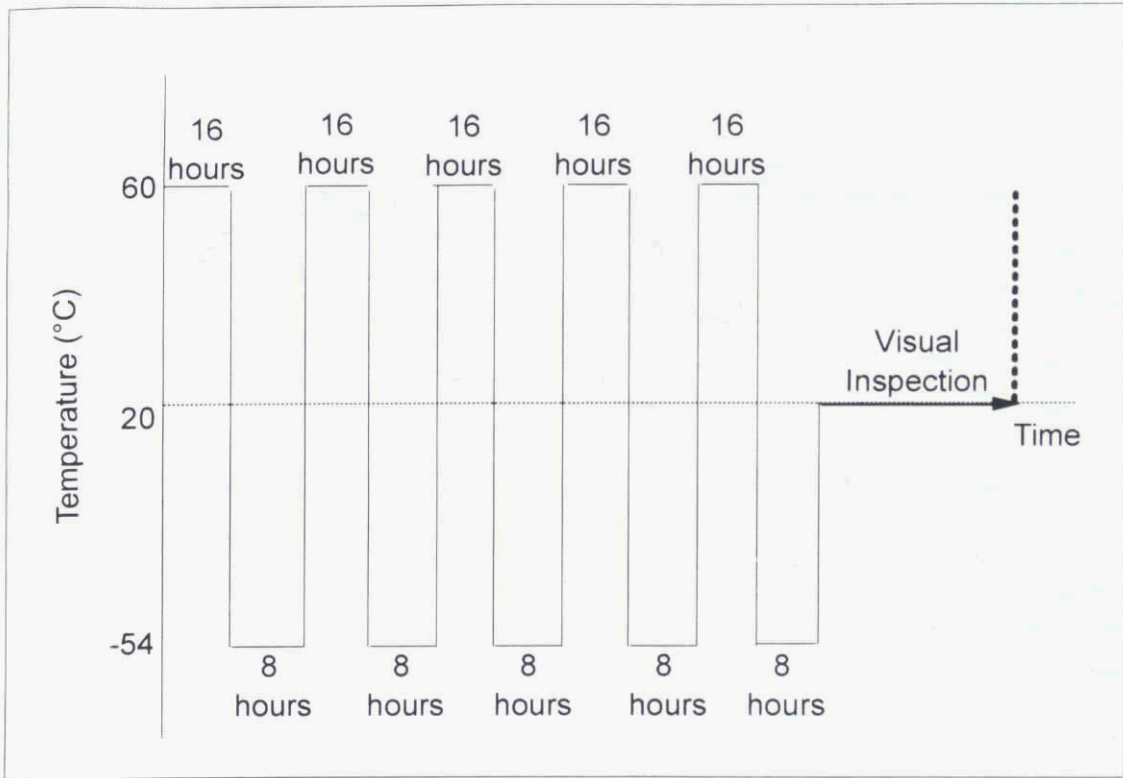


Figure 7-10 : Example of thermal shock cycles

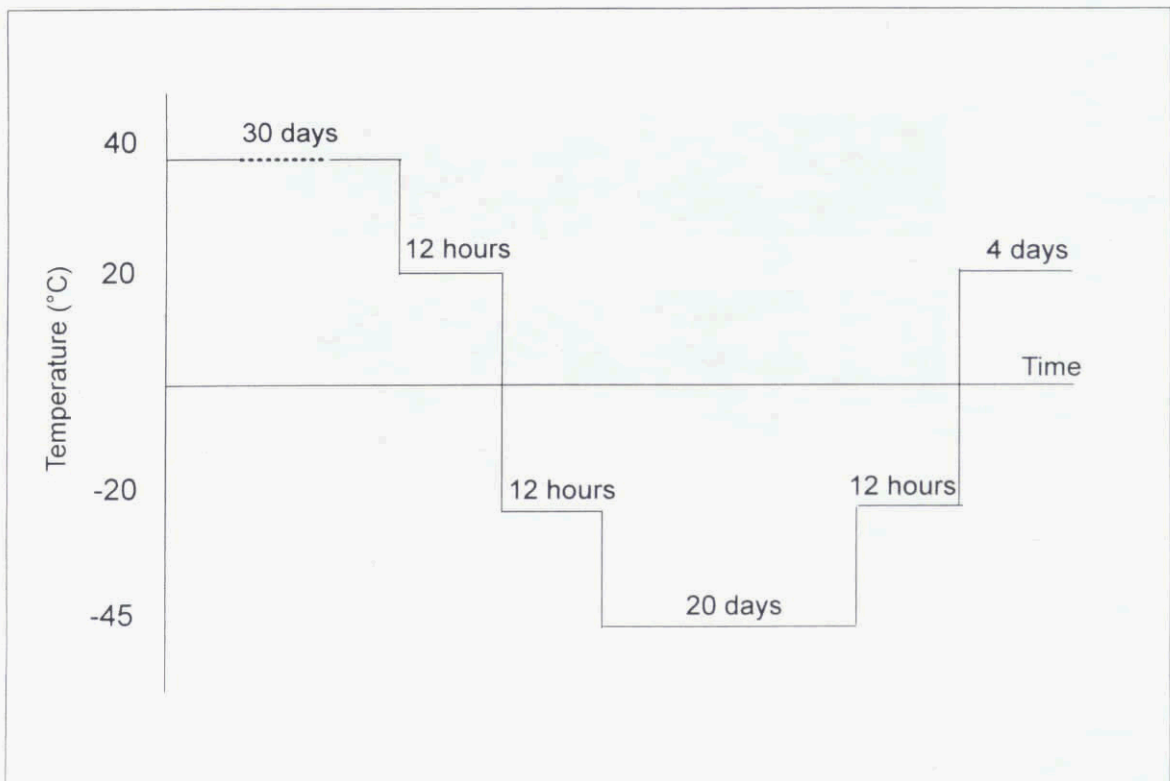


Figure 7-11 : Example of arctic cycles

## 7.6 VERIFICATION USING FULL-SCALE MOTORS

### 7.6.1 Final Design Verification Tests

In order to verify that the propellant grain satisfies the specified operational requirement, a range of verification tests will need to be carried out on the full-scale motor. Results of such tests can be compared to the predictions and test results arising from the development activities so a final evaluation can be made of the motor's Margin of Safety. The main types of test regimes are described below.

### 7.6.2 Environmental Tests

In the Development stage, pre-Qualification tests or limited environmental tests may have been carried out on full-scale motors to assess the capability of the motor to meet the environmental requirements and thereby reduce the risks. In the Verification stage, it will be necessary to conduct a full programme of environmental tests to achieve motor Qualification. The objective of such test programmes is to ensure the motor will perform satisfactorily and safely after being subjected to all environmental conditions within its' life cycle. It may require the sequential application of both typical and extreme climatic and mechanical conditions to replicate elements within the life cycle. To ensure that the conditions to be applied are valid, a review of the operational requirement specification for the system should be carried out. A description of the considerations in such a process is given in Ref [7]. The Qualification test programme will end in either performance testing, including firing under combined load conditions (e.g. acceleration and thermal gradient), or critical examination (e.g. NDT or motor dissection) to ensure a sufficient margin of safety exists. A typical programme of tests for tactical systems is given in the appropriate NATO STANAGs (e.g. Refs [8],[9]), whilst for strategic or space-booster systems these are likely to be specified by the Customer.

### 7.6.3 Overtests.

Some Nations incorporate within their Environmental test programme the option of conducting overttests, where the severity of the environmental stresses or the firing parameters are increased to obtain confidence in the ability of the motor to withstand extreme or abnormal conditions. For cost reasons these overttests are less frequently carried out on full-scale motors, especially on larger systems, nor are they routinely conducted in the USA and some other nations. They can, however, be very valuable for evaluating the Margin of Safety predictions, especially for those applying during the ignition phase. This is usually achieved by firing at temperatures above or below the operational specification; it may also be achieved by reducing the nozzle throat whilst maintaining the maximum pressure (within the case burst strength) and evaluating the effects of the over-pressure that results.

The over test programme may result in either grain failure or its survival. If the grain fails then the Margin of Safety, as predicted using the parameters and boundary conditions in the structural integrity analysis, should be less than zero. This would give a qualitative verification of the structural integrity analysis. The same arguments could be put forward for survivors of an overttest where in this case the predicted Margin of Safety would be greater than zero. However of particular interest is the limit state condition dividing failure and non failure (i.e. Margin of Safety equal to zero) which if identified by this overttest programme would provide a quantitative verification of the structural integrity analysis. Although it is recognised without question that failure data is essential for evaluating the reliability of the solid propellant grain it is also worth noting that survival data provides additional important information. The use of censored data (i.e. failure and survival) will improve the statistical parameter estimations of the reliability distributions. The use of combined survival and failure data also has important application in the Bayesian statistics for a reliability approach (see for example Ref [10]).

### 7.6.4 Ageing Evaluation.

As it is likely that the motor will need to retain the same level of Margin of Safety and reliability throughout its life cycle, it will generally be necessary to verify the influence of ageing on the structural behaviour. In addition to the main elements in the Environmental or Overttest verification programmes, ageing programmes on full-scale motors are therefore applied to evaluate the effects of long term use and storage on the motor. These may use elements of real-time or accelerated ageing, with the latter achieved by the use of higher stress levels (thermal, vibration, etc.) to promote ageing in a shorter test

time; e.g. using the US Navy Type Life cycle or the UK diurnal cycle for hot/wet thermal ageing, or the acceleration of vibration by increased spectra, see Ref.[7]. The structural properties of the grain and bondline system after such ageing are then evaluated, by non-destructive and destructive methods, and the results compared to the predictions made in the strength analysis phase of the assessment or the test results from the Development stage.

#### **7.6.5 Associated Testing.**

Most of the additional methods employed on the full-scale motor to verify the assessment of the overall design are the same as those used on the analogue or sub-scale motors. However, some intrusive methods, such as the use of miniature stress transducers or gauges, may require special agreement or certification before they are acceptable for use in service-standard full-scale motors.

### **7.7 METHODS OF EVALUATION**

#### **7.7.1 Non Destructive Tests :**

Non destructive tests are designed to ensure the quality and integrity of the propellant grain by "inspecting" the most critical areas without altering them. These tests commonly fall into three categories :

- i) propellant bulk inspection to detect cracks, voids or heterogeneities
- ii) examination of the bondlines to detect debonds, cracks or inclusions
- iii) inspection of the geometry to verify the dimensions

These different techniques, described below, are especially useful in detecting a failure when conducting an overttest (e.g. thermal cycling) on an analogue or full scale motor.

#### **a) X-ray Testing (bulk and bonds)**

The most widely used method is X-ray radiography on photographic film which allows inspection of the inner homogeneity of the propellant grain, the quality of the bonds (liner/case, liner/insulator, liner/propellant, propellant/propellant) and also allows a check on the thickness of the various components. Real-time radiography allows a total observation in real time of a moving object by combining the use of television, videotaping and computers. Computer Aided Tomography is the newest and most powerful X-ray technique which permits, the reconstruction of images of successive slices of an object. This method allows the inspection of the inner configuration of the rocket motor in considerable detail [11].

#### **b) Ultrasonic Testing (bonds)**

This technique is based on the observation of the reflection and attenuation of an ultrasonic wave traversing an object, and is used to check the propellant/inhibitor bond.

#### **c) Endoscopic Inspection (inspection of inner bore)**

Endoscopic devices are used to detect the anomalies (voids, cracks) on the surface of the bore. Recent developments using optical techniques allow the 3D measurement of anomalies, without any contact with propellant. This device is used in the quality control of the grain geometry and may also be used to determine grain dimensions and strain levels.

#### **d) Penetrometer**

The penetrometer measures the properties of the propellant in the grain by determining its response to controlled loading conditions of an indenter. From the penetrometer data an assessment can be made of the ageing characteristics of the propellant at the bore of the grain (ref. 12).

### e) Direct Measurements

As in analogue motors (section 7.4.2 ), some direct measurements may be performed in full-scale motors with bore gauges and/or stress transducers. An example of an analysis based on an instrumented rocket motor (CRV-7 motor) stored at the environmental site of Valcartier (Canada) is described in Ref. [13]. Further work is proceeding in the TTCP nations to employ these techniques for examining effects of pressurisation or thermal loading conditions.

## 7.7.2 Destructive Tests

### Dissections

These tests are frequently used either on analogue motors (section 7.4.2) or on actual solid rocket motors (sub-scale or full-scale) . Different samples (propellant and bonds) are cut off the grain and mechanical tests are performed. A comparison of the results obtained shows whether or not significant differences exist between the mechanical properties derived from the actual propellant grain and the propellant used in the characterisation tests. Comparisons are also made after various time periods have elapsed to evaluate the effects of ageing.

### Firing tests

Firing tests are also carried out as part of the verification procedure of the solid rocket motor propellant grain. Tests are carried out under nominal conditions and imposed severe conditions (e.g. overtesting at low temperature extremes under imposed acceleration loads).

## 7.8 REFERENCES

- [1] ICRPG, *Solid Propellant Mechanical Behaviour Manual* , CPIA Publications , 1963
- [2] Thepenier J., Gondouin B, and Menez-Coutanceau H; *Reliability of Solid Propellant grains : mechanical analog motors design and testing* , AIAA. 87.1987; San Diego.
- [3] Final report on KTA-14, *Service life prediction methodologies* , TTCP-WTP4/KTA-14 (November 1994).
- [4] Buswell H.J. and Francis E.C., *Improvements in Rocket Motor Service Life prediction*, Paper No 27 AGARD/PEP Symposium : " Service life of Solid propellant Systems ", Athens , May 1996
- [5] Buswell H.J., Chelner H., Faulkner G.S., and Morell D., *Stress measurement in Solid Rocket Motors* , 18th Transducer Workshop; Colorado Springs, June 1995 .
- [6] Collingwood G., Clark L.M., *Service Life Prediction using Non-linear Viscoelastic Analysis and a Probabilistic Approach* , Paper No 29, AGARD / PEP Symposium : "Service life of Solid propellant Systems" Athens , May 1996
- [7] Maxey I.H, "Environmental Data in Service Life assessment, Paper No 39, AGARD / PEP Symposium : "Service life of Solid propellant Systems" Athens , May 1996
- [8] STANAG 4325, *Standard Environmental & Safety Tests for Air Launched Munitions*, NATO, 1991
- [9] STANAG 4337, *Surface Launched Munitions , Appraisal, Safety & Environmental Tests* , NATO, 1994.
- [10] Nahon.S., Silvestrini.P, Thepenier.J. , *Probabilistic assessment of the design of high reliability objects (> 0.999) such as solid propellant grains* : AIAA 92.3359. Nashville.
- [11] Lamarque P., Tauzia J.M., *Assessment of the Shelf Life of SRM : Prospects provided by High Energy X-Rays Computed Tomography*, Paper No 15, AGARD/PEP Symposium : "Service life of Solid propellant Systems " , Athens , May 1996

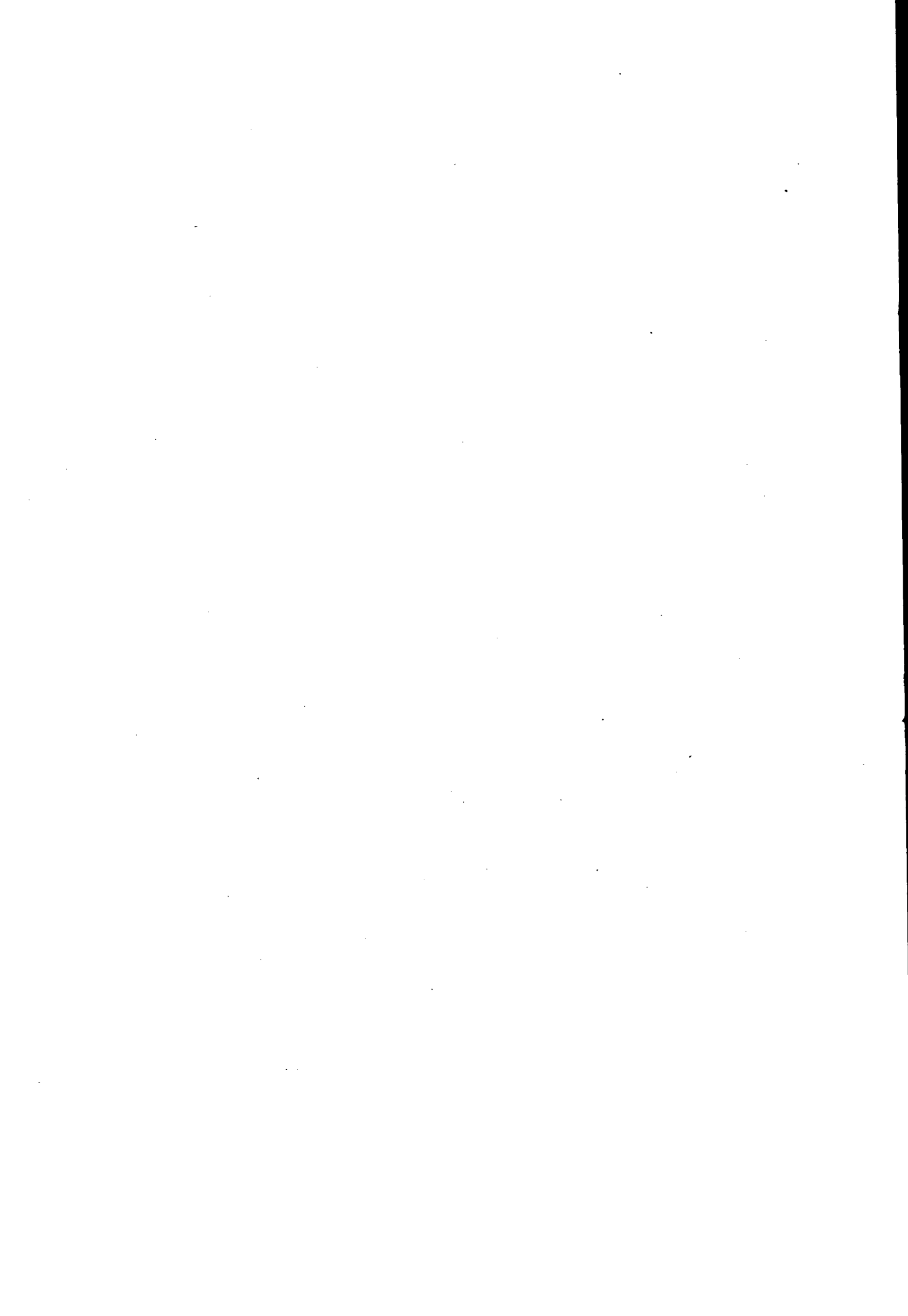
- [12] Faulkner G.S, Thomson A, Buswell H.J., *The penetrometer as a non-destructive test technique* , Paper No 12 , **AGARD/PEP Symposium : " Service life of Solid propellant Systems "** , Athens , May 1996
- [13] Margetson J., Wong F.C., "Service life prediction of solid rocket propellant motors stored in a random thermal environment " , Paper No 36 , **AGARD/PEP Symposium : " Service life of Solid propellant Systems "** , Athens , May 1996

# **CHAPTER 8**

## **RECOMMENDATIONS AND CONCLUSIONS**

### **TABLE OF CONTENTS**

<b>8.1</b>	<b>INTRODUCTION</b>	<b>8-1</b>
<b>8.2</b>	<b>BEST PRACTICE</b>	<b>8-1</b>
8.2.1	General Comments	8-1
8.2.2	Specific Recommendations Concerning Structural Analysis	8-2
<b>8.3</b>	<b>HARMONISATION AND COMMUNICATION</b>	<b>8-2</b>
<b>8.4</b>	<b>RECOMMENDATIONS FOR FUTURE DIRECTIONS</b>	<b>8-3</b>
	<b>APPENDIX 8-1</b> Grain Structural Assessment Report	<b>8-5</b>
	<b>APPENDIX 8-2</b> Recommended Definitions of Terms	<b>8-7</b>



## Chapter 8

### RECOMMENDATIONS AND CONCLUSIONS

This chapter presents the Working Group's conclusions from its programme of work and sets out some recommendations concerning future **structural integrity** assessments of solid rocket motors. It also gives recommendations for standardisation of terminology and methodology which will improve communication among NATO countries.

#### 8.1 INTRODUCTION

There is no doubt that the assessment of grain structural integrity remains a challenging area for solid rocket designers and that there is considerable scope for improvement in the predictive methods currently in use. Furthermore, there are many differing approaches to the theoretical analysis of a solid propellant grain, experimental determination of rheological properties of the propellant and verification of predicted results. Chapter 6 illustrates particularly clearly the need to fully understand the true meaning of terms, the underlying assumptions and built-in allowances for uncertainty contained the method of quantification of the grain's structural margin. These differences create problems when assessing design proposals from another NATO country or entering into joint programmes. This report gives recommendations for harmonisation and provides a reference source describing the various practices currently in use amongst the participating NATO countries. Working Group 25 recommends that the terminology used in this report become a standard for international programmes and that participants use this terminology in future assessments.

The results will be considered under the three major headings of:

- (a) Best Current Practice
- (b) Harmonisation and Communication
- (c) Recommendations for Future Direction

#### 8.2 BEST PRACTICE

##### 8.2.1 General Comments

The previous chapters to this report give a detailed review of the current practice in the field of grain structural assessment but the Working Group would like to emphasise the following important points:

- a) To maximise the safe performance of rocket motors it is essential that realistic specifications of the operating environments are provided whenever available for future systems.
- b) Particular care should be taken so as to ensure that the measured material properties reflect the selected constitutive model to be used and that they provide adequate data from appropriately selected test conditions such as dilation, multi-axiality, hydrostatic pressure, high-rate and combined loading.
- c) The measured failure properties of the materials considered in the assessment must be consistent with the assumed failure criteria.
- d) All these material properties should be measured by the recommended AC310/SGIII methods where possible.
- e) A Failure Mode Effects Analysis (FMEA) should be carried out to verify the critical areas of the grain, and the results of tests to verify the analysis must be recorded in a formalised way. A suggested format is described in section 8.3 and Appendix 8.1.
- f) It is advised that 3D geometry effects are frequently more significant than non-linear behaviour in complex geometry grains and that grain structural analyses take proportionate account of this fact.

### 8.2.2 Specific Recommendations Concerning Structural Analysis (See Chapter 3 for details and discussion)

- a) For traceability, it is strongly recommended that all stages of the structural analysis process are recorded as part of a Grain Structural Assessment Report as in Appendix 8-1.
- b) Problem Definition
  - simplifying assumptions should be used only where appropriate and accuracy is acceptable
  - rigorous 3D modelling techniques should be used for complex geometry
  - symmetry should be used to advantage wherever possible.
- c) FE Model Definition
  - quadratic (second order) elements should be used in general
  - rectangular/brick elements should be used in areas of concentration
  - nodes should be ordered consistently (e.g. counter clockwise)
  - use "reformulated" elements for incompressible / near incompressible materials
  - highly distorted elements should be avoided.
- d) Material Definition
  - Constitutive Laws
    - appropriate (accurate) material laws should be used
    - limits of applicability (i.e. range of material law stability) should be known
  - Case materials
    - it is important to model case accurately (i.e. if filament wound case use composite material definition)
  - Insulation /Inhibitor Materials
    - if non-linear solution procedure used then rubber elastic law should be used
  - Propellant Grain
    - use effective modulus (linear elasticity) only when more detailed data is unavailable
- e) Load Definition
  - superposition should be used for combined loads only if solution procedure is linear.
- f) Solution Procedure
  - geometric non-linear solution procedure should be used when large displacements and/or rotations are expected
- g) Results Interpretation
  - if possible, document mesh sensitivity (i.e. check the accuracy of the mesh by refinement)
  - values of stress/strain computed at integration points should be used whenever possible.

### 8.3 HARMONISATION AND COMMUNICATION

A universally adopted methodology for grain structural assessment across NATO would yield obvious benefits. However it is recognised that each nation now has considerable investment in its procedures not only in terms of an established data base but also in terms of precedence and confidence level. We must therefore expect that full harmonisation will be a slow process. There are however some realisable short term goals that are worth pursuing. The following general recommendations and comments are made:

- a) There is a clear need to determine a set of reasonable and practical procedural requirements that should be followed in structural integrity assessment (see Chapter 2)
- b) In order to provide a framework for the generation of procedural requirements the Working Group recommend that future solid rocket motor projects adopt the use of a Grain Structural Assessment Report (GSAR) and suggest the format and suitable elements to be considered in the GSAR as shown in Appendix 1 to this Chapter.

Assessment Report (GSAR) and suggest the format and suitable elements to be considered in the GSAR as shown in Appendix 1 to this Chapter.

- c) An agreed procedure is needed to formalise and standardise the specification of the minimum required value for the Margin of Safety or reliability together with the method used to derive these figures .
- d) When conducting an independent structural assessment of a given grain it is important to be aware of applicability of the chosen failure criteria and the failure criteria used in the initial analysis together with other associated assumptions.
- e) Recommendations for standard definitions of terms used in structural integrity assessments are given in Appendix 2.

#### 8.4 RECOMMENDATIONS FOR FUTURE DIRECTIONS

The Working Group recommends:

- a) That a unified margin of safety technique for handling multiple loading should be developed and agreed upon among the various NATO countries.
- b) That a probabilistic analysis should be considered as an alternative to the standard Margin of Safety calculation.

The Working Group suggests that the Margin of Safety, Safety Factor and Safety Ratio approaches to structural integrity assessment can lead to misunderstanding and inconsistencies. Although these approaches are regarded as deterministic, they are in fact pseudo-probabilistic in the sense that they rely on the probability of extremes in applying knockdown factors to the load and capacity variables. This is a crude attempt to resolve the problem of uncertainty and only leads to qualitative evaluation with some hidden allowance for statistical variability. It is interesting to note that the probabilistic method links together the Margin of Safety, Safety Factor and Safety Ratio approaches into a uniform procedure and provides a systematic method of analysis. By adopting the probabilistic approach the problems of limited information and levels of confidence can be dealt with using the statistics of small samples a well established branch of statistics. Engineering judgement, in the form of past experience, can be dealt with using Bayesian statistics approach. Two conclusions are worth highlighting. Firstly, many of the misunderstanding and inconsistencies experienced when using the Margin of Safety, Safety Factor and Safety Ratio approaches to structural assessment are eliminated by the use of a probabilistic method. Lastly, many of the other missile system components, like electronic units and the motor cases, are proven statistically from whence it follows that it makes sense to apply a similar approach to the propellant structural assessment problem.

- c) That more emphasis is given to the development of constitutive equations that incorporate damage as the source of material non-linearity. The constitutive law must also be capable of correctly modelling combined loads and multi-axiality.

It has been recognised by this Working Group that the current prediction capability of the stress-strain response in a solid rocket propellant grain and associated bondline system, when subjected to its storage and in-service loads, lacks acceptable precision and in many situations is highly inaccurate. It is therefore proposed that constitutive models are developed which will account for material non-linearity by considering the evolution of damage of microstructure as a function of the applied loading history. Furthermore, these constitutive model should accurately describe combined mechanical and thermal loading conditions. These non-linear thermo-viscoelastic constitutive models must be capable of giving a good correlation with uniaxial behaviour under all forms of combined loading conditions and, furthermore, be capable

of extension to the multiaxial stress state. The constitutive models should be computationally efficient because the finite element solution requirements for the storage and operational loading conditions will be extensive. Significant advances have been made recently in this theoretical field and has been accompanied by important advances in the development of accurate stress measuring devices.

- d) The Working Group considers that the state-of-the-art ability to perform a full mechanical property characterisation of propellant is weak and it needs extra effort to establish the correct procedures and methods.
- e) Finally, and perhaps most importantly, it must be emphasised that the Working Group did not consider Service Life methodologies and predictions related to the use of structural analysis as it was considered beyond the scope of this Working Group. However, the Working Group considered this an essential topic for future study.

## Appendix 8-1

# GRAIN STRUCTURAL ASSESSMENT REPORT

### 1. REQUIREMENT

Within any existing requirement that a motor design authority should provide a Structural Design Record (SDR) for all the structural parts of the motor/missile, a form of the SDR titled the Grain Structural Assessment Report (GSAR) should be created for the grain and bondline system. This GSAR shall be progressively compiled from the initiation of the design; initially in support of the development programme, and progressively reissued or updated until the production standard is reached. It shall subsequently be updated if any significant modifications or requirement changes are introduced and when results from verification testing (before or after production delivery) are made available. The format and content of the GSAR should be agreed before the Development stage commences. The main content and relevant topics which the GSAR may include are given below.

### 2. CONTENT

- 2.1 Introduction - General characteristics/role of the motor, including general information on case and bondline, type of propellant and grain (including designations if appropriate).
- 2.2 Design Features - Description of significant design features and outline basis for design.
- 2.3 Environmental Specification - Description of requirements on which design is based, with references and amplification as necessary.
- 2.4 Design Cases - All significant design cases and loads factors, including:
  - (a) Combination of environmental conditions from which cases derived,
  - (b) Limit loads, including diagrams where necessary,
  - (c) Thermal histories and conditions for each loading,
  - (d) Design and load factors applicable,
  - (e) Assumptions significant to derivation of parameters.
- 2.5 Structural Design Descriptions - to an appropriate level of detail definition, including:
  - (a) General assembly drawings,
  - (b) Complete list of main engineering drawing titles and standard of design,
  - (c) Geometric data,
  - (d) Materials designations and specifications.
- 2.6 Summary of Structural Assessment - a summary of the assessment confirming strength and stiffness of grain, with the following information:
  - (a) Description & Drawing No. of item/assembly,
  - (b) Relevant general dimensional and material specification data,
  - (c) Assumptions made,
  - (d) Method of Structural Analysis,
  - (e) Design cases critical for each item,
  - (f) Theoretical margin of safety, damage factors, etc.,
  - (g) References to supporting and verifying test reports.
- 2.7 Summary of Structural Analysis - covering all stages of structural analysis process, including:
  - (a) Geometry (including dimensions & special features),
  - (b) FE model (element type, etc),

- (c) Materials (properties data, data reduction methods, etc),
- (d) Loads (boundary conditions, etc),
- (e) Constitutive law(s) used (incl. specific parameters),
- (f) Solution procedure (incl. control parameters),
- (g) Results interpretation and assumptions, leading to
- (h) Required inputs to a determination of MS.

2.8 Summary of Strength Analysis - including main methods and assumptions used for:

- (a) Identification of Failure Criteria used,
- (b) Selection of appropriate material models and damage factors where applicable,
- (c) Derivation of MS.

2.9 Structural Appraisal - comments of adequacy, including statements on the following:

- (a) Limitations of simulation,
- (b) Interpretation of test results and comparison to theoretical analysis,
- (c) Assessment of any life limiting aspects,
- (d) Deviations from design requirements,
- (e) Any resulting operating limitations.

2.10 Verification Test Report List - giving for each report a summary of requirements and results.

## Appendix 8-2

### RECOMMENDED DEFINITIONS OF TERMS

#### 1. Structural Integrity Assessment

The Working Group agreed that the term **structural integrity assessment** was the process by which a propellant grain was evaluated to assess its ability to perform satisfactorily under the operating conditions specified throughout its life cycle. The analysis would involve many parts as given in Chapter 2.

#### 2. Margin of Safety

The area where the most confusion existed was in the methodology and calculation of the grain structural capability. It is therefore recommended that the term **margin of safety (MS)**, as given in Chapter 6.2, is used as a measure of the excess of the capability over the requirement.

#### 3. Design Factor

The term **design factor (DF)**, is discussed in Chapter 6, section 6.4.1 and should be used in the MS calculation to take account of the uncertainty in the induced load as set by the requirement. Other terms to be used are also given in Chapter 6.

#### 4. Bondline System

To avoid any confusion with the description of the interface between the propellant grain and the case the term **bondline system** should be used to include all the layers of material between the propellant grain and the case.

The following sub-division of rocket motor type was also agreed:

#### 5. Analogue Motor

A tube filled with a simple geometry grain or alternatively is a specimen designed to simulate specific motor feature used for initial verification tests.

#### 6. Structural Test Vehicle

A case with propellant grain designed to simulate response to complex loading.

#### 7. Sub-scale Motor

Case filled with the same propellant and grain features as the full size motor but of smaller size.

## REPORT DOCUMENTATION PAGE

<b>1. Recipient's Reference</b>	<b>2. Originator's Reference</b> AGARD-AR-350	<b>3. Further Reference</b> ISBN 92-836-1063-6	<b>4. Security Classification of Document</b> UNCLASSIFIED
<b>5. Originator</b> Advisory Group for Aerospace Research and Development North Atlantic Treaty Organization 7 rue Ancelle, 92200 Neuilly-sur-Seine, France			
<b>6. Title</b> Propulsion and Energetics Panel Working Group 25 On Structural Assessment of Solid Propellant Grains			
<b>7. Presented at/sponsored by</b>			
<b>8. Author(s)/Editor(s)</b> Multiple			<b>9. Date</b> December 1997
<b>10. Author's/Editor's Address</b> Multiple			<b>11. Pages</b> 208
<b>12. Distribution Statement</b> There are no restrictions on the distribution of this document. Information about the availability of this and other AGARD unclassified publications is given on the back cover.			
<b>13. Keywords/Descriptors</b>			
Rocket propellant grains Solid propellant rocket engines Solid propellant rockets Gas generators Rocket propulsion Structural analysis	Failure Safety engineering Reliability Service life Mechanical properties Rheological properties	Design Stresses NATO Standardization	
<b>14. Abstract</b>			
<p>Solid propellant rocket motors and gas generators are used in military and civil devices. Missiles, boosters, space propulsion, pyrotechnic actuators are examples. The structural capability of the grain over time and under varying temperature, humidity, and mechanical loads, is of prime concern for the reliability, safety and service life of the device. From 1994 to 1996 an AGARD working group has collected, reviewed and evaluated the methods used for structural analysis of solid propellant grains within the NATO nations and has issued an advisory report consisting of 8 chapters:</p> <ol style="list-style-type: none"> <li>1. Overview of Solid Propellant Rocket Motor Design</li> <li>2. Application of Structural Integrity Assessment</li> <li>3. Structural Analysis</li> <li>4. Material Characterisation</li> <li>5. Failure Criteria</li> <li>6. Margin of Safety Determination</li> <li>7. Verification</li> <li>8. Recommendations and Conclusions</li> </ol> <p>Standardisation and preferable approaches are recommended.</p>			

L'AGARD détient un stock limité de certaines de ses publications récentes. Celles-ci pourront éventuellement être obtenus sous forme de copie papier. Pour de plus amples renseignements concernant l'achat de ces ouvrages, adressez-vous à l'AGARD par lettre ou par télécopie à l'adresse indiquée ci-dessus. *Veuillez ne pas téléphoner.*

Des exemplaires supplémentaires peuvent parfois être obtenus auprès des centres de diffusion nationaux indiqués ci-dessous. Si vous souhaitez recevoir toutes les publications de l'AGARD, ou simplement celles qui concernent certains Panels, vous pouvez demander d'être inclus sur la liste d'envoi de l'un de ces centres.

Les publications de l'AGARD sont en vente auprès des agences de vente indiquées ci-dessous, sous forme de photocopie ou de microfiche. Certains originaux peuvent également être obtenus auprès de CASI.

## CENTRES DE DIFFUSION NATIONAUX

**ALLEMAGNE**

Fachinformationszentrum Karlsruhe  
D-76344 Eggenstein-Leopoldshafen 2

**BELGIQUE**

Coordonnateur AGARD-VSL  
Etat-major de la Force aérienne  
Quartier Reine Elisabeth  
Rue d'Evere, 1140 Bruxelles

**CANADA**

Directeur - Gestion de l'information  
(Recherche et développement) - DRDGI 3  
Ministère de la Défense nationale  
Ottawa, Ontario K1A 0K2

**DANEMARK**

Danish Defence Research Establishment  
Ryvangs Allé 1  
P.O. Box 2715  
DK-2100 Copenhagen Ø

**ESPAGNE**

INTA (AGARD Publications)  
Carretera de Torrejón a Ajalvir, Pk.4  
28850 Torrejón de Ardoz - Madrid

**ETATS-UNIS**

NASA Center for AeroSpace Information (CASI)  
800 Elkridge Landing Road  
Linthicum Heights, MD 21090-2934

**FRANCE**

O.N.E.R.A. (Direction)  
29, Avenue de la Division Leclerc  
92322 Châtillon Cedex

**GRECE**

Hellenic Air Force  
Air War College  
Scientific and Technical Library  
Dekelia Air Force Base  
Dekelia, Athens TGA 1010

**ISLANDE**

Director of Aviation  
c/o Flugrad  
Reykjavik

**ITALIE**

Aeronautica Militare  
Ufficio del Delegato Nazionale all'AGARD  
Aeroporto Pratica di Mare  
00040 Pomezia (Roma)

**LUXEMBOURG**

Voir Belgique

**NORVEGE**

Norwegian Defence Research Establishment  
Attn: Biblioteket  
P.O. Box 25  
N-2007 Kjeller

**PAYS-BAS**

Netherlands Delegation to AGARD  
National Aerospace Laboratory NLR  
P.O. Box 90502  
1006 BM Amsterdam

**PORTUGAL**

Estado Maior da Força Aérea  
SDFA - Centro de Documentação  
Alfragide  
2700 Amadora

**ROYAUME-UNI**

Defence Research Information Centre  
Kentigern House  
65 Brown Street  
Glasgow G2 8EX

**TURQUIE**

Millî Savunma Başkanlığı (MSB)  
ARGE Dairesi Başkanlığı (MSB)  
06650 Bakanlıklar-Ankara

## AGENCES DE VENTE

**NASA Center for AeroSpace Information (CASI)**

800 Elkridge Landing Road  
Linthicum Heights, MD 21090-2934  
Etats-Unis

**The British Library Document Supply Division**

Boston Spa, Wetherby  
West Yorkshire LS23 7BQ  
Royaume-Uni

Les demandes de microfiches ou de photocopies de documents AGARD (y compris les demandes faites auprès du CASI) doivent comporter la dénomination AGARD, ainsi que le numéro de série d'AGARD (par exemple AGARD-AG-315). Des informations analogues, telles que le titre et la date de publication sont souhaitables. Veuillez noter qu'il y a lieu de spécifier AGARD-R-nnn et AGARD-AR-nnn lors de la commande des rapports AGARD et des rapports consultatifs AGARD respectivement. Des références bibliographiques complètes ainsi que des résumés des publications AGARD figurent dans les journaux suivants:

**Scientific and Technical Aerospace Reports (STAR)**

STAR peut être consulté en ligne au localisateur de ressources uniformes (URL) suivant:  
<http://www.sti.nasa.gov/Pubs/star/Star.html>  
STAR est édité par CASI dans le cadre du programme NASA d'information scientifique et technique (STI)  
STI Program Office, MS 157A  
NASA Langley Research Center  
Hampton, Virginia 23681-0001  
Etats-Unis

**Government Reports Announcements & Index (GRA&I)**

publié par le National Technical Information Service  
Springfield  
Virginia 2216  
Etats-Unis  
(accessible également en mode interactif dans la base de données bibliographiques en ligne du NTIS, et sur CD-ROM)



AGARD holds limited quantities of some of its recent publications, and these may be available for purchase in hard copy form. For more information, write or send a telefax to the address given above. *Please do not telephone.*

Further copies are sometimes available from the National Distribution Centres listed below. If you wish to receive all AGARD publications, or just those relating to one or more specific AGARD Panels, they may be willing to include you (or your organisation) in their distribution.

AGARD publications may be purchased from the Sales Agencies listed below, in photocopy or microfiche form. Original copies of some publications may be available from CASI.

## NATIONAL DISTRIBUTION CENTRES

## BELGIUM

Coordonnateur AGARD — VSL  
Etat-major de la Force aérienne  
Quartier Reine Elisabeth  
Rue d'Evere, 1140 Bruxelles

## CANADA

Director Research & Development  
Information Management - DRDIM 3  
Dept of National Defence  
Ottawa, Ontario K1A 0K2

## DENMARK

Danish Defence Research Establishment  
Ryvangs Allé 1  
P.O. Box 2715  
DK-2100 Copenhagen Ø

## FRANCE

O.N.E.R.A. (Direction)  
29 Avenue de la Division Leclerc  
92322 Châtillon Cedex

## GERMANY

Fachinformationszentrum Karlsruhe  
D-76344 Eggenstein-Leopoldshafen 2

## GREECE

Hellenic Air Force  
Air War College  
Scientific and Technical Library  
Dekelia Air Force Base  
Dekelia, Athens TGA 1010

## ICELAND

Director of Aviation  
c/o Flugrad  
Reykjavik

## ITALY

Aeronautica Militare  
Ufficio del Delegato Nazionale all'AGARD  
Aeroporto Pratica di Mare  
00040 Pomezia (Roma)

## LUXEMBOURG

See Belgium

## NETHERLANDS

Netherlands Delegation to AGARD  
National Aerospace Laboratory, NLR  
P.O. Box 90502  
1006 BM Amsterdam

## NORWAY

Norwegian Defence Research Establishment  
Attn: Biblioteket  
P.O. Box 25  
N-2007 Kjeller

## PORTUGAL

Estado Maior da Força Aérea  
SDFA - Centro de Documentação  
Alfragide  
2700 Amadora

## SPAIN

INTA (AGARD Publications)  
Carretera de Torrejón a Ajalvir, Pk.4  
28850 Torrejón de Ardoz - Madrid

## TURKEY

Millî Savunma Başkanlığı (MSB)  
ARGE Dairesi Başkanlığı (MSB)  
06650 Bakanlıklar-Ankara

## UNITED KINGDOM

Defence Research Information Centre  
Kentigern House  
65 Brown Street  
Glasgow G2 8EX

## UNITED STATES

NASA Center for AeroSpace Information (CASI)  
800 Elkridge Landing Road  
Linthicum Heights, MD 21090-2934

## SALES AGENCIES

## NASA Center for AeroSpace Information (CASI)

800 Elkridge Landing Road  
Linthicum Heights, MD 21090-2934  
United States

## The British Library Document Supply Centre

Boston Spa, Wetherby  
West Yorkshire LS23 7BQ  
United Kingdom

Requests for microfiches or photocopies of AGARD documents (including requests to CASI) should include the word 'AGARD' and the AGARD serial number (for example AGARD-AG-315). Collateral information such as title and publication date is desirable. Note that AGARD Reports and Advisory Reports should be specified as AGARD-R-*nnn* and AGARD-AR-*nnn*, respectively. Full bibliographical references and abstracts of AGARD publications are given in the following journals:

## Scientific and Technical Aerospace Reports (STAR)

STAR is available on-line at the following uniform resource locator:

<http://www.sti.nasa.gov/Pubs/star/Star.html>

STAR is published by CASI for the NASA Scientific and Technical Information (STI) Program

STI Program Office  
NASA Langley Res  
Hampton, Virginia  
United States

## Government Reports Announcements &amp; Index (GRA&amp;I)

published by the National Technical Information Service

Springfield  
Virginia 22161  
United States

(also available online in the NTIS Bibliographic



\*348923++P+UL\*